Role of membranes in mammalian stress response: sensing, lipid signals and adaptation

Gábor Balogh

PhD Thesis 2011

Thesis submitted in fulfilment of the requirements of the degree of

Doctor of Philosophy, Cardiff University

Institute of Biochemistry

Biological Research Centre

Hungarian Academy of Sciences

Szeged, Hungary

DECLARATION

This work has not previously been accepted in substance for any degree and is not concurrently submitted in candidature for any degree.

Signed …  (Gábor Balogh) Date **30 November 2011**

STATEMENT 1

This thesis is being submitted in partial fulfillment of the requirements for the degree of **PhD**

Signed …  (Gábor Balogh) Date **30 November 2011**

STATEMENT 2

This thesis is the result of my own independent work/investigation, except where otherwise stated.
Other sources are acknowledged by explicit references.

Signed …  (Gábor Balogh) Date **30 November 2011**

STATEMENT 3

I hereby give consent for my thesis, if accepted, to be available for photocopying and for inter-library loan, and for the title and summary to be made available to outside organisations.

Signed …  (Gábor Balogh) Date **30 November 2011**

SUMMARY

It was suggested that under heat stress the accumulation of denatured proteins alone triggers the expression of heat shock proteins. However, earlier research suggested that during abrupt temperature fluctuations membranes represent the most thermally-sensitive macromolecular structures. The aim of this thesis to confirm experimentally for the membrane sensor theory in mammalian cells and to explore the mechanisms behind membrane lipid structural reorganizations. The main results are as follows:

(i) I provide the first evidence that heat-analogous, chemically-induced membrane perturbation of K562 erythroleukemic cells is indeed capable of activating heat shock protein formation at the growth temperature, without causing measurable protein denaturation;

(ii) I showed that the membrane fluidizer benzyl alcohol acts as a chaperone-inducer also in B16(F10) melanoma cells. Furthermore, following both alcohol and heat treatments, condensation of ordered plasma membrane domains was detected by fluorescence microscopy;

(iii) lipidomic fingerprints revealed that stress achieved either by heat or benzyl alcohol resulted in pronounced and highly specific alterations of membrane lipids in B16(F10) cells. The loss in polyenes with the concomitant increase in saturated lipid species was shown to be a consequence of activation of phospholipases. The accumulation of lipid species with raft-forming properties may explain the condensation of ordered plasma membrane domains detected previously;

(iv) with Laurdan two-photon microscopy it was demonstrated that, in contrast to the formation of ordered domains in surface membranes, the molecular disorder is significantly elevated within the internal membranes of cells preexposed to mild heat stress. These results were compared with those obtained by other probes and visualisation methods. It was found that the structurally different probes revealed substantially distinct alterations in membrane heterogeneity.

The results highlight that even subtle changes in membrane microstructure may play a role in temperature sensing and thermal cell killing and, therefore, could have potential in treatment of several diseases.

ACKNOWLEDGEMENTS

I would like to thank my supervisors, Prof. John Harwood and Prof. László Vígh, for providing me with the opportunity to complete my PhD thesis at the Cardiff University as an external student from the Biological Research Centre in Szeged. I am very grateful for their patience, motivation, enthusiasm, and immense knowledge in lipid, membrane and stress biochemistry. I want to thank László for the many insightful discussions and creating ideas together. He gave me the freedom to design and pursue various projects. Special thanks to John for the continuous support, and the critical questions, corrections and language editing from which I learned a lot.

I am also very grateful to present and past members of the Laboratory of Molecular Stress Biology in BRC, especially to Ibolya Horváth for the discussions and in-depth proofreading of my manuscripts, to Zsolt Török for his advices in biophysical methods, Imre Gombos and Enikő Nagy for their collaboration, and Attila Glatz for his advice about molecular biology. Special thanks to Maria Péter, my closest coworker and generous friend for the everyday helping to finish up the manuscripts and the thesis. I want to thank for the skillful technical assistance Éva Dobóné Barta and Gabi Bogdánné.

I want to thank our collaborators in other groups of the BRC (Elfrieda Fodor and Tibor Páli), and in Italy (Tiziana Parasassi, Giuseppe Maulucci, Marco De Spirito), Germany (Gerhard Liebisch and Gerd Schmitz) and France (Olivier Bensaude), for their kindness, friendship and support. I spent professionally fruitful times in all countries. Their contribution will be detailed in the corresponding chapters of the thesis.

I also thank my wife, Marta for the love, patience and support.

ABBREVIATIONS

AA	arachidonic acid
AM	acetoxymethyl ester
Akt/PKB	protein kinase B
BA	benzyl alcohol
BCA	bicinchoninic acid
BMP	bis(monoacylglycero)phosphate
$[Ca^{2+}]_i$	intracellular free calcium
CaMKII	calcium/calmodulin-dependent protein kinase II
CCCP	carbonyl cyanide *p*-chlorophenylhydrazone
CDP	cytidine diphosphate
CE	cholesteryl ester
Cer	ceramide
CG	cholesteryl glucoside
Chol	cholesterol
CL	cardiolipin
COX	cyclooxygenase
CSR	cellular stress response
DG/DAG	diradylglycerol/diacylglycerol
DGL	diacylglycerol lipase
DHA	docosahexaenoic acid
DHSph	dihydrosphingosine
DMA	dimethyl acetal
DMSO	dimethyl sulfoxide
DPH	1,6-diphenyl-1,3,5-hexatriene
DPH-PA	1,6-diphenyl-1,3,5-hexatriene propionic acid
DRM	detergent-resistant membrane domains
EGFR	epidermal growth factor receptor
EGTA	ethylene glycol tetraacetic acid
EPA	eicosapentaenoic acid
EPR	electron paramagnetic resonance
ER	endoplasmic reticulum
ERK	extracellular signal-regulated kinase
ESI-MS	electrospray ionization tandem mass spectrometry
FA	fatty acid/fatty acyl
FAAH	fatty acid amide hydrolase
FAME	fatty acid methyl esters
FCS	fetal calf serum
FFA	free fatty acid
FFT	fast Fourier transform
fPEG-Chol	fluorescein ester of polyethylene glycol-derivatized cholesterol
GalCer	galactosylceramide
GC-MS	gas chromatography-mass spectrometry
GL	glycerolipid
GluCer	glucosylceramide
GP	generalized polarization
GPI	glycosylphosphatidylinositol
GPL	glycerophospholipid
GSK3	glycogen synthase kinase-3

GSL	glycosphingolipid
HE	heptanol
HER	heregulin
HS	heat stress/heat shock
HSE	heat shock element
HSF	heat shock factor
Hsp	heat shock protein
Hsp	heat shock protein gene
HSR	heat shock response
IGF	insulin-like growth factors
IP_3	inositol triphosphate
JC-1	5,59,6,69-tetrachloro-1,19,3,39-tetraethyl-benzimidazolylcarbocyanine iodide
JNK	c-jun N-terminal kinase
Laurdan	6-dodecanoyl-2-dimethylaminonaphthalene
LD	lipid droplet
L_d	liquid-disordered phase
L_o	liquid-ordered phase
LOX	lipoxygenase
LPA	lysophosphatidic acid
LPC	lysophosphatidylcholine
MAF	MDR activity factor
MAFP	methyl arachidonyl fluorophosphonate
MAPK	mitogen-activated protein kinase
MDR	multidrug resistance
MDR1	multidrug resistant protein
MG/MAG	monoradylglycerol/monoacylglycerol
MGL	monoacylglycerol lipase
MUFA	monounsaturated fatty acid
NIST	National Institute of Standards and Technology
NSAID	non-steroidal anti-inflammatory drug
PA	phosphatidic acid
PAF	platelet activating factor
PBS	phosphate buffered saline
PC	phosphatidylcholine
PC1/PC2/PC3	principal components 1/2/3
PCA	principal component analysis
PC-O	1-alkyl-2-acyl species of phosphatidylcholine
PE	phosphatidylethanolamine
PEMT	phosphatidylethanolamine *N*-methyltransferase
PE-P	1-(1*Z*-alkenyl)-2-acyl species of PE
PG	phosphatidylglycerol
PGA/PGG/PGH/PGJ	different series of prostaglandins
PI	phosphatidylinositol
PI3K	phosphoinositide 3-kinase
PIP2	phosphatidylinositol-4,5-biphosphate ($PI(4,5)P_2$)
PIP3	phosphatidylinositol-3,4,5-triphosphate
PIPn	phosphoinositides
PKA	protein kinase A
PKB/Akt	protein kinase B
PKC	protein kinase C
PL	phospholipid

PLA_1	phospholipase A_1
PLA_2	phospholipase A_2
PLC	phospholipase C
PLD	phospholipase D
PM	plasma membrane
PPO	2,5-diphenyloxazole
PS	phosphatidylserine
PSL	phosphosphingolipid
PTEN	phosphatase and tensin homologue protein
PUFA	polyunsaturated fatty acid
Rac1	Ras-related C3 botulinum toxin substrate 1
ROI	Region-of-Interest
5- and 16-SASL	5- and 16-(4',4'-dimethyloxazolidine-*N*-oxyl)stearic acid spin labels
SD	standard deviation
SDS	sodium dodecyl sulfate
SEM	standard error of mean
S1P	sphingosine-1-phosphate
SFA	saturated fatty acid
SIRT1	sirtuin 1
SL	sphingolipid
SM	sphingomyelin
Sn	stereospecific numbering
SPC	sphingosyl phosphorylcholine
Sph	sphingosine
THL	tetrahydrolipstatin
TG/TAG	triradylglycerol/triacylglycerol
TGL	triacylglycerol lipase
TMA-DPH	1-(4-trimethylammoniumphenyl)-6-phenyl-1,3,5-hexatriene
TPL	total polar lipid
$\Delta\Psi_m$	mitochondrial membrane potential

CHAPTER 1. INTRODUCTION

“Without stress, there would be no life”
Hans Selye

1.1. STRESS

Hans Selye discovered *stress* in 1936 as a syndrome occurring in laboratory rats which he termed the "general adaptation syndrome" (Selye, 1936). In 1950 he summarised his thesis concerning stress: "Anything that causes stress endangers life, unless it is met by adequate adaptive responses; conversely, anything that endangers life causes stress and adaptive responses. Adaptability and resistance to stress are fundamental prerequisites for life, and every vital organ and function participates in them." (Selye, 1950). Nowadays Selye's notion of a universal non-specific reaction has become accepted, and biochemists and physiologists use stress as a unifying concept to understand the interaction of organic life with the environment.

General adaptation can be divided into three stages. The first stage is called the alarm reaction, the second resistance or adaptation and the third exhaustion (Selye, 1936). In the first two phases the stress response does not lead to adverse health outcomes; rather, it protects an organism from harm by increasing alertness, mobilizing energy, and protecting against pathogens. Every time the stress response is activated, however, physiological adjustments must be made, and over time, these adjustments may lead to cumulative exhaustion (Piazza et al., 2010).

The beneficial effect of stress is to enable the organism to cope with a subsequent, more severe stress. This ability is called stress tolerance. In a positive case of mild stress with no apparent damage this phenomenon is called hormesis. However, if damage overwhelms the adaptation, it results in functional decline, a so-called distress. The organismal adaptation response is mediated by the vegetative nervous system and the hypothalamo-pituitary-adrenal axis (Söti and Csermely, 2007). But how can the organisms cope with stress at the cellular level?

1.2. CELLULAR STRESS

Acute and chronic stresses are able to cause deleterious effects on cellular infrastructure and disturb cellular homeostasis. Most types of environmental stress, including osmotic

stress (Hochachka and Somero, 2002), thermal stress (Hochachka and Somero, 2002), heavy metal stress (Farrer and Pecoraro, 2002), ionizing radiation (Kempner, 1993), baric stress (Somero, 1992), oxidative stress (Kasprzak, 2002) and hypoxia/ischemia (Borkan and Gullans, 2002), manifest themselves with changes in protein conformation. Likewise, many of these various stresses are also known to cause DNA damage (Galloway et al., 1987; Kasprzak, 2002; Kültz and Chakravarty, 2001; Liu, 2001; Rydberg, 2001). Lipids are also well-known targets of oxidative (see e.g. Catalá, 2010) and heat stresses (Yatvin and Cramp, 1993), X-ray (Yukawa et al., 2005) and UV (Roshchupkin and Murina, 1998) irradiations. Moreover, the stress response in eukaryotic cells often inhibits translation initiation and leads to the formation of cytoplasmic RNA-protein complexes referred to as stress granules (Buchan and Parker, 2009).

As a consequence, organisms have developed the capacity to initiate a number of adaptive cellular response pathways that attempt to reduce damage and maintain or re-establish cellular homeostasis (Gupta et al., 2010). The cellular stress response (CSR) is a universal mechanism of extraordinary physiological/pathophysiological significance (Kültz, 2003). Many aspects of CSR are not stressor-specific because cells monitor stress based on macromolecular damage regardless of the type of stress that causes such damage; cellular mechanisms activated by DNA, protein and membrane (lipid) damage are interconnected and share common elements. Other cellular responses directed at re-establishing homeostasis are stressor-specific and often activated in parallel to the CSR. All organisms have stress proteins, and universally conserved stress proteins can be regarded as the minimal stress proteome. Functional analysis of the minimal stress proteome yields information about key aspects of the cellular stress response, including physiological mechanisms of sensing membrane lipid, protein, and DNA damage; redox sensing and regulation; cell cycle control; macromolecular stabilization/repair; and control of energy metabolism. In addition, cells can quantify stress and activate a death program (apoptosis) when tolerance limits are exceeded (Kültz, 2005).

1.2.1. Heat stress at cellular level

A major type of damage observed in response to heat stress (HS) conditions, especially in eukaryotes, are defects of the cytoskeleton (Richter et al., 2010). In Figure 1.1 an unstressed cell is compared to a heat-stressed cell. Mild HS leads to the reorganization of actin filaments into stress fibres, while severe HS results in the aggregation of

vimentin or other filament-forming proteins (microtubuli), leading to the collapse of intermediary, actin, and tubulin networks (Welch and Suhan, 1985; Welch and Suhan, 1986). Along with the disruption of the cytoskeleton, the loss of the correct localization of organelles and a breakdown of intracellular transport processes are observed. The Golgi system and the endoplasmic reticulum (ER) become fragmented under stress conditions, and the number and integrity of mitochondria and lysosomes decreases (Welch and Suhan, 1985). The uncoupling of oxidative phosphorylation and the loss of mitochondria are connected to a dramatic drop in ATP levels during HS (Patriarca et al., 1992). The nucleoli, sites of ribosome assembly, swell, and large granular depositions, the stress granula, become visible in the cytosol in addition to protein aggregates. Finally, there are changes in the membrane morphology, aggregation of membrane proteins, and an increase in membrane fluidity. Together, all these effects stop growth and lead to cell-cycle arrest as indicated by non-condensed chromosomes in the nucleus.

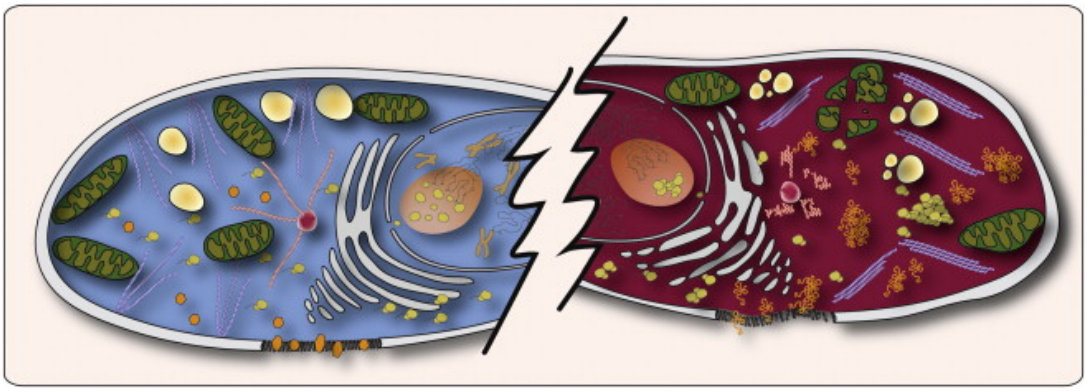

Figure 1.1. Effects of heat shock on the organization of the eukaryotic cell (Richter et al., 2010). An unstressed eukaryotic cell (left) is compared to a cell under heat stress (right). The different subcompartments are colour-coded: actin filaments, blue; microtubuli, red; endoplasmic reticulum, white; mitochondria, green; lysosomes, yellow-white gradient; stress granula, yellow; protein aggregates (hexagonal versus spaghetti style), orange.

1.3. THE HEAT SHOCK RESPONSE

An important subclass of CSR is the heat shock response (HSR). According to the definition of Westerheide and Morimoto, the HSR is an ordered genetic response to diverse environmental and physiological stressors that results in the immediate induction of genes, called stress genes or heat shock genes, encoding molecular chaperones, proteases, and other proteins (Westerheide and Morimoto, 2005). These are essential for protection and recovery from cellular damage associated with the expression of misfolded proteins and/or other compromised cell sensory elements such

as RNA, redox sensors and membranes (see later). The list of "stressors" that activate transcription of stress genes is large and includes various acute and chronic conditions such as elevated temperatures, heavy metals, small molecule chemical toxicants, infection, and oxidative stress.

However, from a survey of the literature it is clear that hyperthermia causes an increase in cholesterol and a rearrangement in phospholipid composition in cellular membranes as well (Yatvin and Cramp, 1993). Furthermore, the functional changes in membrane lipids at high temperature – linked with the alterations in fatty acid unsaturation and with other subtle changes in membrane lipid composition – can influence the response of organisms to high temperature (Guschina and Harwood, 2006). Therefore, in this thesis I use the term HSR in a wider sense including also processes which not necessarily or directly lead to stress gene induction and protein expression, but cause membrane remodelling in response to stress (see also Chapters 3–5).

1.4. HEAT SHOCK PROTEINS

In the early 1960s, Ritossa made the seminal discovery of temperature-induced puffs in polytene chromosomes of *Drosophila melanogaster* larvae salivary glands (Ritossa, 1962). A decade later, it was shown that the puffing pattern corresponded to a robust activation of genes encoding the heat shock proteins (Hsps) (Lindquist, 1986; Tissières et al., 1974). Many of these proteins function as molecular chaperones to guide conformational states critical in the synthesis, folding, translocation, assembly, and degradation of proteins (Bukau and Horwich, 1998; Hartl, 1996). Some of the major chaperones are present at high concentrations in non-stressed cells reaching 1–5 % of total cellular protein, which shows that a continuous intense demand is present to guard the protein conformational homeostasis.

A meta-analysis of microarray data (Figure 1.2) showed that a short sub-lethal HS (43 °C, 60 min) upregulated about 2 % of the human genes more than 3.16-fold (in monocyte leukemia THP-1 cells). Chaperone genes were 17 times more likely to be induced by heat than non-chaperone genes and 20 % of the chaperome was massively (>20-fold) induced by elevated temperature. Despite this general high propensity of the chaperones to be induced by heat, a majority of chaperone genes (66 % for human) still remained uninduced (Finka et al., 2011). The terms "chaperones" and "Hsps" are often indiscriminately used in the literature. However, the above analysis clearly confirms the

importance of not confusing Hsps with chaperones and vice versa, because most Hsps are not chaperones, and most chaperones are not Hsps (Finka et al., 2011).

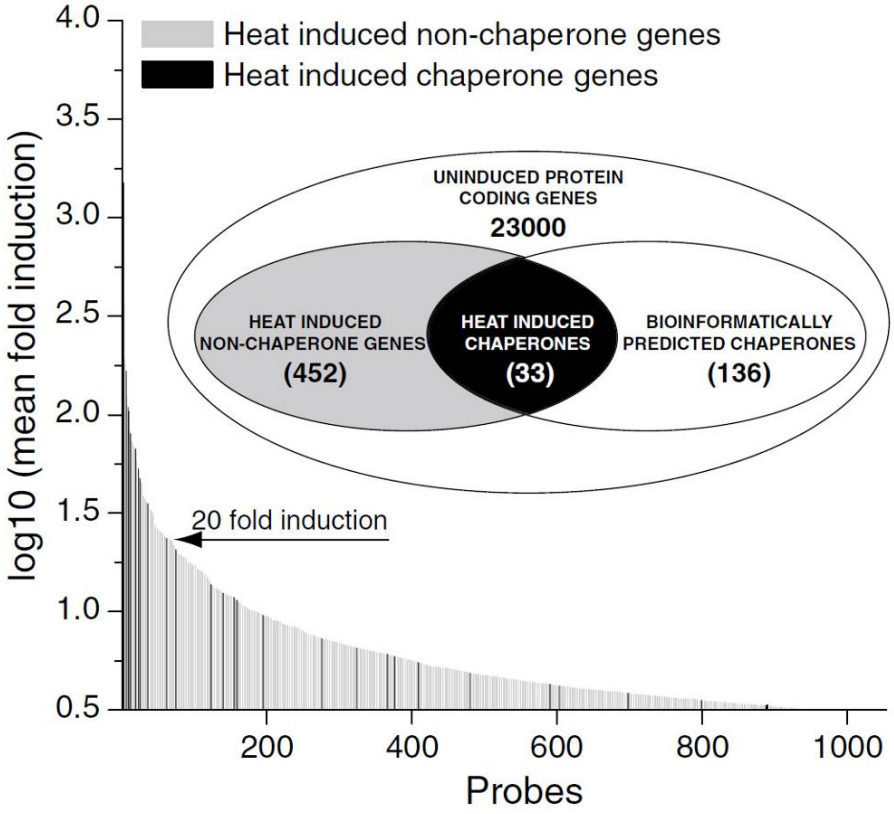

Figure 1.2. Distribution and fold-expression levels of heat-induced genes in human monocyte leukemia THP-1 cells (adapted from Finka et al., 2011). Cells were heat stressed at 43 °C for 1 h. Microarray probes corresponding to bioinformatically-predicted chaperone genes are in white, non-chaperone genes are grey and heat-induced chaperones are black.

In the present work I use the term "Hsp" in a narrower sense by focusing on heat-induced chaperones (black intersection in Figure 1.2). (Hsp) ***chaperones*** display various activities in the cell, such as:

1. proper folding of nascent polypeptide chains,
2. facilitating protein translocation across various cellular compartments,
3. modulating protein activity via stabilization and/or maturation to functionally-competent conformation, masking mild mutation at the conformational level
4. promoting multiprotein complex assembly/disassembly,
5. refolding of misfolded proteins,
6. protecting against protein aggregation,
7. targeting ultimately damaged proteins in degradation,

8. sequestering damaged proteins to aggregates,
9. solubilizing protein aggregates for refolding/degradation.

Moreover, chaperones work in concert with co-chaperones and regulate local protein and signalling networks of the cell (Pratt and Toft, 2003; Söti and Csermely, 2000; Söti and Csermely, 2007; Söti et al., 2005; Young et al., 2004).

Activation and induction of Hsps are the molecular basis of both aquired ***thermotolerance and cross-tolerance*** (Kültz, 2005). When organisms are grown at normal temperatures and shifted suddenly to severe temperatures they die rapidly. However, if they are given a brief pretreatment at a more moderate but Hsp-inducing temperature they have a higher chance of survival at severe temperatures. The effects of pretreatments are very dramatic. Differences in survival between naive and conditioned organisms are often in the range of 100- to 1000-fold. This phenomenon is also called acquired thermotolerance. Conditioning heat treatment also provides tolerance to many other types of stress, such as sodium arsenite or heat in yeast (Parsell et al., 1993). Similarly, ischemic preconditioning and mild hyperthermia induce Hsp70 and decrease reperfusion injury of human muscle and kidney (Lepore et al., 2001).

A moonlighting function of Hsps is linked to their ***membrane association***. A subpopulation of Hsps is present either on the surface or within cellular membranes (Horváth et al., 2008). On the basis of prokaryotic models, it was suggested earlier that a lipid-selective association of a subpopulation of Hsps (GroEL and sHsps) with membranes, leading to increased molecular order, may in turn result in down-regulation of *hsp* gene expression (Horváth et al., 1998; Török et al., 1997; Török et al., 2001). Such hypothetical 'cross-talk' between the membrane primary stress sensors and Hsps suggests a feedback loop mechanism in the regulation of *hsp* genes (Escribá et al., 2008; Vigh et al., 1998; Vigh et al., 2007a). sHsps have been shown to modulate major attributes of the membrane lipid phase such as the fluidity, permeability, or non-bilayer propensity via their specific membrane lipid interactions. It is emphasized that different Hsps have been found to associate to a variable extent with detergent-resistant microdomains ("rafts"), and the association of the Hsps with these microdomains can be modulated by stress (Broquet et al., 2003). Further important aspects of membrane-associated stress proteins, e.g. the membrane quality control by lipid–sHsp interactions, the membrane expression of Hsp70 and its release into the extracellular milieu, and the question, how Hsp70 promotes cell survival by inhibiting lysosomal membrane permeabilization, are not discussed in details in this thesis. However, exhaustive information can be found in a recent review (Horváth et al., 2008).

1.4.1. Hsp families

Hsp chaperone families include members whose expression is constitutive, developmentally/organ-specifically regulated, and/or responsive to heat or other abiotic stresses (Finka et al., 2011), indicating that molecular chaperones take part in many physiological and stress-related cellular processes.

The heat shock gene superfamily is organized by molecular size and functional class, including the Hsp100, Hsp90, Hsp70, Hsp60, Hsp40 (J-domain proteins), and small heat shock protein (sHsp) families.

Hsps were originally identified as stress-responsive proteins required to deal with thermal and other proteotoxic stresses. It became clear shortly thereafter that Hsp families also encode constitutively expressed members like Hsc70 (HSPA8) in the Hsp70 family. With the sequencing of the human genome and the computational annotation of its genes, it became apparent that most Hsp families contain additional members.

The expanding number of members in the various human Hsp families and the inconsistencies in their nomenclature have often led to confusion (Kampinga et al., 2009). The nomenclature of the human Hsp families with the alternative names and the mouse orthologs are listed in Tables 1.1–1.5 in order to help orientate the reader.

Table 1.1. HSP Nomenclature. HSP70 superfamily: HSPA (HSP70) and HSPH (HSP110) families (Kampinga et al., 2009).

	Gene name	Protein name	Old names	Human gene ID	Mouse ortholog ID
HSP A					
1	*HSPA1A*	HSPA1A	HSP70-1; HSP72; HSPA1	3303	193740
2	*HSPA1B*	HSPA1B	HSP70-2	3304	15511
3	*HSPA1L*	HSPA1L	hum70t; hum70t; Hsp-hom	3305	15482
4	*HSPA2*	HSPA2	Heat-shock 70kD protein-2	3306	15512
5	*HSPA5*	HSPA5	BIP; GRP78; MIF2	3309	14828
6	*HSPA6*	HSPA6	Heat shock 70kD protein 6 (HSP70B′)	3310	unknown
7	*HSPA7* [a]	HSPA7	Heat shock 70kD protein 7	3311	unknown
8	*HSPA8*	HSPA8	HSC70; HSC71; HSP71; HSP73	3312	15481
9	*HSPA9*	HSPA9	GRP75; HSPA9B; MOT; MOT2; PBP74; mot-2	3313	15526
10	*HSPA12A*	HSPA12A	FLJ13874; KIAA0417	259217	73442
11	*HSPA12B*	HSPA12B	RP23-32L15.1; 2700081N06Rik	116835	72630
12	*HSPA13* [b]	HSPA13	Stch	6782	110920
13	*HSPA14*	HSPA14	HSP70-4; HSP70L1; MGC131990	51182	50497
HSP H					
1	*HSPH1*	HSPH1	HSP105	10808	15505
2	*HSPH2* [b]	HSPH2	HSPA4; APG-2; HSP110	3308	15525
3	*HSPH3* [b]	HSPH3	HSPA4L; APG-1	22824	18415
4	*HSPH4* [b]	HSPH4	HYOU1/Grp170; ORP150; HSP12A	10525	12282

[a]Annotated as pseudogene, but possibly a true gene

[b]Under consultation with the HUGO Gene Nomenclature Committee (HGNC) and the scientific community

Table 1.2. HSP Nomenclature. The DNAJ (HSP40) family (Kampinga et al., 2009).

	Gene name	Protein name	Old names	Human gene ID	Mouse ortholog ID
DnaJA					
1	*DNAJA1*	DNAJA1	DJ-2; DjA1; HDJ2; HSDJ; HSJ2; HSPF4; hDJ-2	3301	15502
2	*DNAJA2*	DNAJA2	DNJ3; mDj3; Dnaj3; HIRIP4	10294	56445
3	*DNAJA3*	DNAJA3	Tid-1; Tid1l	9093	83945
4	*DNAJA4*	DNAJA4	Dj4; Hsj4	55466	58233
DnaJB					
5	*DNAJB1*	DNAJB1	HSPF1; HSP40	3337	81489
6	*DNAJB2*	DNAJB2	HSJ1; HSPF3; Dnajb10; MDJ8	3300	56812
7	*DNAJB3*	DNAJB3	Hsj3; Msj1; MSJ-1; Hcg3[a]	414061[a]	15504
8	*DNAJB4*	DNAJB4	Hsc40	11080	67035
9	*DNAJB5*	DNAJB5	Hsc40; HSP40-3	25822	56323
10	*DNAJB6*	DNAJB6	Mrj; mDj4	10049	23950
11	*DNAJB7*	DNAJB7	Dj5; mDj5	150353	57755
12	*DNAJB8*	DNAJB8	mDj6	165721	56691
13	*DNAJB9*	DNAJB9	Mdg1; mDj7; ERdj4	4189	27362
14	*DNAJB11*	DNAJB11	Dj9; ABBP-2; Erdj3	51726	67838
15	*DNAJB12*	DNAJB12	Dj10; mDj10	54788	56709
16	*DNAJB13*	DNAJB13	Tsarg6; Tsarg 3 protein	374407	69387
17	*DNAJB14*	DNAJB14	EGNR9427; FLJ14281	79982	70604
DnaJC					
19	*DNAJC1*	DNAJC1	MTJ1; ERdj1; ERj1p; Dnajl1	64215	13418
20	*DNAJC2* [b]	DNAJC2	Zrf1; Zrf2; MIDA1;M-phase phosphatase protein 11; MPP11; zuotin; ZUO1	27000	22791
21	*DNAJC3*	DNAJC3	p58; mp58; Prkri; Dnajc3; p58IPK; Dnajc3b	5611	100037258
22	*DNAJC4*	DNAJC4	HSPf2; Mcg18	3338	57431
23	*DNAJC5*	DNAJC5	Csp	80331	13002
24	*DNAJC5B*	DNAJC5B	CSP-beta	85479	66326
25	*DNAJC5G*	DNAJC5G	MGC107182; gamma-CSP	285126	231098
26	*DNAJC6*	DNAJC6	mKIAA0473; auxilin	9829	72685
27	*DNAJC7*	DNAJC7	Ttc2; mDj11; mTpr2	7266	56354
28	*DNAJC8*	DNAJC8	AL024084; AU019262; splicing protein (spf31)	22826	68598
29	*DNAJC9*	DNAJC9	AU020082; RcDNAJ9	23234	108671
30	*DNAJC10*	DNAJC10	JPDI; ERdj5; macrothioredoxin	54431	66861
31	*DNAJC11*	DNAJC11	FLJ10737; dJ126A5.1	55735	230935

	Gene name	Protein name	Old names	Human gene ID	Mouse ortholog ID
32	*DNAJC12*	DNAJC12	Jdp1; mJDP1	56521	30045
33	*DNAJC13*	DNAJC13	Rme8; RME-8; Gm1124	23317	235567
34	*DNAJC14*	DNAJC14	HDJ3; LIP6; DRIP78	85406	74330
35	*DNAJC15*	DNAJC15	Dnajd1; MCJ; Cell growth-inhibiting 22 protein	29103	66148
36	*DNAJC16*	DNAJC16	mKIAA0962	23341	214063
37	*DNAJC17*	DNAJC17	C87112	55192	69408
38	*DNAJC18*	DNAJC18	MGC29463	202052	76594
39	*DNAJC19*	DNAJC19	TIM14; TIMM14	131118	67713
40	*DNAJC20*[b]	DNAJC20	JAC1; HSC20; HscB	150274	100900
41	*DNAJC21*	DNAJC21	GS3; JJJ1; DNAJA5	134218	78244
42	*DNAJC22*	DNAJC22	FLJ13236; Wurst	79962	72778
43	*DNAJC23*[b]	DNAJC23	Sec63; AI649014	11231	140740
44	*DNAJC24*[b]	DNAJC24	DPH4; zinc finger, CSL-type containing 3	120526	99349
45	*DNAJC25*	DNAJC25	bA16L21.2.1; DnaJ-like protein; AAH48318; LOC552891; G-protein gamma 10	548645	72429
46	*DNAJC26*	DNAJC26	GAK; cyclin G associated kinase; auxilin-2	2580	231580
47	*DNAJC27*[b]	DNAJC27	RBJ; RabJ	51277	217378
48	*DNAJC28*	DNAJC28	Orf28 open reading frame 28; C21orf55, oculomedin	54943	246738
49	*DNAJC29*[b]		Sacsin; SACS	26278	50720
50	*DNAJC30*	DNAJC30	WBSCR18; Williams–Beuren syndrome chromosome region 18 homolog (human)	84277	66114

[a]Hcg3 is the closest human homologue of, and is syntenic with, MSJ-1 which encodes both N- and C-terminal domains in the same transcript but there is a reported frame shift between these domains

[b]Under consultation with HGNC and the scientific community

Table 1.3. HSP Nomenclature. The HSPB family (small heat shock proteins) (Kampinga et al., 2009).

	Gene name	Protein name	Old names	Human gene ID	Mouse ortholog ID
1	*HSPB1*	HSPB1	CMT2F; HMN2B; HSP27; HSP28; HSP25; HS.76067; DKFZp586P1322	3315	15507
2	*HSPB2*	HSPB2	MKBP; HSP27; Hs.78846; LOH11CR1K; MGC133245	3316	69253
3	*HSPB3*	HSPB3	HSPL27	8988	56534
4	*HSPB4* [a]	HSPB4	crystallin alpha A; CRYAA, CRYA1	1409	12954
5	*HSPB5* [a]	HSPB5	crystallin alpha B, CRYAB; CRYA2	1410	12955
6	*HSPB6*	HSPB6	HSP20; FLJ32389	126393	243912
7	*HSPB7*	HSPB7	cvHSP; FLJ32733; DKFZp779D0968	27129	29818
8	*HSPB8*	HSPB8	H11; HMN2; CMT2L; DHMN2; E2IG1; HMN2A; HSP22	26353	80888
9	*HSPB9*	HSPB9	FLJ27437	94086	75482
10	*HSPB10* [a]	HSPB10	ODF1; ODF; RT7; ODF2; ODFP; SODF; ODF27; ODFPG; ODFPGA; ODFPGB; MGC129928; MGC129929	4956	18285
11	*HSPB11*	HSPB11	HSP16.2; C1orf41; PP25	51668	72938

[a]Under consultation with HGNC and the scientific community

Table 1.4 HSP Nomenclature. The HSP90/HSPC family (Kampinga et al., 2009).

	Gene name	Protein name	Old names	Human gene ID	Mouse ortholog ID
1	*HSPC1* [a]	HSPC1	HSP90AA1; HSPN; LAP2; HSP86; HSPC1; HSPCA; HSP89; HSP90; HSP90A; HSP90N; HSPCAL1; HSPCAL4; FLJ31884	3320	15519
2	*HSPC2* [a]	HSPC2	HSP90AA2; HSPCA; HSPCAL3; HSP90ALPHA;	3324	unknown
3	*HSPC3* [a]	HSPC3	HSP90AB1; HSPC2; HSPCB; D6S182; HSP90B; FLJ26984; HSP90-BETA	3326	15516
4	*HSPC4* [a]	HSPC4	HSP90B1;ECGP; GP96; TRA1; GRP94; endoplasmin	7184	22027
5	*HSPC5* [a]	HSPC5	TRAP1; HSP75; HSP90L	10131	68015

[a]Under consultation with HGNC and the scientific community

Table 1.5. HSP Nomenclature. Chaperonins and related genes (Kampinga et al., 2009).

	Gene name	Protein name	Old names	Human gene ID	Mouse ortholog ID
HSPD					
1	*HSPD1*	HSPD1	HSP60; GroEL	3329	15510
HSPE					
1	*HSPE1*	HSPE1	HSP10; chaperonin 10; GroES	3336	15528
CCT					
1	*CCT1* [a]	CCT1	TCP1; CCTA; CCT-alpha; TCP-1-alpha	6950	21454
2	*CCT2*	CCT2	CCTB; CCT-beta; TCP-1-beta	10576	12461
3	*CCT3*	CCT3	CCTG; CCT-gamma; TCP-1-gamma; TRiC-P5	7203	12462
4	*CCT4*	CCT4	CCTD; CCT-delta,;TCP-1-delta; SRB	10575	12464
5	*CCT5*	CCT5	CCTE; CCT-epsilon; TCP-1-epsilon	22948	12465
6	*CCT6A*	CCT6A	CCT6; CCTZ; CCT-zeta; CCT-zeta1; TCP-1-zeta; HTR3; TCP20	908	12466
7	*CCT6B*	CCT6B	CCTZ2; CCT-zeta2; TSA303	10693	12467
8	*CCT7*	CCT7	CCTH; CCT-eta; TCP-1-eta	10574	12468
9	*CCT8*	CCT8	CCTQ; CCT-theta; TCP-1-theta; KIAA002	10694	12469
Other chaperonin-like					
1	*MKKS*	MKKS	McKusick–Kaufman syndrome; MKS; Bardet–Biedl syndrome 6; BBS6	8195	59030
2	*BBS10*	BBS10	Bardet–Biedl syndrome 10	79738	71769
3	*BBS12*	BBS12	Bardet–Biedl syndrome 12	166379	241950

[a]Under consultation with HGNC and the scientific community

Small Hsps (sHsps or HSPB in mammals) are ATP-independent low-molecular mass chaperones found in every kingdom. sHsps are characterized by the presence of a conserved crystallin domain flanked by a variable N-terminus and C-terminus. The N- and C-termini, together with part of the crystallin domain, are involved in substrate binding (Vos et al., 2008). One of the most notable features is their large oligomeric structure with conserved structural organization. It is well documented that sHsps can capture unfolding, aggregation-prone proteins to form stable complexes and prevent their irreversible aggregation. The release of substrate proteins from the transient reservoirs, i.e. complexes and aggregates with small heat shock proteins, and their refolding require cooperation with ATP-dependent chaperone systems (Nakamoto and Vigh, 2007).

Hsp90 is an evolutionarily conserved molecular chaperone involved in the folding, stabilization, activation, and assembly of its 'client' proteins (Csermely et al., 1998; Pearl et al., 2008; Pratt et al., 2008), and is an essential component of the protective heat shock response (Heads et al., 1995; Taipale et al., 2010). In non-stressed cells, Hsp90 is highly abundant and associates with a wide array of client proteins that depend on its chaperoning function to acquire their active conformations. Hsp90's ATPase activity, which is essential for its chaperone function, is regulated and coupled with the conformational changes of Hsp90 dimer (Hahn, 2009). The protein folding by Hsp90 is involved in signal transduction, protein trafficking, receptor maturation and innate and adaptive immunity. In doing so, Hsp90 interacts with more than 20 co-chaperones, which guide its recognition of client proteins and modulate its biochemical activities. These activities are closely coupled to environmental perturbations (Taipale et al., 2010).

Recently, it was found that ***Hsp110*** members act as nucleotide exchange factors for both mammalian and yeast Hsp70 proteins (Dragovic et al., 2006; Raviol et al., 2006). Hsp110 proteins are known to have the capacity to hold unfolded proteins in a folded competent state. As both heat-inducible substrate binders and heat-inducible nucleotide exchange factors, Hsp110 proteins may be particularly relevant under (heat) stress conditions during which it may hold substrates (like sHSPs) to be passed on to Hsp70 for further handling after the stress (Vos et al., 2008).

Chaperonins represented by ***Hsp60*** homologues are found in bacteria (***GroEL***), mitochondria, chloroplasts and in the cytosol of eukaryotes (***TIRC***). A functional Hsp60 complex comprises 14 identical subunits arranged in two stacked heptameric rings, requiring two heptameric co-chaperones, ***Hsp10/GroES*** (Azem et al., 1995). Artificially

denatured proteins become prevented from aggregating upon binding to purified GroEL and, moreover, become subsequently refolded to the native state in a strict GroES- and ATP-dependent manner (Finka et al., 2011; Goloubinoff et al., 1989).

Hsp70s are ubiquitous molecular chaperones that function in a myriad of biological processes, modulating polypeptide folding, degradation and translocation across membranes, as well as protein–protein interactions (Kampinga and Craig, 2010). However, Hsp70s have never been found to function alone. Much of their functional diversity is driven by a diverse class of cofactors, J-proteins (also called Hsp40s). Often, multiple J-proteins function with a single Hsp70. Some target Hsp70 activity to clients at precise locations in cells; others bind client proteins, thereby delivering specific clients to Hsp70, directly determining their fate.

All cellular functions of the ***Hsp70/Hsp40 core machine*** (Figure 1.3) use the same mechanism of ATP-driven polypeptide binding and release; binding and hydrolysis of ATP regulates their interactions with unfolded polypeptide substrates and are essential both *in vitro* and *in vivo* for the chaperone activity (Mayer and Bukau, 2005; Young, 2010).

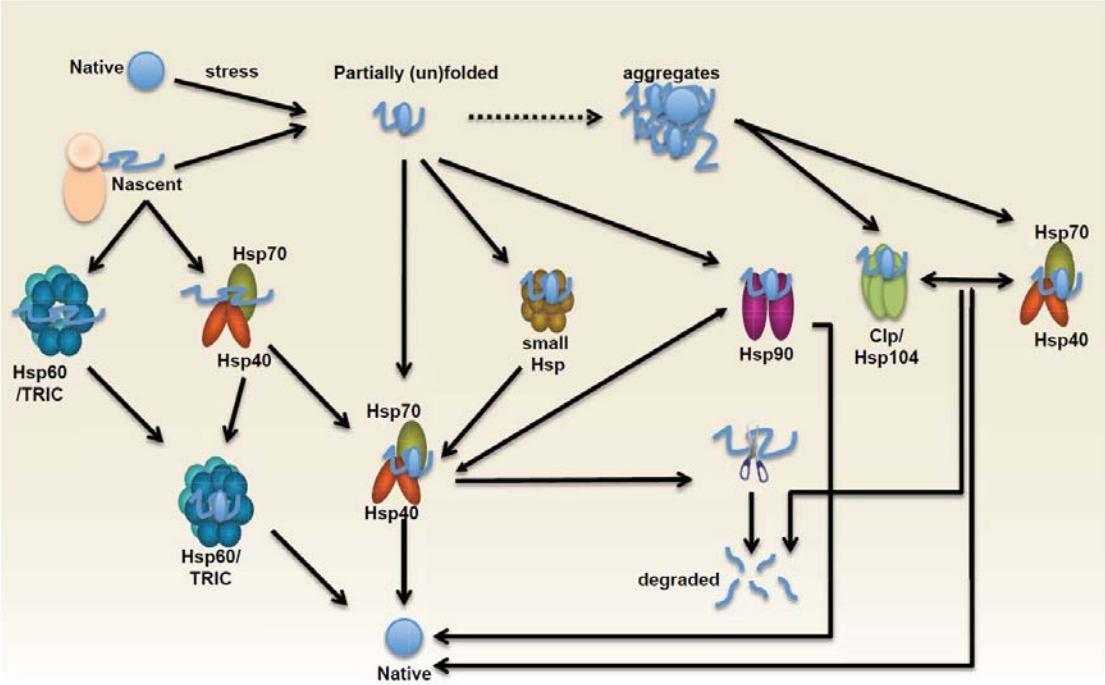

Figure 1.3. Chaperone networks; the arrows indicate client transfer to and from the various chaperone complexes (see Kampinga and Craig, 2010).

The core machines can form partnerships with at least three other Hsp families. These include partnerships with the ATP-dependent chaperonins (Hsp60/TRIC family),

the Hsp90 family and the ATP-independent chaperones of the small Hsp families. Each of these families is composed of several members and the size of these families (especially the small Hsps) has increased substantially during evolution. In various processes, the Hsp70 core machine can act simultaneously or sequentially with these other Hsp families in protein (re)folding, -assembly, -degradation, or even -disaggregation (Figure 1.3).

A summary of the properties of different human HSPs is given in Table 1.6.

Table 1.6. Properties of the human HSP families (Vos et al., 2008).

	molecular size (kDa)	**tissue distribution**	**subcellular localization**	**clients/ substrates**	**associated disease**
sHSP family					
HSPB1	22.8	ubiquitous	cytosol	cytoskeletal components, ubiquitin, cytochrome *c*	Charcot-Marie-Tooth disease, distal hereditary motor neuropathy
HSPB2	20.2	heart and skeletal muscle	cytosolic granules/mitochondria	myotonic dystrophy protein kinase	–
HSPB3	17	muscle	unknown	–	
HSPB4	19.9	eye lens	cytoplasm	–	cataract
HSPB5	20.2	ubiquitous	cytosol/nucleus	cytoskeletal components	cataract, desmin-related myopathy
HSPB6	17.1	heart, muscle, brain	cytosol	14-3-3 γ, Bax	–
HSPB7	18.6	heart and skeletal muscle	cytosol/nucleus	α-filamin	upregulated in muscular dystrophy
HSPB8	21.6	muscle, brain, keratinocytes , placenta	cytosol/plasma membrane	BAG-3	Charcot-Marie-Tooth disease, distal hereditary motor neuropathy
HSPB9	17.5	testis	cytosol/nucleus	DynLT1	upregulated in certain tumors
HSPB10	28.4	testis	sperm cell tails	–	–
HSPB11	16.3	unknown	cytosol/nucleus	Hsp90	upregulated in certain tumors
HSP90 family					
HSPH1	96.9	ubiquitous	cytosol/nucleus	–	–
HSPH2	94.3	ubiquitous	cytosol/nucleus	–	–
HSPH3	94.5	testis, brain, kidney, liver, lung, spleen	cytosol/nucleus	–	–

HSPH4	111.3	ubiquitous	endoplasmic reticulum (ER)	–	–
HSP70 family					
HSPA1A	70	ubiquitous	cytosol	promiscuous	upregulated in certain tumors
HSPA1B	70	ubiquitous	cytosol	promiscuous	upregulated in certain tumors
HSPA1L	70.4	testis	cytosol	–	rs2075800 G allele associates with sarcoidosis
HSPA2	70	testis/ubiquitous	cytosol/nucleus	–	upregulated in certain tumors
HSPA5	71	ubiquitous	ER	ATF6	–
HSPA6	71	brain, liver, ovary, saliva	cytosol/nucleus	–	in the proximity of a susceptibility locus for schizophrenia
HSPA7	ND	unknown	unknown	–	in the proximity of a susceptibility locus for schizophrenia
HSPA8	70.9	ubiquitous	cytosol/nucleus	many growth factors	upregulated in certain tumors
HSPA9	73.7	B cell, brain, liver, ovary, platelet, saliva	mitochondria	mitochondrial proteins, p53	–
HSPA12A	141	endothelia, brain, heart, kidney, muscle, testis	unknown	–	associates with atherosclerosis
HSPA12B	75.7	endothelia, ubiquitous	unknown	–	associates with atherosclerosis
HSPA13	51.9	unknown	microsomes	–	–
HSPA14	54.8	unknown	unknown	–	–
HSP40 family					
DNAJA1	44.9	ubiquitous	cytosol	promiscuous	–
DNAJA2	45.7	brain, heart, kidney, liver	cytosol	promiscuous	–
DNAJA3	52.5	fetus, mammary gland, B cell	mitochondria	–	protects against dilated cardiomyopathy
DNAJA4	44.7	brain	membranes	promiscuous	–
DNAJB1	38.2	ubiquitous	cytosol	promiscuous	protects against various neuronal misfolding diseases
DNAJB2	35.6/30.6	heart, muscle, brain	cytosol/ER	–	–
DNAJB3	26.7	testis	unknown	–	–
DNAJB4	37.8	ubiquitous	unknown	G protein β subunit	

DNAJB5	39.1/26.9	brain, heart, liver, pancreas, skeletal muscle, spleen	unknown	–	–
DNAJB6	36.1	ubiquitous	cytosol/nucleus	keratin-18	–
DNAJB7	35.4	ubiquitous	unknown	–	–
DNAJB8	25.7	testis	unknown	–	–
DNAJB9	25.5	ubiquitous	ER	–	–
DNAJB10	30.6/28.6	unknown	unknown	–	–
DNAJB11	40.5	ubiquitous	ER	APOBEC1	
DNAJB12	41.9	blood plasma	unknown	–	–
DNAJB13	36.1	fetus, spermatozoa, testis	unknown	–	–
DNAJB14	42.5/33.5	unknown	unknown	–	–

1.5. TRANSCRIPTIONAL REGULATION OF HSP RESPONSE

When summarising the regulation of Hsp response it is usual to follow a bottom-up style. The Hsps consist the main well-characterized group of the effector molecules, as summarised above. As we approach the earlier events, our knowledge becomes weaker – the interconnecting steps are often missing.

In eukaryotes the Hsp response is regulated mainly at the level of transcription by heat shock factors (HSFs). HSF1 is a master regulator of the heat shock genes in mammalian cells (Björk and Sistonen, 2010) and by far the best-characterized member of the HSF family. *Hsf1*-knockout mouse and cell models have revealed that HSF1 is a prerequisite for the transactivation of *hsp* genes, maintenance of cellular integrity during stress and development of thermotolerance (Akerfelt et al., 2010).

HSF1 is constitutively expressed in most tissues and cell types. Its activation cycle is depicted in Figure 1.4. In its resting state, the DNA-binding activity and transactivating capacity of HSF1 are subject to negative regulation, i.e., the majority of HSF1 exists diffusely distributed in the nucleus or cytosol in an inert monomeric form through intra- and intermolecular interactions, including interactions with Hsps (Figure 1.4). In response to stress, HSF1 is rapidly converted into a transcriptionally active form involving nuclear accumulation, a monomer-to-trimer transition, extensive post-translational modifications (phosphorylation, sumoylation, acetylation) and DNA-binding through a regulatory upstream promoter element, called the heat shock element (HSE) (Anckar and Sistonen, 2011). Sumoylation (small ubiquitin-like modification)

occurs rapidly without affecting the DNA-binding capacity, but it is diminished upon more severe profound and sustained stress. The stress-inducible hyperphosphorylation of the key serines within the regulatory domain could function as a trigger, relieving the inhibition of the transactivation domain to enable activation of the target genes.

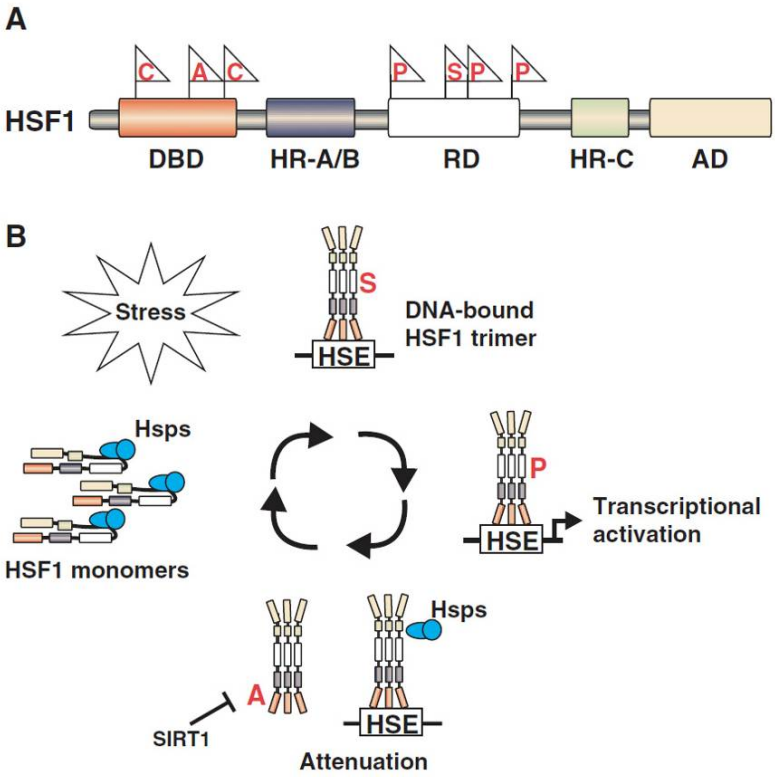

Figure 1.4. Functional domains and acetylation cycle of HSF1 (see Björk and Sistonen, 2010). (A) Schematic presentation of HSF1 with its functional domains. Some of the sites subjected to stress-induced posttranslational modifications are marked with flags. (B) The activation cycle of HSF1. A, acetylation; AD, transactivation domain; C, cysteine residues subjected to disulfide bond formation; DBD, DNA-binding domain; HR-A/B and HR-C, hydrophobic heptad repeats; P, phosphorylation; RD, regulatory domain; S, sumoylation.

Despite numerous studies conducted in different laboratories, the impact of multisite phosphorylation on HSF1 functions has remained elusive (Björk and Sistonen, 2010). Only a small number of the phosphorylation sites of human HSF1 identified to date (Ser^{121}, Ser^{230}, Ser^{292}, Ser^{303}, Ser^{307}, Ser^{314}, Ser^{319}, Ser^{320}, Ser^{326}, Ser^{344}, Ser^{363}, Ser^{419} and Ser^{444}) appears to play a role in activation of the factor during a stress (Ser^{230}, Ser^{326}) or inactivation subsequent to a stress (Ser^{303}, Ser^{307}, Ser^{363}) (Voellmy and Boellmann, 2007). Moreover, certain sites are constitutively phosphorylated whereas others are stress-inducible (Holmberg et al., 2001). During the attenuation phase the

transactivation capacity of HSF1 is repressed through a negative-feedback loop via binding to Hsps. The DNA-binding activity of HSF1 is inhibited by acetylation of several lysines within the DNA-binding domain (Akerfelt et al., 2010). The attenuation phase is regulated by the deacetylase sirtuin 1 (SIRT1).

The induction of HSF by diverse stressors and the wide variety of posttranslational modifications suggests that HSF may be a convergence point for several signalling pathways thus functioning as a stress integrator. Indeed, the stress-activated signal transduction pathways, (see below) leave their signatures on the HSF protein. A number of protein kinases are activated by heat shock and can profoundly influence the Hsp response in positive or negative ways (Figure 1.5) (Calderwood et al., 2010).

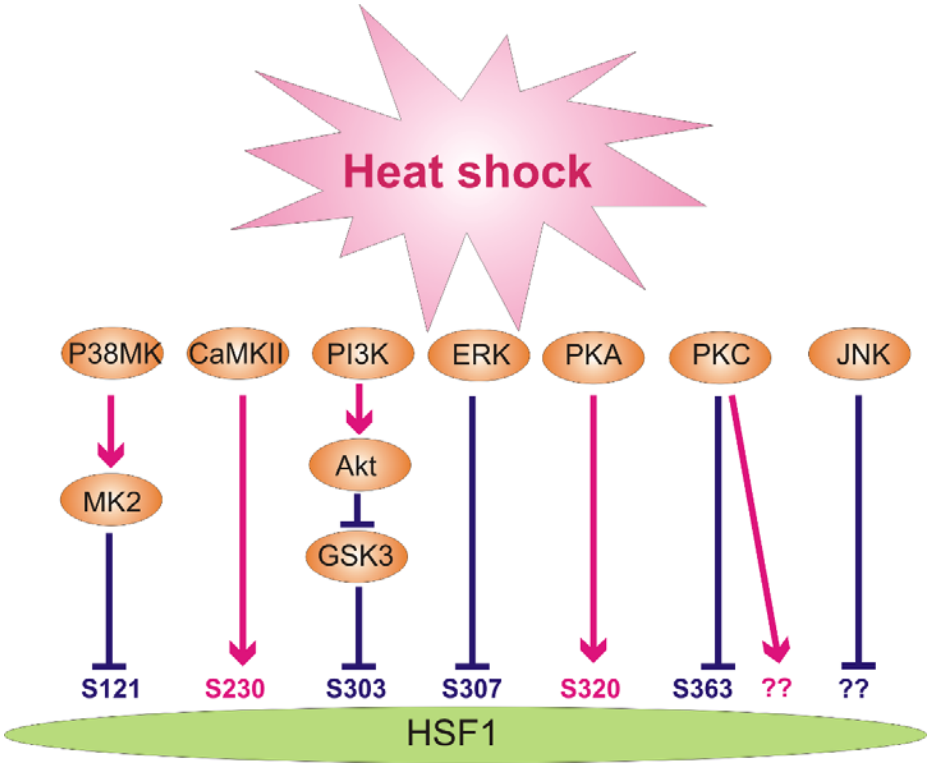

Figure 1.5. Signalling kinase cascades activated by HS and their downstream (serine) targets (based on Calderwood et al., 2010) on HSF1. p38MK, p38 mitogen-activated protein kinase; CaMKII, calcium/calmodulin-dependent protein kinase II; PI3K, phosphoinositide 3-kinase; ERK, extracellular signal-regulated kinase; PKA, protein kinase A; PKC, protein kinase C; JNK, c-jun N-terminal kinase; MK2, MAPK-activated protein kinase 2; Akt, protein kinase B; GSK3, glycogen synthase kinase-3; HSF1, heat shock factor 1.

These HS-activated signal transducing kinases comprise the three mitogen-activated protein kinase (MAPK) pathways, namely the extracellular signal-regulated

kinase (ERK), c-jun N-terminal kinase (JNK) and p38. Protein kinase B (PKB/Akt) is another important kinase rapidly stimulated by HS. The early induction of the pathways leading to MAPK and PKB induction can either serve to trigger adaptive responses or be used to signal cell death (Nadeau and Landry, 2007).

It was demonstrated in NIH 3T3 fibroblasts that early upstream signalling events in response to HS may involve activation of phosphoinositide 3-kinase (PI3K), tyrosine kinases and growth factor receptors such as epidermal growth factor receptor (EGFR). Activation of important downstream pathways occur by divergent signalling mechanisms similar to growth factor stimulation (Lin et al., 1997). Interestingly, the activation of EGFR by HS is ligand-independent. This mode of induction resembles the activation of the ERK pathway by UV light, hyperosmolarity and hydrogen peroxide (H_2O_2), which all hijack growth factor receptors from their normal physiological function to initiate stress signals (Nadeau and Landry, 2007) and refs therein). Calcium/calmodulin-dependent protein kinase II (CaMKII) signalling is involved in the positive regulation of HSF1-mediated transactivation (Holmberg et al., 2001). It has been reported that activation of protein kinase C (PKC) induced Hsps (Kiang and Tsokos, 1998). Furthermore, intracellular protein kinase A (PKA) levels and phosphorylation of HSF1 at Ser^{320} were both required for HSF1 to be localized to the nucleus, bind to response elements in the promoter of an HSF1 target gene (*hsp70.1*) and activate *hsp70.1* after stress (Murshid et al., 2010). Taken together, several kinases are activated in response to HS and all of them are participate in direct regulation of HSF1 or in other apoptotic or antiapoptotic pathways.

1.6. STRESS SENSING

Heat (and other stresses) is rapidly sensed by physico-chemical perturbations of various biomolecules in the plasma membrane (PM), cytosol and subcellular organelles of cells, which provoke particular signals for the Hsp response. However, no consensus has been reached as to the actual stress sensors. The possible sensors of (heat) stress are summarised in Figure 1.6 (Vigh et al., 2007a).

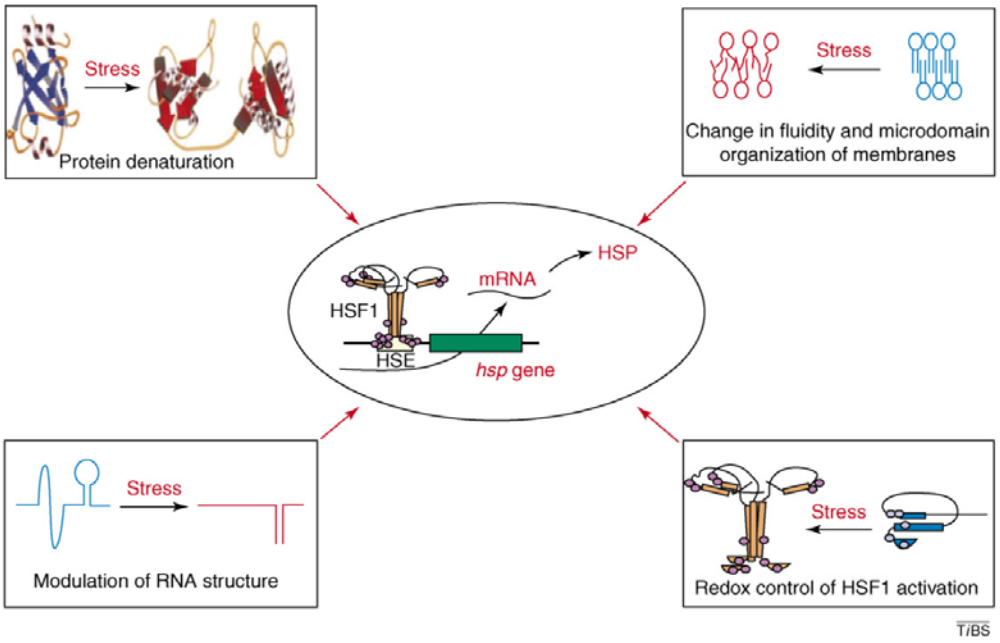

Figure 1.6. Sensors of the HSR in mammalian cells. Four examples are indicated: protein denaturation, membrane fluidity or microdomain organization, RNA structure and redox control (see Vigh et al., 2007a).

Although HSF1 can be activated by diverse stimuli, according to the ***denatured protein sensor*** hypothesis (Figure 1.7), a common denominator might be misfolded or aggregated proteins disturbing protein homeostasis (Morimoto, 1998). The suggestion that denaturation of intracellular proteins may be produced by metabolic stresses to induce the activation of the *hsp* genes was examined by co-injection of purified proteins and *hsp* genes into frog oocytes. Activation of *hsp* genes was observed if the proteins were denatured prior to injection but not if they were introduced in their native form (Ananthan et al., 1986).

As a defence mechanism, HSFs induce the synthesis of Hsps that act as molecular chaperones through binding to the hydrophobic surfaces of unfolded proteins, thereby facilitating refolding of peptides and preventing protein aggregation (Björk and Sistonen, 2010; Morimoto, 1998). The discovery of an interaction between HSF1 and Hsps, such as Hsp70/Hsp40 and Hsp90, led to the hypothesis of a negative-feedback loop, where excess Hsps under non-stress conditions keep HSF1 inactive (Morimoto, 1998). Upon exposure to stress, the Hsps are sequestered to denatured proteins and HSF1 is released from the chaperone complexes to induce transcription of the genes encoding additional Hsps. Once the pools of Hsps are saturated, they can again bind HSF1 and inhibit its function (Figure 1.7).

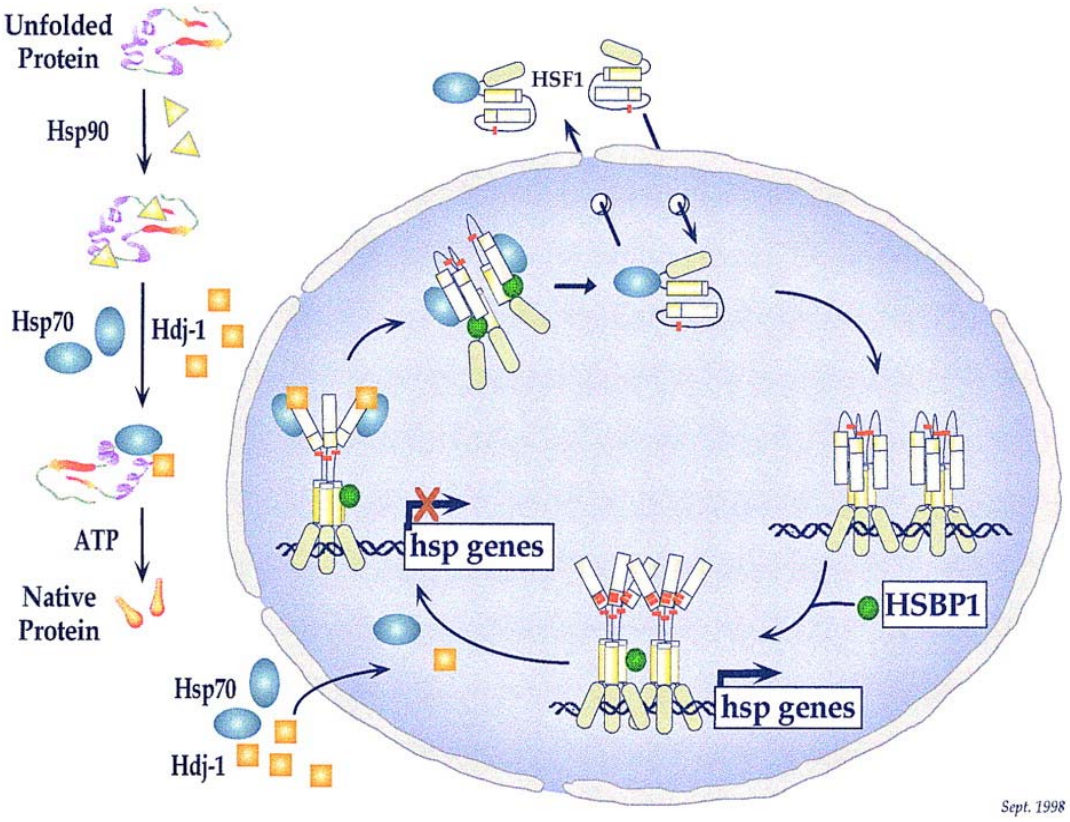

Figure 1.7. Regulation of the HSR sensed by unfolded proteins (see Morimoto, 1998).

The concept of an ***RNA thermometer*** is not new – a few bacterial examples have been described previously (Johansson et al., 2002; Morita et al., 1999). Recently it was proposed that the translation elongation factor eEF1A and a novel non-coding RNA, HSR1, act in tandem to activate HSF during HS in mammalian cells (Shamovsky et al., 2006). Curiously, eEF1A is one of the most conserved and most abundant proteins in eukaryotic cell, and HSR1 appears to be highly conserved as well. eEF1A has been implicated in a variety of cellular processes in addition to its canonical role in mRNA translation during protein synthesis. Notably, it is the key component regulating the actin cytoskeleton architecture in the cell. The authors assigned a new function to eEF1A as a co-activator of HSF1 and suggest that this ubiquitous protein has a multifaceted role in the response to HS. HS leads to two major physiological perturbations in the cell − translational shutdown and cytoskeleton collapse. These events might cause the release of eEF1A, which then becomes available for interaction with HSR1 and HSF1 to initiate the Hsp response (Figure 1.8) (Shamovsky and Nudler, 2008; Shamovsky et al., 2006).

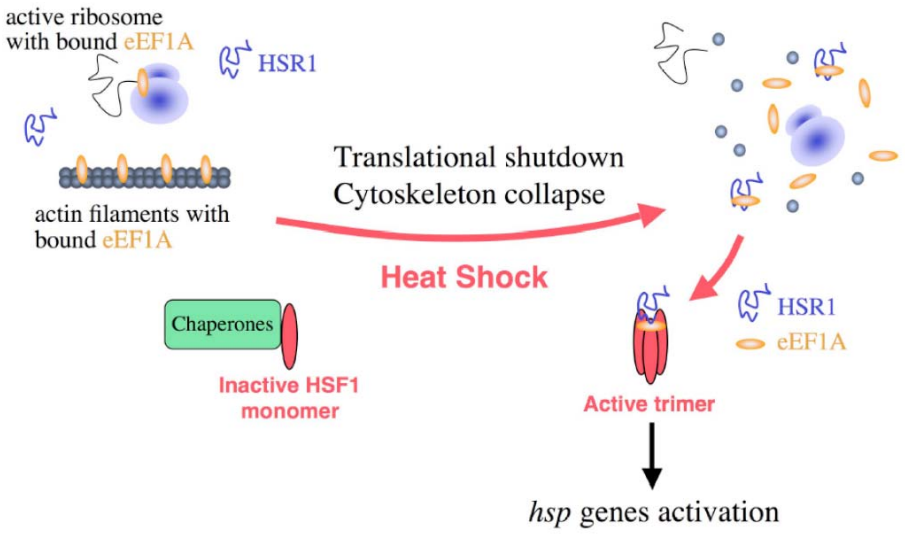

Figure 1.8. An integrated model of HSR activation in mammalian cells implying RNA as stress sensor (see Shamovsky et al., 2006).

Mammalian HSF1 was shown to directly sense heat and oxidative stress *in vitro* to assemble into a homotrimer in a reversible and ***redox-regulated*** manner that requires cysteine residues at two positions within or adjacent to the DNA-binding domain. Cysteine residues (C35 and C105) required for HSF1 redox regulation are essential for stress activation of HSF1 multimerization, DNA-binding, nuclear accumulation, *hsp* target gene activation, and the protection of mammalian cells from stress-induced apoptosis. Furthermore, mutation of the cysteine residues rendered HSF1 refractory to stress (Ahn and Thiele, 2003).

Several essential cellular activities depend on proper membrane function. Thus, membrane lipid composition and membrane lipid dynamics have received significant attention for over a decade (Vigh et al., 1998). It is well known that, following a temperature change, cells compensate for stress-induced cellular disturbances through physiological and biochemical mechanisms of homeoviscous adaptation adjusting its membrane lipid composition to maintain fluidity. Here and throughout the thesis I use the term fluidity, nevertheless, the fluidity of cell membranes is an imprecise concept which is generally considered in terms of the relative motion of constituents of the membrane. The property is attributed solely to the lipid constituents but membrane fluidity as assessed by a variety of physical techniques is known to be markedly affected by membrane proteins (Quinn, 1981). The structural order of the membrane lipids is related to the degree of molecular packing and this suggest its inverse relationship to the lateral diffusion of membrane lipids and proteins (Van Blitterswijk et al., 1981). Microviscosity should be regarded as an operational term which was introduced for the

application of classical hydrodynamic expression of microscopic fluid regions (Shinitzky and Barenholz, 1978). Microviscosity is the measure of frictional resistance to rotational and translational motions of molecules and often considered as the reciprocal to fluidity (Demchenko et al., 2009). However, others (Heyn, 1979; Van Blitterswijk et al., 1981) argued against this notion, mentioning that "lipid fluidity" may be defined as the reciprocal of the lipid structural order parameter rather than of the microviscosity (Van Blitterswijk et al., 1981).

The natural modulators of lipid fluidity can be divided into chemical modulators and physical effectors. The main modulators are the cholesterol (Chol) level, the degree of unsaturation of the phospholipid (PL) acyl chains, the level of sphingomyelin (SM), and the level of membrane proteins. The stationary levels of these modulators in a biological membrane can change in response to a regulatory signal or stress. The physical effectors of lipid fluidity are temperature, pressure, pH, membrane potential and Ca^{2+}, and their effect is practically instantaneous (Shinitzky, 1984).

To my knowledge, in 1992 Dietz and Somero (by studying two extremely eurythermal goby fishes) provided the first example of seasonal changes in the temperature at which enhanced synthesis of a specific type of Hsps was induced (Dietz and Somero, 1992). Therefore, it turned into a useful tool to alter the fluidity of cell membranes by temperature acclimation or by addition of a fluidizer (e.g. alcohols) and test the membrane physical state-dependent variation in HSR threshold temperatures in different organisms (in details see later). The early findings using the above-mentioned approaches led to the formulation of a hypothesis in 1998 by Vigh, Maresca and Harwood that membranes can sense environmental changes and, as a consequence of changes in their phase state and microdomain organisation, transmit HS signals that activate *hsp* transcription (Vigh et al., 1998).

To better understand the details of the ***membrane sensor hypothesis*** I feel it important to give first an overview on membrane/membrane lipid structure and organizations.

1.6.1. Membranes and membrane lipids

Membranes provide the structural framework that divides cells from their environment and that, in eukaryotic cells, permits compartmentation (Vigh et al., 1998). This compartmentalization enables segregation of specific chemical reactions for the

purposes of increased biochemical efficiency and restricted dissemination of reaction products.

The unique property of lipids, particularly in an aqueous environment, is self-aggregation, i.e. biological lipids generally form aggregates of various sorts, mostly extended sheet-like structures, known as bilayers. The bilayer, the structural basis of the cell membrane, is formed by 'amphipathic' lipid molecules, i.e. molecules that possess both a hydrophilic portion in contact with the water, and a lipophilic portion which remains isolated from the aqueous medium. Biological membranes are thus water-immiscible structures consisting of a microenvironment composed of lipids and proteins which allow a considerable degree of freedom to diffuse, both rotationally and laterally, in the plane of the membrane (van Meer et al., 2008).

The Singer–Nicolson fluid mosaic model, which is near its 40th anniversary, with some restrictions is still valid. The fluid mosaic structure is formally analogous to a two-dimensional oriented solution of integral proteins (or lipoproteins) in the viscous phospholipid bilayer solvent (Singer and Nicolson, 1972) and predicts lateral and rotational freedom and random distribution of molecular components in the membrane. Now it is known, however, that this freedom of protein (and lipid) mobility is far from being unrestricted (Vereb et al., 2003), i.e., most membrane proteins do not enjoy the continuous unrestricted lateral diffusion characteristic of a random, two-dimensional fluid. Instead, proteins diffuse in a more complicated way that indicates considerable lateral heterogeneity in membrane structure, at least on a nanometer scale (Jacobson et al., 1995).

Progress in biophysics, chemistry and genetics has attracted renewed attention to the biological roles of the great variety of membrane lipids. In addition to the barrier function, lipids provide membranes with the potential for budding, tubulation, fission and fusion, characteristics that are essential for cell division, biological reproduction and intracellular membrane trafficking. The membrane and its constituent lipids are also indispensable participants in many events of signal transduction and enzyme activity.

1.6.1.1. Lipid structure and diversity

Lipids are small molecules of enormous chemical diversity, and currently there is an increasing awareness across many disciplines of the critical importance of lipids in all aspects of life (Wenk, 2010). Unlike other major biomolecules, they are not genetically encoded. Instead, they are the result of anabolic and catabolic reactions that are under complex dietary and physiological control. It is thus difficult to define, name, and

categorize lipids in a coherent and comprehensive fashion (Christie and Han, 2010; Fahy et al., 2005; Fahy et al., 2009). The graphical overview in Figure 1.9 focuses, according to the subject of this thesis, on the main mammalian lipids including the most important structural, mediator and storage molecules, and is based on the three main backbone structures (squalene, glycerol and sphingoid base).

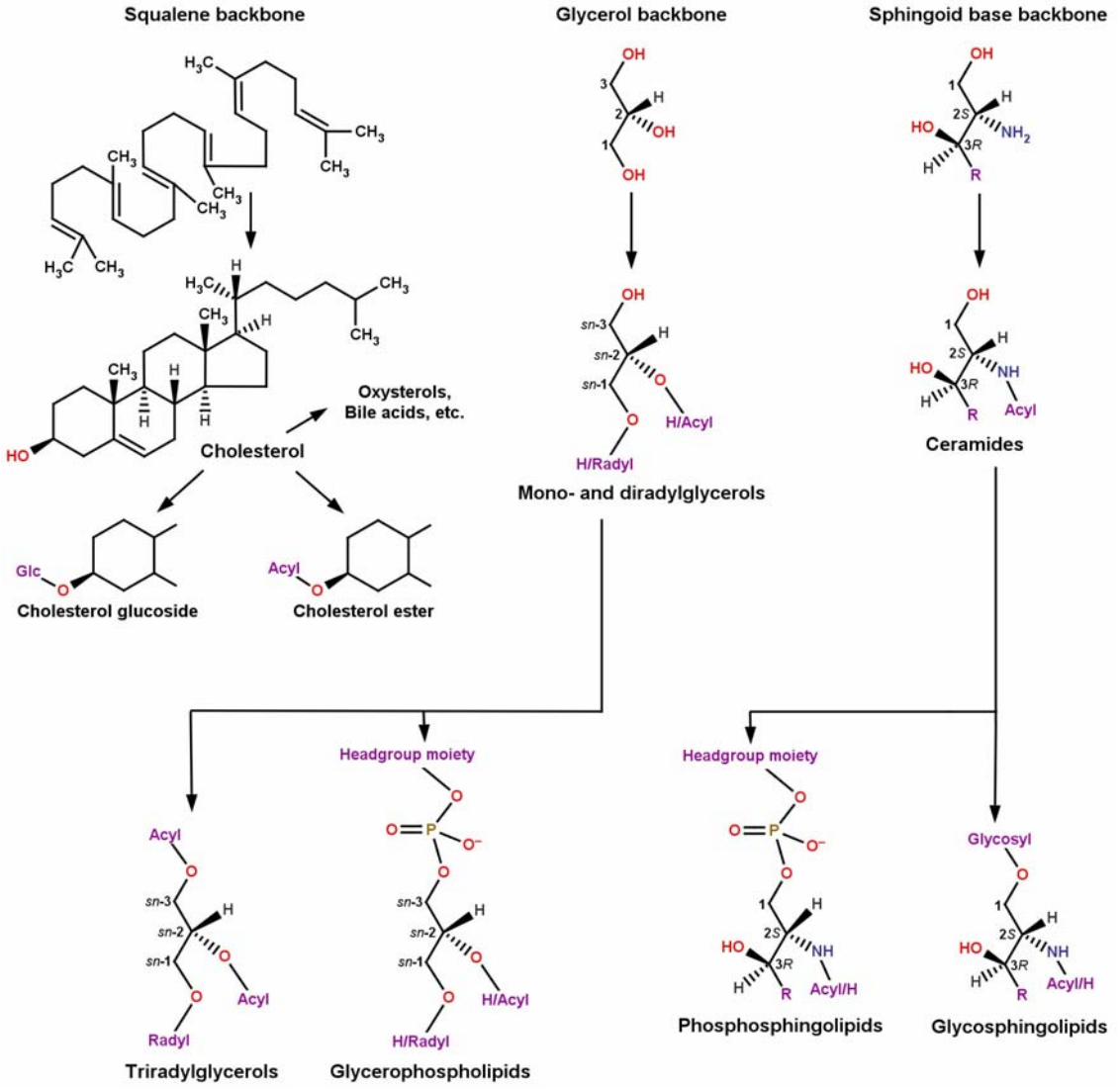

Figure 1.9. Main classes of mammalian lipids.

Several reaction steps on the squalene backbone lead to one of the most unique mammalian lipids, cholesterol (Chol). Chol itself has a dominant part in modulating membrane fluidity, it is a major component of specific membrane subdomains (rafts), but also its derivatives play important roles in signalling such as the glucose-derivative cholesterol glucoside, or in energy storing such as the fatty acid (FA)-derivative subclass cholesteryl ester (CE).

The other two backbones, the trifunctional alcohol glycerol and the long-chain amino diol sphingoid base bear similarities (both real and apparent) in many respects. The OH groups of glycerol, attached to carbons C-1 and C-2, can be stepwise substituted to get first the intermediate signalling lipids mono- (MG) and diradylglycerols (DG) (see below for explanation of "radyl"). DGs play a central role in glycerolipid (GL) metabolism (see later), and this is exactly the case for ceramide (Cer) which functions as a hub for sphingolipid (SL) metabolism and can be obtained from the corresponding sphingoid base by addition of a FA to the amino group attached to the C-2 carbon.

Upon substitution, the C-2 carbon in glycerol becomes chiral (i.e., possesses 4 different subsituents), and in complex mixtures the designation of the resulting enantiomers become difficult. To avoid such problems the "stereospecific numbering" (*sn*) system was recommended by a IUPAC-IUB commission, in which the prefix *sn* is placed before the stem name of the GL if its stereochemistry is known. In the SL category stereochemistry should be specified only in cases when it differs from the 2*S*,3*R* configuration of the natural core base (see later).

By further substitution of the OH group on the *sn*-3 carbon in DG, and on the C-1 carbon in Cers, the main structural and storage lipids can be formed. Triradylglycerols (TG), major constituents of the cell's storage compartments (i.e., lipid droplets), can be formed with an additional radyl group from DGs.

In case of GLs, the addition of different phosphate-containing headgroups to the *sn*-3 OH results in the formation of the most widely studied glycerophospholipids (GPLs) in mammals. Figure 1.10 represents the sources of structural diversity of this lipid class originating from differences in headgroup moieties, different O-radyl linkage types and variability of the hydrocarbon chain R in the hydrophobic tail.

The simplest GPL is phosphatidic acid (PA), where the headgroup is the phosphate itself. The other derivatives can be derived by esterification of the phosphate of PA with an alcohol-type agent, such as ethanolamine in phosphatidylethanolamine (PE), serine in phosphatidylserine (PS), glycerol in phosphatidylglycerol (PG), choline in phosphatidylcholine (PC), and inositol in phosphatidylinositol (PI). The size (relative to the hydrophobic tail) and polarity/charge of these hydrophilic headgroup moieties largely determines the shape and electronic properties of the resulting lipids, and the differences that arise lead to diverse discrete additional functions beyond the common structural role. For example, PC with the zwitterionic phosphocholine headgroup has a cylindrical shape and is, therefore, a typical bilayer-forming lipid, while PE, according

to its smaller headgroup, has a conical shape, which creates a stress in the bilayer and this non-bilayer-forming property is believed important for membrane curvature. The influence of lipid shapes in determining this arrangement in membranes has been described well by Israelachvili (1978).

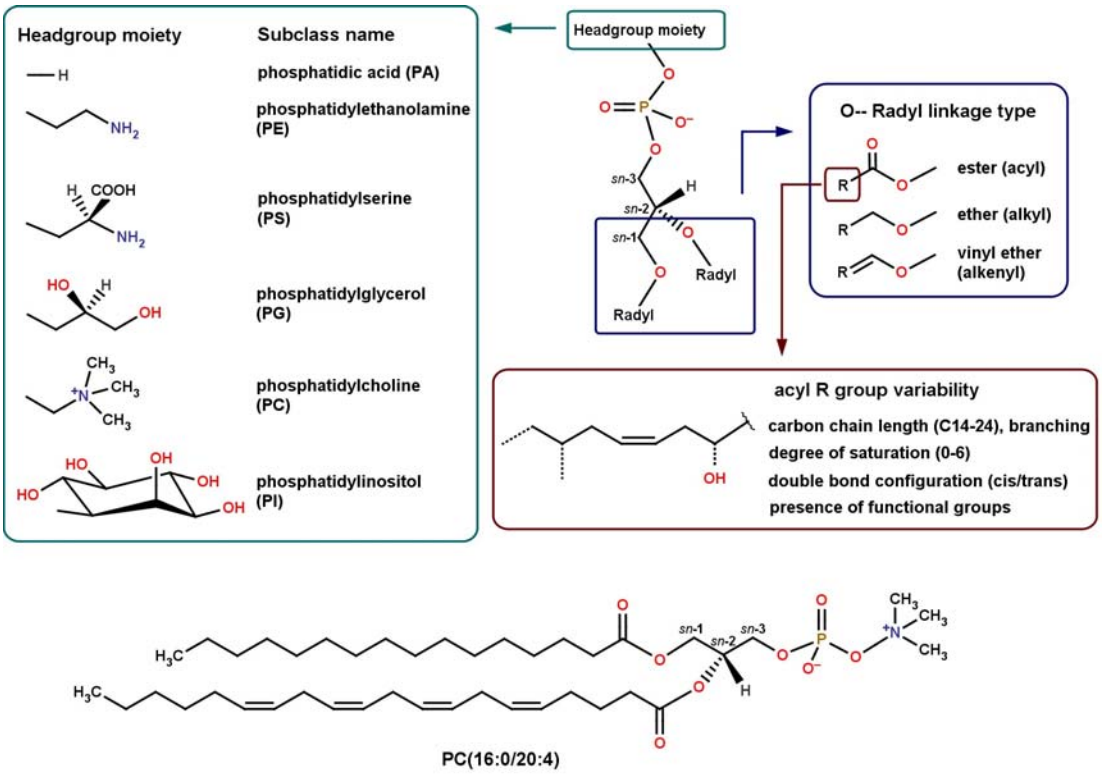

Figure 1.10. Sources of glycerophospholipid variability.

A further variation possibility originates from the linkage type of the radyl groups to the oxygen atoms of the glycerol hydroxyls. The general term "radyl" is used to denote either acyl, alkyl, or 1*Z*-alkenyl substituents corresponding to an ester, an ether, or a vinyl ether linkage, respectively, allowing for coverage of diacyl, alkyl-acyl (plasmanyl) and 1Z-alkenyl-acyl (plasmenyl, plasmalogen) glycerols. Among these, the most abundant linkage type is the ester, when the glycerol hydroxyl(s) in *sn*-1 and/or *sn*-2 position are esterified by fatty acids. In ether-type lipids the alkyl or alkenyl substituent is found generally in *sn*-1 position (with an acyl substituent in *sn*-2). Although occurring in lesser amount, these compounds play important roles as signal lipids, such as the ether lipid platelet-activating factor, whereas plasmalogens may serve as a store of polyunsaturated fatty acids (PUFAs) or as antioxidants due to the presence of the vinyl ether double bond (Brites et al., 2004).

The diversity of GPLs can be still largely expanded by varying the hydrocarbon chain R in case of the ester linkage type, i.e. in the esterifying FA, as detailed in Figure

1.10. In most naturally occurring unsaturated fatty acids the double bonds are in the *cis* configuration, while a *trans* double bond is typically a result of human processing (e.g., hydrogenation). As an example, 1-hexadecanoyl-2-arachidonoyl-*sn*-glycero-3-phosphocholine is shown, which can be designated by the "Headgroup(*sn*-1/*sn*-2)" format, where the structures of the side chains (chain length of the FA and, after the colon, the number of double bonds) are indicated within parentheses, i.e. PC(16:0/20:4). Additionally, presence of an alkyl ether linkage can be represented by an "O-" identifier, as in PC(O-16:0/18:1), whereas "P-" denotes a 1*Z*-alkenyl ether linkage, as in PE(P-16:0/18:1).

The substitution of different Cers on the C-1 carbon produces the corresponding phosphosphingo- (PSLs) and glycosphingolipids (GSLs). Figure 1.11 represents the sources of structural diversity of these complex SLs originating from differences in the sphingoid base (Pruett et al., 2008) and the amide-linked FAs, and also from variability in headgroup moieties (both for phosphate- and sugar-containing ones).

The commonest sphingoid base in animal tissues is sphingosine (Sph), (2*S*,3*R*,4*E*)-2-amino-4-octadecen-1,3-diol or 4*E*-sphingenine, with a C18 aliphatic chain, hydroxyl groups in positions 1 and 3 and an amino group in position 2; importantly, the double bond in position 4 has the *trans* (*E*) configuration. It is usually accompanied by the saturated analogue, dihydrosphingosine (DHSph) or sphinganine.

Among PSLs by far the most abundant is SM, a structural analogue of the glycerophospholipid PC, containing a phosphocholine head. It is a stable and chemically resistant building block of the outer leaflet of the plasma membrane. Nevertheless, the similarity between PC and SM is superficial, and there are great differences in the hydrogen bonding capacities and physical properties of the two lipids. SM has an amide bond at position 2 and a hydroxyl on position 3 of the sphingoid base that can both participate in hydrogen bonding. The *trans* double bond also appears to assist intermolecular interactions in membranes resulting in tight packing capability. On the contrary, in acyl-containing PCs, the two ester carbonyl groups can only act as hydrogen acceptors. The degree of unsaturation in the hydrophobic tails in each lipid is very different, and this gives them significantly different packing properties in membranes. SM and Chol have a high affinity for each other and are usually located together in microdomains of membranes. As an example, *N*-(octadecanoyl)-sphing-4-enine-1-phosphocholine is shown, which can be designated by the shorthand SM(d18:1/18:0). In the parentheses first the number of hydroxyl groups (e.g., "d" for the two hydroxyls of Sph and DHSph), the number of carbon atoms, and after the colon

the number of double bonds of the sphingoid base are indicated followed by the *N*-acyl chain composition (FA chain length and saturation).

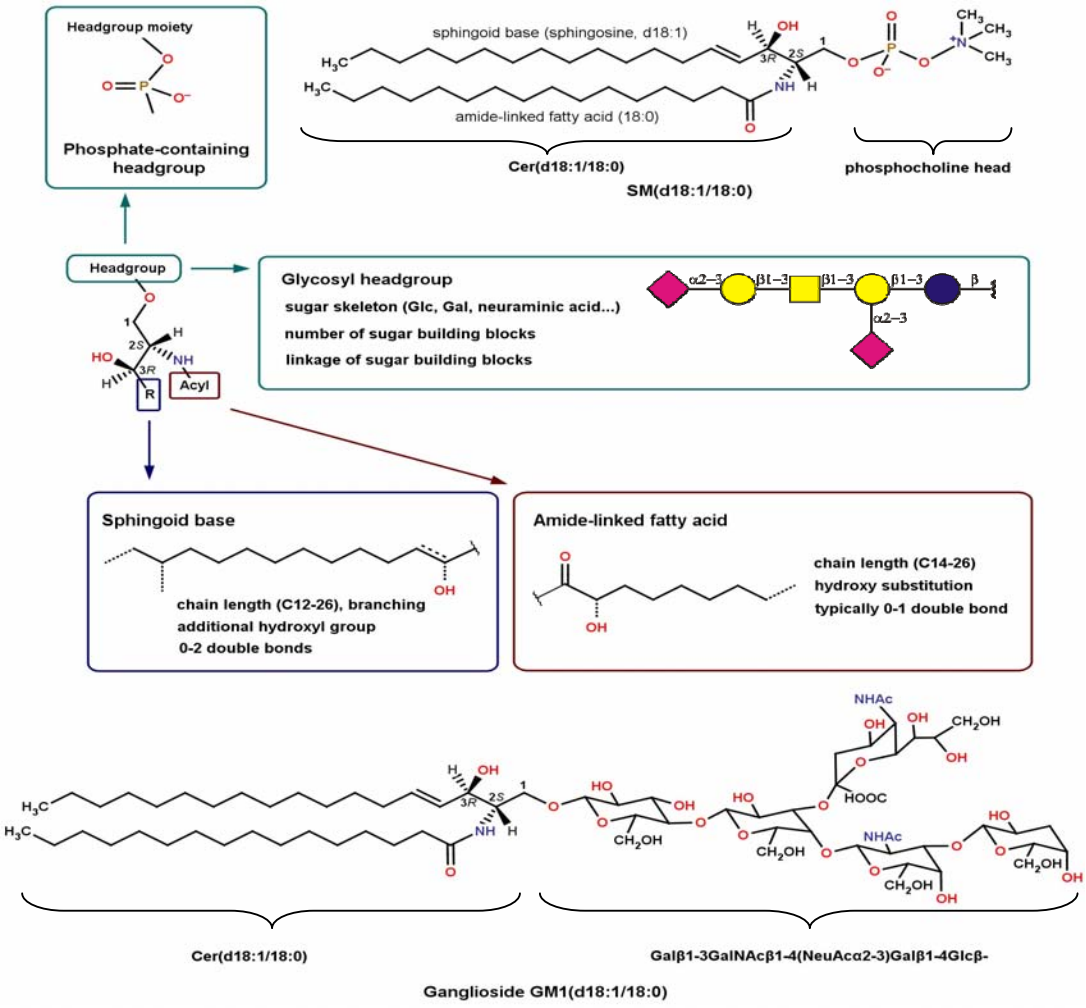

Figure 1.11. Sources of sphingolipid variability.

Glycosphingolipids (GSLs) are composed of the two-tail Cer backbone with a wide variety of carbohydrate headgroups. Based on the extreme variability of headgroup structure (quality and substitution of sugars, number and linkage of sugar building blocks), four principal classes can be distinguished: monoglycosylceramides (mostly glucosylceramide (GluCer) and galactosylceramide (GalCer)), non-acidic oligoglycosylceramides, and two classes of acidic GSLs, gangliosides which contain the characteristic *N*-acetylneuraminic acid (sialic acid, NeuAc) residues, and sulfogalactoceramides (sulfatides). Acidic GSLs are considered as 'un-lipid-like' lipids, because they are rather water-soluble. In the conventional lipid extraction methods they partition predominately into the aqueous layer rather than with the "classical" lipids in the organic (chloroform) layer. GSLs can be found exclusively in the outer plasma

membrane leaflet, and all of them are important as membrane microdomain substituents. The very large surface area occupied by the oligosaccharide chain, (e.g., in gangliosides) imparts a strong positive curvature to the membrane. In addition, they may have other vital biological functions, for example as cellular messengers or as part of the immune system. As an example, a GM1 ganglioside, Galβ1-3GalNAcβ1-4(NeuAcα2-3)Galβ1-4Glcβ-Cer(d18:1/18:0) is shown.

There are also (partly) deacylated counterparts of more complex lipids which contain a hydrogen instead of a corresponding radyl or acyl group. The so-called lysolipids can be specified with a letter “L” in the abbreviation, for example, lysophosphatidylcholine as LPC. Lysolipids are minor lipid components compared to the major membrane lipids. They are produced during the metabolism of higher order molecules. However, they are not simple metabolic intermediates, but exhibit biological properties resembling those of extracellular growth factors or signalling molecules. The most biologically significant lysolipids are sphingosine-1-phosphate (S1P), lysophosphatidic acid (LPA), LPC, and sphingosyl phosphorylcholine (SPC).

The above-shown staggering structural diversity of lipids is accompanied by diversity in polarity covering the whole palette from the hydrocarbon-soluble TGs to the water-soluble gangliosides. Above all, also the range which should be covered during an analysis of the individual elements of a complex mixture – ranging from the bulk structural lipids to minor signalling components – reaches (or even exceeds) 5–6 orders of magnitude difference in concentration. This multi-level diversity could only be studied during the past decade when technological developments, especially in mass spectrometry and bioinformatics, have revealed that living cells contain (ten)thousands rather than dozens of different lipids (van Meer and de Kroon, 2011). Cellular lipidomics must, however, not only determine which lipids are present but also the concentration of each lipid at each specific intracellular location in time; it must include the enzymes of lipid metabolism and transport, their specificity, localization and regulation; and it requires a thorough understanding of the physical properties of lipids and membranes, especially lipid–lipid and lipid–protein interactions. In the context of a cell, the complex relationships between and within the different layers of determinants (genome, transcriptome, proteome and metabolome) can only be understood by viewing them as an integrated system by means of systems biology, i.e., lipidomics (as a part of metabolomics) should also be integrated into the "omics" trends. The first studies combining genomics and lipidomics have just been published. Given the central role of lipids as key metabolites with remarkably diverse biological roles, the field of

lipidomics may follow a steeply ascending trajectory comparable to the developments seen in genomics and proteomics over the past decade (Wenk, 2010).

The biosynthetic pathways of lipids are very complex with several additional intermediate molecules and junctions, and work in concert with catabolic events. The reactions build up a highly complex network in which the synthesis of a given compound means, at least in part, the degradation of another one. Moreover, often the reactions are reversible, and also the production and catabolism of a certain molecule is multi-directional. The same lipid class can be synthesised in different compartments in different ways (e.g., PE in ER vs. mitochondria) or even in the same organelle in several ways (e.g., PC by the PE *N*-methyltransferase vs. cytidine diphosphate-choline pathways in ER). Many times the enzymes that catalyse the formation or degradation of lipids possess high product selectivity (e.g., chain length selectivity of Cer synthases) or substrate selectivity/specificity (e.g. headgroup- or FA chain-specificity of phospholipases) leading to compositionally different pools of lipids (e.g. two DG pools in the nucleus). In the following sections I give a brief overview of lipid biosynthesis.

1.6.1.2. Fatty acids – nomenclature, families and metabolism

In addition to acting as constituents of higher-order glycero- (GLs) and sphingolipids (SLs) and cholesteryl esters (CEs), free (non-esterified) fatty acids (FFAs) (and their derivatives) are themselves individual lipids with several vital metabolic and signalling functions. FAs play essential roles in the biosynthesis of more complex lipids. In their CoA-activated form they participate as "co-substrates" in several anabolic steps, and very importantly, they are "by-products" in numerous catabolic reactions catalysed by a wide range of hydrolytic enzymes (e.g., phospholipases, sphingomyelinases) – see below. The diversity of FAs (as acyl chains in complex lipids) was summarised in Figure 1.10 (section 1.6.1.1). In assigning the position of an individual double bond I follow the "n-" nomenclature, in which the position of the first double bond from the methyl end is described. This "reversed" convention is particularly useful is designating groups of FAs derived from the same parent compound as metabolic reactions do not occur on the methyl end of an existing double bond. If not specified otherwise, the double bond configuration is always *cis* and the double bonds are methylene interrupted (Cook and McMaster, 2004).

FA biosynthesis is a stepwise assembly using acetyl-CoA (but units mostly as malonyl-CoA, derived from glycolysis/lipolysis) by a fatty acid synthase (FAS) complex in the cytoplasm (Figure 1.12). The usual FA produced by FAS is palmitate

(hexadecanoic acid, 16:0), an abundant saturated FA (SFA). When the C16 stage is reached, palmitic acid can be released from the enzyme and can then undergo separate elongation and/or desaturation steps to yield other FA molecules although FAS in most organisms can form stearic acid (18:0) as well. Elongation and desaturation occur predominantly in the ER, but also in the mitochondria, from both endogenously synthesized and dietary FAs. Elongation involves condensation of acyl-CoA groups with malonyl-CoA yielding the corresponding two carbons longer FA, e.g., stearate (18:0) from palmitate. There are three main FA desaturase enzymes in mammals designated as Δ9, Δ6 and Δ5 FA-CoA desaturases according to the position, counted from the carboxyl end, where they insert the double bond. The first double bond introduced into a SFA is generally in the Δ9 position, thus yielding monounsaturated FAs (MUFAs). Oleate (18:1 n-9) and palmitoleate (16:1 n-7) represent the majority of MUFAs present in membrane PLs, TGs, and CEs. The ratio of SFA to MUFA in membrane PLs is critical to normal cellular function and alterations in this ratio have been correlated with several pathological/disease states, such as diabetes, obesity, cardiovascular disease and cancer.

Since the mammalian desaturases cannot introduce sites of unsaturation beyond C-9, they cannot synthesize either 18:2 n-6 (linoleic) or 18:3 n-3 (α-linolenic acids). These polyunsaturated FAs (PUFAs) must be acquired from the diet and are needed for good health. They are, therefore, referred to as essential FAs (see Gurr et al., 2002).

Linoleic acid is important in that it is required for the synthesis of arachidonic acid (AA), 20:4 n-6, an abundant PUFA in most animal tissues. When cells are stimulated by a variety of external stimuli, arachidonic acid is released from cell membranes through the action of phospholipases (see later). The released arachidonic acid then serves as the precursor for the synthesis of the biologically active eicosanoids (prostaglandins, thromboxanes and leukotrienes) which function in diverse biological phenomena such as inflammation, immunity, or as second messengers in the central nervous system.

Once taken up, the essential α-linolenic acid (18:3 n-3) is converted to 20:5 n-3 (eicosapentaenoic acid, EPA) and then to 22:6 n-3 (docosahexaenoic acid, DHA) which serve as important precursors for the potent anti-inflammatory lipids called resolvins and protectins. EPA also gives rises to non- (or poorly) inflammatory eicosanoids. They have also been shown to be important for normal brain development and function.

In the n-9 series a 20-carbon long PUFA is worth a mention, 20:3 n-9, the so-called Mead acid. Animals can make it *de novo* from oleic acid; its elevated presence is

an indication of essential FA deficiency and attention should be paid to its amount in controlling cell culture conditions.

FAs in the form of acyl-CoA molecules are broken down by the process of β-oxidation in mitochondria and/or in peroxisomes to generate acetyl-CoA, the entry molecule for the citric acid cycle. β-oxidation and FA synthesis share essentially reversal chemistry with a few (but not discussed here) key differences (see Gurr et al., 2002).

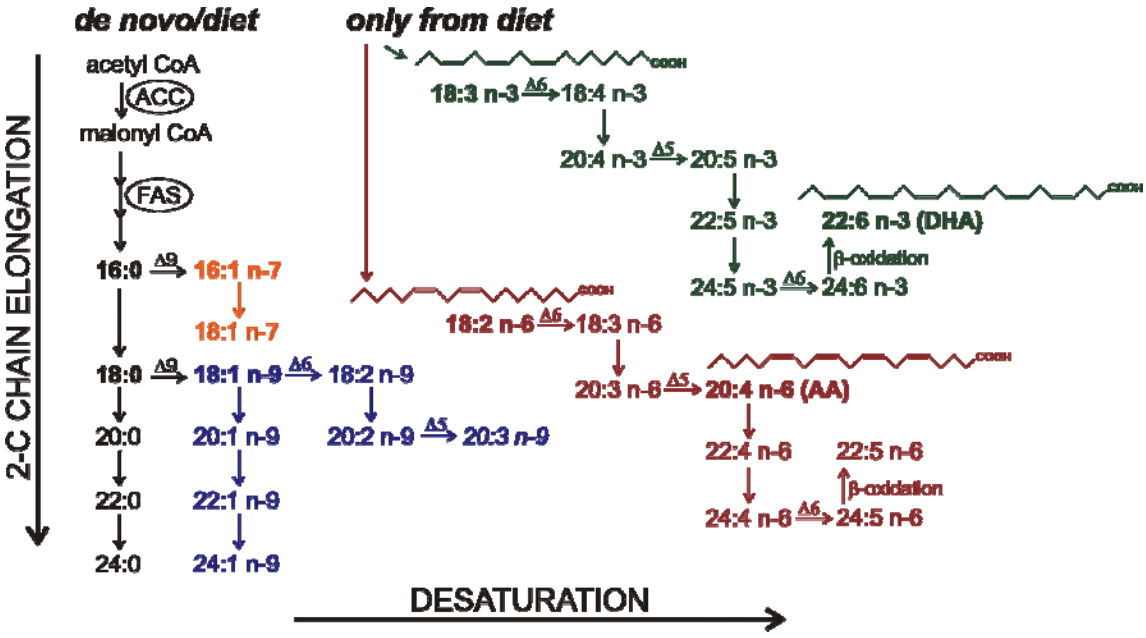

Figure 1.12. Major pathways of FA synthesis in animal tissues. The predominant FA families are shown with different colours: n-9, red; n-7, orange; n-6, blue; n-3, green. AA, arachidonic acid; DHA, docosahexaenoic acid; ACC, acetyl-CoA carboxylase; FAS, fatty acid synthase; Δ9, Δ6 and Δ5 denote the corresponding fatty acyl-CoA desaturases (based on Cook and McMaster, 2004).

1.6.1.3. Sites of lipid synthesis

The main lipid biosynthetic organelle is the endoplasmic reticulum (ER), which produces the bulk of the structural GPLs, Chol, and SLs to Cer (and GalCer) (Figure 1.13).

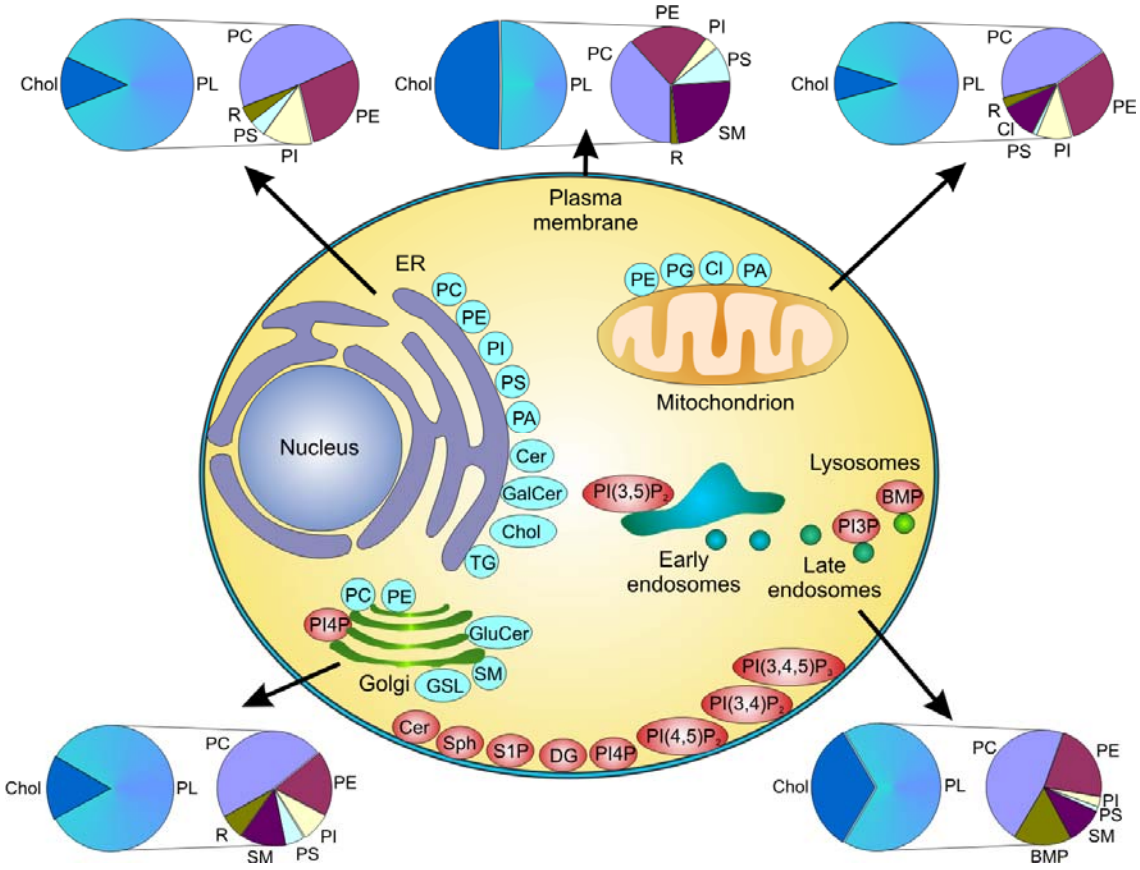

Figure 1.13. Sites of lipid synthesis and steady-state composition of cell membranes (based on van Meer et al., 2008). The lipid compositional data (shown in graphs) are expressed as a percentage of the total phospholipid (PL) in mammals (blue). As a measure of sterol content, the molar ratio of cholesterol (Chol; in mammals) to PL is included. The figure shows the site of synthesis of the major phospholipids (blue) and lipids that are involved in signalling and organelle recognition pathways (red). PC, phosphatidylcholine; PE, phosphatidylethanolamine; PI, phosphatidylinositol; PS, phosphatidylserine; PA, phosphatidic acid; PG, phosphatidylglycerol; CL, cardiolipin; BMP, bis(monoacylglycero)phosphate; Cer, ceramide, GalCer, galactosylceramide, GluCer, glucosylceramide; Chol, cholesterol; TG, triradylglycerol; SM, sphingomyelin; GSLs, complex glycosphingolipids; DG, diradylglycerol; $PI(3,4)P_2$, phosphatidylinositol-(3,4)-bisphosphate; $PI(3,5)P_2$, phosphatidylinositol-(3,5)-bisphosphate; $PI(4,5)P_2$, phosphatidylinositol-(4,5)-bisphosphate; $PI(3,4,5)P_3$, phosphatidylinositol-(3,4,5)-trisphosphate; PI4P, phosphatidylinositol-4-phosphate; S1P, sphingosine-1-phosphate; Sph, sphingosine; R, remaining lipids.

Both the ER and lipid droplets (LDs) participate in CE and TG synthesis. Significant levels of lipid synthesis occur in the Golgi which specializes in higher-order SL synthesis, such as SM, GluCer and complex GSLs. Mitochondria are also an active lipid synthetic site, almost half of its PLs autonomously synthesized here. Moreover, PG and cardiolipin (CL, diphosphatidylglycerol) are confined to that organelle, i.e. they are mitochondrial marker lipids, whereas bis(monoacylglycero)phosphate (BMP) is a major

PL in the inner membranes of late endosomes and lysosomes. Phosphoinositides (PIPn), different phosphate derivatives of PI, are specialized for different organelles (PM, Golgi, early and late endosomes) and, to an extent, can be used as marker lipids for these sites. Due to intensive and specific sorting events (van Meer et al., 2008), which, however, cannot be discussed here, the lipid composition of different organellar membranes varies significantly throughout the cell as shown in Figure 1.13.

1.6.1.4. Glycerolipid metabolism

GLs arise by several mechanisms, most sharing PA and DG as key intermediates (Figure 1.14) (Snyder et al., 2004; Vance, 2004). Most of PA is generated through *sn*-glycerol-3-phosphate (G3P) and acyl LPA (1-acyl-sn-glycerol-3P) via the Kornberg/Pricer pathway with the successive additions of CoA-activated FA chains, but acyl LPA can also be obtained from dihydroxyacetone phosphate (DHAP) via 1-acyl-DHAP in peroxisomes. A portion of PA is synthesized from DG via the action of diacylglycerol kinase (DGK) or it may originate upon the action of PLD from a GPL (see below). The other GLs can be obtained from PA by two mechanisms. One utilizes cytidine-diphosphate (CDP)-activated DG and the polar headgroups inositol and G3P to yield PI and PG, respectively. From PI its position-specific phosphate derivatives (PIP_n) with important signalling properties can be produced, while PG is the precursor for CL and BMP formation. In the other mechanism first DG is formed from PA by PA-phosphatase (PAP) which is then converted to TG by DG acyltransferase (DGAT) (the whole process from G3P to TG is the so-called Kennedy pathway). DG can be produced in the reversed reaction by triacylglycerol lipase (TGL), and upon the action of PLC from a GPL as well. In addition, DG can also be coupled with the corresponding CDP-activated polar headgroups (CDP-choline and CDP-ethanolamine) to produce PC and PE; from these PS is synthesised by an exchange reaction with L-serine. In addition, the mitochondrial PS-decarboxylase produces half of the cellular PE from PS. A second pathway for biosynthesis of PC involves sequential methylation of PE with mono- and dimethyl-PE as intermediates and catalysed by the enzyme PE *N*-methyltransferase (PEMT pathway). Importantly, a third route of PC synthesis occurs in the SL network (Figure 1.16) during the degradation of SM to Cer by sphingomyelinase (SMase) when PC is simultaneously formed from DG. It has been suggested that the ratios of PC/SM and DG/Cer are intrinsically related, with possible implications for cross-talk between glycerolipid and sphingolipid signalling.

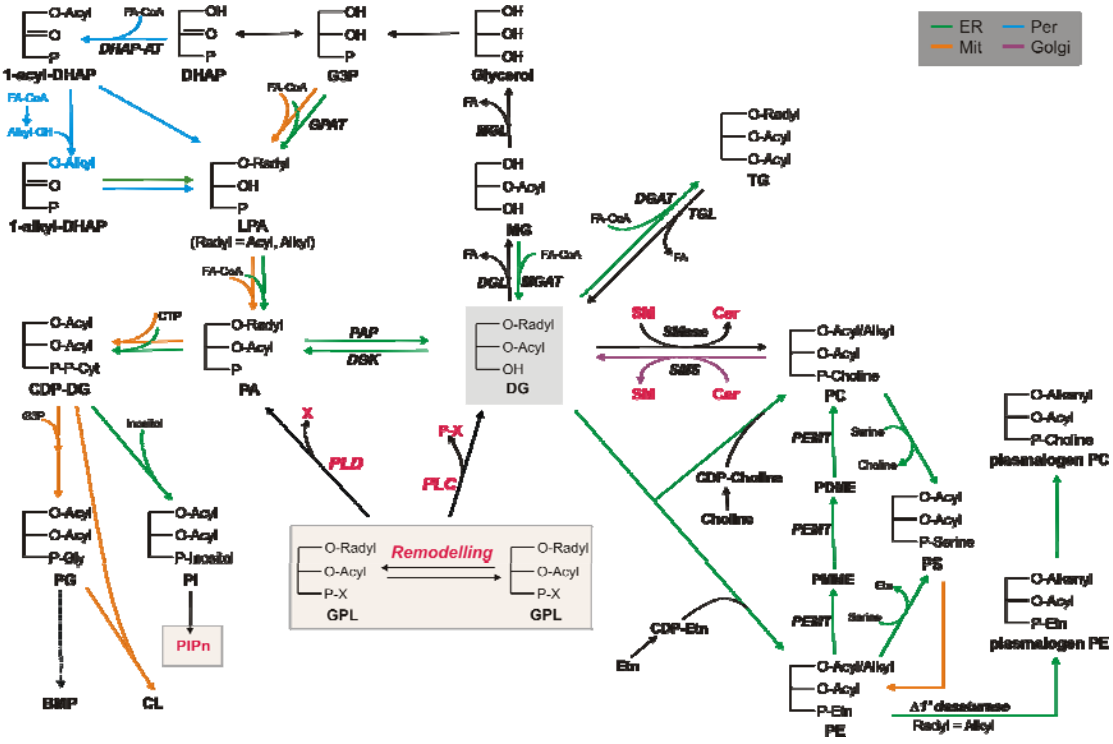

Figure 1.14. Overview of glycerolipid metabolism (based on Gurr et al., 2002). Major sites of synthesis are colour-coded: ER - green, peroxisome - blue, mitochondria - orange, Golgi - purple. P, phosphate; X, headgroup moiety; CTP, cytidine triphosphate; DHAP, dihydroxyaceton-phosphate; G3P, glycerol-3-phosphate; LPA, lysophosphatidic acid; PA, phosphatidic acid; DG, diradylglycerol; CDP-, cytidine-diphosphate-; TG, triradylglycerol; MG, monoradylglycerol; PG, phosphatidylglycerol; PI, phosphatidylinositol; PIPn, phosphoinositide; BMP, bis(monoacylglycero)phosphate; CL, cardiolipin; PC, phosphatidylcholine; PE, phosphatidylethanolamine; PMME, phosphatidylmonomethylethanolamine; PDME, phosphatidyldimethylethanolamine; PS, phosphatidylserine; Etn, ethanolamine; SM, sphingomyelin; Cer, ceramide. Enzymes: DHAP-AT, dihydroxyaceton-phosphate acyltransferase; FA-CoA, fatty acyl coenzyme A; GPAT, glycerolphosphate acyltransferase; PAP, phosphatidic acid phosphatase; DGK, DG kinase; PEMT, PE *N*-methyltransferase; SMS, SM synthase; SMase; sphingomyelinase, PLC, phospholipase C; PLD, phospholipase D, MGAT, monoacylglycerol acyltransferase; DGAT, diacylglycerol acyltransferase; MGL, monoacylglycerol lipase; DGL, diacylglycerol lipase; TGL, triacylglycerol lipase.

In case of the ether-type glycerols, the first two biosynthetic reaction steps are carried out in the peroxisomes, where DHAP is converted to 1-alkyl-DHAP by introducing the ether bond. The following reduction step is the fusion point between ether and acyl lipid synthesis resulting in the formation of 1-alkyl-G3P (alkyl LPA). It is then converted to the corresponding 1-alkyl-2-acyl-PE by the same enzyme system used for diacyl GL synthesis. The final step involves the insertion of the vinyl ether bond to form plasmalogen PE that, in turn, can be transformed to the plasmalogen PC analogue.

Breakdown of the fully or partially substituted GLs goes through several intermediates which are generated in course of hydrolytic processes, such as cleavage of radyl (acyl) groups, headgroups or headgroup moieties (Figures 1.14 and 1.15). The enzymes that catalyse these reactions are called phospholipases. Although the phospholipase denomination is specifically used for GPLs, analogous reactions take place on the simple glycerolipids MG, DG and TG upon the release of the radyl (acyl) substituents from the glycerol backbone. In this respect, as mentioned above, DG is the hydrolysis product of TGL from TG. At the same time, DG is the precursor of MG formation by DG lipase (DGL), which, in turn, can be further hydrolyzed by MG lipase (MGL) to glycerol and a non-esterified (free) FA. This reaction is an important source of AA production, while glycerol can be re-delivered into the GL biosynthetic cycle (Figure 1.14).

According to the site of action four different families can be distinguished, phospholipases A_1, A_2, C and D (Figure 1.15) (Wilton and Waite, 2004). In some tissues, such as intestine, there is a phospholipase B that cleaves both fatty acid esters – but this is exceptional.

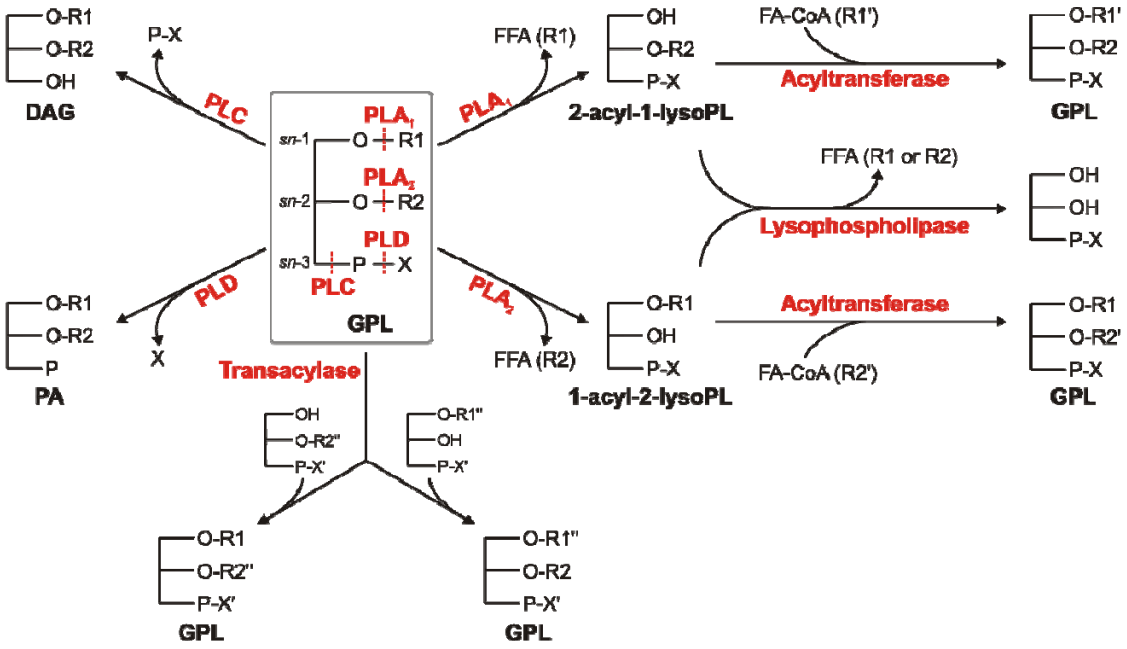

Figure 1.15. Glycerophospholipid degradation and remodelling (as an example a diacyl GPL is shown). PLA_1, phospholipase A_1; PLA_2, phospholipase A_1; PLC, phospholipase C; PLD, phospholipase D; FFA, free fatty acid; GPL, glycerophospholipid; PA, phosphatidic acid; DAG, diacylglycerol; P, phosphate; X, headgroup moiety; R1 and R2; fatty acyl chains.

Phospholipase A_2 (PLA_2) cleaves the *sn*-2 ester bond of a diacyl GPL specifically, generating a free fatty acid (FFA) and a 1-acyl lysophospholipid (lysoPL), while phospholipase A_1 (PLA_1) is able to hydrolyse the *sn*-1 ester bond. The resulting lysoPLs can be further hydrolysed by lysophospholipases or can be re-acylated by CoA-dependent acyltransferases and CoA-dependent/independent transacylases (Yamashita et al., 1997). Subsequent hydrolysis and re-acylation/transacylation of GPLs (often referred to Lands' cycle) is an apparently extensive re-modelling process which post-synthetically determines the FA compositions and positional distributions on the glycerol moiety (Figure 1.15). The turnover of glycerolipid acyl chains functions not only to form specific glycerolipid molecular species, but in part to repair membranes by removing oxidized fatty acids.

The PLA_2 superfamily includes 15 enzymes which comprise four main types including the secreted $sPLA_2$, cytosolic $cPLA_2$, calcium independent $iPLA_2$, and platelet activating factor (PAF) acetyl hydrolase/oxidized lipid lipoprotein associated (Lp)PLA_2 (Burke and Dennis, 2009). The groups are designated by a comprehensive Group numbering system; assignment of the enzymes to a certain group is based on the catalytic mechanism as well as functional and structural features. The most well-studied is the cytosolic GIVA PLA_2. It requires Ca^{2+} for activity, and it is the only PLA_2 with a preference for arachidonic acid (AA) in the *sn*-2 position of phospholipids. This enzyme has been proposed to play a major role in inflammatory diseases. The $iPLA_2$s (Group VI) have high molecular masses (about 85 kDa), do not require Ca^{2+} for activity and are not selective for AA-containing phospholipids. PLA_2s often possess lysophospholipase and transacylase activity, too.

Phospholipase C (PLC) cleaves the phosphate-containing headgroup thus yielding diacylglycerol (DAG), while PLD hydrolyzes the headgroup moiety and generates PA. These phospholipases possess high headgroup specificity, i.e., the FA compositions of the released products reflect the composition of the parent phospholipids. In particular, DAGs derived from PIs (and PIPn) via PI-specific PLC are highly enriched in molecular species containing stearic acid in position *sn*-1 and AA in position *sn*-2, the most abundant FA chain combinations in PI. Nevertheless, in the cell nucleus it appears that there are two distinct pools of DAGs with very different compositions produced from PIPn (polyunsaturated) via the action of a PI-specific PLC and from PC (saturated and monoenoic) via the action of a PC-specific PLC by specific stimuli, and these may have different functions (Carrasco and Mérida, 2007).

Phospholipase D (PLD) uses normally (albeit not exclusively) PC to generate the lipid second messenger PA and choline. There are two mammalian isoforms: PLD1 and PLD2. PLD has been implicated in a variety of physiological cellular functions, such as intracellular protein trafficking, cytoskeletal dynamics, membrane remodelling and cell proliferation in mammalian cells (Gomez-Cambronero, 2010).

1.6.1.5. Sphingolipid metabolism

In the SL metabolic network Cer (and dihydroceramide (DHCer) to a lesser degree) can be considered to be a metabolic hub because it occupies a central position in SL biosynthesis and catabolism as depicted in Figure 1.16 (Hannun and Obeid, 2008). Briefly, mammalian SLs are predominantly synthesized de novo from serine and palmitate by serine palmitoyltransferase (SPT) yielding the saturated dihydrosphingosine (DHSph), (2*S*,3*R*)-2-aminooctadecane-1,3-diol, one of the major sphingoid bases (d18:0). In turn, it is acylated by highly specific (dihydro)-ceramide synthases (also known as Lass or CerS). Cer is formed by the desaturation of DHCer. In SL biosynthetic pathways, Cer (and DHCer) can be phosphorylated by ceramide kinase (CK), glycosylated by glucosyl or galactosyl ceramide synthases (GluCS or GalCS), or can receive a phosphocholine headgroup from PC in the biosynthesis of SM through the action of SM synthases (SMSs), which thereby also serve to generate DG from PC.

Breakdown of complex SLs proceeds through the action of specific hydrolases (Merrill, 2008), leading to the formation of GluCer and GalCer. In turn, specific β-glucosidases and galactosidases hydrolyse these lipids to regenerate ceramide. The breakdown of SM is catalysed by sphingomyelinases (SMases) that are distinguished according to their pH optima and subcellular localization and, to date, several have been characterized: lysosomal acid sphingomyelinase (aSMase), zinc ion-dependent secretory sphingomyelinase (sSMase), neutral magnesium ion-dependent SMase (nSMase), and alkaline SMase (bSMase). These are all categorized as SMase C enzymes, i.e., cleave the phosphodiester bond on the side of the linkage to Cer, so the products are Cer and choline phosphate (in the presence of DG, PC is produced, see above). Ceramide may be broken down by one of several ceramidases (CDases) leading to the formation of sphingosine (Sph), which seems to have one of two fates (Hannun and Obeid, 2008). Sph may be ‘salvaged’ or recycled into SL pathways, or it can be phosphorylated by one of two Sph kinases (SKs). The product S1P can be dephosphorylated to regenerate Sph through the action of specific intracellular S1P phosphatases (SPPases) and, possibly, non-specific extracellular lipid phosphate phosphatases. Alternatively, S1P lyase can

irreversibly cleave S1P to generate ethanolamine phosphate (Etn-P) and hexadecenal which, in turn, can be reduced to palmitate and subsequently reincorporated into lipid metabolic pathways.

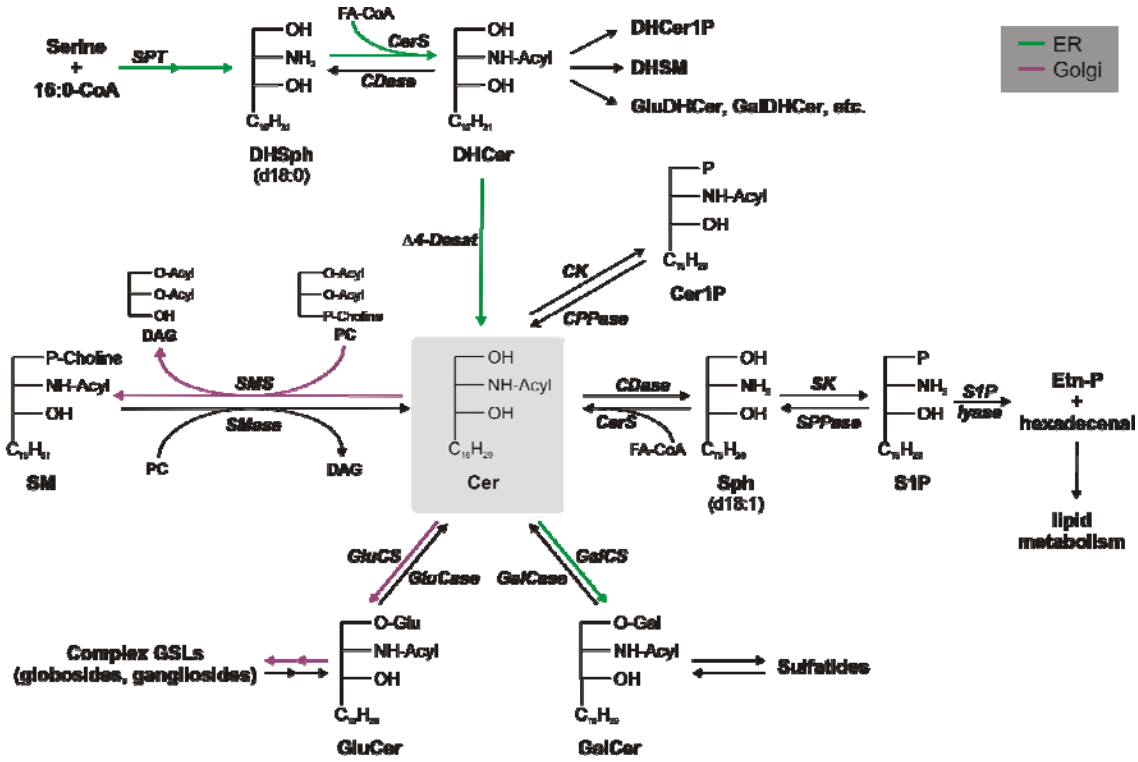

Figure 1.16. Sphingolipid metabolism and interconnection of bioactive SLs (based on Hannun and Obeid, 2008). DHSph, dihydrosphingosine; DHCer, dihydroceramide; DHSM, dihydrosphingomyelin; DHCer1P, dihydroceramide-1-phosphate; Glu/GalDHCer, glucosyl/galactosyl dihydroceramide; Sph, sphingosine; Cer, ceramide; SM, sphingomyelin; Cer1P, ceramide-1-phosphate; Glu/GalCer, glucosyl/galactosyl ceramide; GSL, glycosphingolipid; S1P, shpingosine-1-phosphate; Etn-P, ethanolamine phosphate; PC, phosphatidylcholine; DAG, diacylglycerol. Enzymes: SPT, serine palmitoyl transferase; CerS, ceramide synthase; CDase, ceramidase; CK, ceramide kinase; CPPase, ceramide-1-phosphate phosphatase; SK, sphingosine kinase; SPPase, sphingosine-1-phosphate phosphatase; S1P lyase, sphingosine-1-phosphate lyase; GluCase/GalCase, glucosyl/galactosyl ceramidase; GluCS/GalCS, glucosyl/galactosyl ceramide synthase; SMase, sphingomyelinase; SMS, sphingomyelin synthase.

It should be emphasized that the phosphorylated vs. non-phosphorylated intermediates in the SL network imply completely opposite biological roles, i.e. Cer and Sph induce apoptosis and cell-cycle arrest, while Cer1P and S1P take part in cell survival and proliferation. The significance of proper functioning of the SL network can be well illustrated by the fact, that a whole set of disorders, collectively called as sphingolipidoses (Harwood et al., 2007), can be connected practically to every step of the catabolic flow starting from complex SLs towards Cer. Such sphingolipidoses

include Niemann-Pick (SMase disorder) and Gaucher disease (GCase disorder) and are caused by the absence of specific catabolic enzymes, thus leading to accumulation of their substrate.

1.6.1.6. Cholesterol metabolism

In animals, cells can obtain the Chol they require either from the diet via the circulating low-density lipoproteins, or they can synthesise it themselves. Chol biosynthesis involves a highly complex series of at least thirty different enzymatic reactions (Liscum, 2004), a subject that cannot be treated in detail here. Basically, Chol is built up from acetyl-CoA transported from the mitochondria to the cytosol, where also the first reaction steps are carried out generating mevalonic acid. All the subsequent reductive reactions of Chol biosynthesis use membrane-bound ER-localized enzymes and NADPH as a major cofactor. The isoprenoid intermediates, with squalene as a key structure (shown in Figure 1.9), can be diverted to either sterol or non-sterol pathways. CEs, i.e. with long-chain FAs linked to the hydroxyl group, are much less polar than free Chol and represent a biologically inert form of Chol (and other derivatives, too) for storage in LDs and transport in lipoproteins (Gurr et al., 2002). Chol is also a precursor of signalling molecules, such as Chol glucoside, and of oxysterols, bile acids and steroid hormones, all possessing versatile biological functions.

1.6.1.7. Membrane heterogeneity

As I have shown above, lipid concentrations and compositions may vary between organelles, but importantly, it may be different between the two leaflets of the lipid bilayer and even within the lateral plane of the membrane resulting in membrane (leaflet) asymmetry and the existence of membrane microdomains (often referred as rafts), respectively.

In 1971, Bretscher first hypothesized that the PLs of the human erythrocyte membrane were arranged asymmetrically (Bretscher, 1971). A critical discussion of these early data and the techniques used can be found in (Boon and Smith, 2002)).

PLs in the PM of eukaryotic cells are highly regulated so that cells are able to maintain a non-random distribution of PLs across the PM. Thus, in general, the amino phospholipids PS and PE are restricted to the cytoplasmic leaflet of the PM, whereas PC, SM and GSLs are enriched in the exoplasmic leaflet (Pomorski and Menon, 2006). A detailed table can be found in Boon and Smith (2002) containing several results with

references for lipid asymmetry in different cell types and species. The basis for this transmembrane lipid asymmetry lies in the fact that GLs are primarily synthesized on the cytosolic and SLs on the non-cytosolic surface of cellular membranes (van Meer, 2011). In addition, this asymmetric lipid arrangement is thought to come about as a result of the action of energy-dependent flippases that use ATP hydrolysis to move specific lipids against a concentration gradient (Pomorski and Menon, 2006) (Figure 1.17). In the PM of eukaryotic cells, flip-flop of PLs is constrained owing to the absence of constitutive bi-directional flippases. Thus, ATP-dependent flippases can maintain an asymmetric phospholipid distribution by moving specific lipids towards (P-type ATPase family members) or away from the cytosolic leaflet (ABC transporters). Alternatively, ABC transporters could flip the lipid molecule to present it for release to an acceptor (A).

Cellular activation can collapse the lipid asymmetry by the transient activity of an ATP-independent scramblase. As shown originally for activated platelets, many cell membranes harbour a Ca^{2+}-dependent mechanism that can rapidly move PLs back and forth between the two membrane leaflets (lipid scrambling), leading to a loss of membrane PL asymmetry. The loss of lipid asymmetry in the PM and the appearance of the anionic PLs such as PE and, particularly, PS on the cell surface have been implicated in numerous biological processes, including blood coagulation, myotube formation, vesicle fusion, cell division, sperm capacitation, and phagocytic recognition and clearance of apoptotic cell corpses (Fadeel and Xue, 2009 and refs therein). Various scramblase candidates have been proposed but none has been validated (Bevers and Williamson, 2010).

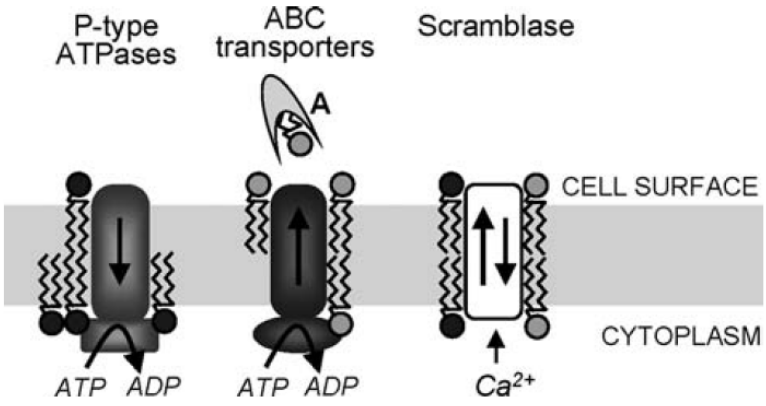

Figure 1.17. Lipid flippases in the PM of eukaryotic cells (see Pomorski and Menon, 2006). A, lipid acceptor.

Chol plays a unique role among the many lipids in mammalian cells. This is based partly on its biophysical properties, which allow it to be inserted into or extracted from membranes relatively easily. Additionally, it plays a special role in organizing the biophysical properties of other lipids in a bilayer (Maxfield and van Meer, 2010). Chol has been shown by many biophysical approaches to have a preferential interaction with SM and, therefore, was supposed to be mostly localised in the outer leaflet of PM. However, like the findings in erythrocytes (Schroeder et al., 1991), also in nucleated cells (Mondal et al., 2009) all (indirect) evidence points to an enrichment of Chol in the cytosolic leaflet of the PM (van Meer, 2011). This is counter-intuitive because the SLs in the non-cytosolic leaflet should enrich the sterols there. In addition, at the typical PM content of 40 mol % cholesterol (and with a Chol surface area half that of PC), restriction of the Chol to one leaflet would yield a ratio Chol/PL in that leaflet of 2, which is the limiting solubility of Chol in PC but (far) above that of PE-containing membranes (van Meer, 2011). Even after nearly 40 years of intense research on the transbilayer organization of lipids, there are still dramatic gaps in our knowledge (van Meer, 2011). The understanding, e.g., how Chol is distributed could be essential for the clarification of raft structure mentioned below.

The Singer–Nicholson model of membranes postulated a uniform lipid bilayer randomly studded with floating proteins. However, it became clear almost immediately that membranes were not uniform and that clusters of lipids in a more ordered state existed within the generally disordered lipid milieu of the membrane. These clusters of ordered lipids (with proteins) are now referred to as membrane rafts (Pike, 2009). Early descriptions of membrane rafts noted their enrichment with Chol and GSLs and focused on their ability to resist extraction by non-ionic detergents (Brown and Rose, 1992). They are a heterogeneous collection of domains that differ in protein and lipid composition as well as in temporal stability. A role for the protein components of rafts in their organization has also become apparent (Pike, 2009). This new concept is embodied in the consensus definition of a lipid raft developed at the 2006 Keystone Symposium of Lipid Rafts and Cell Function: “Lipid rafts are small (10–200 nm), heterogeneous, highly dynamic, sterol- and sphingolipid-enriched domains that compartmentalize cellular processes. Small rafts can sometimes be stabilized to form larger platforms through protein–protein and protein–lipid interactions.” (Pike, 2006). The distinctive lipid composition of membrane rafts was discovered by lipidomic analyses. Different types of rafts have been reported – some are enriched in Chol while others are enriched in SLs. Chol levels in rafts are generally double those found in the

PMs from which they were derived. Likewise, SM levels are elevated by approximately 50 % compared with PMs. The elevated SM levels are offset by decreased levels of PC so the total amount of choline-containing lipids is similar in rafts and the rest of the PM (Pike et al., 2002; Pike, 2009). PS levels are elevated 2- to 3-fold in rafts as compared with the bulk PMs. This suggests that rafts may be a source for the rapid externalization of PS during apoptosis or platelet activation. Rafts are also enriched in ethanolamine plasmalogens, particularly those containing AA (Pike et al., 2002; Pike et al., 2005). Plasmalogens can function as antioxidants and the presence of these compounds in rafts may serve to detoxify molecules that are internalized via lipid rafts or caveolae. It is also possible that rafts serve as an enriched source of AA-containing PLs for hydrolysis by PLA_2 enzymes. As with proteomic studies of lipid rafts, lipidomic studies of these domains have been done using rafts prepared by both detergent-free and detergent-containing protocols. When direct comparisons of the various preparations have been done, significant differences in lipid composition have been identified (Pike et al., 2005; Pike, 2009).

Separation of artificial membranes into liquid-ordered (L_o) and liquid-disordered (L_d) phases is regarded as a common model for lateral heterogeneity. The models have focused on L_o phases that are formed between SM and Chol. This has stemmed from studies characterising the motional constraints on the lipids in dispersions of the PL with Chol and resistance of such phases to solubilisation by Triton X-100 at 4 °C. However, examination of the presently available data on the lipid composition of membrane rafts indicates that a L_o phase of SM and Chol represents less than 25 % of the raft lipids (Quinn, 2010). Thus, in cell membranes, which are dynamic systems not in thermodynamic equilibrium, the underlying propensity of the lipids to phase separate is likely modulated by the presence of proteins and their state of aggregation as well as the continuous trafficking of lipids to and from the PM (Pike, 2009). Moreover, a recent study (Lingwood et al., 2008) suggested that L_o phases are not equivalent to stabilized raft domains at physiological temperature. The selective inclusion of transmembrane proteins suggests that this phase possesses a quality in addition to the lipid basis for L_o–L_d phase separation seen in model membranes (Lingwood and Simons, 2010). Indeed, the raft ganglioside GM1 phase in PM spheres exhibited considerably lower order than that of the L_o domain of model membranes as measured by the membrane order-sensing dye Laurdan. This is consistent with different partitioning of lipid and transmembrane protein markers suggesting additional interactions between proteins and lipids (Kaiser et al., 2009).

In order to cope with the above-mentioned controversies of raft formation, the lipid matrix model of raft structure was proposed (Quinn, 2010) consisting of four main types of membrane domains. These include (i) ordered structures in which membrane proteins are the principle architects; (ii) fluid domains in which oligomeric protein structures are packaged into the fluid bilayer matrix by lipids that typically form non-bilayer structures; (iii) liquid-ordered domains formed by interaction of sterols with polar membrane lipids (in mammalian membranes this is a stoichiometric complex formed between symmetric molecular species of SLs and Chol in molar proportions 1.7:1); and (iv) quasi-crystalline domains that form between asymmetric SLs and PLs. All these structures have their special role which cannot be discussed here.

In a very recent review, Simons and Sampaio also summarised their view on raft structure and function (Simons and Sampaio, 2011). In living cells, raft assemblies can be stabilized by specific oligomerization of raft proteins or lipids with little energy input. The merger of specific nanoscale rafts into larger and more stable platforms brings into function specific rafts in membrane trafficking both in biosynthetic and endocytic pathways as well as in signal transduction and other raft-associated processes as illustrated in Figure 1.18 (Simons and Sampaio, 2011).

Resting-state rafts are dynamic, nanoscopic assemblies of lipids and proteins that persist for a certain period of time, i.e. they are metastable. Most raft proteins are either solely lipid-anchored (glycosylphosphatidylinositol (GPI)-anchored) in the exoplasmic (1) or doubly acylated in the cytoplasmic leaflet (2). They may contain acyl chains besides their transmembrane domain (3), they could undergo a conformational change when partitioning into rafts (4) or following binding to GSLs (5). After oligomerization of raft proteins by multivalent ligands (6) or cytoplasmic scaffolds (7), the small raft domains coalesce and become more stable by forming *small raft clusters*. They may contain more than one family of raft proteins. Although still having a size below the resolution limits of light microscopes, they could already function as signalling platforms. *Large raft clusters* are probably assembled only when due to protein modifications (like phosphorylation) the number of protein–protein interactions increases and it leads to the coalescence of small clusters into larger domains on the scale of several hundred nanometres (8).

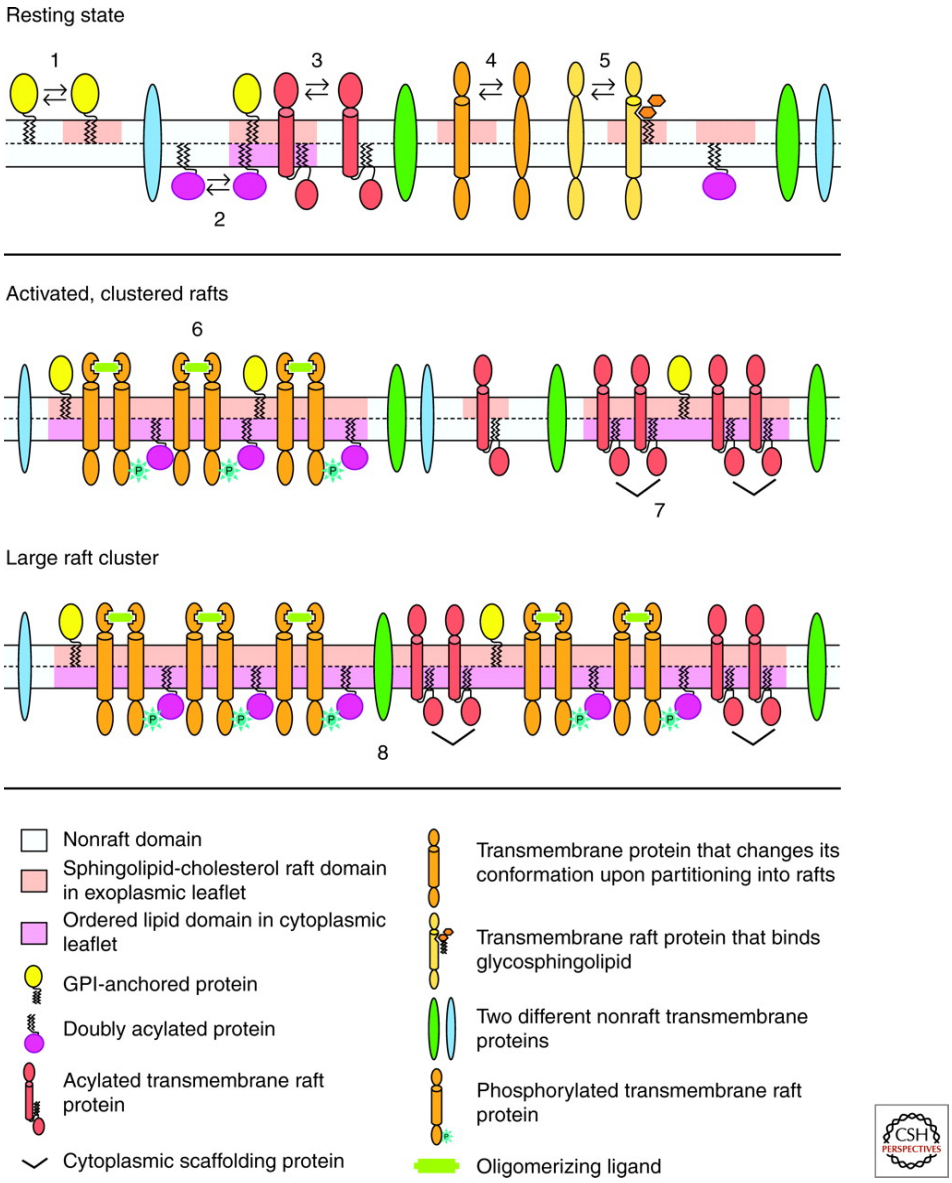

Figure 1.18. The tuneable states of rafts (see Simons and Sampaio, 2011); the different states are explained in the text).

1.7. ROLE OF MEMBRANES AND LIPIDS IN TEMPERATURE ADAPTATION AND STRESS RESPONSE

1.7.1. Cold

One of the most important feature of a lipid bilayer is the relative mobility of the individual lipid molecules and how this mobility alters with temperature. This response is known as the phase behaviour of the bilayer. Basically, at a given temperature a lipid

bilayer can exist in either a gel or a liquid phase. Upon increasing temperature all lipids have a characteristic temperature, referred to as the transition temperature, at which they undergo a transition from the viscous gel (frozen) to the fluid (melted) liquid phase upon increasing temperature. Lowering the ambient temperature of poikilotherms is likely to cause an increase in membrane lipid order. Because of the mixture of lipid classes and lipid molecular species in biological membranes, this will mean that one or more of these molecular species will be below its liquid to gel phase transition temperature. As soon as this phenomenon becomes significant then phase separation of the affected lipids can take place (Guschina and Harwood, 2006). When the growth temperature of poikilotherms is lowered, a number of changes in their membrane lipids have been observed (re-tailoring of membrane species, increase in FA unsaturation, chain shortening, alteration of FA type, changes in lipid classes and lipid/protein ratio changes) which are commensurate with attempts to maintain lipid order at physiologically-advantageous values. These alterations could, therefore, be viewed as adaptation. Rigidification of membrane lipids has been thought to be a general mechanism which could provide a simple way in which homeostatic regulation of membrane properties could be achieved (see reviews: Guschina and Harwood, 2006; Vigh et al., 1998). As an example, it has been shown that modification of the membrane's physical state by surface membrane selective catalytic lipid hydrogenation induces the cold-responsive Δ12 desaturase (*desA*) gene in *Synechocystis* PCC 6803 under isothermal conditions (Vigh et al., 1993). Catalytic hydrogenation of a small pool of PM FAs in live *Synechocystis* cells stimulated the transcription of the *desA* gene in the same way as chilling. In addition, hydrogenated cells displayed an elevated sensitivity to cold stress, indicating that hydrogenation and cooling have "additive effects" on *desA* induction and that cold perception is mediated through changes in membrane fluidity.

1.7.2. Heat stress

If heat is truly transduced into an intracellular signal at the level of membranes, then any manipulation that modulates membrane physical parameters (fluidity, lipid domain organization) should alter the profile and temperature threshold of the HSR.

It was demonstrated in the yeast *S. cerevisiae* that a series of aliphatic alcohols (from methanol to n-pentanol) can lower the temperature required for the maximum induction of a HS-inducible promoter by 3 °C and that the concentration needed to

achieve this decreases as alcohol hydrophobicity increases (Curran and Khalawan, 1994). The lipid–water partition coefficient of alcohols increases with increasing carbon chain length. That a proportionally lower concentration of alcohol elicited the same shift in the maximum HSR threshold as the carbon chain length increased, supports the hypothesis that the membrane plays a role in modulating the cell's response to an increase in temperature. Furthermore, the HS and ethanol stress responses exhibited an extensive similarity and functional overlap. The Hsps required a temperature above ca. 35 °C or ethanol levels above a threshold level of 4–6 % (v/v) for strong induction (Piper, 1995). It was shown that genetic modification of lipid unsaturation and the membrane fluid state, obtained by over-expression of a desaturase gene in the yeast *S. cerevisiae*, resets the optimal temperature of HSR (Carratù et al., 1996).

To confirm the "membrane sensor" hypothesis in the cyanobacterium *Synechocystis* PCC 6803, Northern blot analysis was performed on cells acclimated to contrasting temperatures (22 °C vs. 36 °C), or treated by the membrane fluidizer benzyl alcohol (BA) before various heat exposures (Horváth et al., 1998). The results showed that in cells acclimated to 36 °C all four *hs* genes tested (*dnaK*, *groEL*, *cpn60*, and *hsp17*) were activated at significantly elevated temperatures in comparison with the low temperature-grown counterparts (Figure 1.19). The threshold temperature for the maximal activation was 44 °C in 36 °C samples whereas this value downshifted to 38–40 °C in 22 °C-grown cells. Moreover, unlike *dnaK*, *groEL*, and *cpn60*, the *hsp17* gene was transcribed exclusively at 44 °C and above in samples of 36 °C-grown cells.

These results also demonstrated that the temperature setpoint for the activation of the *hsp* genes is not a fixed value but is clearly affected by the growth temperature. The main factors governing the long-term acclimation in cyanobacteria to ambient temperatures are changes in the level of lipid unsaturation and ratio of proteins to lipids in the membrane (Horváth et al., 1998; Török et al., 1997), which in turn, cause an alteration in the membrane physical state. To test whether correlation between growth temperature, thylakoid thermosensitivity, and activation of *hsp* genes are truly mediated via changes in the membrane physical state, the membrane fluidity of isothermally grown cells was modulated before temperature stress (Figure 1.19). Administration of BA to 36 °C-grown cells, causing reduced molecular order in both the cytoplasmic and thylakoid membranes, dramatically lowered the threshold temperature of heat shock gene activation. Further supporting its unique feature, the administration of the fluidizer increased the hsp17 either at mRNA or protein level throughout the whole temperature range tested.

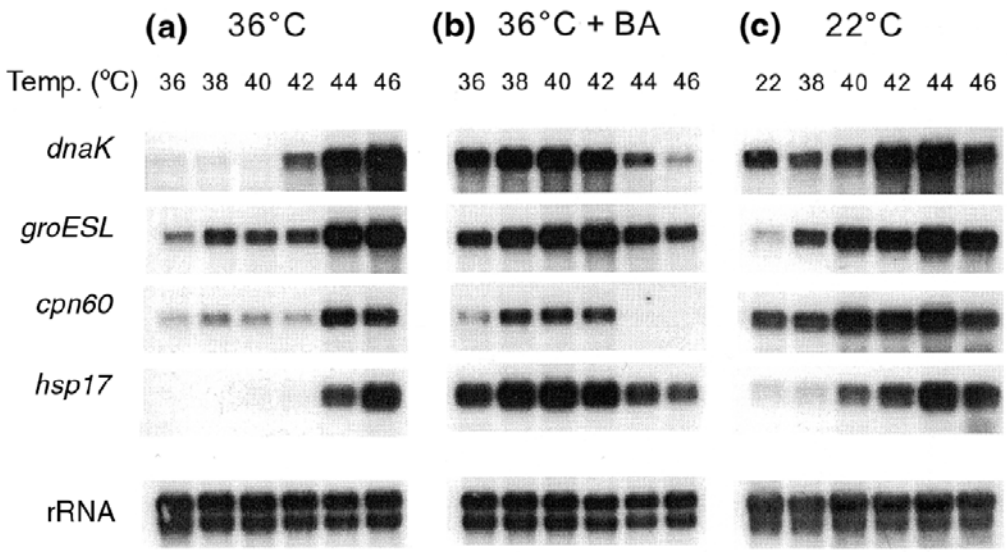

Figure 1.19. Effect of membrane modulations on the temperature profile of *hsp* gene (*dnaK*, *groESL*, *cpn60*, and *hsp17*) expression in *Synechocystis* (adapted from Horváth et al., 1998). Cells, acclimated to 36 °C, 22 °C, grown at 36 °C and treated with 30 mM BA (36 °C +BA), were incubated at indicated temperatures, and the extracted total RNA were subjected to Northern analysis. Hybridizations with rRNA were served as loading controls.

The precise mechanism(s) by which *Escherichia coli* cells sense environmental stress and transduce signals affecting the expression of genes involved in defence, recovery, and stress acclimation are still unclear. To address whether membrane changes directly participate in generating signals for the activation of heat shock genes, a study was conducted on wild type (*wt*) and *rpoH* (encoding the major heat shock sigma factor, σ32) deletion mutant *E. coli* strains exposing cells to HS and BA treatment (Shigapova et al., 2005). In the wt cells, both GroEL and dnaK, representing the two major chaperone systems of *E. coli*, could be activated by a temperature upshift or BA treatment at the growth temperature. It is known that the transcription of the heat shock genes is strongly reduced in the absence of σ32 (Zhou et al., 1988). Interestingly, in the strain lacking σ32, transcripts of both *groEL* and *dnaK* (this latter in a relatively large amount) were already present at 30 °C and their levels were slightly reduced rather than induced upon BA administration. In contrast, a transcriptional activation of these genes upon temperature upshift to 43 or 46 °C was observed. Western blot experiments were carried out to follow the accumulation of the major Hsps, DnaK and GroEL. Surprisingly, in contrast to a short HS (43 or 46 °C, 20 min), resulting in the formation of both *hsp* transcripts and Hsps, BA treatment accumulated *hsp* transcripts but did not cause sizable formation of the Hsps.

Interestingly, the amount of Hsps that were induced in *P. patens* by a specific HS did not depend only on the inducing temperature, but also on the basal growth temperature (Saidi et al., 2009a; Saidi et al., 2010). When mosses which had been pre-acclimated at 22 °C were treated 1 h at 34 °C they showed a 4-fold higher HSR compared to mosses pre-acclimated at 30 °C. This correlated with a massive increase in the lipid saturation of their membranes at 30 °C as compared to 22 °C.

Furthermore, the exposure of moss cells to compounds that increase membrane fluidity has led to a significant activation of Hsps at non-inducing temperatures (Saidi et al., 2007; Saidi et al., 2009a). Membrane fluidizers like BA induced a major (albeit transient) elevation of cytosolic Ca^{2+}, activated Hsp promoters and improved *P. patens* thermotolerance (Saidi et al., 2009a; Saidi et al., 2010). Exposure to BA also evoked the opening of a non-selective Ca^{2+} channel in excised PM patches, which was very similar, in conductance and ion selectivity, to the heat-activated channel. Moreover, BA-mediated HSR was strictly dependent on extracellular Ca^{2+} and addition of Ca^{2+} chelators abolished the BA-mediated thermotolerance (Saidi et al., 2009a).

In their study, Samples and colleagues showed that leukocytes, isolated from the pronephros of rainbow trout *Oncorhynchus mykiss*, acclimated to 5 or 19 °C expressed elevated levels of *hsp70* mRNA when heat-shocked at 5 °C above their respective acclimation temperature (Samples et al., 1999). Supplementation with exogenous DHA or AA followed by HS enhanced the levels of *hsp70* mRNA. These authors suggested that HS initiates changes in membrane physical state, which when acted upon by phospholipases, may release lipid mediators that could serve as triggering signals during the HSR.

Another example for the HS threshold alteration due to the acclimation was given by examining the HSR in testis (Sarge et al., 1995; Sarge, 1995). A unique feature of the male gonads of many species is their location outside the main body cavity, so that testis cells have a significantly lower growth temperature relative to cells of other tissues. In the mouse, testis temperature is tightly regulated at 30 °C, 7 °C lower than the body cavity temperature at which other tissues such as liver are maintained. It was demonstrated that HSF1 DNA-binding is induced at significantly lower temperatures in a preparation of mixed male germ cell types relative to other mouse cell types (Sarge et al., 1995). This result suggested the possibility that the growth temperature experienced by a particular cell type *in vivo* plays a primary role in determining the HSF1 activation temperature in that cell type. Interestingly, the phenomenon of reduced HSF1 activation temperature in testis is a property unique to male germ cell types within this tissue, as it

is exhibited by pachytene spermatocytes but not by somatic testis cell types (Sarge, 1995).

Attenuation of cardiac Hsp expression has been shown in some pathological conditions, such as cardiac hypertrophy and aging. For example, it has been shown that the expression of Hsp70 in response to heat and ischemic stress is also diminished in hearts of rats fed a Chol-enriched diet (Csont et al., 2002). Since hyperlipidemia is known to alter lipid composition (Hexeberg et al., 1993) and, thereby, the physical state of myocardial membranes, it also likely limits the capacity of cells to accumulate Hsps under various stress conditions (Vigh and Maresca, 2002).

1.7.3. Lipid-interacting non-toxic drugs

Bimoclomol, a hydroxylamine derivative (N-[2-hydroxy-3-(1-piperidinyl)propoxy]-3-pyridine carboximidoylchloride maleate), and its analogues was shown to have potential therapeutic uses in the treatment of diabetes, cardiac dysfunction and cerebrovascular disorders (Chung et al., 2008; Jednákovits et al., 2000; Kürthy et al., 2002; Vigh et al., 1997). Arimoclomol, a closely related bimoclomol analogue, delayed the disease progression in amyotrophic lateral sclerosis (Kieran et al., 2004). The first evidence that these non-toxic compounds are coinducers of Hsps (i.e., they cannot amplify the *hsp* gene expression without a concomitant stress, but the stress-induced increase in Hsp levels is further elevated by their presence) was provided 15 years ago (Vigh et al., 1997). The precise mechanism of Hsp coinduction by these new drugs is still unknown, but they have been documented not to interact with a number of known conventional pharmacological targets. Coinducing effects of bimoclomol on Hsp expression were shown to be mediated by means of HSF1 (Hargitai et al., 2003). It was also demonstrated (Török et al., 2003), however, that the presence of bimoclomol does not affect protein denaturation in various mammalian cells. Instead, it was documented that the compound (and its analogues) specifically interacts with and significantly increases the fluidity of negatively charged membrane lipids. On the other hand, bimoclomol is an efficient inhibitor of bilayer–nonbilayer lipid phase transitions. This was the first evidence that non-toxic compounds possess the capability of Hsp coinduction in the absence of the production of unfolded proteins. It was suggested that bimoclomol and the related compounds modify those membrane domains where the thermally or chemically induced perturbation of lipid phase is sensed and transduced into a cellular signal, leading to enhanced activation of heat shock genes (Török et al., 2003).

1.7.4. Lipid signalling of HS

Requirements and availability together determine the amount of a certain lipid (in membranes) by a very intimate regulation of the anabolic and catabolic pathways of lipid metabolism. Because of this, the actual local concentration of a lipid, is decisive in terms of functionality, and can be largely influenced by changing stress conditions. This fact has important consequences during the process of stress response, since even subtle changes in lipid concentration/composition may result in alterations in lipid–lipid and lipid–protein interactions leading to altered functional properties such as in signalling.

Lipids of cell membranes can serve as a source of those mediators which can be involved in the activation or attenuation of Hsp signalling pathways. Stresses and clinical conditions can induce alterations in the metabolism of membrane lipids in producing a unique set of lipid mediators with the potential of retailoring the pre-existing Hsp profile (Escribá et al., 2008). Thus, it has been shown that exogenous PLA_2, which stimulates AA release, and AA itself both activate the HSR (Jurivich et al., 1994; Jurivich et al., 1996).

HS and other agents that induce the stress response activate PLC and PLA_2 in different cell lines, including cells of human, rat, mouse, and hamster origin (Calderwood and Stevenson, 1993) producing AA (Calderwood et al., 1989) and inositol triphosphate (IP_3) as a result of $PI(4,5)P_2$ hydrolysis (Calderwood et al., 1987; Calderwood et al., 1988). Furthermore, in human epidermoid A431 cells U-73122 (an inhibitor of PLC) treatment reduced the levels of heat-induced Hsp72 almost by half (Kiang et al., 1994).

On the other hand, during HS, AA is used in the synthesis of eicosanoids via cyclooxygenases (COX) and lipoxygenases (LOX) (Calderwood et al., 1989). The cyclopentenone prostaglandins PGA_1, PGA_2 and PGJ_2 also lead to activation of HSF1 (Amici et al., 1992; Amici et al., 1993; Ianaro et al., 2003; Ohno et al., 1988). Hsp70 induction by these compounds is mediated by cycloheximide-sensitive activation of HSF1, and sustained for long periods of time (12–24 h, depending on the type of prostaglandin) in human cells (Santoro, 2000). Moreover, certain lipoxygenase products of AA, such as 12-hydroxyeicosatetraenoic acid, have also been shown to induce the expression of individual Hsps in human leucocytes (Köller and König, 1991).

Non-steroidal anti-inflammatory drugs (NSAIDs) partially activate components of the HSR and often work in conjunction with a secondary stress signal for full induction of Hsp70 expression (Westerheide and Morimoto, 2005). Sodium salicylate (Jurivich et

al., 1992) and other NSAIDs such as indomethacin (Lee et al., 1995) induce both HSF1 DNA binding and hyperphosphorylation of HSF1 and drug pretreatment lowers the temperature threshold of HSF1 activation (Lee et al., 1995). Conventional non-steroidal anti-inflammatory drugs are non-selective inhibitors of COX-1 and COX-2 enzymes (Wu, 1998). COX is a bifunctional enzyme, containing the COX activity that catalyzes the bisoxygenation of AA to form PGG and a peroxidase activity, which catalyzes the reduction of PGG to PGH (Smith and Marnett, 1991). Therefore, inhibition of COX results in an elevated AA level. Taken together, one possible explanation for the mechanism of Hsp coinducing activity of NSAIDs could be that these compounds are able to elevate the AA level during stress conditions. However, Roussou et al. suggested that indomethacin at moderate temperatures increases the level of denatured proteins in the cell, thus lowering the temperature threshold for HSR (Roussou et al., 2000).

It has been shown that the binding of HSF to HSE can be activated by Ca^{2+}. Treatment with Ca^{2+} ions resulted in a concentration- and time-dependent activation of HSF *in vitro* in cell-free HeLa system (Mosser et al., 1990). In permeabilized NIH3T3 cells, Ca^{2+} activated HSF binding only in combination with HS (Price and Calderwood, 1991). In intact fibroblast cells HS elevated intracellular Ca^{2+}, but raising intracellular Ca^{2+} failed to activate the HSR (Stevenson et al., 1987), indicating that Ca^{2+} alone is insufficient to activate expression of the heat shock genes. Hyperthermia caused a large (3- to 5-fold) increase in intracellular free calcium ($[Ca^{2+}]_i$) in HA-1 fibroblasts. Increased $[Ca^{2+}]_i$ appeared initially to be due to release of Ca^{2+} from an internal store. These heat-induced changes in Ca^{2+} homeostasis were correlated with a rapid release of IP_3 within 1 min at 45 °C (Calderwood et al., 1988). However, in human epidermoid A431 cells heat activates the Na^{+}–Ca^{2+} exchange system so as to increase $[Ca^{2+}]_i$ and reduce $[Na^{+}]_i$ (Kiang et al., 1992).

Increases in $[Ca^{2+}]_i$ induced by ionomycin (a Ca^{2+} ionophore) promote Hsp70 production in A431 cells (Ding et al., 1996), MDCK cells (Yamamoto et al., 1994), and rat luteal cells (Khanna et al., 1995). Furthermore, inhibition of increases in $[Ca^{2+}]_i$ in A-431 cells by removal of external Ca^{2+}, addition of the chelator EGTA in the medium, or treatment with an intracellular Ca^{2+} chelator, greatly attenuates HSF translocation from the cytosol to the nucleus, HSF binding to HSE, *hsp70* gene expression, and protein synthesis (Kiang et al., 1994).

In cells that overexpress Hsp70 as a result of HS or *hsp70* gene transfection, increases in $[Ca^{2+}]_i$ induced by HS, air hypoxia, or chemical hypoxia are attenuated (Kiang and Tsokos, 1998). It was suggested by Kiang and Tsokos (Kiang and Tsokos,

1998) that IP_3 itself is important in the regulation of the expression of Hsps because treatment with pertussis toxin, cholera toxin, or forskolin increases the production of IP_3 (Kiang and McClain, 1993). This increased production leads to the increased levels of *hsp70* mRNA and protein in human epidermoid A431 cells. They hypothesized that induction of Hsp70 may be a result of IP_3 binding to its receptors (Kiang and Tsokos, 1998).

Investigating the roles of membrane fluidity and Cer in hyperthermia and alcohol stimulation of TRAIL apoptosis, Moulin and coworkers showed (Moulin et al., 2007), that HS, BA or ethanol treatment, had the ability to up-regulate total cellular Cer levels in Jurkat cells. Cer is widely considered as an effector promoting cell cycle arrest and apoptosis, which are important components of the stress response. However, the increase in Cer does not necessarily lead to cell death since B16 cells remain viable after 41–43 °C heat or 40 mM BA treatment for 1 h (Nagy et al., 2007). A similar distinction of heat-induced Cer generation and apoptosis induction was demonstrated in Molt-4 cells (Jenkins et al., 2002). Nevertheless, when the damage is extensive (i.e. due to a heating over 44 °C or prolonged HS) cells undergo apoptosis (Zhang et al., 2009). Moreover, a direct link between heat-induced Cer production and specific stress protein induction was reported on NIH WT-3T3 cells (Chang et al., 1995), where HS at 42.5 °C for 2 h caused a 2-fold increase of total Cer. Application of exogenous C2 (acetyl)-Cer or increased endogenous intracellular Cer was found to induce a sHsp αB-crystallin, but not the structurally similar Hsp25.

SPC is naturally produced via breakdown of SM by SM deacylase. SPC (but not S1P) activates Hsp27 via the p38 MAPK pathway in isolated rat cerebral arteries (Mathieson and Nixon, 2006). In contrast, in osteoblast-like MC3T3-E1 cells and aortic smooth muscle A10 cells S1P stimulates the induction of Hsp27 via p38 MAPK and PI3K/Akt pathways (Kozawa et al., 1999a; Kozawa et al., 1999b; Takai et al., 2006).

In addition, during HS Chol can be rapidly converted to cholesteryl glucoside (Kunimoto et al., 2000). Exogenous cholesteryl glucoside rapidly activated HSF1 and induced the synthesis of Hsp70 in fibroblast cells (Kunimoto et al., 2002).

The stress response-modulating lipid mediators are summarised in Figure 1.20 which is based on the original figure published in a recent review (Escribá et al., 2008).

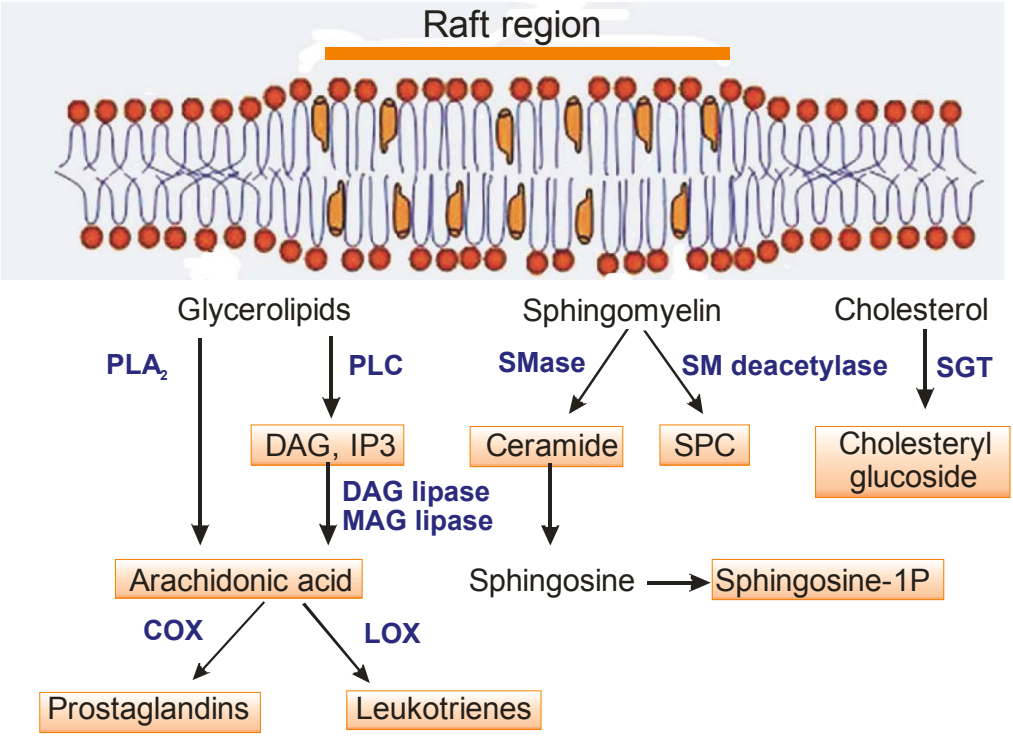

Figure 1.20. Some typical lipid mediators capable of altering the HSR. SMase: sphingomyelinase; SGT: sterol glucosyltransferase; COX: cyclooxygenase and LOX: lipoxygenase (adapted from Escribá et al., 2008).

1.7.5. HS signals through growth factor receptors

It was suggested (Escribá et al., 2008; Park et al., 2005; Vigh et al., 2005) that signalling from the transmembrane growth factor receptors to *hsp* genes may link PM events to Hsp expression induced by mild HS and membrane fluidizers. Membrane rearrangement by mild HS or chemical fluidizers may activate growth factor receptor tyrosine kinases by causing their non-specific clustering (Vigh et al., 2005). Ligand-independent activation of the EGFR by lipid raft disruption was demonstrated on keratinocytes (Lambert et al., 2006). The authors hypothesized that Chol depletion leads to the release of EGFR from the damaged rafts of methyl-β-cyclodextrin-treated cells into small confined areas of the membrane, where the receptor molecules are likely to be spontaneously activated owing to a very high density and/or separation from the inhibitory factors remaining in the surrounding portions of the membrane.

PI3Ks are activated by growth factor receptor tyrosine kinases, either directly or through interaction with the insulin receptor substrate family of adaptor molecules. This activity results in the production of PIP3. A bifurcation of the signalling pathway exists downstream of PI3K and PIP3, so that Akt and Rac1 (a member of the Rho family of

small GTPases) activation occur in parallel (Ishikura et al., 2008). The serine/threonine kinase Akt links growth factor signalling with cellular growth, proliferation, metabolism, survival (Akhavan et al., 2010) and Hsp response by inhibiting GSK3. Rac1 plays a fundamental role in a wide variety of cellular processes, including actin cytoskeletal reorganization, cell transformation, the induction of DNA synthesis, superoxide production, axonal guidance, cell migration (Bosco et al., 2009) and also in Hsp response (Han et al., 2001).

Moderate HS (43 °C) has been shown to activate PI3K in NIH3T3 fibroblasts (Lin et al., 1997). Additionally, mild HS (41–42 °C) induces phosphorylation and activation of Akt in a PI3K-dependent manner in NIH3T3 fibroblasts (Bang et al., 2000; Han et al., 2002), and in human neuroblastoma SHSY5Y cells (Bijur and Jope, 2000). HS treatment of SHSY5Y cells also caused a rapid increase in HSF1 DNA-binding activity that was partially dependent on PI3K activity. HS-induced activation of PI3K and the inhibitory effect of GSK-3b on HSF1 activation and Hsp70 expression imply that Akt-induced inhibition of GSK-3b contributes to the activation of HSF1 (Bijur and Jope, 2000). *In vivo* experiments also showed that mild HS (41 °C, 30 min) application induces PI3K activation and GSK-3b inactivation (Maroni et al., 2000).

Mild HS (39–42 °C, 15–20 min) has been shown to activate Rac1 pathway as demonstrated by pull-down assay using the Rac1-binding domain of p21-activated kinase. Overexpression of Rac1N17, a dominant negative mutant Rac1, completely prevents HSF1 activation and Hsp expression in response to mild or moderate HS (40–43 °C, 20 min), but not to severe HS (44–45 °C, 20 min) (Han et al., 2001), indicating that the Rac1 GTPases play a critical role in stress-induced HSF1 activation and Hsp70 expression (Park et al., 2005). The signalling pathways are summarised in Figure 1.21 (based on Akhavan et al., 2010; Escribá et al., 2008; Park et al., 2005; Vigh et al., 2005).

As mentioned above, raft perturbation may result in ligand-independent growth factor receptor activation. An important HS-induced process resulting in raft rearrangement is Cer generation. Cer, which has the unique property of fusing membranes, appears to drive the coalescence of raft microdomains to form large, Cer-enriched membrane platforms, which exclude Chol (Grassme et al., 2007; Gulbins and Kolesnick, 2003), in other words elevated Cer level rapidly displaces Chol from membrane/lipid-“Chol-raft” and forms “Cer-raft” (Patra, 2008). It was hypothesised that extracellular stimuli employ Cer-enriched platforms to achieve a critical density of

receptors and other signalling molecules that are required for biochemical transfer of the stress across the PM.

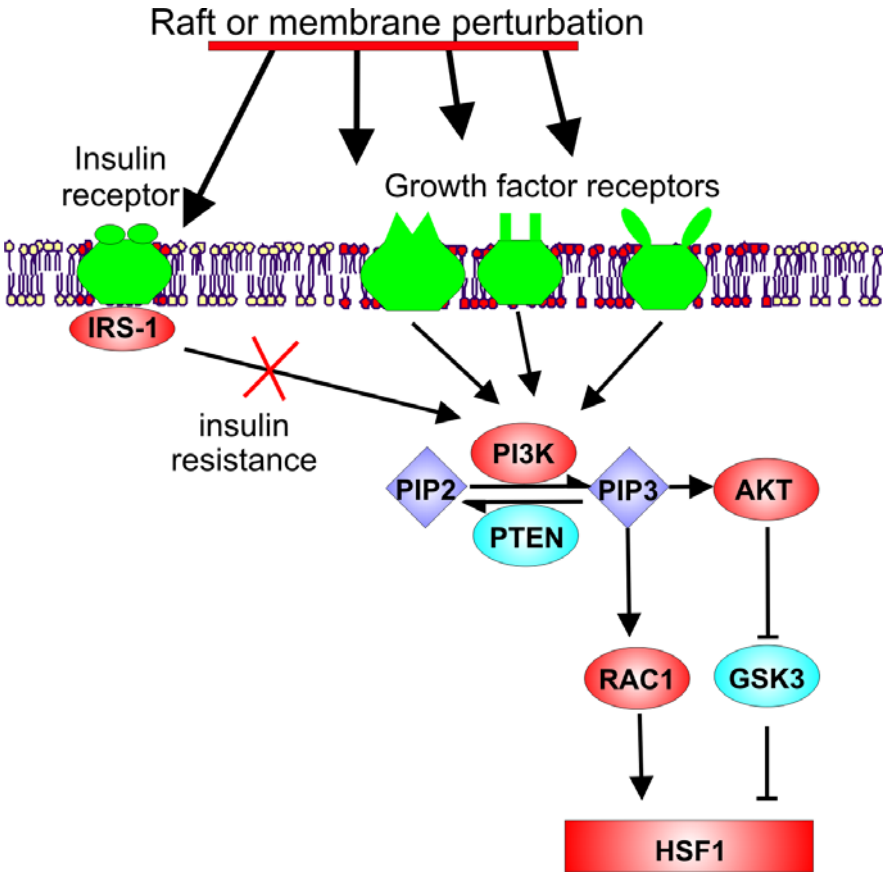

Figure 1.21. Cascade of possible HS signal generation and transduction events linking plasma membrane (growth factor signalling) to heat shock genes during Hsp response induced by mild HS and membrane fluidizers (based on Akhavan et al., 2010; Escribá et al., 2008; Park et al., 2005; Vigh et al., 2005). IGF-1, insulin-like growth factor 1; IRS-1, insulin receptor substrate 1; PIP2, phosphatidylinositol biphosphate; PIP3, phosphatidylinositol triphosphate; Akt, protein kinase B; Rac1, a small GTPase protein; GSK3, glycogen synthase kinase-3; HSF1, heat shock factor 1; PI3K, phosphoinositide 3-kinase; PTEN, phosphatase and tensin homologue protein.

1.7.6. Altered HSR in diabetes and cancer

Insulin resistance and type 2 diabetes are known to be associated with low Hsp levels, and with decreased PI3K and enhanced GSK3 activities. Stimulation of the translocation of GLUT4 glucose transporters in muscle and adipose tissue shares the PI3K-Akt pathway with HSR, therefore common insulin and Hsp signal attenuation in type 2 diabetes has been suggested (see in Figure 1.21) (Chung et al., 2008). Using rodent models, it has been demonstrated that the localization of insulin receptor in the

caveolae is interrupted by elevated levels of the endogenous ganglioside GM3 during a state of insulin resistance (Kabayama et al., 2007). In agreement, diseases or treatments, which alter raft lipid composition, also change insulin sensitivity and presumably the HSR as well (Vigh et al., 2007a). Certain lipid-interacting non-toxic drugs (see above) have been reported to improve insulin sensitivity. Using BGP-15 to achieve an elevation of Hsp72 protein, protection against diet or obesity-induced hyperglycaemia, hyperinsulinemia, glucose intolerance and insulin resistance was observed (Chung et al., 2008). It is highly probable that these drugs may influence the above-mentioned common signal pathways.

On the other hand, in cancer HSF1 becomes activated and its activity is associated with transformation and maintenance of the malignant phenotype. As documented by Khaleque et al. (2005), Hsp elevation in tumour cells can be induced by the malignant growth factor heregulin (HER), which causes homo- and heterodimerization between each member of the four ErbB receptor molecules (Khaleque et al., 2005). The formation of raft-associated growth factor receptor dimers is followed by tyrosine phosphorylation of their intracellular domains. The major downstream signalling pathways include the Ras–Raf1–Mek–ERK and PI3K–PDK1–Akt pathways (Escribá et al., 2008; Khaleque et al., 2005). HER appears to be linked to Hsp expression by its activation of HSF1 through inhibition of the constitutive kinase GSK3. As GSK3 is inhibitory for HSF1, HER2/Akt signalling can then activate HSF1 by blocking inhibitory signalling (Calderwood et al., 2010).

Elevated Hsp expression promotes cancer by inhibiting programmed cell death (Hsp27, Hsp70) and by promoting autonomous growth (Hsp90) and leads to resistance to chemotherapy and hyperthermia. Tumour Hsps have another property that can be exploited in therapy. They are immunogenic and can be used to form the basis of anticancer vaccines. Elevation in Hsp levels may thus have competing effects in tumour growth, being required for tumour cell survival but conferring a hazard for cancer cells due to their immunogenic properties (Calderwood and Ciocca, 2008).

Membrane fluidizing treatments such as mild hyperthermia, aliphatic alcohols and local anaesthetics change the lipid dynamics of cell membranes resulting in an increase in local fluidity. The use of fluidizing treatments in combination with chemotherapeutic agents may therefore allow more efficient entry of the drugs into the tumour cell. Such combination therapies may also allow the use of lower drug concentrations, thereby limiting the damage to normal cells (see reviews: Baritaki et al., 2007 and Grimm et al., 2009). In addition to causing cell membrane fluidization, hyperthermia treatment causes

vasodilation of local blood vessels and increases oxygenation which, when combined with chemotherapy may result in improved delivery of the drug (Dempsey et al., 2010). Moreover, synergistic effects of compounds able to alter membrane fluidity could also be exerted with cytotoxic drugs or radiation leading finally to apoptotic cell death (Baritaki et al., 2007).

1.7.7. Mild and severe heat stress: the significance of fever

It is important to distinguish between mild (natural and usually beneficial) and severe (mostly destructive) HS. The severity of HS is determined by heat dose, meaning both temperature and exposure time. Furthermore, HS sensitivity varies depending on biological factors, including cell types, tissue origin, developmental stage, a cell cycle phase of the cell line analyzed and the cellular events measured. Thus, the criteria for grading HS should be considered in both their arithmetic and biological aspects. The major difference between the cellular responses to mild and severe HS is adaptation of growth conditions (mild) versus cell death or morbidity (severe) (Park et al., 2005).

The prevalence of fever in modern day members of the 2 major animal divisions, Deuterostomia (vertebrates) and Protostomia (arthropods and annelids), suggests that it must have first appeared approximately 600 millions years ago. The persistence of fever for over 600 million years despite its considerable metabolic cost offers persuasive evidence that it is protective to the infected host (Hasday and Singh, 2000).

It is known that mild hyperthermia alters cellular immune function (Peer et al., 2010). In 2000 Hasday and Singh proposed four ways by which fever might protect the infected host: (i) exposure to fever-like temperatures might be directly cytostatic or cytotoxic or for attacking microbial pathogens, it can shorten disease duration and speed up pathogen clearance; (ii) fever might confer protection during infection by inducing Hsp expression in host cells, it can elevate their resistance to the chemical stresses originated from the infected microenvironment; (iii) fever might defend the infected host by stimulating the pathogens to produce Hsps, many of which are effective activators of host innate immune defences; (iv) fever might ameliorate survival potential during infection by helping to optimize and orchestrate the host immune response through the use of components of the HSR (Hasday and Singh, 2000).

HSF1 has been shown to be involved in the thermal attenuation of the production of cytokines like TNFα (Singh et al., 2000) and the CXC family of chemokines (Nagarsekar et al., 2005). For adaptive immunity, stress proteins are able to chaperone

intracellular peptide antigens, protect them from degradation and transport them from the cell. They might be seen as portable vehicles of immune surveillance and appear to have played a significant role in immunity for long stretches of evolutionary time. In addition, Hsps might be a component of an endogenous immunoregulatory mechanism functioning to control and resolve inflammatory events (Pockley et al., 2008).

1.7.7.1. What could be the sensors of HSR in fever?

Fever appears to be an evolutionarily conserved response to bacterial or viral infection, which implies it may have survival benefits (Peer et al., 2010). It is important to note that the overexpression of Hsps can be activated under mild physiological conditions that are unlikely to cause any protein denaturation in the cell (Saidi et al., 2007; Saidi et al., 2010; Vigh et al., 1998; de Marco et al., 2005). It is noted that phospholipase activation plays a central role both in HSR (discussed above) and inflammation. Since Milton and Wendlandt discovered the pyrogenic activity of prostaglandins of the E series (Milton and Wendlandt, 1970), and Vane found that non-steroidal anti-inflammatory drugs block fever by inhibiting prostaglandin synthesis (Vane, 1971), it has been accepted that fever is mediated by prostaglandins, specifically PGE_2 (Elmquist et al., 1997; Engblom et al., 2002; Ivanov and Romanovsky, 2004) which are synthesized from AA released by PLA_2 from membrane PLs. Moreover, a plethora of data is available in the literature that mammalian MAP kinase signal transduction pathways are activated by both stress (discussed above) and inflammation (reviewed in detail by (Kyriakis and Avruch, 2001).

The sensing of HSR therefore shares certain common mechanisms with inflammation with possible initiation points coupled to the functional changes at cellular membranes. It is conceivable that HS sensor(s) evolved in parallel to the fever response in vertebrates by detecting the elevation of temperature without any recognisable damage to the main cellular functions (e.g. in the absence of protein denaturation), thereby supplying the evolutionary basis for the membrane sensor theory.

Considering its obvious importance in several aspects for living organisms, as shown in this Chapter, the experimental work to be presented in the following sections was planned and carried out to evaluate further the membrane sensor hypothesis.

1.8. AIMS OF THE THESIS

Earlier research on prokaryotes and yeast clearly suggested that during abrupt temperature fluctuations membranes represent the most thermally sensitive macromolecular structures.

The aims of this thesis were to test experimentally the membrane sensor theory in mammalian cells and to explore the mechanisms behind the lipid signals and membrane lipid structural reorganizations leading to heat stress response and adaptation. The experiments to achieve this objective were:

1) To test the membrane sensor hypothesis on K562 mammalian cells comparing the effect of two distinct membrane fluidizer (alcohols and heat stress) on membrane microviscosity and the heat shock response (HSR).
2) To check whether the fluidizers applied at heat shock-inducing conditions act primarily on membranes without effect on protein denaturation.
3) To investigate the Ca^{2+} signals and mitochondrial membrane potential alterations elicited by heat or membrane perturbing agents.
4) To extend the validity of membrane sensor hypothesis to B16(F10) cells and test the induction of major *hsp* genes comparing heat and benzyl alcohol (BA) as stressors.
5) To explore further commonalities in plasma membrane rearrangement through testing the cholesterol-rich domain structure alterations by heat or BA treatment.
6) To systematically map the lipid changes following membrane perturbation caused by heat or BA treatment by means of lipidomic mass spectrometry measurements in order to uncover novel lipid alterations during the initial phase of the stress response.
7) To identity possible lipid signalling pathway elements.
8) To gain further insights into the role of membrane organisation alterations during hyperfluidization-induced stress by different visualization methods which use different reporters regarding structure, charge and localization.

CHAPTER 2. GENERAL MATERIALS AND METHODS

2.1. GENERAL MATERIALS

Most of the chemicals such as solvents, buffers, reagents were from Sigma (Steinheim, Germany) unless otherwise indicated, and were of the best available grade

2.2. CELL CULTURE

K562 (ATCC: CCL-243) human erythroleukemic cells and B16(F10) (ATCC CRL-6475) mouse melanoma cells were cultured in RPMI-1640 medium supplemented with 10 % fetal calf serum (FCS) and 2 mM glutamine in a humidified 5 % CO_2, 95 % air atmosphere at 37 °C and routinely subcultured three times a week.

Cells were plated in $3x10^6$ cell number/10 cm plate and grown additionally for 1 day. For heat shock treatments, the plates were immersed in a water bath set to the indicated temperature (±0.1 °C). For BA treatment, the growth medium was changed to fresh growth medium containing BA at the indicated concentrations.

Because it was found that culture conditions (e.g. cell number, serum quantity) affect lipid composition and metabolism in B16 cells, very careful attention was paid to the above conditions and only cultured for a few passages. Independently-grown samples were used as replicates.

2.3. PROTEIN DETERMINATION

For protein measurement the enhanced bicinchoninic acid (BCA) assay (available in kit form from Pierce, Rockford, Illinois) was applied according to the manufacturers instructions. The absorbtion of the purple-coloured reaction product formed by the chelation of two molecules of BCA with one Cu^{1+} ion was measured at 562 nm. A series of dilutions of bovine serum albumin in the concentration range of 5-250 µg/mL were prepared and assayed in order to determine the standard curve.

2.4. MEMBRANE ISOLATION

Subcellular fractions of K562 cells were isolated based on the method of (Maeda et al., 1980). Cells ($5x10^7$) were harvested by centrifugation (1000 *g*, 5 min) and washed with ice-cold phosphate buffered saline (PBS) twice. All further procedures were carried out at 4 °C. Cells were resuspended in 4 ml TNM buffer (10 mM Tris-HCl pH 7.5, 10 mM NaCl, 1.5 mM $MgCl_2$, 1mM PMSF 2 µM leupeptin) for 5 min. After swelling cells were disrupted with Dounce homogenizer (40 strokes). Intact cell and nuclei were removed by centrifugation (1000 *g*, 5 min). The supernatant were centrifuged (8000 *g*, 15 min) in order to pellet the PM and mitochondrial/lysosomal fraction. The resulting supernatant contains the microsomal fraction. The pellet was resuspended in 8 mL TNM buffer, layered over 36 % sucrose (dissolved in TNM) and centrifuged in a Beckman ultracentrifuge (Beckman L7, Beckman Coulter, Inc.) equipped with SW-41 rotor (90,000 *g*, 2.5 h). The band on sucrose layer (PM fraction) and the pellet (mitochondrial/lysosomal fraction) was removed and resuspended in 8 mL TNM. These two fractions and the supernatant containing the microsomal fraction were centrifuged (100,000 *g*, 40 min). The resultant pellets (PM, mitochondrial/lysosomal fraction and microsomal fraction) were resuspended in 0.5 mL 10 mM Tris, 10 mM NaCl (pH 7.5) for further analysis. Protein content was measured by BCA kit (see above) and lipid content was determined as described in Chapter 4.1.5.

The purity of PM fraction was checked in two representative preparations by enzymatic assays (Table 2.1). The microsomal and mitochondrial fractions were combined and compared with the PM fraction. The activity of marker enzymes of PM (ouabain sensitive Na, K-ATPase), mitochondria (oligomycin sensitive Mg-ATPase) and microsomes (glucose-6-phosphate dehydrogenase) were determined from a portion of these fraction corresponding to 100 µg protein per assay.

Ouabain sensitive Na, K-ATPase activity (PM marker) was assayed as the difference between phosphate (P_i) liberated from ATP after a 10-min time interval (see below). 100 µg protein was incubated in the presence of K^+ (167 mM NaCl, 50 mM KCl, 33.3 mM imidazole, pH 7.2) and in the absence of K^+ but in the presence of ouabain (217 mM NaCl, 33.3 mM imidazole, 1 mM ouabain, pH 7.2) (Kimelberg and Papahadjopoulos, 1974). The reaction was initiated by adding 3.3 mM ATP.

Oligomycin sensitive Mg-ATPase activity (mitochondrial marker) was assayed as the difference between P_i production in the presence and absence of 1 µg oligomycin for 4 min at 30 °C in a total volume of 0.45 mL (10 mM $MgCl_2$, 8.3 mM imidazole buffer,

pH 6.9). For reaction initiation 0.15 mL ATP was then added in a final concentration of 10 mM (Futai et al., 1974). From the difference in P_i production (see below) the oligomycin sensitive activity was calculated.

In the above assays the ATPase reactions were stopped by addition of 100 µL 20 % sodium dodecyl sulfate (SDS). The P_i formed was determined from a 0.1 mL aliquot of the reaction mixture (Baginski et al., 1967). It was mixed with 0.25 mL of reagent A (3 % ascorbic acid in 0.5 M HCl and 0.5 % ammonium molybdate solution) and the tubes were incubated on ice for 10 min. Then 0.5 mL of reagent B (2 % sodium-arsenite, 2 % trisodium citrate and 2 % acetic acid) was added. The colour developed after 10 min at 37 °C was measured at 850 nm (HP 8452A Diode Array Spectrophotometer, Hewlett Packard, USA). The enzyme activities were expressed as nmol P_i/mg prot/min.

Glucose-6-phosphate dehydrogenase (microsomal marker) was assayed in 2.7 mL 55 mM Tris-HCl buffer (pH 7.8) containing 3.3 mM $MgCl_2$ at 30 °C. The reaction was started with 0.1 mL 6 mM nicotinamide adenine dinucleotide phosphate (monosodium salt). The increase in the absorbance difference A_{340} - A_{374} (in dual wavelength mode) resulting from the reduction of NADP to NADPH was recorded for 4 min. The glucose-6-phosphate dehydrogenase activity was expressed as nmol NADP/mg prot/min (an absorption coefficient of 6.0 $mM^{-1} * cm^{-1}$ was used) (Hino and Minakami, 1982).

Table 2.1. The activity of marker enzymes of PM (ouabain sensitive Na, K-ATPase), mitochondria (oligomycin sensitive Mg-ATPase) and microsomes (glucose-6-phosphate dehydrogenase) in the membrane fractions of K562 cells (n=2).

Fraction	Ouabain sensitive Na, K-ATPase[#]	Oligomycin sensitive Mg-ATPase [#]	Glucose-6-phosphate dehydrogenase[##]
Plasma membrane	112.1 ± 21.5	8.2 ± 3.8	7.2 ± 1.9
microsomes+mitochondria	4.2 ± 1.7	75 ± 12.3	23.6 ± 5.4

nmol P_i/mg prot/min, ## nmol NADP/mg prot/min

2.5. FLUORESCENCE ANISOTROPY

In fluorescence anisotropy measurements, the light filtered by a monochromator passes through a vertical polarizing filter and excites fluorescent molecules in the sample tube. Only those molecules that are closely oriented in the vertically polarized plane absorb

light, become excited with the highest probability (called photoselection) and subsequently emit light. The emitted light is measured passing through horizontal and vertical polarizing filters. The anisotropy (r) is defined as the ratio of the polarized components to the total intensity $r=(I_{\parallel} - I_{\perp})/(I_{\parallel} + 2I_{\perp})$. The probability distribution function determines the maximum photoselection and therefore the theoretical maximum anisotropy can be calculated: $r_{max}= 0.4$ for single photon excitation, while r=0 when the emission is completely depolarized (Lakowicz, 2006). The anisotropy reflects the average angular displacement of the probe molecule between the time points of excitation and emission.

The measurement of fluorescence anisotropy is well suitable to estimate certain aspects of the membrane physical state, because the characteristic time constant of the rotational diffusion (rotational correlation time (Φ)) is comparable to the average time the fluorophore (e.g. DPH) stays in its excited state (lifetime (τ)). Based on a model by (Perrin, 1926) derived from the theory of Brownian motion, the rotational correlation time (for a spherical probe) can be estimated as follows: $\Phi= \eta V/RT$, where η = solvent viscosity, T = temperature, R = gas constant and V = molecular volume of the fluorescent probe. Therefore, anisotropy provides information on local viscosities of the fluorophore environment. Furthermore, anisotropy depends on the temperature and molecular volume (and shape) of the fluorophore. The determination of the instrumental response factor (G) and the anisotropy are described in Figure 2.1.

In systems, where the fluorescent probe molecules are dispersed in lipid bilayer membranes, it is expected that the long axis of the rodshaped molecules, like 1,6-diphenyl-1,3,5-hexatriene (DPH) and its analogues, is more or less preferentially aligned along the normal of the membrane. Moreover, the motion of these dipoles expected to reflect closely the motion of neighbouring hydrophobic parts of lipids. The structure of DPH and its derivatives, 1-(4-trimethylammoniumphenyl)-6-phenyl-1,3,5-hexatriene (TMA-DPH) and 1,6-diphenyl-1,3,5-hexatriene propionic acid (DPH-PA) are depicted in Figure. 2.2.

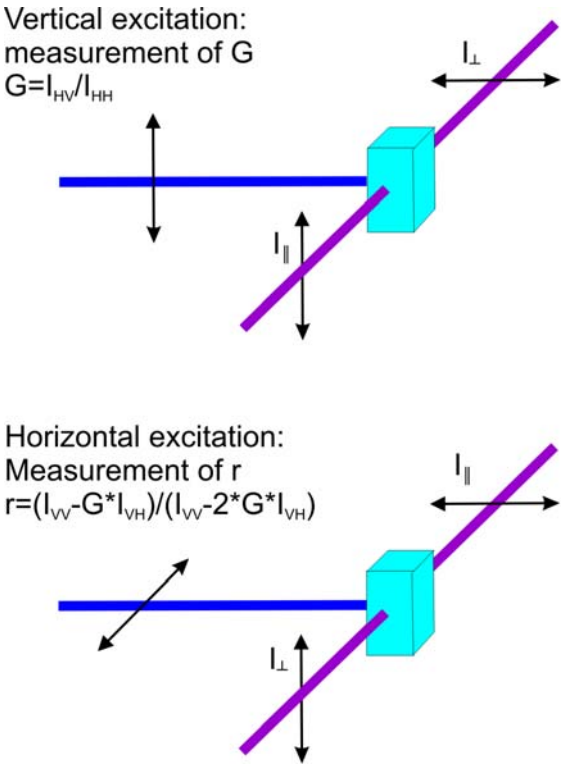

Figure 2.1. Diagram of T-format fluorescence anisotropy measurement. I_{VV} and I_{VH} are the parallel and perpendicular polarized fluorescence intensities measured with the vertically polarized excitation light, I_{HV} and I_{HH} are the same fluorescence intensities measured with the excitation light horizontally polarized, and G is the instrumental correction factor.

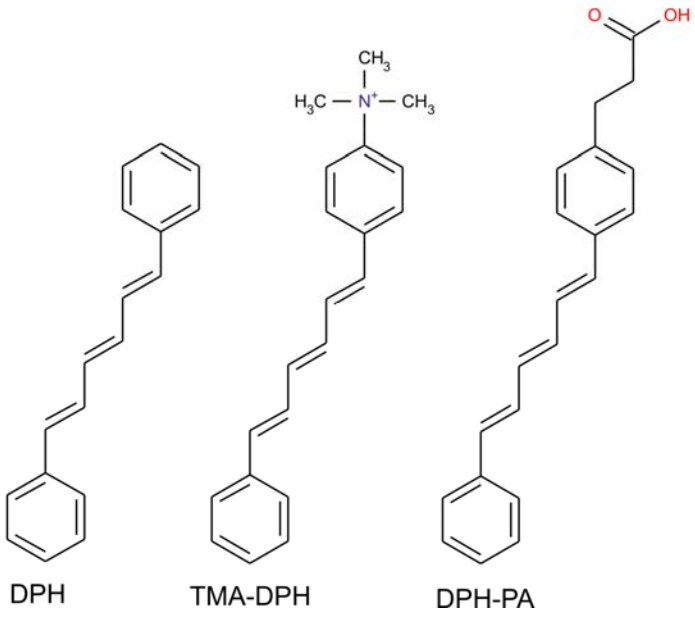

Figure 2.2 Structure of DPH analogues.

2.5.1. Membrane fluidity measurements

The PM fraction of K562 cells was isolated as described above (Maeda et al., 1980). Isolated PMs were labelled in 10 mM Tris, 10 mM NaCl (pH 7.5) or PBS with 0.2 μM DPH or its derivatives, TMA-DPH and DPH-PA, at a molar ratio of about 1:200 probe/phospholipid for 5–10 min. For *in vivo* fluidity measurements, K562 cells were rinsed and resuspended in PBS at OD_{430}=0.1 in the fluorimeter cuvette. The cells were labelled with 0.2 μm DPH for 30 min, or with DPH-PA and TMA-DPH for 5 min (these times are appropriate for the individual probes, (Kitagawa et al., 1991).

Steady-state fluorescence anisotropy was determined in a PTI spectrofluorometer (Quanta Master QM-1, Photon Technology International, Inc., Princeton, NJ, USA). Excitation and emission wavelengths were 360 and 430 nm, respectively (5-nm slits) (Török et al., 1997). The details of the instrument architecture are shown on Fig 2.3. The temperature in the cuvette was followed by a sensor and recorded by computer.

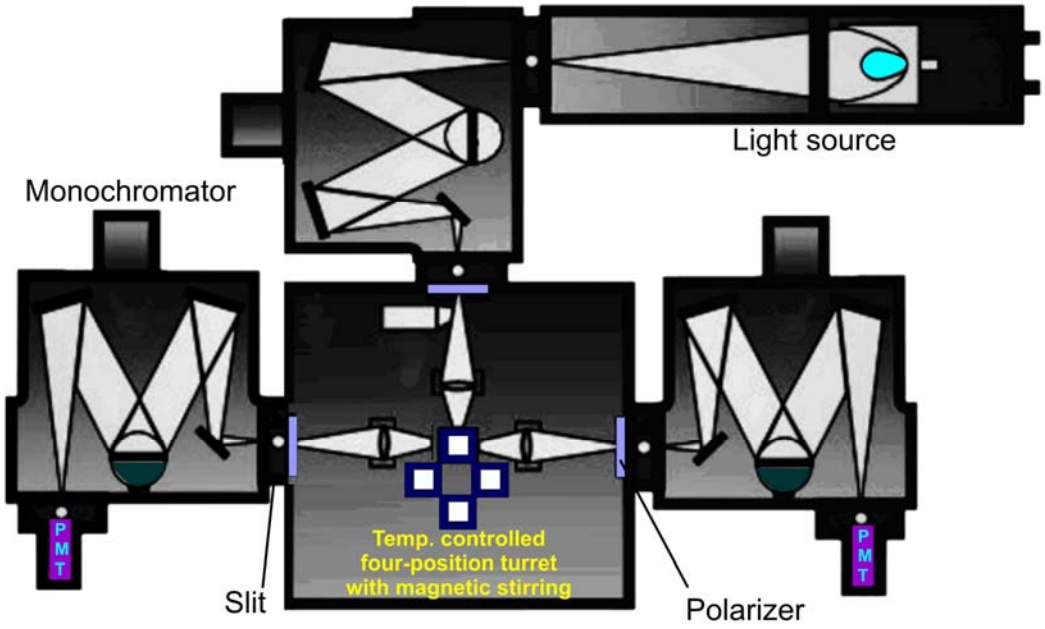

Figure 2.3 Diagram of the Quanta Master T-format spectrofluorometer equipped for steady state fluorescence anisotropy measurement. The temperature of the turret was controlled by a heating and cooling circulating water temperature controller with built-in PID algorithms.

CHAPTER 3. THE HYPERFLUIDIZATION OF MAMMALIAN CELL MEMBRANES ACTS AS A SIGNAL TO INITIATE THE HEAT SHOCK RESPONSE

The experiments presented in this chapter were conceived and designed in collaboration with László Vígh. All experiments, evaluation and statistical analysis were performed by myself, with the following exceptions: Luciferase assays were performed in collaboration with Olivier Bensaude in Paris. Electron microscopy analysis was performed by Zsófia Hoyk. Zsolt Török, Olivier Bensaude, Zsófia Hoyk, Enikő Nagy and Ibolya Horváth took valuable part in the interpretation of results. The paper published from that research was written in collaboration with László Vígh, Ibolya Horváth. The contribution of all co-authors is gratefully acknowledged.

Up to now, most published studies have focused mainly on the cellular responses to severe HS, which causes the unfolding of pre-existing proteins and the misfolding of nascent polypeptides (Sarge et al., 1993). Therefore, it has been proposed that the denaturation of a portion of the cellular proteins during severe heat serves as the primary heat-sensing machinery which triggers the up-regulation of the *hsp* gene expression. Because mild HS is not coupled with the extended unfolding of cellular proteins, it was suggested that it is sensed by a different mechanism (Park et al., 2005). Moreover, many results support the notion that instead of proteotoxicity, an alteration in membrane fluidity may be the first event that detects a change in temperature. Thus, it may be considered as a thermosensor under such circumstances (Carratù et al., 1996; Horváth et al., 1998; Shigapova et al., 2005; Vigh and Maresca, 2002). Fever-range hyperthermia may cause the activation of membrane proteins, e.g. multiple growth factor receptors, by affecting the membrane microdomain structure and mobility (Park et al., 2005). In turn, the activation of growth factor receptors may activate the Ras/Rac1 pathway, which has been shown to play a critical role in HSF1 activation and Hsp up-regulation (Han et al., 2001).

It has been documented that specific alterations in the membrane's physical state for prokaryotes and yeasts, can act as an additional stress sensor (Carratù et al., 1996; Horváth et al., 1998; Shigapova et al., 2005). It was assumed that membrane-controlled signalling events might exist temporarily if a re-adjustment of the membrane hyperstructure is completed after stress (Vigh and Maresca, 2002; Vigh et al., 1998). Here, I furnish the first evidence that chemically-induced perturbations in membranes of K562 erythroleukemic cells, analogous to heat-induced PM fluidization, are indeed capable of activating Hsp production even at normal growth temperatures without

resulting in measurable protein denaturation. I also demonstrate that, similarly to the response to HS, after the administration of membrane fluidizers there are prompt elevations in $[Ca^{2+}]_i$ level and mitochondrial membrane potential, $\Delta\Psi_{m,}$. Thus, it is highly possible that alterations in the PM fluidity, which is affected considerably by environmental stress, are well suited for cells to sense stress. In a wider sense, even subtle changes or defects in the lipid phase of membranes (known to be present under pathophysiological conditions or during aging) should affect membrane-initiated signalling processes that lead to a dysregulated stress response.

3.1. MATERIALS AND METHODS

3.1.1. Cell culture

K562 cells were cultured in RPMI-1640 medium supplemented with 10 % FCS and 2 mM glutamine in a humidified 5 % CO_2, 95 % air atmosphere at 37 °C and routinely subcultured three times a week.

3.1.2. Membrane fluidity measurements

The PM fraction of K562 cells was isolated, labelled and membrane fluidity was measured as detailed in Chapter 2.5. When the temperature dependence of fluidity was followed, the temperature was gradually (0.4 °C/min) increased and the anisotropy data were collected every 30 s.

DPH-labelled membranes were incubated with different concentrations of heptanol (HE) or BA for 5 min at 37 °C, and DPH anisotropy was measured at 37 °C.

For *in vivo* fluidity measurements, K562 cells were labelled with 0.2 μM DPH for 30 min or TMA-DPH for 5 min, (these times are appropriate for the individual probes, (Kitagawa et al., 1991), and incubated further with BA (0–50 mM) or HE (0–6 mM) for an additional 5 min. Steady-state fluorescence anisotropy was monitored (Török et al., 1997).

3.1.3. In vivo protein labelling

Cells (1 mL of 10^6/mL) were treated with various concentrations of BA or HE for 1 h at different temperatures, as indicated in Figure 3.3. The cells were then washed and further incubated in serum-completed medium for 3 h at 37 °C. Next, the medium was changed for 1 mL buffer A (1.2 mM $CaCl_2$, 2.7 mM KCl, 1.5 mM KH_2PO_4, 0.5 mM $MgCl_2$, 136 mM NaCl, 6.5 mM Na_2HPO_4, 5 mM D-glucose) containing 10 μL L-[U-^{14}C]-labelled amino acid mixture (mixture of Ala, Arg, Asp, Glu, Gly, His, Ile, Leu, Lys, Met, Phe, Pro, Ser, Thr, Tyr and Val in water containing 2 % ethanol, Radiochemical Centre, Amersham, Bucks., UK; product code: CFB25, radioactive concentration 50 μCi/mL). The cells were incubated for 1 h at 37 °C, then harvested and resuspended in SDS sample buffer. Proteins were separated by SDS polyacrylamide gel electrophoresis (SDS-PAGE, acrylamide concentration 8 %) and prepared for fluorography.

In fluorography, radioactively-labelled substances emit radiation that excites a scintillator molecule (e.g. 2,5-diphenyloxazole, PPO) that is present in the gel. Upon relaxation to its ground state, the scintillator emits a photon of visible or ultraviolet light that is detected by an X-ray film at low temperature (−80 °C). For PPO incorporation, the gel was soaked in acetic acid for 5 min, then in acetic acid containing 20 % (w/v) PPO for l.5 h. Thereafter the gel was immersed in water containing 5 % glycerol for 30 min, layered over a Whatman 3MM blotting paper (Whatman International Ltd, UK), covered with plastic foil and dried under vacuum in a gel dryer at 70 °C. Finally, the gel was exposed to preflashed X-ray film for one week at -80 °C (Skinner and Griswold, 1983). After development, the *de novo* synthesized proteins could be visualized on the film. The method allowed the sensitive detection of newly produced Hsp70 following stress treatments.

3.1.4. Measurement of intracellular free Ca^{2+} level

Measurement of $[Ca^{2+}]_i$ was performed by applying Fura-2 AM (Molecular Probes, Eugene, USA), a ratiometric dye. The analysis with Fura-2 can usually be performed over a long period of time without significant loss of fluorescence resulting from either bleaching or leakage. The acetoxymethyl ester (AM) derivative of Fura-2 is a membrane-permeant uncharged molecule, therefore it is useful for non-invasive intracellular loading. Inside the cell, the AM group is hydrolysed by non-specific

esterases producing the charged non-membrane-permeant form. Moreover, Fura-2 has a good selectivity for Ca^{2+} over other divalent cations (Grynkiewicz et al., 1985).

K562 cells were washed in buffer A and loaded with 5 mM Fura-2 AM (Molecular Probes, Eugene, USA) at 37 °C for 45 min. They were then washed with buffer A and loaded into the measuring cell at D_{510} = 0.25 at 37 °C and treated with BA or HE or subjected to 42 °C. The fluorescence signal was measured with a PTI spectrofluorometer (Photon Technology International, Inc., South Brunswick, NJ, USA) with emission at 510 nm and dual excitation at 340 and 380 nm (slit width 5 nm). The 340/380 nm excitation ratio (R_{fl}) was directly calculated by the fluorimeter software. The autofluorescence from the cells not loaded with the dye was subtracted from the Fura-2 signal. The Fura-2 leakage at 37 °C was assessed as in (Khaled et al., 2001).

When the contribution of the $[Ca^{2+}]_i$ mobilization was tested, the cells were resuspended in buffer A without Ca^{2+}, but containing 10 mM ethylene glycol tetraacetic acid (EGTA). Following the experimental treatment, the Fura-2 responses were calibrated using the calcium ionophore ionomycin (10 μM) followed by addition of 1 mM $CaCl_2$ to obtain the fluorescence ratio of maximal response, R_{max}. Thereafter, 10 mM EGTA was added to yield the Ca^{2+}-independent fluorescence ratio of Fura-2, R_{min}. $[Ca^{2+}]_i$ was then calculated according to the formula: $[Ca^{2+}]_i = K_d\ [R_{fl} - R_{min})/(R_{max} - R_{fl})]$, where K_d for Fura-2 = 224 nM (Grynkiewicz et al., 1985).

3.1.5. Measurement of mitochondrial membrane potential $\Delta\Psi_m$

Lipophilic fluorescent dyes bearing a delocalized positive charge can be used to measure the membrane potential of the cells because they are membrane permeable and bind to the membranes with low affinity. Cations are attracted to the negative potential across the inner mitochondrial membrane, and thus, they accumulate into the mitochondria in living cells. 5,59,6,69-tetrachloro-1,19,3,39-tetraethyl-benzimidazolylcarbo-cyanine iodide (JC-1) dye is more specific for mitochondrial versus PM potential and more consistent in its response to depolarization than some other cationic dyes such as DiOC6 and rhodamine 123 (Cottet-Rousselle et al., 2011). JC-1 forms a concentration-dependent fluorescent nematic phase consisting of J-aggregates. The monomers emit light at 527 nm and J-aggregates at 590 nm (λ_{ex}= 490 nm). It is known that increasing concentrations of JC-1 above a certain level cause a

linear rise in the J-aggregate fluorescence. The intact mitochondria accumulate JC-1 into the matrix with subsequent formation of J-aggregates (Reers et al., 1991).

$\Delta\Psi_m$ was analyzed as in Khaled et al. (2001) by using JC-1 (Molecular Probes, Eugene, USA). K562 cells (0.5 x 10^6) were incubated with JC-1 (5 μg/mL) during the last 15 min of any treatment in the dark and were immediately analyzed with a FACScan flow cytometer (Becton-Dickinson, USA) equipped with a 488 nm argon laser. Dead cells were excluded by forward and side scatter gating. JC-1 aggregates were detectable in the FL2 (585 ± 21 nm), and JC-1 monomers were detectable in the FL1 (530 ± 15 nm) channel. Data on 10^4 cells per sample were acquired and analyzed with Cell Quest software. The mean fluorescence intensity of J-aggregates was used to determine the $\Delta\Psi_m$. Cells treated with carbonyl cyanide *p*-chlorophenylhydrazone (CCCP), causing quick mitochondrial membrane depolarization, served as positive control.

3.1.6. Estimation of the level of *in vivo* and *in vitro* protein denaturation in response to heat stress and membrane fluidizing alcohols

The heat-induced denaturation of luciferase was described first in 1945 (Johnson et al., 1945). In order to study the effects of HS on proteins, it was suggested to follow the activity of exogenous well characterized enzymes (e.g. firefly luciferase) (Nguyen et al., 1989).

The effects of heat or fluidizer treatment on *in vivo* protein denaturation were followed via measurement of the luciferase activity expressed in HeLa cells as in Qian et al. (2004) using a bioluminescence assay. HeLa cells $5x10^5$/tube were grown in tissue culture tubes in 10% FCS-supplemented DMEM medium. The cells were incubated at 37 °C with 30 mM BA or 4.5 mM HE or at 42 °C for 5, 15, 30 and 45 min. Immediately after treatment, the cells were cooled to 4 °C and lysed. A brief wash with ice-cold PBS was followed by the cell lysis in 0.5 mL of lysis buffer (25 mM H_3PO_4/Tris, pH 7.8, 10 mM $MgCl_2$, 1 % Triton X-100 (v/v), 15 % glycerol (v/v), 1 mM EDTA) containing 0.5 % 2-mercaptoethanol (v/v). The lysates were kept frozen at −20 °C before measurement of luciferase activity. Luciferase activities were determined in a Berthold Lumat 9501 luminometer for 10 s after the addition of substrates (1.25 mM ATP and 87

mg/mL luciferin (Sigma) in lysis buffer) (Nguyen and Bensaude, 1994). For inactivation experiments, the activity before treatment was taken as 100 %.

In vitro protein denaturation was followed using diluted cytosolic fraction of K562 cells. Cells ($5x10^8$) were disrupted by 40 strokes of potter homogenizer in 4 mL buffer-Cyt containing 50 mM Hepes, 150 mM KCl, 20 mM $MgCl_2$ (pH 7.4). The debris was removed by pelleting at 1000 *g* for 5 min. The supernatant was adjusted to 12 mL and centrifuged in Beckman ultracentrifuge equipped with SW-41 rotor (100,000 *g*, 40 min). 250 µL supernatant was mixed with 250 µL buffer-Cyt in the absence or presence of 60 mM BA (final conc. 30 mM) or 9 mM HE (final conc. 4.5 mM). The test tubes were incubated at 37 °C or heat treated at 40, 42 or 44 °C for 1 h. The tubes were cooled on ice for 5 min and centrifuged at 15,000 *g* for 15 min at 4 °C. The supernatant was carefully removed and the pellet was redissolved in solubilisation buffer containing 50 mM Tris-HCl (pH 8.0), 5 mM EDTA, 150 mM NaCl, 0.1 % SDS, 1mM dithiothreitol and 1 % Triton X-100. It should be noted that a small amount of insoluble proteins was formed during 1 h incubation even at 37 °C. The protein content was determined with BCA method against the solubilisation buffer (blank). The level of insoluble proteins after treatments was normalized to the 37 °C control samples.

3.1.7. Electron microscopy

Cells were prepared for electron microscopy according to standard procedures. Briefly, they were fixed with 4 % paraformaldehyde and 2.5 % glutaraldehyde overnight at 4 ^oC then washed in 0.1 M phosphate buffer (pH 7.4) and osmicated in phosphate buffer containing 1 % OsO_4 for 1 h. Following postfixation they were dehydrated and embedded in Araldite. Ultrathin sections were stained with lead citrate and uranyl acetate, then viewed with a Zeiss EM 902 electron microscope (Zeiss, Germany).

3.1.8. Statistics

All data are expressed as mean ± SD (standard deviation). Student's paired *t*-test ($\alpha = 0.05$) with the Bonferroni adjustment was used to compare groups.

3.2. RESULTS

3.2.1. Selection of the critical concentrations of membrane perturbers equipotent in fluidization with temperature upshifts

It has been proposed that the membrane lipid phase plays a central role in the cellular responses that take place during pathological states and acute HS (Carratù et al., 1996; Horváth et al., 1998; Shigapova et al., 2005; Vigh and Maresca, 2002; Vigh et al., 1998). However, direct correlation between the Hsp response and the membrane fluidization of the lipid region has not been unambiguously established for mammalian cells. By intercalating between membrane lipids the two structurally unrelated membrane fluidizers (BA and HE) induced a disordering effect. This was due to weakening the van der Vaals interactions between the lipid acyl chains (Shigapova et al., 2005). As for HS, the initial fluidity elevations caused by these membrane perturbants were followed by a rapid relaxation period *in vivo* (see Chapter 5 for more details). Therefore, isolated membranes were used for detailed comparison and assessment of the levels of the thermally- and chemically-induced primary alterations in the membrane physical orders. As demonstrated in Figure 3.1A, the PM fraction of K562 cells was labelled with DPH and the steady-state fluorescence anisotropy (Carratù et al., 1996; Horváth et al., 1998; Shigapova et al., 2005) was recorded as a function of temperature. In parallel, the fluidity changes were monitored at various concentrations of the two alcohols (Figure 3.1B, C). In such a way, it was possible to determine the critical concentrations of each of the two fluidizers at which their addition to membrane isolates resulted in membrane fluidity enhancements identical to that found after a temperature increase to 42 °C. As highlighted by the arrows in Figure 3.1A–C, PM hyperfluidization resulting from HS at 42 °C (i.e. a reduction of the steady-state DPH anisotropy value by ~ 0.015 units) can be achieved by the addition of 30 mM BA or 4.5 mM HE. The critical concentrations of the membrane perturbers proved to be essentially equipotent in causing membrane hyperfluidization *in vivo* (Figure 3.2). The decrease in the lipid order was monitored in the membrane interior of the K562 cells by following the DPH anisotropy alteration. The fluidizing effects of the alcohols in the glycerol and upper acyl regions were also determined using the charged (not membrane permeable) derivative of DPH, TMA-DPH.

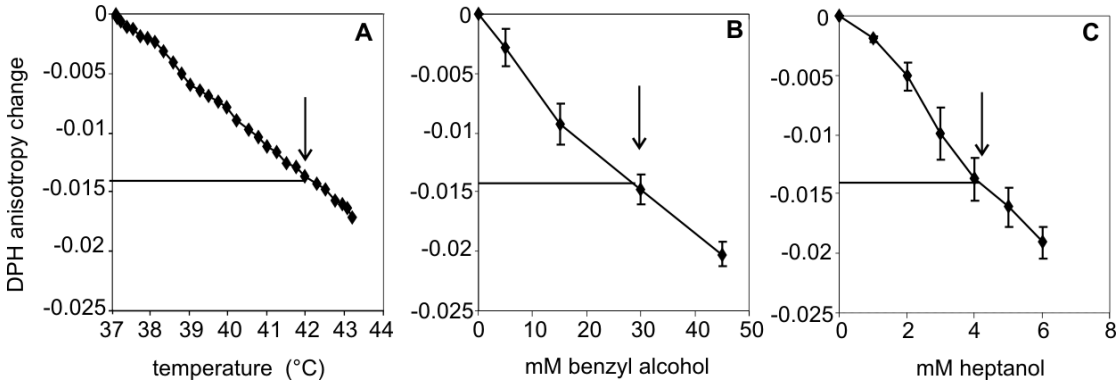

Figure 3.1. Heat stress- or membrane fluidizer-induced alterations in isolated PM fluidity, measured with DPH. Isolated PMs were labelled with DPH and (A) the effects of heat or (B) different concentrations of BA or HE on the steady-state fluorescence anisotropy were detected. The arrows show the concentrations of the alcohols that exert a fluidizing effect equivalent to that caused by exposure to 42 °C. Mean ± SD, n = 4.

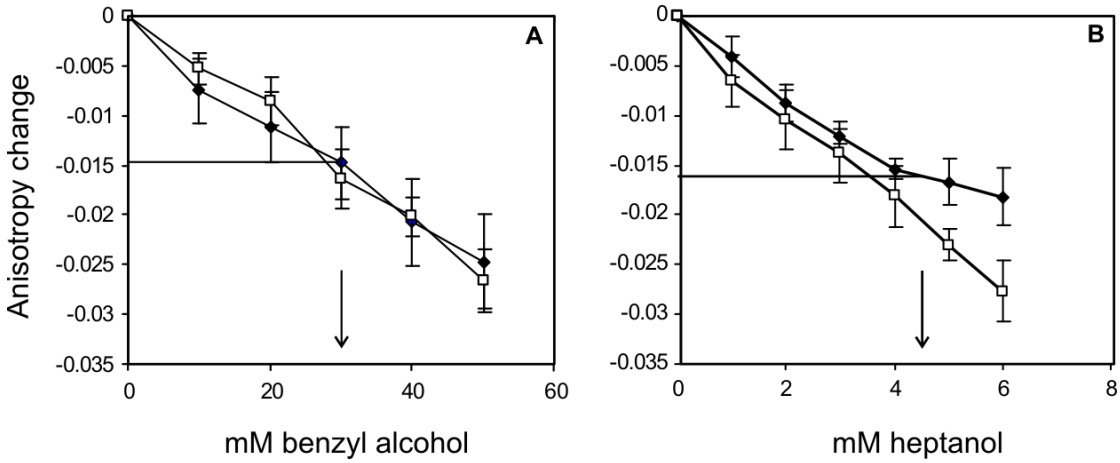

Figure 3.2. Membrane fluidity measurements *in vivo*. K562 cells were labelled with 0.2 μM DPH (◆) for 30 min or TMA-DPH (□) for 5 min, and then further incubated with various concentrations of BA or HE. The fluorescence steady-state anisotropy was measured and the differences from the controls were calculated. The arrows indicate the concentrations of the alcohols at which similar levels of Hsp70 synthesis were detected at 37 °C. Mean ± SD, n = 6.

3.2.2. Membrane fluidizers lower the set-point temperature of Hsp70 synthesis

K562 cells were treated at various temperatures in the presence or absence of different concentrations of BA or HE for 60 min. After a 3-h recovery period at 37 °C, the cells were labelled with a ^{14}C amino acid mixture for 60 min to follow the *de novo*

synthesized Hsp70 level. Co-treatment of the cells with BA or HE during HS resulted in a temperature- and dose-dependent Hsp70 synthesis (Figure 3.3). Apparently, the gradual temperature rise shifted the peak of HSR towards the lower alcohol concentration range. It indicates a cooperative triggering mechanism in the induction of Hsp70 synthesis. The maximum responses at 37 °C were obtained by the administration of 4.5 mM HE or 30 mM BA. These critical fluidizer concentrations were exactly those that resulted in identical PM fluidization levels *in vitro* and *in vivo* (Figures 3.1 and 3.2). In other words, the increase in the PM fluidity as a result either of heat treatment or of chemical perturbations was followed equally by Hsp induction. Similarly to HS, higher doses of BA or HE caused a complete inhibition of protein synthesis. Thus, at 42 °C the highest tolerable concentrations of BA and HE were only 10 and 2 mM, respectively.

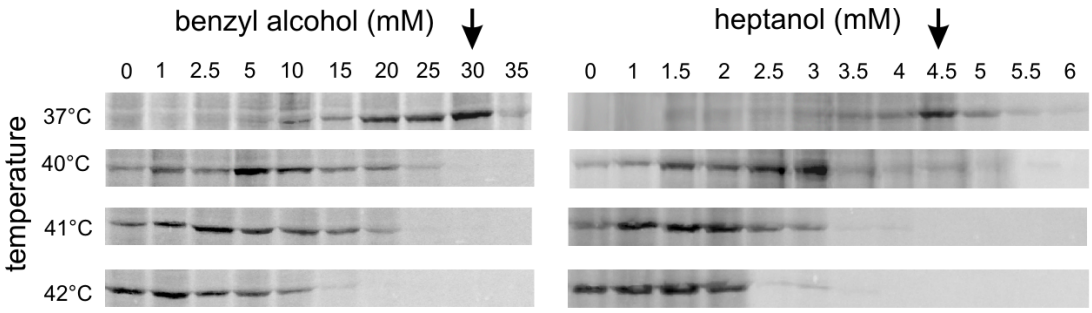

Figure 3.3. Hsp70 induction in K562 cells treated with BA or HE and subjected to HS. Cells were treated with different concentrations of BA or HE for 1 h at various temperatures. After a 3 h recovery period, the cells were labelled for 1 h with L-[U-^{14}C]-labelled amino acid mixture and, after SDS-PAGE, prepared for fluorography. The Hsp70 lane of the fluorograph is shown. The arrows indicate the most effective concentrations of the alcohols at 37 °C.

3.2.3. Effects of heat and membrane fluidizers on the cellular morphology and the cytosolic free Ca^{2+} level

It is known that HS induces distinct morphological alterations in mammalian cells (Welch and Suhan, 1985). In the present study, by the use of electron microscopy, a moderate membrane blebbing was revealed when K562 cells were incubated with 30 mm BA or 4.5 mm HE or heat shocked at 42 °C for 1 h (Figure 3.4). However, no major changes were observed in the ultrastructure of cells after these treatments (Figure 3.4.).

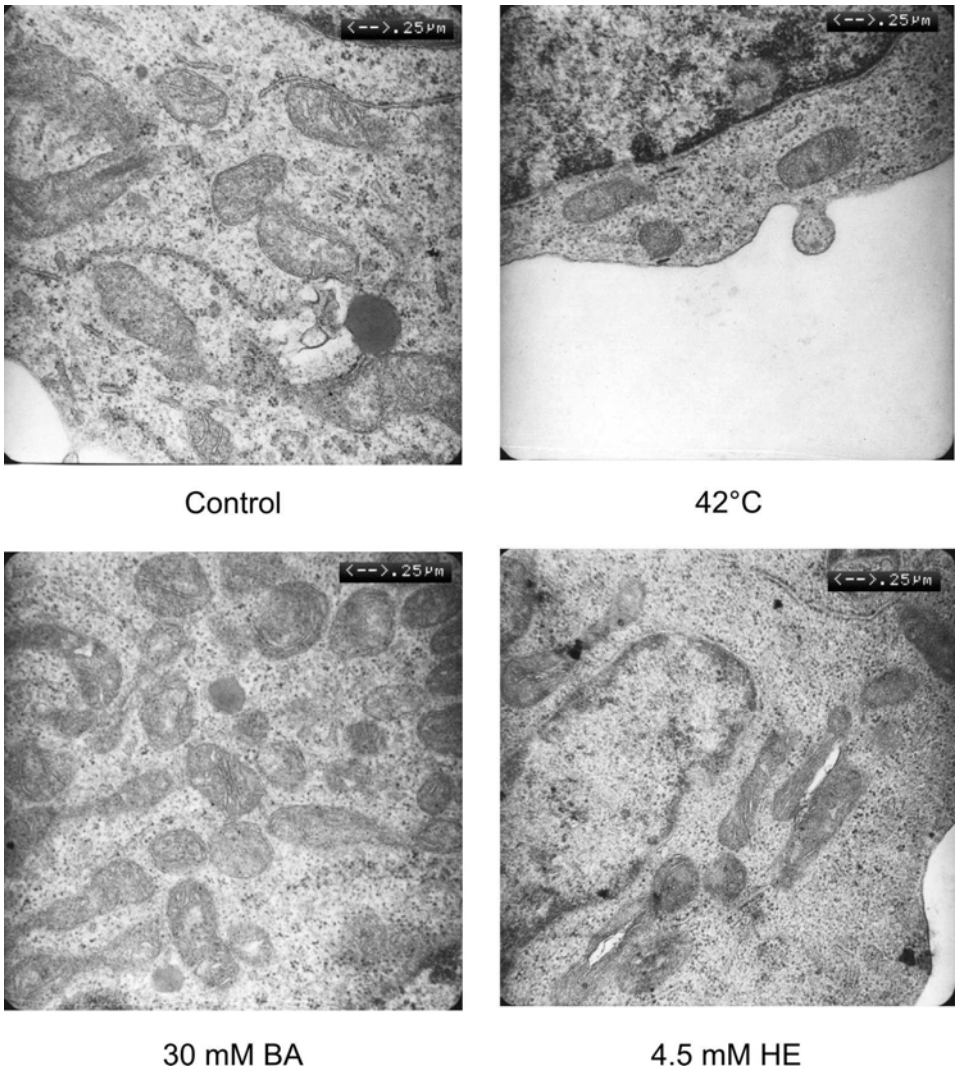

Figure 3.4. Representative transmission electron microscopy images of K562 cells subjected to various stresses for 1 h (42 °C, 30 mM BA or 4.5 mM HE) or left untreated.

It is known that the $[Ca^{2+}]_i$ concentration is a tightly regulated key signalling element of the HSR in mammalian cells. Though it was found that an increase in $[Ca^{2+}]_i$ promoted the synthesis of Hsp70, the overexpression of Hsp70 attenuated $[Ca^{2+}]_i$ elevations (Kiang et al., 1994; Kiang et al., 1998). It was earlier documented that membrane fluidizer anaesthetics may displace Ca^{2+} from external and internal binding sites and modulate the functioning of different Ca^{2+} regulatory systems (Grant and Acosta, 1994; Kültz, 2005). Therefore, changes in $[Ca^{2+}]_i$ after the addition of the membrane fluidizer alcohols were monitored in a dose-dependent manner in order to compare the findings with the $[Ca^{2+}]_i$ increase as a result of HS. Cells were treated with these alcohols (at concentrations equipotent in membrane fluidization and in the induction of Hsp70) and Fura-2 fluorescence was continuously monitored. It was found

that BA and HE enhanced the $[Ca^{2+}]_i$ in a very similar and strictly dose-dependent fashion (Figure 3.5A).

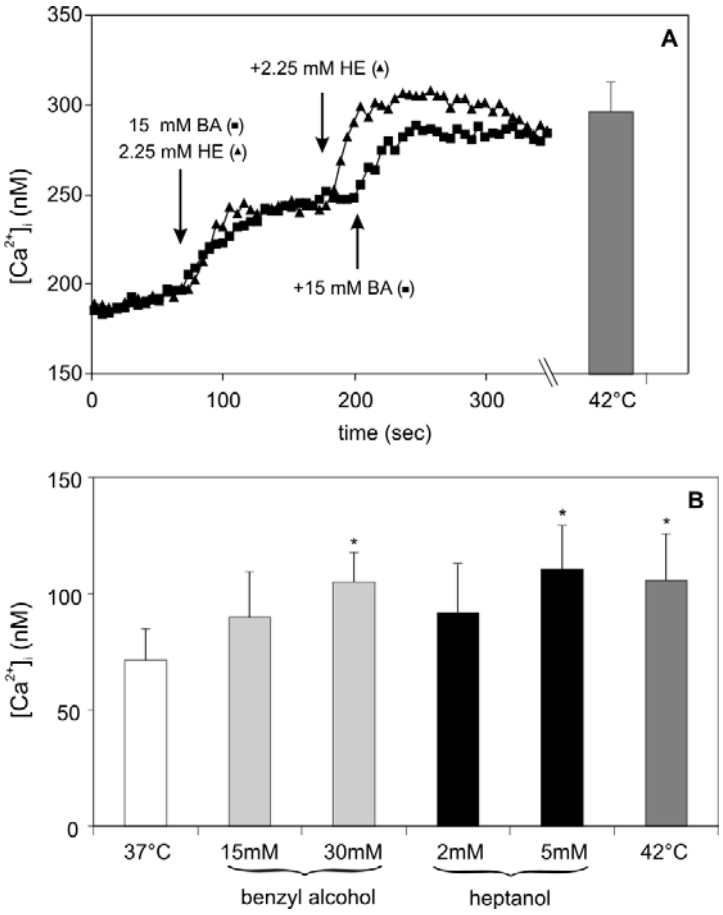

Figure 3.5. $[Ca^{2+}]_i$ increase induced by membrane fluidizers or heat. $[Ca^{2+}]_i$ was measured at 37 °C by using Fura-2 AM. (A) Time course of $[Ca^{2+}]_i$ rise induced in 1.2 mM $CaCl_2$-containing buffer by HE or HE (the arrows show the increase in fluidizer concentration; final concentrations were 30 mM for BA and 4.5 mM for HE) or treatment at 42 °C. (B) $[Ca^{2+}]_i$ in Ca^{2+}-free buffer containing EGTA, measured in samples treated with alcohol or heat for 5 min. Data are presented as mean ± SD, n = 4*p < 0.05 compared with 37 °C control.

$[Ca^{2+}]_i$ rose to its plateau level within ≈ 30 s (from 185 nM to 290 nM for 30 mM BA and from 185 nM to 305 nM for 4.5 mM HE). In case of HS at 42 °C for 5 min, the averaged $[Ca^{2+}]_i$ value is depicted by the bar in Figure 3.5A. It revealed that the HS at 42 °C caused a similar rise in $[Ca^{2+}]_i$ to that produced by the corresponding alcohol doses (at which equal Hsp70 synthesis was reported).

To assess the contribution of intracellular Ca^{2+} mobilization, cells were suspended in a buffer without Ca^{2+}, but containing the Ca^{2+}-chelator EGTA. While the absolute values dropped to about one-third, the pattern of $[Ca^{2+}]_i$, obtained after the addition of

membrane fluidizers or HS, was not affected by the depletion of external Ca^{2+} (Figure 3.5B).

3.2.4. The effects of membrane fluidizers and heat stress on mitochondrial membrane potential ($\Delta\Psi_m$)

It is known that an $[Ca^{2+}]_i$ overload (together with several other stimuli) is able to elicit structural and functional alterations in the mitochondria. Therefore, it was examined whether the strikingly similar alterations in $[Ca^{2+}]_i$ – seen after membrane hyperfluidization elicited either by HS or by equipotent membrane fluidizers – were paralleled by similar tendencies in changes in $\Delta\Psi_m$. A two-dimensional display of JC-1 red vs. green fluorescence demonstrates the changes in $\Delta\Psi_m$ that took place following membrane perturbations (Figure 3.6A). A higher intensity of red fluorescence is assumed to indicate a higher $\Delta\Psi_m$ (hyperpolarization). Cells treated with CCCP served as methodological control for mitochondrial depolarization. Figure 3.6B shows histograms in which $\Delta\Psi_m$ (detected via the J-aggregate fluorescence) is plotted against the number of cells. For HS at 42 °C and fluidizer treatments – besides the equal extent of membrane hyperfluidization together with identical degrees of Hsp70 induction –, very similar increases in $\Delta\Psi_m$ were observed. The quantification of $\Delta\Psi_m$ in response to gradually increasing heat and increasing concentrations of membrane fluidizers is displayed in Figure 3.7. Both membrane hyperfluidization with these alcohols and HS led to the closely similar extent of mitochondrial hyperpolarization.

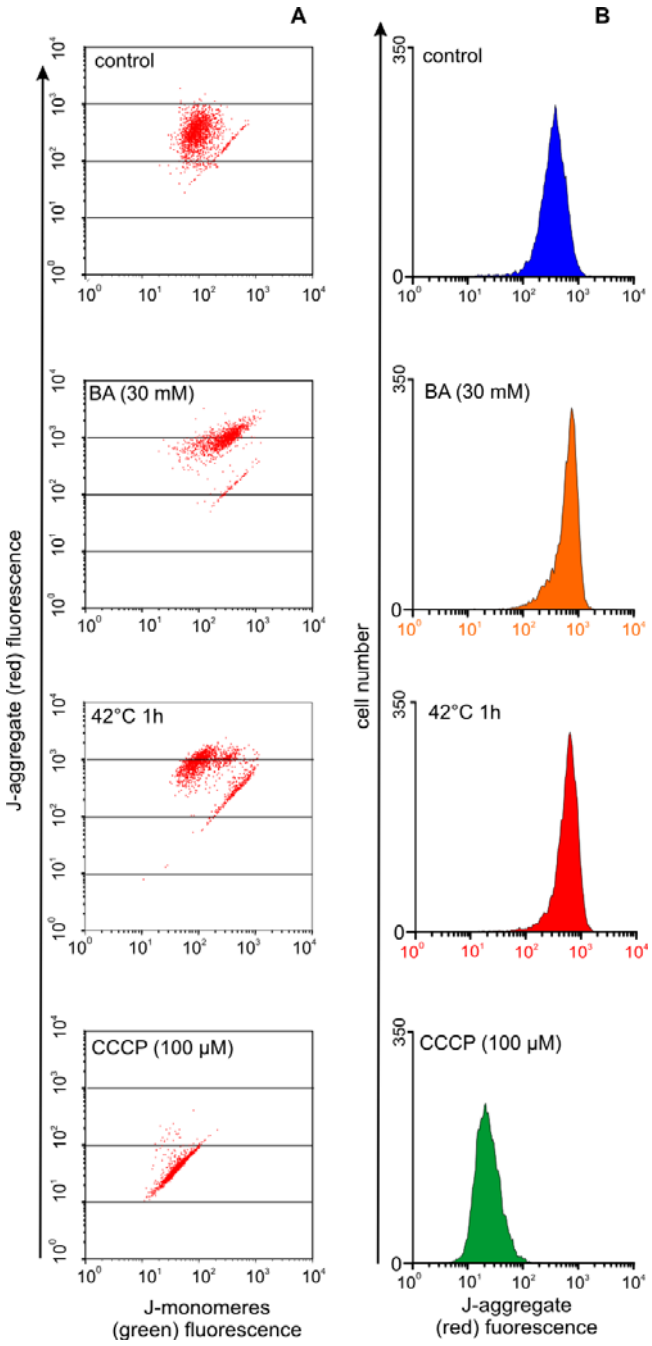

Figure 3.6. Analysis of mitochondrial membrane potential of K562 cells by flow cytometry. Cells were left untreated or treated with BA, heat or CCCP for 1 h as indicated. Cells were then stained with JC-1 and assayed by flow cytometry. (A) Dot plots of JC-1 red fluorescence vs. green fluorescence. (B) Corresponding histograms in which the J-aggregate fluorescence is plotted against the number of cells.

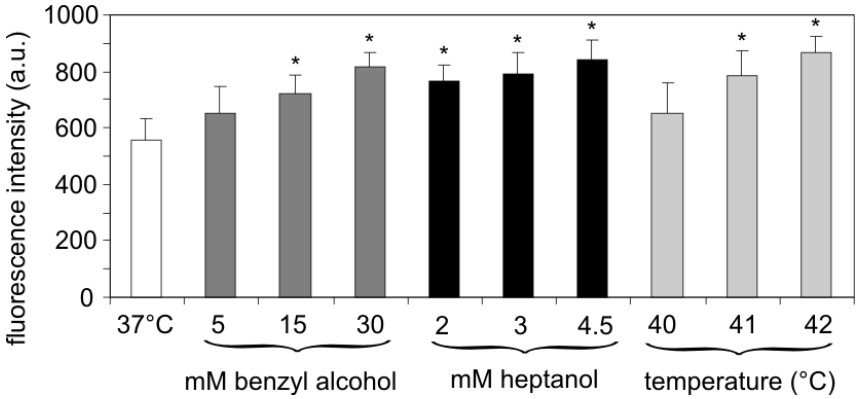

Figure 3.7. Quantitative changes in $\Delta\Psi_m$ caused by gradually increasing HS or increasing membrane fluidizer concentrations. Cell were treated with BA, HE or subjected to HS for 1 h as indicated. The samples were analyzed as in Figure 3.5. The mean fluorescence intensity of J-aggregates was used to determine the $\Delta\Psi_m$. Mean ± SD, n = 4, $*p < 0.05$ compared with control.

3.2.5. The chemical membrane fluidizers exert no measurable effect on protein denaturation

HS can inactivate the firefly luciferase when it is expressed in mammalian cells. The loss of enzymatic activity correlates with the loss of its solubility and can be considered as a direct evidence of protein denaturation. This method served as a sensitive tool for testing the proteotoxicity of Hsp-inducing compounds (Török et al., 2003). In the present study, HeLa cells expressing cytoplasmic firefly luciferase were used. The presence of either 30 mM BA or 4.5 mM HE did not exert a significant effect on luciferase activity when the cells were tested at their growth temperature. However, the loss of enzyme activity was observed in cells exposed to 42 °C (Figure 3.8). The same tendency was noticed in an *in vitro* protein denaturation assay using lysates of K562 cells (Figure 3.9).

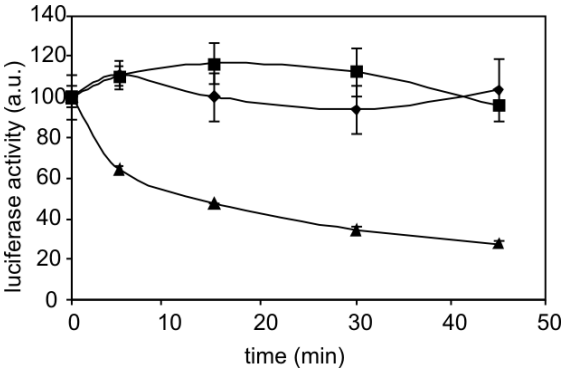

Figure 3.8. *In vivo* protein denaturation assay. The effects of BA, HE or HS treatment on protein denaturation were followed by measurement of the cytosolic luciferase activity expressed in HeLa cells. Cells were treated with 30 mM BA (◆), 4.5 mM HE (■) or submitted to HS at 42 °C (▲). At different time points cells were lysed and analyzed for luciferase activity. Enzyme activity of cells before treatment was taken as 100 %. Data are presented as mean ± SD, n = 3.

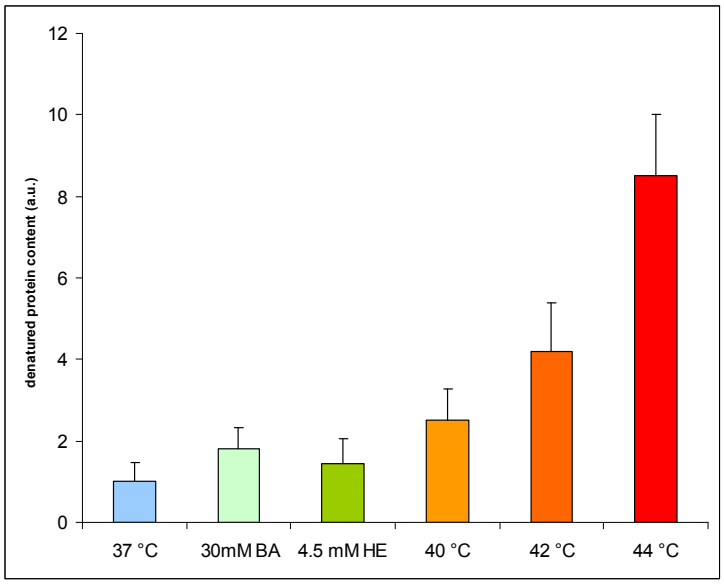

Figure 3.9. *In vitro* protein denaturation assay. The effects of BA, HE or HS on protein denaturation were followed by measurement of insoluble protein content in the cytosolic fraction of K562 cells. Cells were left untreated at 37 °C or treated with 30 mM BA, 4.5 mM HE or submitted to HS at 40 °C, 42 °C or 44 °C for 1 h. The level of insoluble proteins after treatments was normalized to the 37 °C control samples. Data are presented as mean ± SD, n = 3.

3.3. DISCUSSION

In spite of that the importance of Hsps in the pathogenesis of several diseases is well established, our knowledge about stress sensing and signalling that lead eventually to an altered Hsp expression is still very limited (Pockley, 2001). According to an early

observation the majority of the stressors and agents with the ability to induce Hsps proved to be proteotoxic. This finding gave rise to the suggestion that protein denaturation may be the sole initiating signal for the activation of *hsp* genes (Hightower and White, 1981).

In the course of the present study, K562 cells were treated with BA or HE at concentrations that induce a HSR at the normal growth temperature, as highlighted by monitoring of the synthesis of one of the major Hsps, Hsp70. The critical concentrations of the membrane fluidizers were determined so that their addition to the cells resulted in identical increases in the PM fluidity level as it was found after HS at 42 °C. It has been demonstrated that, independently on the origin of the membrane perturbations, the formation of isofluid membrane states is accompanied by an essentially identical HSR in K562 cells. HS at 42 °C or the addition of 30 mM BA or 4.5 mM HE (which are structurally distant compounds) proved equally effective in the up-regulation of Hsp70 production.

At the cellular level Ca^{2+} is derived from internal and external sources. It is proposed that the mechanism by which the fluidizer alcohols and HS altered the Ca^{2+} homeostasis resulted from their action on Na^{+}/Ca^{2+} exchangers and subsequent Ca^{2+} mobilization from different intracellular Ca^{2+} pools (Kiang et al., 1998). Furthermore, lipid rearrangement can induce alterations in membrane permeability, and the altered activity of mechanosensitive ion channels during stress may also promote Ca^{2+} influx into the cytosol (Kültz, 2005). In parallel with the induction of Hsp synthesis, HS and the membrane fluidizer treatments elicited nearly identical rises in $[Ca^{2+}]_i$ both in Ca^{2+}-containing and in Ca^{2+}-free media. It is suggested that the elevation in $[Ca^{2+}]_i$, that occurs as a response to HS, is due to the release of the Ca^{2+}-regulatory compound IP_3 following phosphoinositide-specific PLC activation (Calderwood and Stevenson, 1993). The co-stimulation of phospholipases such as PLA_2 and PLC by HS and the resultant release of lipid mediators could enhance the subsequent membrane association and activation of PKC. In turn, PKC activation can drive the phosphorylation of HSFs (see Chapter 1). In separate studies, elevation in $[Ca^{2+}]_i$ not only stimulated HSF1 translocation into the nucleus, resulting in Hsp70 expression (Ding et al., 1996), but proved to be essential for the multistep activation of HSFs (Price and Calderwood, 1991). Similarly to the results obtained in this study, a sudden $[Ca^{2+}]_i$ rise and an *in vivo* alteration in membrane lipid order after the addition of the calcium ionophore ionomycin have been reported. It was paralleled with the activation of stress-activated

protein kinase, increased HSF–HSE interaction and elevated Hsp70 synthesis (Sreedhar and Srinivas, 2002).

$[Ca^{2+}]_i$ overload elicited by phospholipase activation (or by other mechanisms) is known to cause structural and functional alterations in the mitochondria. In severe cases these include swelling, the disruption of electron transport, mitochondrial depolarization, and the opening of mitochondrial membrane permeability transition pores (Qian et al., 2004). However, from recent papers it became clear that the change in $\Delta\Psi_m$ during cellular attack is not associated exclusively with apoptosis and exhibits a severity-dependent biphasic profile. Instead, mitochondrial hyperpolarization may represent an early and reversible switch in cellular signalling acting as one of the major checkpoints of cell death pathway selection (Perl et al., 2004; Zaragoza et al., 2001). It is important to note that mitochondrial hyperpolarization, when developed e.g. due to the Ca^{2+}overload-activated dephosphorylation of cytochrome c oxidase, was suggested to be a cause of subsequent reactive oxygen species production (Perl et al., 2004). The latter are required to promote the transcriptional activation of the NF-κB pathway leading to a cellular adaptive response that includes proliferation and Bcl-xL-mediated resistance to apoptosis. It was demonstrated recently that, after HS, NF-κB controls the selective removal of misfolded or aggregated proteins via modulating the BAG3-HspB8 complex (Nivon et al., 2012). In accordance with these findings, it was documented in this work that the increase in $\Delta\Psi_m$ may serve as a key event in the stress signalling of K562 cells without causing any sign of apoptosis. An example of the delicate interrelationship between changes in $\Delta\Psi_m$ and HSR is that, disruption of HSF1, while resulting in a reduced Hsp expression, led to elevated $\Delta\Psi_m$ in renal cells (Yan et al., 2005). On the other hand, the overproduction of Hsp70 by HS prevented the H_2O_2-induced decline in mitochondrial permeability transition and the swelling of the mitochondria (Yan et al., 2005).

Previous reports on the regulation of the HSR in different prokaryotic model systems showed that the threshold temperature for activation of the major *hs* genes was significantly lowered by BA treatment (Horváth et al., 1998; Shigapova et al., 2005). BA stress activated the entire set of *hs* genes when the solubility of the most aggregation-prone protein homoserine *trans*-succinylase was tested, but it failed to cause *in vivo* protein denaturation in *Escherichia coli* (Shigapova et al., 2005). The Hsp co-inducer bimoclomol and its derivatives, just like other chaperone inducers and co-inducers, appear to be non-proteotoxic (Qian et al., 2004; Sachidhanandam et al., 2003; Vigh et al., 1997; Yan et al., 2004). It has been proposed that bimoclomol and related

compounds interact specifically with acidic membrane lipids, thereby modifying those membrane domains where the thermally- or chemically-induced perturbation of the lipid phase is sensed and transduced into a cellular signal, leading to elevated *hsp* gene activation (Qian et al., 2004). In the present study, the effects of BA and HE on protein stability at non-HS temperatures were tested via the heat-induced inactivation of heterologously expressed cytoplasmic firefly luciferase in HeLa cells. Neither of the fluidizers exerted measurable effect on protein denaturation. To summarise, the above facts lend further support to the view that, in addition to the formation of denatured proteins, changes in the lipid phase of cell membranes, alone or together with consequent changes in $[Ca^{2+}]_i$ and $\Delta\Psi_m$, may participate in the sensing and transduction of environmental stress into a cellular signal.

It has been documented that shear stress-induced fluidity alterations in endothelial cells are sufficient to initiate signal transduction (Butler et al., 2002), i.e. alterations in PM lipid dynamics can serve as a link between chemical signalling and mechanical force. Indeed, BA was able to mimic the effect of step-shear stress by enhancing ERK and JNK activities. On the other hand, the membrane fluidity reduction by Chol administration resulted in diminished activities of both MAPKs. This finding was attributed to the effect of membrane rigidification on the dynamics of microdomains and subsequent signalling events. Cell activation by shear stress is hypothesized to occur via the lipid modification of integral and peripheral membrane proteins, or signalling complexes organized in Chol-rich microdomains (rafts, focal adhesions, caveoli, etc., see Vereb et al., 2003). Moreover, the phospholipid bilayer was capable of mediating shear stress-induced activation of membrane-bound G proteins, even in the absence of G protein receptors, by changing the physical properties and composition of lipids (Gudi et al., 1998).

The mechanisms highlighted above possibly operate in the present case as well. The heat-induced activation of kinases such as Akt has been reported to increase HSF1 activity. Enhanced Ras maturation by HS was associated with an increase in ERK activation, a key mediator of both mitogenic and stress signalling pathways in response to subsequent growth factor stimulation (Shack et al., 1999). Due to the importance of the PM in linking growth factor receptor activation to the signalling cascade, it is conceivable that any modulation in surface membrane fluidity could significantly influence ERK activation. Indeed, ERK activation in aged hepatocytes was reduced in response to either stressful treatments or proliferative stimuli (Guyton et al., 1998). The level of membrane-associated PKC was also diminished in elderly, hypertensive

subjects (Escribá et al., 2003). It is suggested that this effect is strictly controlled by age-related fluidity changes and the polymorphic phase state of the membranes (Escribá et al., 2003). Thus, strategies aimed at changing the membrane's physical state can be useful to elevate the stress responsiveness in aging cells or under disease conditions such as diabetes, where reduced Hsp levels are causally linked to less fluid, stiffer membranes (Hooper and Hooper, 2005).

Finally, heat and other types of stress are associated not only with changes in the fluidity, permeability, tension or surface charges of membranes, and in protein and lipid rearrangements, but are also coupled with the production of lipid peroxides and lipid adducts (Garbe and Yukawa, 2001). It may be noted that 4-hydroxynonenal, a highly reactive end-product of lipid peroxidation, is an Hsp inducer. It has been proposed to play a significant role in the initial phase of stress-mediated signalling in K562 cells (Cheng et al., 2001).

In conclusion, our results strongly indicate that mammalian cell membranes play a critical role in thermal sensing as well as signalling. The exact mechanism of the perception of membrane stress imposed on K562 cells by BA and HE, coupled with the activation of Hsp expression, awaits further studies. It is reasonable to suggest that changes in the compositions of particular lipid molecular species involved directly in lipid–protein interactions (Vigh and Maresca, 2002; Vigh et al., 1998), the appearance of specific microdomains (Vereb et al., 2003) with an abnormal hyperfluid state or locally formed non-bilayer structures (Escribá et al., 2003), rather than the overall changes in the physical state of membranes, are potentially all equally able to mediate a stimuli for the activation of *hs* genes (Vigh et al., 2005). Very recently a new technology was developed for the direct imaging of PMs of life cells by single molecule microscopy. In the resting state, Chol-dependent homo-association of fluorescent raft markers in the PM of intact CHO and Jurkat T cells was detected, thereby demonstrating the existence of small, mobile, long-lived platforms containing these probes. Furthermore, it was demonstrated that during fever-type HS, which caused Hsp27 induction, the homo-association of the raft markers disappeared in the PM. It revealed, in fact, the role of microdomain reorganization during HSR (Brameshuber et al., 2010).

CHAPTER 4. MEMBRANE CHANGES DURING EARLY STRESS RESPONSES IN A MURINE MELANOMA CELL LINE

I would like to acknowledge the work performed by Enikő Nagy (under my supervision) concerning the stress response of B16 cells (RT-PCR and domain size analysis together with Imre Gombos). These experiments have been included within the introductory section, and experimental details have been incorporated into the Materials and methods section of this chapter. All experiments, evaluation and statistical analysis were performed by myself, with the following exceptions: Cell culturing and stress treatments were done in collaboration with Enikő Nagy and Andriy Maslyanko. Measurements for GC-MS analysis and TLC lipid class separations were performed in collaboration with Mária Péter. ESI-MS analysis was carried out with the help of Gerhard Liebisch in the laboratory of Gerd Schmitz in Regensburg. Data evaluation was performed in collaboration with Gerhard Liebisch and Mária Péter. Zsolt Török, Sándor Benkő and Ibolya Horváth took valuable part in the interpretation of results. The paper published from that research was written by myself and Mária Péter, and critically reviewed by László Vígh, Ibolya Horváth and John L. Harwood. The contribution of all co-authors is gratefully acknowledged.

Recent data show that most anticancer agents provoke apoptosis through changes of membrane fluidity of tumour cells (Baritaki et al., 2007). Numerous potential therapeutic applications, including hyperthermia, directed at such fluidity have been suggested (Baritaki et al., 2007; Grimm et al., 2009; Issels, 2008). Hsps were first identified as stress proteins that confer resistance to environmental stresses such as temperature elevation in all cellular organisms. Elevated Hsp expression promotes cancer by inhibiting the major known apoptosis pathways (Calderwood and Ciocca, 2008) or autophagy (Kirkegaard et al., 2010) and causes resistance to heat- (thermotolerance) or chemotherapy. Therefore, it would be desirable not to increase the intracellular level of Hsps in cancer cells when attempting different antitumour treatments. In contrast, the upregulation of the surface expression of Hsps has been demonstrated to enhance immunogenicity of tumour cells (Horváth et al., 2008). In addition, mild HS may confer radiosensitization of cancer cells probably through effects on membrane structure (Grimm et al., 2009). In this investigation B16(F10) cells (which are a highly metastatic cancer cell line) were used, in order to clarify the role of membrane lipids in this dichotomic feature of thermal stress.

It has been suggested that, during abrupt temperature fluctuations, membranes represent the most thermally-sensitive macromolecular structures (Morenilla-Palao et al., 2009; Yatvin and Cramp, 1993). Thus, alterations in the physical state of

membranes of *Synechocystis, E. coli* or yeast (Carratù et al., 1996; Horváth et al., 1998; Shigapova et al., 2005) have been reported to affect essentially the temperature-induced expression of *hsp* genes. Opposite alterations in membrane fluidity mimic HS or cold activation of different plant MAPK pathways (Sangwan et al., 2002). When *Saccharomyces cerevisiae* was exposed to increased temperatures in the presence of alcohols, the amount of alcohol required decreased as its hydrophobicity increased and the temperature needed for the maximal activation of the *hsp* promoter was diminished (Curran and Khalawan, 1994). In the moss *Physcomitrella patens* it was published that early sensing of mild temperature elevations took place at the PM independently on cytosolic protein unfolding. The heat signal was translated into an effective HSR by a specific membrane-regulated Ca^{2+} influx, and led to thermotolerance (Saidi et al., 2009b). An abrupt H_2O_2 burst occurred in tobacco BY2 cells in response to membrane fluidity increases. It could be triggered by treatment of cells with BA or by HS. This induction of H_2O_2 production was required for the synthesis of sHsps in plants (Königshofer et al., 2008).

In Chapter 3 it has been demonstrated that, irrespective of the origin of membrane perturbations, the formation of isofluid membrane states was accompanied by an essentially identical HSR in K562 cells. The addition of 30 mM BA or HS at 42 °C was found to be evenly effective in the up-regulation of Hsp70 production. The fluidity increase of isolated membranes after BA treatment was identical to that seen during a thermal upshift to 42 °C. The different stressors induced a rapid rise in $[Ca^{2+}]_i$ and caused mitochondrial hyperpolarization to a similar extent as well (Balogh et al., 2005). However, the precise mechanism of BA-induced stress protein signalling through membrane perturbation remained unresolved.

It was shown that several membrane intercalators possessing a small polar headgroup as a common denominator, such as Cer(18:1/16:0) or hexadecanol (Alanko et al., 2005), not only gave rise to bulk membrane hyperfluidization but also possessed the ability to displace Chol from pre-existing Chol/SM microdomains. It is noteworthy that a membrane intercalator molecule such as deoxycholic acid was also found to activate raft-associated growth factor receptors in a ligand-independent manner (Jean-Louis et al., 2006). Overall, the importance of Chol as a key component of the regulation of signal transduction through membrane lipid-ordered microdomains is well established (Vigh et al., 2007a; Zeyda and Stulnig, 2006).

In order to learn more about the details of the mechanism of action of BA and HS, the induction of *hs* genes due to stress treatments was followed in B16 cells. To assess

the initial expression changes, the mRNA levels of *hsp70*, *hsp25*, *αB-crystallin*, *hsp90*, and *hsp105* were determined immediately after exposure of cells to increasing concentrations of BA (35–46 mM) or subject to heat (41 °C or 42 °C) (Figure 4.1). BA treatment resulted in elevation in the levels of *hsp70* and *hsp25* mRNAs, which peaked at 40 mM. The *hsp70* amount was higher than that of *hsp25* in BA-treated cells. It was in contrast to that seen after mild heat exposure at 41 °C (i.e., less *hsp70* than *hsp25*). Interestingly, the expressions of other *hsp* family members were not enhanced in the BA-treated samples under the same conditions. Overall, the membrane fluidizer BA induced a distinct HSR at the growth temperature, which manifested by increases of mRNA levels of only two *hsp* classes.

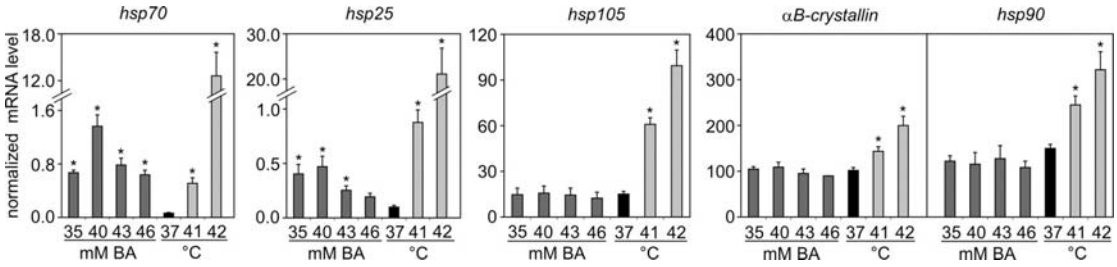

Figure 4.1. Effects of BA on *hsp* gene mRNA levels. B16(F10) cells were left untreated (37 °C) or treated with BA at the indicated concentrations or exposed to heat for 1 h. *Hsp* mRNA levels were followed immediately after the treatments by quantitative real-time RT-PCR. The amounts of *hsp70*, *hsp25*, *hsp105*, *αB-crystallin*, and *hsp90* mRNAs were determined and normalized to 10^3 *β-actin*. The data are shown as mean ± SEM, n = 3–15, **p* < 0.05 compared with control as analyzed by Student's unpaired *t*-test with the Bonferroni adjustment.

In parallel, possible rearrangements of membrane microdomains were recorded. It was recently shown that a non-toxic fluorescent probe, fluorescein ester of polyethylene glycol-derivatized cholesterol (fPEG-Chol), specifically recognizes sterol-rich membrane domains and is co-localized with various raft markers (Sato et al., 2004). Unlike filipin and other Chol probes, this agent could be added as an aqueous dispersion to various samples. When applied for intact mammalian cells, fPEG-Chol was distributed only in the outer PM leaflet (Sato et al., 2004). Therefore, it was expected that the monitoring of fPEG-Chol-labelled structures may provide information about the alterations in the dynamics of Chol-rich domains in B16 cells due to different stress conditions. B16(F10) cells treated with 40 mM BA, or exposed to HS (41 or 43 °C) were incubated with fPEG-Chol, and the labelled 'spots' were visualized by confocal microscopy. The detected domains were separated into six classes on a diameter basis (Figure 4.2).

When the cells were exposed to heat, a characteristic rearrangement of the membrane microdomains was observed (Figure 4.2). In response to more severe HS (43 °C), the number of smaller domains decreased, while the larger domains piled up. The amplitude of the effects observed was proportional to the temperature: the effect of mild heat (41 °C) showed the same tendency, however, these changes were not significant. A very similar result was seen after the addition of BA, with the exception of a domain classified into the range 1100–1900 nm, where BA promoted an obviously larger elevation. In other words, equally to severe HS, the Chol-rich surface membrane microdomains fused into larger platforms upon the administration of BA.

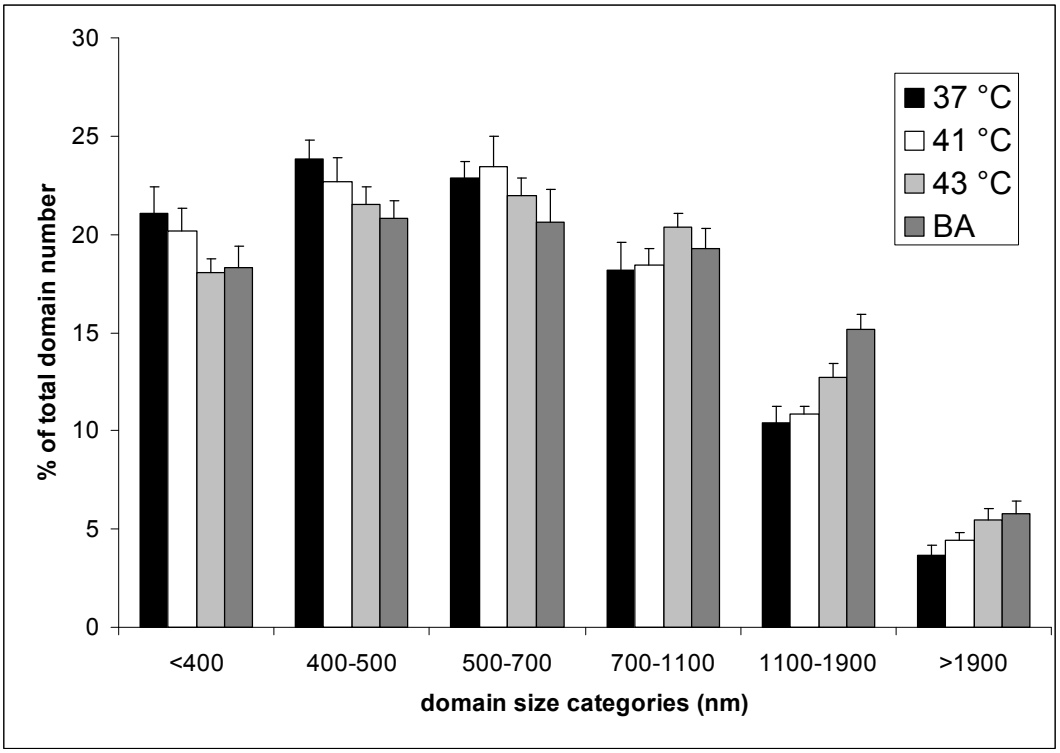

Figure 4.2. Redistribution of Chol-rich membrane domains on the surface of B16(F10) cells monitored by fluorescence microscopy. Cells were left untreated at 37 °C, heat-stressed at 41 °C or 43 °C or treated with 40 mM BA for 1 h. They were then labelled with fPEG-Chol for 20 min and imaged. The domain size distribution was determined. The data shown are mean values ± SEM, n = 3. Samples treated at 43 °C and with BA differed from the control (37 °C) significantly ($p < 0.05$) as analyzed by the Kolmogorov–Smirnov test (for details see Materials and methods).

These results suggest that a distinct reorganization of Chol-rich microdomains may also be required for the generation and transmission of sufficient stress signals to activate *hsp* genes. Furthermore, it is reasonable to propose that the mode of action of the Hsp inducer BA may be analogous to shear stress. Hemodynamic shear stress, an

important determinant of vascular remodelling and atherogenesis, was able to enhance Hsp expression under isothermal conditions in response to balloon angioplasty, acute hypertension or advanced lesions of atherosclerosis. The Hsp70 expression induced by mechanical stress has been shown to be regulated by the small G proteins Ras and Rac through PI3K (Xu et al., 2000). Active Rac1 can bind preferentially to Chol-rich membranes. The binding step is determined specifically by the physical state and composition of membrane lipids (del Pozo et al., 2004). Analogously, moderate HS induced membrane translocation of Rac1 and membrane ruffling in a Rac1-dependent manner, in parallel with the activation of HSF1 and an increased Hsp expression (Han et al., 2001).

The above described data fully supported the paradigm shift toward the "membrane sensor" hypothesis that membranes can act as temperature sensors (Escribá et al., 2008; Vigh et al., 2005; Vigh et al., 2007a; Vigh et al., 2007b). It is well established that numerous lipid mediators released following different stresses can serve as stress-response modulating factors. Thus, HS induced elevations in inositol phosphate levels which were comparable in magnitude to those achieved after stimulation with growth factors. It indicates that HS might initiate transmembrane signalling cascades with potential importance in cellular regulation (Calderwood and Stevenson, 1993). Common cellular responses to growth factors and heat include feedback modulation of PLC by its products and the parallel stimulation of PLA_2 activity (Calderwood et al., 1993).

It was reported that extracellular exposure of HeLa cells to AA induced *hs* gene transcription in a dose-dependent manner via acquisition of phosphorylation and DNA-binding activity of HSF1. Moreover, addition of AA in low concentrations to the cells lowered the temperature threshold for HSF1 activation showing that increased *hs* gene expression can be a direct consequence of an AA-mediated cellular response (Jurivich et al., 1994).

This part of my thesis work was aimed at systematically mapping the lipid changes after membrane perturbation elicited by heat or fluidizer treatment in order to identify any novel lipid alterations during the initial phase of the stress response. These data can highlight the possible links between different microdomain reorganizational and lipid compositional changes in membranes that lead to the generation of stress signals.

4.1. MATERIALS AND METHODS

4.1.1. Materials

Methyl arachidonyl fluorophosphonate (MAFP), U-73122, tetrahydrolipstatin (THL, also referred to as orlistat), RPMI-1640 medium and Hanks' balanced salt solution were purchased from Sigma (Steinheim, Germany). Calcein AM was from Molecular Probes (Eugene, OR, USA), 1-palmitoyl-2-[1-^{14}C]oleoyl-phosphatidylcholine was from DuPont NEN Research Products (Boston, USA) and the Flo Scint II scintillation cocktail was from PerkinElmer (Waltham, Massachusetts, USA). Lipid standards were obtained from Avanti Polar Lipids (Alabaster, AL, USA). fPEG-Chol (Sato et al., 2004) was a generous gift from Toshihide Kobayashi (RIKEN Discovery Research Institute, Saitama, Japan). The solvents used for extraction and for mass spectrometric analyses were of gas or liquid chromatographic grade and BA of analytical grade was from Merck (Darmstadt, Germany). All other chemicals were purchased from Sigma and were of the best available grade.

4.1.2. Inhibitors

The inhibitors were dissolved in ethanol in the mM concentration range and kept at −80 °C. Upon usage this solution was added to the serum-free medium so that the final inhibitor concentrations were 10 μM for MAFP, 30 μM for THL and 5 μM for U-73122. The final concentration of ethanol was 0.1 % or less and this concentration had no detectable effect on growth or metabolism.

4.1.3. Cell culturing and treatments

B16(F10) (ATCC CRL-6475) mouse melanoma cells were cultured in RPMI-1640 medium supplemented with 10 % (v/v) fetal bovine serum and 4 mM L-glutamine at 37 ºC. Cells were plated in $3x10^6$ cell number/10 cm plate and grown additionally for 1 day. For ESI-MS studies, the cells were treated in the plates. Thus, for HS experiments, the plates were immersed in a water bath set to the indicated temperature (±0.1 °C). For BA treatments, the growth medium was changed to fresh growth medium containing 40 mM BA. After 1 h, the cells were scraped into 2 mL ice-cold water and extracted. To

measure AA release, the cells were first scraped, resuspended in 12 mL serum-free medium containing 0.5 % FA-free BSA and treated by BA or heat as above. At the indicated time points, 2 mL aliquots (about $3x10^6$ cells) were taken out and immediately extracted. For inhibitor studies, the cells were resuspended in a small amount of serum-free medium, divided into equal parts ($6x10^6$ cells/experiment), diluted to 2 mL with serum-free medium containing the inhibitor at the appropriate concentration and incubated at 37 ºC. After 20 min, 2 mL serum-free medium containing the inhibitor (at the appropriate concentration with 1 % FA-free BSA) was added to the reaction flasks to control and heat-shocked samples and, for BA treatments, the medium contained additional BA to a final concentration of 40 mM. The treatments were applied for 60 min. The reactions were stopped by placing the flasks on ice and the reaction mixture was immediately extracted for lipids.

Because it has been observed that culture conditions (e.g. serum quantity, cell number) affect lipid metabolism and composition in B16 cells, very careful attention was paid to the above conditions and cells were cultured only for a few passages. Independently-grown samples were used as replicates.

4.1.4. Lipid extraction

Lipids were extracted according to a modified Folch procedure (Folch et al., 1957). Briefly, to 2 mL portions of cell suspensions in water or serum-free medium, 5 mL methanol (containing 0.001 % butylated hydroxytoluene as antioxidant) and 2.5 mL chloroform were added to form one phase (chloroform:methanol:water (1:2:0.8, by vol.)). The mixture was left at room temperature for 1 h with periodical vortexing. 7.5 mL chloroform and 1.75 mL 0.2 M KCl were then added for phase separation to occur (final composition of chloroform:methanol:water (2:1:0.75, by vol.)). After vortexing, the sample was centrifuged at 600 *g* for 10 min and the lower chloroform phase, containing lipids, was evaporated and the residue was redissolved in chloroform:methanol (2:1, by vol.).

4.1.5. GC-MS analysis of lipid classes

Qualitative and quantitative analyses of total lipid extracts for further ESI-MS studies were carried out by a gas chromatography-mass spectrometry (GC-MS) system (GCMS-QP2010, Shimadzu) equipped with a BPX-70 capillary column (10m x 0.1 mm

ID, 0.2 μm film thickness). One tenth of the extracts was methylated in 1 mL 5 % acetyl chloride in methanol at 80 °C for 2 h in the presence of C15:0 fatty acid (FA) as internal standard. The resulting fatty acid methyl esters (FAME) were extracted with hexane, the solvent was evaporated and the residue redissolved in 50 μL benzene. A 1 μL aliquot was injected onto the column maintained at 150 °C for 2 min, programmed at 6 °C/min to 215 °C, then at 20 °C/min to 235 °C and maintained isothermally for 2 min. Identification and calibration of FAMEs was made by comparison with authentic standards and confirmed with NIST (National Institute of Standards and Technology, Gaithersburg, MD 20899-8380 USA) MS library spectra.

For AA release and inhibitor studies, the extracted lipids were separated on Kieselgel 60 silica gel TLC plates (20 x 20 cm, Merck) using hexane:diethylether:acetic acid (50:50:2, by vol.). The main lipid classes were identified using authentic standards and visualized with 8-anilino-naphtalene-1-sulfonate (0.05 % in methanol) under UV. For the spots of interest (i.e. total polar lipid fraction (TPL), diacylglycerol (DAG), monoacylglycerol (MAG) and free (non-esterified) fatty acid (FFA)), a known amount of C15:0 FFA was added as an internal standard for quantitation. The spots were scraped and the scrapings were directly methylated and analyzed as above. Phospholipid class analyses were carried out similarly except that the lipids were separated using chloroform:methanol:glacial acetic acid:water (60:40:2:2, by vol.).

Quantitative analysis of MAG was carried out by silylation in the presence of C15:0 FFA as internal standard. MAG was recovered from the TLC plates by adding 1 mL chloroform:methanol (1:1, by vol.) to the scrapings. After centrifugation the supernatant was evaporated, the residue redissolved in 50 μL benzene followed by addition of 5 μL *N,O*-bis(trimethylsilyl)acetamide and kept at room temperature for an hour. A 1 μL aliquot of the resulting trimethylsilyl ether derivative of MAG was injected onto a BPX-1 capillary column (10m x 0.1mm x 0.1μm film thickness) programmed at 15 °C/min from 150 to 320 °C, and maintained isothermally for 3 min. Identification of MAG species was made on the base of spectra presented in (Isidorov et al., 2007). Quantitation was calibrated in the presence of an authentic MAG (1-18:0-MAG) standard.

Both the methyl esters and silyl ether derivatives were analyzed on GC-MS by using the selected ion monitoring mode in order to obtain more precise and reliable data. In this method, instead of detection of total ion chromatograms, a limited number of fragment ions are recorded by the MS. For FAMEs, the fragment ion series was selected to include the main fragments of the individual FA groups, but to exclude

known ions from the background main impurities. Based on this idea, fragment ions m/z 74, 87, 81, 67, 83, 79, and 91 for FAMEs, m/z 75 for dimethyl acetals (formed from plasmalogen species) as well as m/z 73, 103, 129, 147 and 419 for trimethylsilyl ether derivatives of MAG were chosen. This improvement led to two important advantages, i.e. a ca. 10-fold increase in sensitivity as well as avoidance of overquantitation of a given peak due to co-eluting impurities (Figure 4.3).

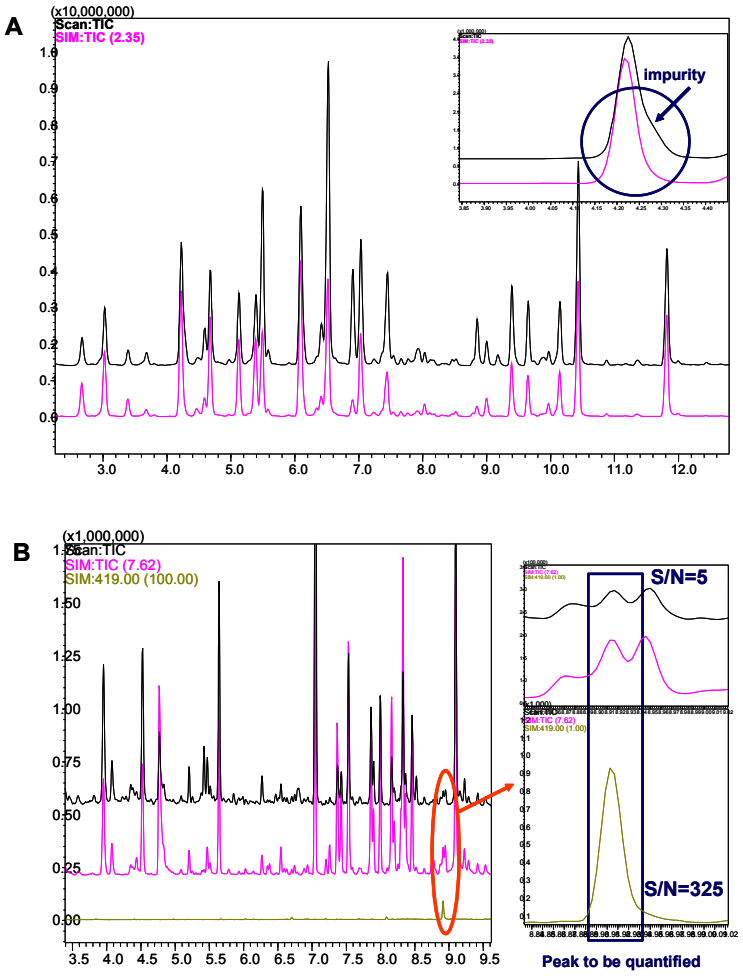

Figure 4.3. Advantages of the application of selected ion monitoring mode in GC-MS. Representative chromatograms are shown to demonstrate (**A**) avoiding overquantitation caused by a co-eluting impurity peak and (**B**) increased sensitivity, i.e. signal-to-noise ratio (S/N). Total ion chromatograms (Scan: TIC) are drawn in black, while selected ion chromatograms (SIM: TIC) in pink and green.

4.1.6. Quantitative analysis of lipid classes using ESI-MS/MS

Lipid molecular species were analysed by electrospray ionization tandem mass spectrometry (ESI-MS/MS) in positive ion mode (Brügger et al., 1997) applying a triple

quadrupole mass spectrometer (Quattro Ultima, Micromass, Manchester, UK). The following lipid classes were measured: diacyl and 1-alkyl-2-acyl species of phosphatidylcholine (PC and PC-O), lysophosphatidylcholine (LPC), diacyl phosphatidylethanolamine (PE), 1-(1*Z*-alkenyl)-2-acyl species of PE (PE-P), phosphatidylglycerol (PG), cardiolipin (CL), phosphatidylinositol (PI), phosphatidylserine (PS), sphingomyelin (SM), ceramide (Cer), cholesterol (Chol) and cholesteryl ester (CE). To quantify these lipid classes, specific lipid molecular species in chloroform were added as internal standards to the total lipid extract as follows: PC(14:0/14:0), PC(22:0/22:0), PE(14:0/14:0), PE(20:0/20:0) (di-phytanoyl), PS(14:0/14:0), PS(20:0/20:0) (di-phytanoyl), PG(14:0/14:0), PG(20:0/20:0) (di-phytanoyl), CL(14:0/14:0/14:0/14:0), PI(16:0/16:0), LPC(13:0), LPC(19:0), Cer(d18:1/14:0), Cer(d18:1/17:0), deuterated D7-Chol, CE17:0 and CE22:0. The mixture was dried under nitrogen and redissolved in methanol:chloroform (3:1, by vol.) containing 10 mM ammonium acetate at a concentration of 40 µg FA/mL of the total lipid extract. 20 µL of this solution was injected and data were acquired for 1.3 min.

Samples were quantified by direct flow injection using the analytical setup and the data analysis algorithms as described previously (Liebisch et al., 2004). A precursor ion scan of m/z 184 specific for phosphocholine-containing lipids was used for PC, SM (Liebisch et al., 2004) and LPC (Liebisch et al., 2002). Neutral loss scans of m/z 141 and m/z 185 were used for PE and PS, respectively (Brügger et al., 1997). Fragment ions of m/z 364, 380 and 382 were used for the plasmalogen PE species containing 16:0, 18:0 and 18:1 in the *sn*-1 position, respectively (Zemski Berry and Murphy, 2004). Ammonium-adduct ions of PG and PI were analysed by neutral loss scans of m/z 189 and 277, respectively (Matyash et al., 2008). Chol and CE were quantified after acetylation using a fragment ion of m/z 369 (Liebisch et al., 2006). Sphingosine (d18:1)-based Cer were analyzed by product ion of m/z 264 similar to a previously described method (Liebisch et al., 1999). After identification of relevant lipid species, selected reaction monitoring analysis was performed to increase precision of the analysis for the following lipid classes: PE, PE-P, PG, PI, PS, LPC, Cer, CE.

Quantification was achieved by calibration lines generated by the addition of naturally-occurring lipid species to cell homogenates (Leidl et al., 2008). All lipid classes were quantified with internal standards belonging to the same lipid class, except SM (PC internal standard) and PE-based plasmalogens (PE internal standards). Calibration lines were generated for the following naturally-occurring species: PC(34:1), (36:2), (38:4), (40:0) and PC(O-16:0/20:4); SM(d18:1/16:0), (d18:1/18:1),

(d18:1/18:0); LPC(16:0), (18:1), (18:0); PE(34:1), (36:2), (38:4), (40:6) and PE(P-16:0/20:4); PS(34:1), (36:2), (38:4), (40:6); Cer(d18:1/16:0), (d18:1/18:0), (d18:1/20:0), (d18:1/24:1), (d18:1/24:0); Chol, CE 16:0, 18:2, 18:1, 18:0. These calibration lines were also applied for uncalibrated species, as follows: concentrations of saturated, monounsaturated and polyunsaturated species were calculated using the closest related saturated, monounsaturated and polyunsaturated calibration line slope, respectively. For example PE(36:2) calibration was used for, PE(36:3), PE(36:4); PE(38:4) calibration was used for PE(38:3) and PE(38:5) and so on. Alkyl ether PC species were calibrated using PC(O-16:0/20:4) and PE-based plasmalogens were quantified independent from the length of the ether linked alkyl chain using PE(P-16:0/20:4).

4.1.7. Annotation of lipid species

Lipid species were annotated according to the updated comprehensive classification system for lipids (Fahy et al., 2009). For glycerophospholipids, the "Headgroup(*sn*-1/*sn*-2)" format specifies one or two radyl side chains where the structures of the side chains are indicated within parentheses, e.g., PC(16:0/18:1). In cases where the glycerophospholipid total composition was known, but side chain regiochemistry was unknown, abbreviations, such as PE(36:1), were used to indicate total numbers of carbons and double bonds for all chains. Presence of an alkyl ether linkage typically at *sn*-1 of glycerol was represented by an "O-" identifier (also referred as plasmanyl species), as in PC(O-34:1), whereas "P-" denotes a 1*Z*-alkenyl ether (vinyl ether) linkage typically at the *sn*-1 position (also referred as plasmenyl species or plasmalogens), as in PE(P-16:0/18:1). Lysophospholipids were specified with a letter "L" in the abbreviation, for example, LPC(16:0).

For sphingolipids, first the number of hydroxyl groups (e.g., "d" for the two hydroxyls of sphingosine and sphinganine), the number of carbon atoms and then the number of double bonds are indicated followed by the *N*-acyl chain composition, such as SM(d18:1/16:0).

4.1.8. Multidrug resistant (MDR) activity

Malignant cells are often resistant to a wide range of hydrophobic cytostatic chemicals which may seriously impair the effectiveness of tumour chemotherapy. The main feature of these multidrug resistant (MDR) cells is an energy-dependent outward

transport of drugs by multidrug transporter proteins such as MDR1. It was demonstrated that hydrophobic acetoxymethyl ester (AM) derivatives of various fluorescent indicators, such as Fura-2, Fluo-3 or calcein, are actively extruded from cells by MDR1 (Homolya et al., 1993).

Calcein AM, a non-fluorescent hydrophobic molecule, rapidly penetrates the cell membrane. In the cytoplasm it is readily cleaved by non-specific endogenous esterases into the fluorescent free acid form of the indicator, which becomes trapped due to its hydrophilic character. In MDR1-expressing cells calcein AM is extruded by the multidrug transporter before its intracellular conversion to the free calcein. However, when this calcein AM extrusion is blocked by an agent that interferes with the MDR1 pump activity, the non-fluorescent calcein AM rapidly accumulates. Based on these findings a calcein assay has been proposed to discriminate between drug resistant and drug sensitive cells (Homolya et al., 1996). Furthermore, it was shown that the decrease in dye accumulation rate correlates both with the level of MDR1 expression and drug resistance (Homolya et al., 1996). It provided the opportunity for the quantitative determination of the MDR1 function. If dye extrusion is entirely blocked by an MDR inhibitor (e.g. verapamil), the difference between the dye uptake rates before and after the addition of inhibitor reflects the MDR1 pumping activity. In order to avoid alterations arising from different experimental conditions, the MDR1 activity factor (MAF) was expressed as a dimensionless parameter: MAF = (F* -F)/F*, where F* and F designates the dye accumulation rates in the presence and absence of an MDR1 inhibitor, respectively. Because calcein AM was found to be a high-affinity substrate of the MDR1 transporter (Homolya et al., 1993), the calcein accumulation assay was suggested to give an overall reflection of the cellular multidrug resistance. The theoretical value of MAF ranges between 0 and 1. A MAF value <0.2 can be regarded as MDR negative, while MAF value >0.25 is indicative of positive MDR activity (according to several commercially available MDR Quantitation Kits, e.g. Sigma, Chemicon).

To find out whether MDR activity could be responsible for the ineffectiveness of certain phospholipase inhibitors (see in the Results section), calcein assay measurements were performed according to Homolya et al. (1996). B16 cells were trypsinized and then washed and resuspended in Hanks' balanced salt solution containing 0.25 μM calcein AM at a concentration of $2x10^5$ cells/mL. As MDR inhibitors sodium orthovanadate (500 μM) or verapamil (100 μM) were used. The fluorescence signal was followed at 37 °C with gentle stirring in a PTI

spectrofluorometer (Photon Technology International, Inc., South Brunswick, NJ, USA) with emission at 515 nm and excitation at 493 nm (slit width 5 nm). Calibration of dye concentration was based on the measurement of free calcein fluorescence in the same instrument under identical conditions. MAF was calculated from the dye accumulation rates in the presence and absence of verapamil, respectively.

4.1.9. PLA_2 activity in vitro

In order to prove the potency of MAFP as a PLA_2 inhibitor, PLA_2 *in vitro* activity was assayed according to Hayakawa et al. (1993) with slight modifications.

4.1.9.1. Cell lysate preparation

B16 cells ($5x10^7$) were mixed with 500 µL lysis buffer: 10 mM Hepes pH 7.5, 1 mM EDTA, 0.34 M sucrose and protease inhibitors (1 mM benzamidine, 1 mM phenylmethylsulphonyl fluoride, 1 mM caproic acid). The sample was vortexed and sonicated at 0 °C for three periods of 30 sec with a 30 sec pause between each period and then centrifuged at 100,000 *g* (at 4 °C), for 40 min. The supernatant was assayed for PLA_2 activity (see below).

4.1.9.2. Lipid preparation

1-Palmitoyl-2-[1-^{14}C]oleoyl-phosphatidylcholine, PC(16:0/18:1[1-^{14}C]), 28 nmol (1.5 µCi) in toluene:ethanol (1:1, by vol.)) was dried and resuspended in 2 mL PLA_2 assay buffer (400 µM Triton X-100, 100 mM Hepes pH 7.5, 1 mM $CaCl_2$, 0.1 mg/mL fatty acid-free BSA, 2 mM DTT) and mixed micelles were created by repeated vortexing and heating in hot water until the solution clarified.

4.1.9.3. PLA_2 assay conditions

The total volume of the assay was 560 µL (450 µL mixed micelles and 110 µL cell lysate); for inhibitor experiment MAFP (final concentration 10 µM) was also added. The cell lysate was incubated with substrate for 80 min at 40 °C. Then the reaction mixture was extracted and separated on Kieselgel 60 silica gel TLC plates (20 x 20 cm, Merck) in hexane:diethylether:acetic acid (85:25:2, by vol.) as described above. It was expected that the isolated PLA_2 in the cell lysate supernatant should preferentially

hydrolyse the radioactive PC(16:0/18:1[1-^{14}C]) in the *sn*-2 position resulting in the formation of radioactive 18:1[1-^{14}C] FFA and non-radioactive LPC(16:0), and – depending on the conversion rate – non-reacted radioactive PC. Authentic FFA and PC standards were run on both sides of the TLC plate. Sample spots at the height of these standards were scraped and the scrapings were redissolved in 500 µL hexane:isopropanol (3:2, by vol.) to recover the released FFA and unchanged PC (both should possess radioactivity). 10 mL Flo Scint II scintillation cocktail was added to the samples and the mixtures were counted in a Wallac 1409 Liquid Scintillation Counter (Wallac, Turku, Finland) for 2 min. Inhibition was calculated by comparison of radioactivity in the presence and absence of MAFP.

4.1.10. Quantitative real-time RT-PCR

RNA was isolated by using the NucleoSpin RNA II kit (Macherey-Nagel, Duren, Germany). Two micrograms of RNA was reverse-transcribed through use of the RevertAid H Minus First Strand cDNA Synthesis kit (Fermentas, St. Leon-Rot, Germany). *Hsp70* (Mm01159846s1), *hsp25* (Mm00834384_g1), *hsp90* (Mm00658568_gH), *hsp105* (Mm00442865_m1), *αB-crystallin* (Mm00515567_m1), and *β-actin* (Mm00607939s1) primers with TaqMan probes were purchased from Applied Biosystems (Foster City, CA). TaqMan Universal PCR Master Mix (Applied Biosystems) was used to prepare the reaction mixtures. The PCR runs were performed in a Rotor-Gene 3000 instrument (Corbett Research, Sydney, Australia). Relative quantities of mRNAs were normalized to *β-actin*.

4.1.11. fPEG-Chol labelling, confocal microscopy, and domain size analysis

B16(F10) cells were heat stressed at 41 °C or 43 °C or treated with 40 mM BA for 1 h. They were then incubated with 0.2 µM fPEG-Chol for 20 min as in (Sato et al., 2004). After fPEG-Chol staining, the cells were washed and imaged with an Olympus Fluoview 1000 microscope (Melville, NY) by using the 488-nm argon ion laser line for the excitation of fluorescein. Pictures were taken with a resolution of 1,600 x 1,600; the final magnification was x300. The freeware ImageJ software (http://rsbweb.nih.gov/ij/) was used for selecting areas of images for domain size analysis. Subsequently, a fast

Fourier transform (FFT) bandpass filter (5–100 pixel) was applied to get rid of noisy background. CellProfiler (www.CellProfiler.org) was used for detecting, segmenting and measuring objects which corresponded to fluorescently-labelled domains. The analysed domains were sorted into classes according to diameter. The ranges were selected by taking into account that the number of larger domains are less than that of smaller ones. Therefore, the domain size intervals were determined on an exponential basis by increasing the interval lengths by a factor of 2 to include sufficient number of domains into the individual ranges. Diameters were calculated as $2X(N_{pix}/\pi)-2$, where X is the size of a pixel in nanometres, and N_{pix} is the number of pixels covering the actual domain. A representative image of how the data was captured and processed is shown in Figure 4.4.

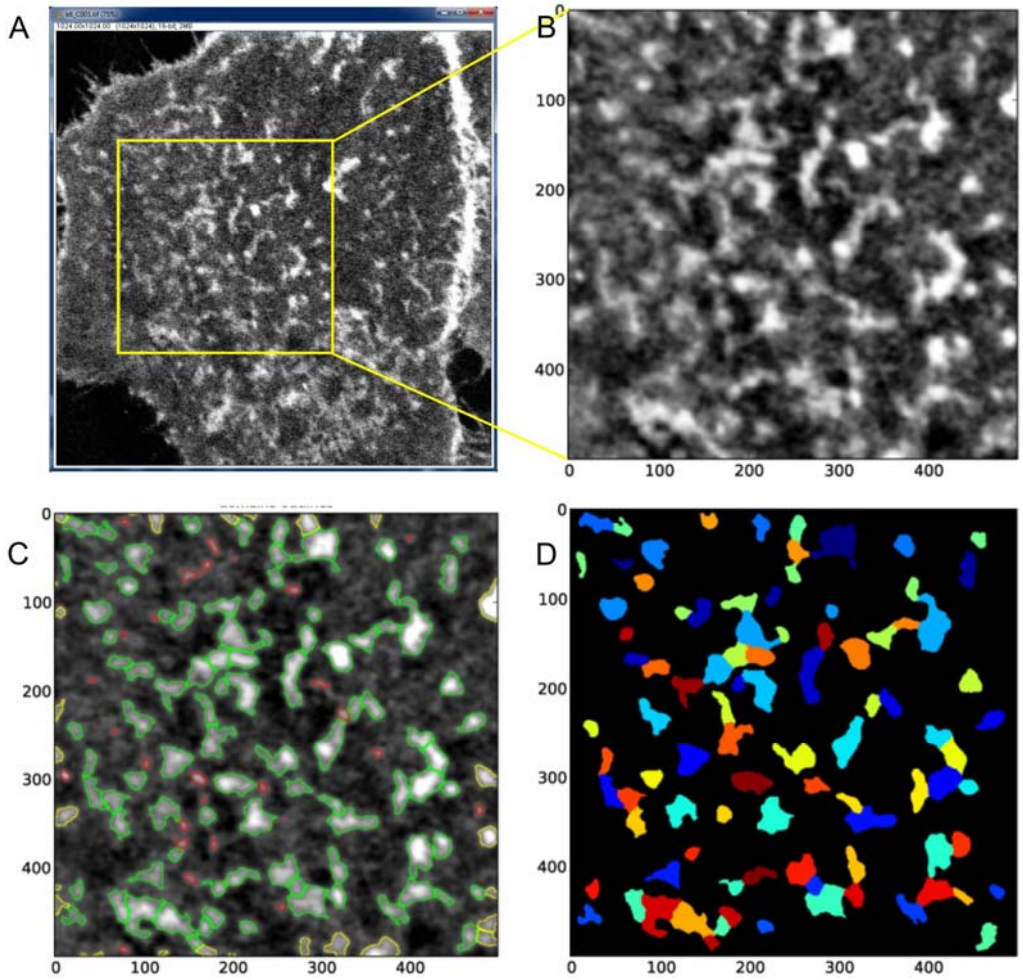

Figure 4.4. Representative images of data processing for domain size distribution analysis. (**A**) Original confocal image of a B16 cell labelled with fPEG-Chol. (**B**) A FFT bandpass filter was applied on the previously selected area. (**C**) Domains detected and outlined by CellProfiler software. (**D**) RGB identification of detected domains.

4.1.12. Statistics

Correction of isotopic overlap and quantification of lipid species were performed by self programmed Excel Macros for all lipid classes according to the principles described previously (Liebisch et al., 2004). For all lipid species those data are presented which accounted for above 1 mol % of the corresponding lipid class for at least one treatment group. ESI-MS results are shown as mean ± SD of four independent experiments. The statistical analysis was performed according to Storey and Tibshirani (2003) measuring statistical significance calculating the *q* values based on the concept of the false discovery rate. The goal is to identify as many significant changes in lipidome as possible, while keeping a relatively low proportion of false positives. The *q* value is similar to the well-known *p* value, except it is a measure of significance in terms of the false discovery rate rather than the false positive rate.

For enzyme inhibition studies, data obtained for individual lipids, such as AA or 20:4-MAG and 20:4-DAG were normalized to the TPL content. Results are presented as means ± SD of five independent analyses. Student's *t*-test with the Bonferroni correction was used for statistical analysis.

Principal Component Analysis (PCA) was performed by PAST software (Hammer et al., 2001). Data for each molecular species were centred to the controls and normalized with the geometric mean of the SD's as follows:
$y_{i,j} = x_{i,j}\text{-mean}(x_{37c,j})/\text{SQRT}((\text{SD}(x_{37c,j})^{2+}\text{SD}(x_{41C,j})^{2+}\text{SD}(x_{43C,j})^{2+}\text{SD}(x_{BA,j})^2)/4)$, where *i* is the index of the individual experiments for the *jth* molecular species.

For PLA_2 assay and MDR activity measurements, data are presented as means ± SD of three independent analyses and compared with Student's *t*-test.

For the analysis of *hsp* gene mRNA levels, data are expressed as mean ± SEM (standard error of mean). Student's paired *t*-test ($\alpha = 0.05$) with the Bonferroni adjustment was used to compare groups.

Because from the point of view of possible microdomain rearrangements following various stresses, it is not the significance of the individual domain size ranges, but far more the alterations in the domain size distribution that counts. In statistics, the Kolmogorov–Smirnov test (K–S test) is a non-parametric test for the equality of one-dimensional probability distributions that can be applied to compare two samples (two-sample K–S test). Therefore, it was well suited for comparison of domain size distributions under control and stress conditions. The two-sample K–S statistic is one of the most useful and general non-parametric methods for comparing two samples,

as it is sensitive to differences in both location and shape of the empirical cumulative distribution functions of the two samples.

4.2. RESULTS

4.2.1. Characterization of the B16 lipidome

For quantitative and comprehensive characterization of B16 cells' lipidome, two mass spectrometric methods were used. FA profiling of B16 cell total lipid extracts using GC-MS (Table 4.1) showed a ratio of saturated:monounsaturated:polyunsaturated FAs (SFA:MUFA:PUFA) of about 45:43:12. However, this ratio was essentially different for the individual phosphoglyceride classes. Though PC, PI and PS contained high amounts of SFA (ca. 45-55 %), in PC this was predominantly palmitic acid, while in PI and PS stearic acid. The larger proportions of PUFAs in PE and PI (20 %) compared to PC and PS were also remarkable. For PE, n-3 and n-6 PUFAs were fairly evenly distributed, while the PUFAs in PI were dominated by AA. The n-3 PUFAs, docosapentaenoic and docosahexaenoic acids, were significant in PS and PE but very low in PI and PC. Although oleate was present in similar amount in all phosphoglyceride classes (about 27 %), PC contained significant levels of hexadecenoate also. Interestingly, in view of their shared biosynthetic pathways, the acyl compositions of PC and PE were quite different.

Lipid class analysis (Figure 4.6 and Table 4.2 (at the end of the Chapter)) demonstrated a ratio of PC to ethanolamine-containing PLs of around 2:1. Plasmalogens accounted for about 40 mol % of PE species and they were almost exclusively detected in PE in B16 cells. Anionic PLs represented ca. 15 mol %, with PI and PS being the most predominant ones, whereas the total amount of detectable SL species was much lower, at about 3 mol % of TPL fraction. The Chol/TPL ratio was 0.16.

Molecular species information about different lipid classes is presented in Table 4.2. Combining molecular species data with the FA profiles, the main species in PC was 34:1, probably mainly 16:0/18:1. In PE 36:2 (mainly 18:1/18:1), in PS 36:1 (mainly 18:0/18:1) and in PI 38:4 (mainly 18:0/20:4) dominated.

Table 4.1. Percentage composition of major FAs in B16 cells

	Total FA	PC	PE	PS	PI
14:0	1.5 ± 0.7	2.2 ± 0.2	0.6 ± 0.1	1.3 ± 0.4	1.2 ± 0.3
16:0	25.3 ± 0.3	39.2 ± 1.0	10.4 ± 0.5	10.5 ± 0.9	14.4 ± 0.4
16:1 n-9	2.5 ± 0.5	4.1 ± 0.1	0.9 ± 0.2	0.9 ± 0.2	1.1 ± 0.1
16:1 n-7	3.9 ± 0.6	5.5 ± 0.2	2.5 ± 0.2	1.9 ± 0.2	1.9 ± 0.2
18:0	12.2 ± 1.9	5.9 ± 0.7	9.9 ± 0.8	37.4 ± 1.7	27.8 ± 1.4
18:1 n-9	27.2 ± 1.0	27.6 ± 0.5	26.8 ± 0.3	27.2 ± 1.4	26.8 ± 0.7
18:1 n-7	7.1 ± 0.5	7.1 ± 0.3	7.2 ± 0.5	6.1 ± 0.4	7.5 ± 0.3
18:2 n-6	1.0 ± 0.1	1.1 ± 0.1	0.9 ± 0.1	1.0 ± 0.3	0.9 ± 0.0
20:0	0.4 ± 0.1	0.4 ± 0.1	0.3 ± 0.1	1.4 ± 0.2	0.0 ± 0.2
20:3 n-9	2.1 ± 0.4	0.9 ± 0.1	3.4 ± 0.0	0.5 ± 0.1	4.4 ± 0.3
20:3 n-6	0.9 ± 0.1	0.7 ± 0.0	1.2 ± 0.0	1.6 ± 0.1	0.4 ± 0.4
20:4 n-6	3.8 ± 0.2	1.2 ± 0.1	5.0 ± 0.5	0.8 ± 0.0	12.5 ± 1.2
20:5 n-3	0.4 ± 0.1	0.3 ± 0.0	0.9 ± 0.1	0.4 ± 0.0	0.1 ± 0.0
22:5 n-3	1.7 ± 0.1	0.8 ± 0.1	3.4 ± 0.1	2.5 ± 0.2	0.5 ± 0.1
22:6 n-3	2.0 ± 0.2	0.9 ± 0.1	4.2 ± 0.3	3.4 ± 0.4	0.5 ± 0.1
24:0	0.8 ± 0.1	1.2 ± 0.1	0.0 ± 0.0	3.0 ± 0.3	0.0 ± 0.0
16:0 DMA	3.3 ± 0.1	0.6 ± 0.0	9.8 ± 0.6	0.0 ± 0.0	0.0 ± 0.0
18:0 DMA	1.7 ± 0.2	0.3 ± 0.0	5.3 ± 0.4	0.0 ± 0.0	0.0 ± 0.0
18:1 DMA	1.1 ± 0.0	0.0 ± 0.0	3.8 ± 0.3	0.0 ± 0.0	0.0 ± 0.0
18:1 DMA	1.0 ± 0.0	0.0 ± 0.0	3.4 ± 0.3	0.0 ± 0.0	0.0 ± 0.0
SFA:MUFA:PUFA	***45:43:12***	***50:44:6***	***36:45:19***	***54:36:10***	***44:37:19***
n-6:n-3	1.4	1.6	0.8	0.5	12.1
AA % in PUFA	***32***	***21***	***27***	***8***	***65***

FAs of untreated cells were quantified by GC-MS after methylation. DMA denotes dimethyl acetal from plasmalogen species. Values are expressed as weight % of total FA and expressed as means ± SD (n = 4).

4.2.2. Principal Component Analysis (PCA) shows that B16 cell lipidome is altered in a stimulus-specific manner due to membrane stress

B16 cells were exposed to mild (fever-like, 41 °C) or severe (43 °C) temperatures or to 40 mM BA for 1 h. The lipid molecular species composition was determined by ESI-MS/MS and a comprehensive analysis of lipid classes (PC, PC-O, LPC, PE, PE-P, PG, PI, PS, SM, Cer, Chol and CE) was performed. The filtered data included 157 molecular species, each of them accounted for more than 1 % within its lipid class (Table 4.2).

The results obtained and listed in Table 4.2 (i.e. 157 molecular species x 4 different treatments x 4 independent replicates) served as a base for PCA. PCA is an unsupervised multivariate statistical method which is able to reveal the internal structure of high-dimensional data explaining the variance in them. PCA produces linear combinations of the original variables to generate the linearly uncorrelated principal components. Each successive component displays a decreasing among of variance. With other words, each component is orthogonal to each other and has the highest variance possible (the first principal component (PC1) has the largest variance). Using only the first few principal components (accounting for the most of the variance) result in the reduction of dimensionality of multivariate dataset. This process simplifies the visualization of complex data sets for exploratory analysis. By applying this method the aim was to test for possible lipid alterations caused by the distinct treatments and also to assess overall experimental variation. Projection of the resulting sample scores for the first, second and third principal components (PC1, PC2 and PC3, respectively) clearly separated the samples into four non-overlapping clusters corresponding to the individual stresses (Figure 4.5). The analysis revealed that the three highest ranking components PC1, PC2 and PC3 accounted for 58 %, 18 % and 6 % of the total variance (altogether 82 %), respectively. PC1 captured most of the variations between the control and stressed samples, PC2 distinguished BA and heat treatments and PC3 separated the mild heat from the severe heat stress. Therefore, PCA revealed that the individual stresses resulted in marked and distinct alterations in the membrane lipid profiles.

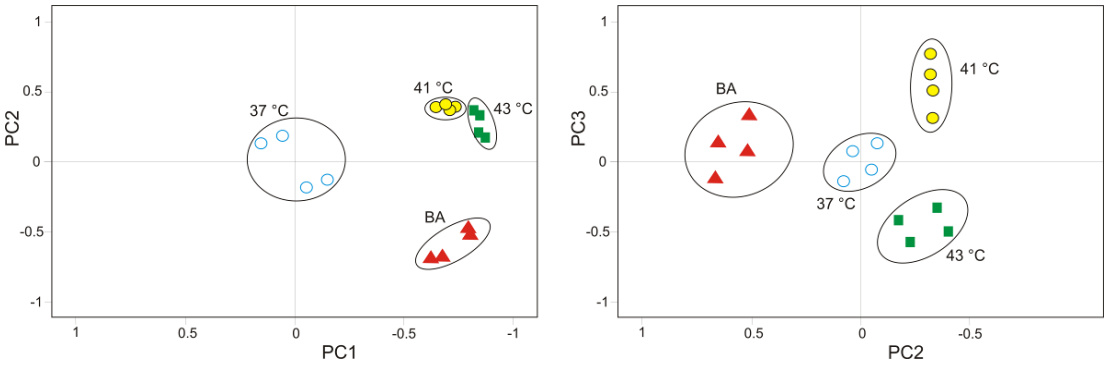

Figure 4.5. Principal component analysis (PCA) score plots. Values for 4 independent experiments are shown for PC1/PC2 (left) and PC2/PC3 (right) of the control and stressed cells. B16 cells were left untreated at 37 °C (open circles), treated at 41 °C (filled circles), 43 °C (filled squares) or with 40 mM BA (filled triangles) for 1 h (n = 4). Lipids were quantified by ESI-MS/MS. PCA data were filtered, centred to the average of the 37 °C controls and normalized.

4.2.3. Stress-induced lipid remodelling

Because PCA had shown such obvious differences in the lipidomes of B16 cells subjected to different stress conditions, these changes were analyzed in more detail. Comparison of the molecular species patterns for control incubations (37 °C) with individual stress conditions (heat or BA), demonstrated 116 statistically-significant distinctions, which are shown in Table 4.2. In order to select appropriate changes with explanatory relevance, results were grouped according to alterations in lipid class, fatty acyl chain length and/or degree of unsaturation.

Lipid class analysis (Figure 4.6) revealed that both mild and severe heat and BA stresses induced remarkably the level of Chol. The sphingolipid Cer displayed a similar elevation (irrespective of its molecular species composition). SM, a potential source of Cer, was diminished due to stress but not significantly so.

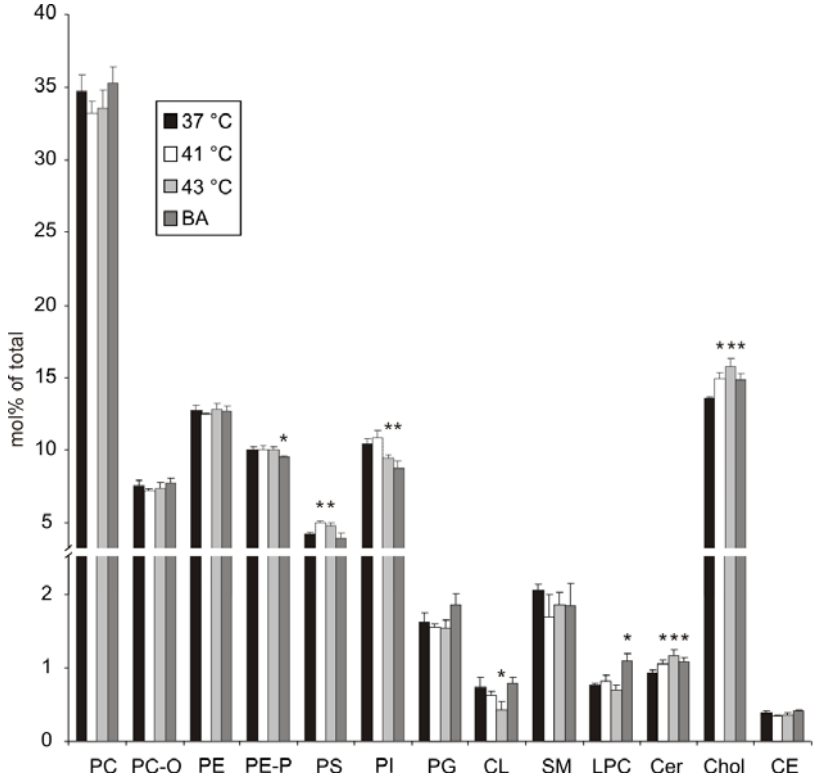

Figure 4.6. Lipid class compositional changes in B16 cells. B16 cells were left untreated at 37 °C, treated at 41 °C, 43 °C or with 40 mM BA for 1 h. Lipids were quantified by ESI-MS/MS. Data are expressed as mol % of analyzed lipids and presented as means ± SD (n = 4), *$q < 0.025$ compared to 37 °C (q is based on false discovery rate, see (Storey and Tibshirani, 2003).

The levels of the most abundant phospholipid, PC, (as well as PE and PG) were no significantly altered by any of the stress conditions. In contrast, the enhanced amount

of LPC following BA addition may indicate a metabolic change in PC. PE-P levels were lowered in the BA-treated samples, whereas PS increased after both mild and severe HS (the alterations for the different PS molecular species were similar: see Table 4.2.) but not with BA. CL was reduced remarkably by severe heat (43 °C) while the PI amount depleted in response to both BA and 43 °C, but not upon 41 °C exposure.

Distinct alterations in the molecular species of individual PL classes were visualised by grouping such species according to the total number of their double bonds (Figure 4.7).

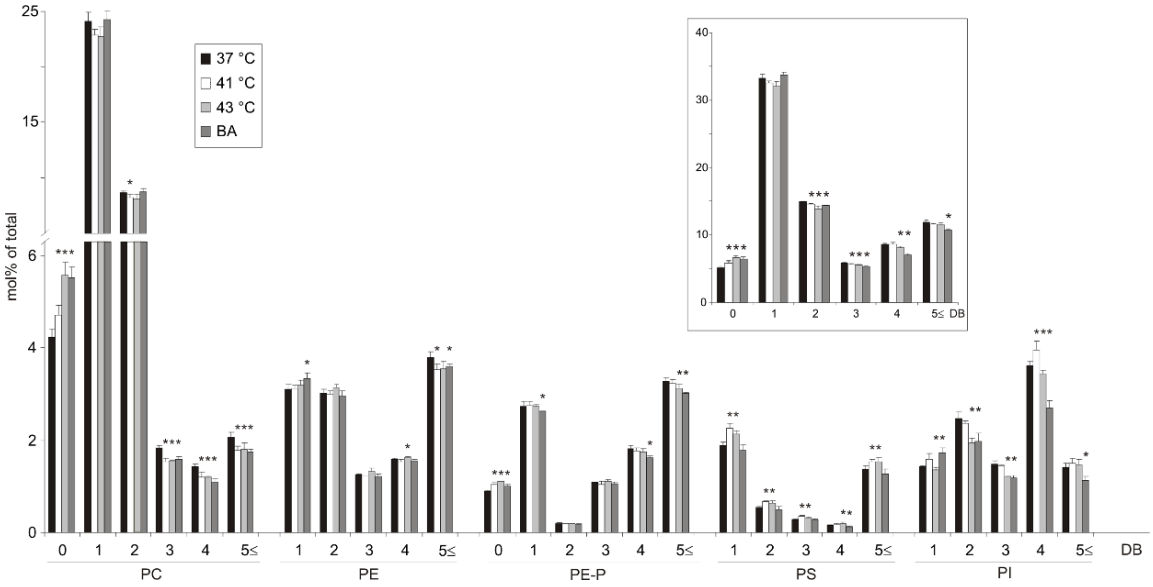

Figure 4.7. Effect of stress on the double bond composition of lipid classes (insert: sum of double bond compositions). B16 cells were left untreated at 37 °C, treated at 41 °C, 43 °C or with 40 mM BA for 1 h. Lipids were quantified by ESI-MS/MS. Data are expressed as mol % of analyzed lipids and presented as means ± SD (n = 4), *$q < 0.025$ compared to 37 °C.

In PC, the significant increase of disaturated species following heat and BA stresses was paralleled by the decrease in polyunsaturated chains. Because disaturated phosphoglycerides are known to play role in membrane raft formation and the latter may be involved in stress responses, results for these molecular species were collected in Figure 4.8. The data showed a large contribution of shorter chain FAs (PC(30:0), PC(32:0)) to the elevated disaturated PC. Furthermore, an increase in the amounts of PE-P species containing 16:0 or 18:0 was found as well. It is noteworthy that another major raft component, Chol, was also significantly increased by heat or BA stress (Figure 4.6).

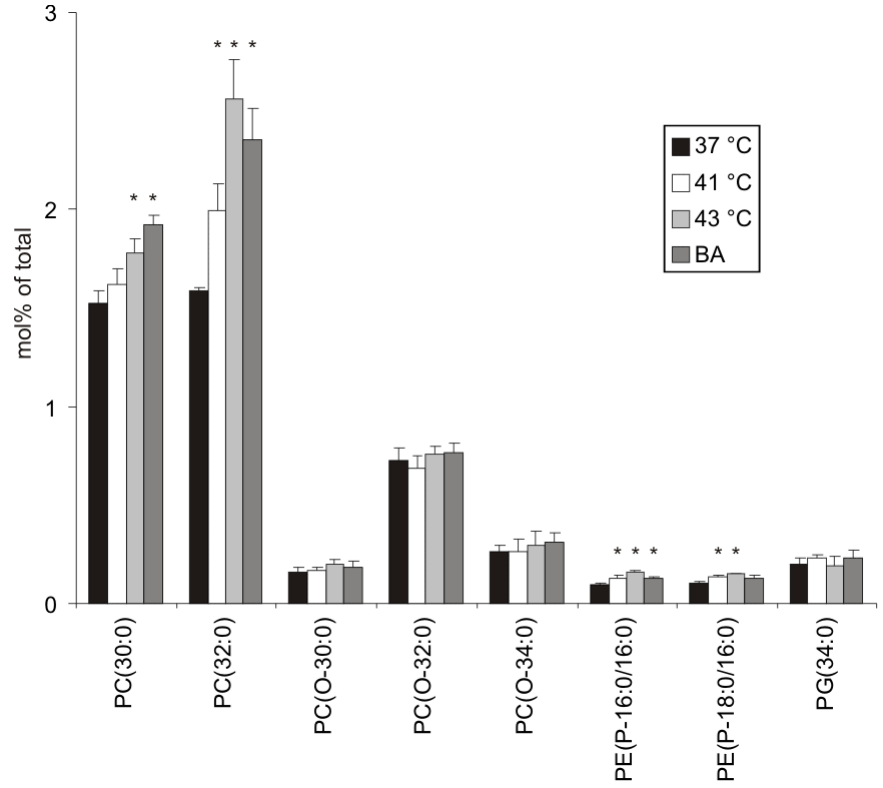

Figure 4.8. Alterations in disaturated phospholipid molecular species elicited by stress. B16 cells were left untreated at 37 °C, treated at 41 °C, 43 °C or with 40 mM BA for 1 h. Lipids were quantified by ESI-MS/MS. Data are expressed as mol % of analyzed lipids and presented as means ± SD (n = 4), *$q < 0.025$ compared to 37 °C.

Although a measurable portion of PC and ethanolamine plasmalogen contained SFA moieties only, in diacyl PE, PS and PI only molecular species with at least one double bond were detected (Figure 4.7). In PE the reduced level of highly unsaturated polyenes (double bonds≥5) after BA treatment was counterbalanced by elevated monoenoic species. Moreover, the reduction in total PI amount after severe heat (43 ºC) or BA stress (Figure 4.6) occurred as a result of the depletion in unsaturated (double bonds≥2) species (Figure 4.7).

From these data it can be concluded that BA and heat stresses (especially 43 ºC) caused increased levels of saturated lipids and decreased amounts of polyenoic species (Figure 4.7 insert). This demonstrated the concerted alterations in the lipidome which take place after the applied stress treatments in B16 cells.

4.2.4. Proposed involvement of phospholipases

The above results, i.e. the overall polyene reduction, may point to the involvement of phospholipases in stress-mediated lipid remodelling. Because AA is a known and potent

Hsp modulator among PUFAs, those molecular species were examined further that contained AA. As shown in Figure 4.9, remarkable losses were observed, especially in BA-treated samples, in PE(P-16:0/20:4), PC(36:4), PE(38:5) and, especially, in PI(38:4). Based on the abundance of 16:0 among saturated and the high enrichment of AA among the PUFAs of PC, the main species of PC(36:4) probably corresponds to 16:0/20:4. Due to the observed increase in LPC levels following BA addition (Figure 4.6), it is reasonable to suggest a PLA_2 enzyme activation. This cleaves the ester bond in *sn*-2 position of a PL leading to the production of the corresponding lyso derivative and release of the *sn*-2 FA, in this case mainly AA. Although LPE was not analyzed, it is known that PE species are also good substrates for mammalian PLA_2 enzymes (Balsinde et al., 2002). In PE-P the presence of 20:4-containing species was apparent. In addition, the large contribution of the 18:1/20:4 species to the total composition of PE(38:5) was suggested to be due to the high proportion of 18:1 in the monoene and the abundance of AA in the polyene fraction of diacyl PE. This species (PE(38:5)) was diminished significantly upon BA stress (Figure 4.9). The most striking alterations were seen in PI(38:4) which accounts for, by far, the largest portion (about 30 %) among the lipids depicted in Figure 4.5. The largest ratio of PI(38:4) can be mainly attributed to the 18:0/20:4 species, considering that in PI the FAs 18:0 and 20:4 are the dominant SFA and PUFA, respectively (Table 4.1). When exposed to severe heat or, especially to BA treatment, this molecular species was lowered very remarkably (in the case of BA treatment by 30 %). It should also be noted, that the amount of PI(36:4) (most probably 16:0/20:4) enriched significantly following both heat stresses. However, the pronounced depletion observed in PI and especially in the PI(38:4) species after severe membrane stress (43 °C and 40 mM BA) may denote the involvement of a phosphoinositide-specific PLA_2 and/or PLC. In the latter case, PLC would cleave the phosphodiester bond. The DAG produced so could then be hydrolysed in two sequential steps to form first MAG and finally free AA.

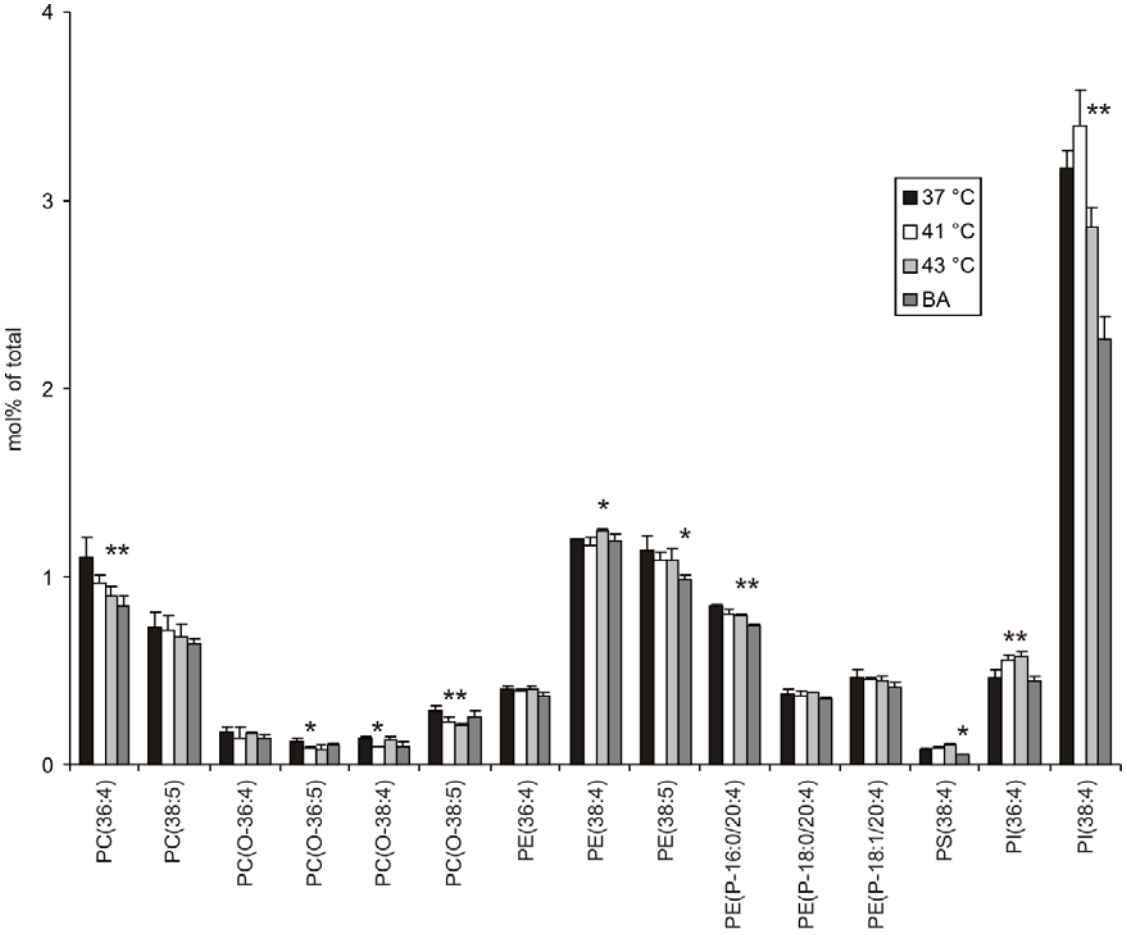

Figure 4.9. Changes in phospholipid molecular species containing 4 or 5 double bonds in response to stress. These species probably contained AA (see text). B16 cells were left untreated at 37 °C, treated at 41 °C, 43 °C or with 40 mM BA for 1 h. Lipids were quantified by ESI-MS/MS. Data are expressed as mol % of analyzed lipids and presented as means ± SD (n = 4), *q < 0.025 compared to 37 °C.

To confirm the suggestion that in many cases the decrease found in AA-containing lipids was due to phospholipase action, the level of FFAs were measured. The FA compositional changes in the FFA fraction due to stress treatments are shown in Figure 4.10. Among PUFAs AA was preferentially released by stress (Figure 4.10). Therefore, time-course alterations are presented for this FA in Figure 4.11. At 37 °C the AA amount displayed a slight elevation during a 1 h incubation. Following mild HS (41 °C) no further significant increase was found as compared to the control, while at 43 °C a remarkable 4-fold rise was detected, and BA treatment caused in the highest increase of AA with a further 2.5-fold elevation compared to HS at 43º C (Figure 4.11).

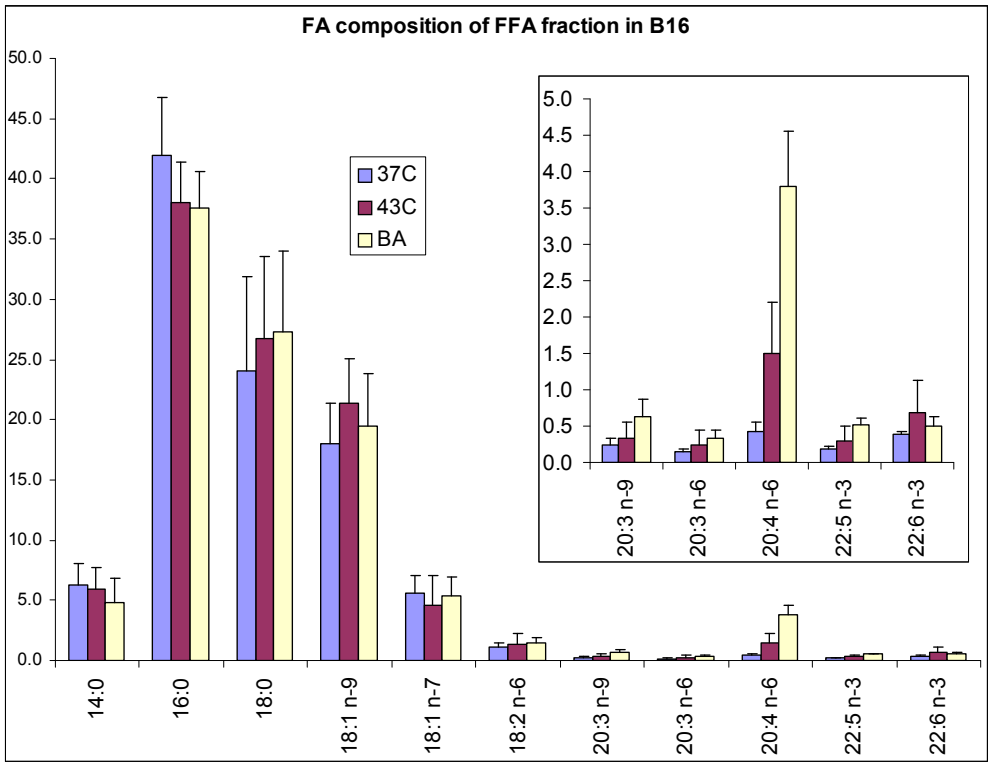

Figure 4.10. FA compositional changes in the FFA fraction of B16 cells after stress. B16 cells were left untreated at 37 °C, treated at 43 °C or with 40 mM BA for 1 h. FAs were quantified by GC-MS. Data are expressed as weight % of total and presented as mean ± SD (n = 5).

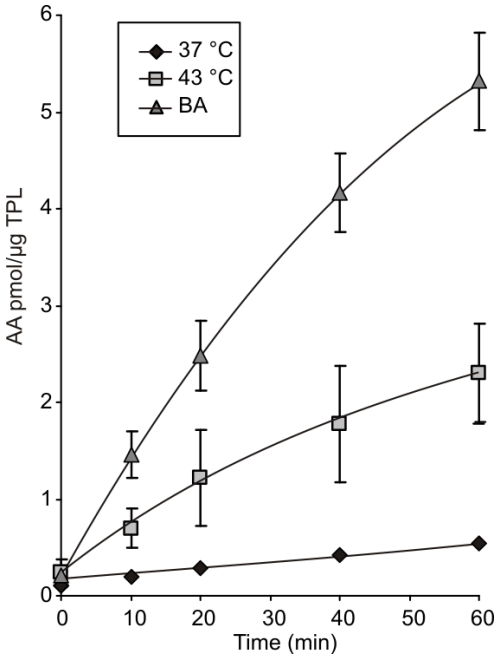

Figure 4.11. Time-course changes in free AA levels after stress. B16 cells were left untreated at 37 °C, treated at 43 °C or with 40 mM BA for 1 h. AA was quantified by GC-MS. Data are expressed in pmol/µg TPL and presented as means ± SD (n = 5).

4.2.5. Inhibitor studies to uncover the mechanism of arachidonate release

It is known from the literature that AA can be produced mainly by two types of phospholipases, the above-mentioned PLA_2 and/or PLC (Figure 4.12). In order to determine the role and/or contribution of the different AA-producing pathways, selective inhibitors were used and alterations in the amount of the relevant lipid metabolites, i.e. arachidonate-containing DAG and MAG as well as AA were determined (Figure 4.14).

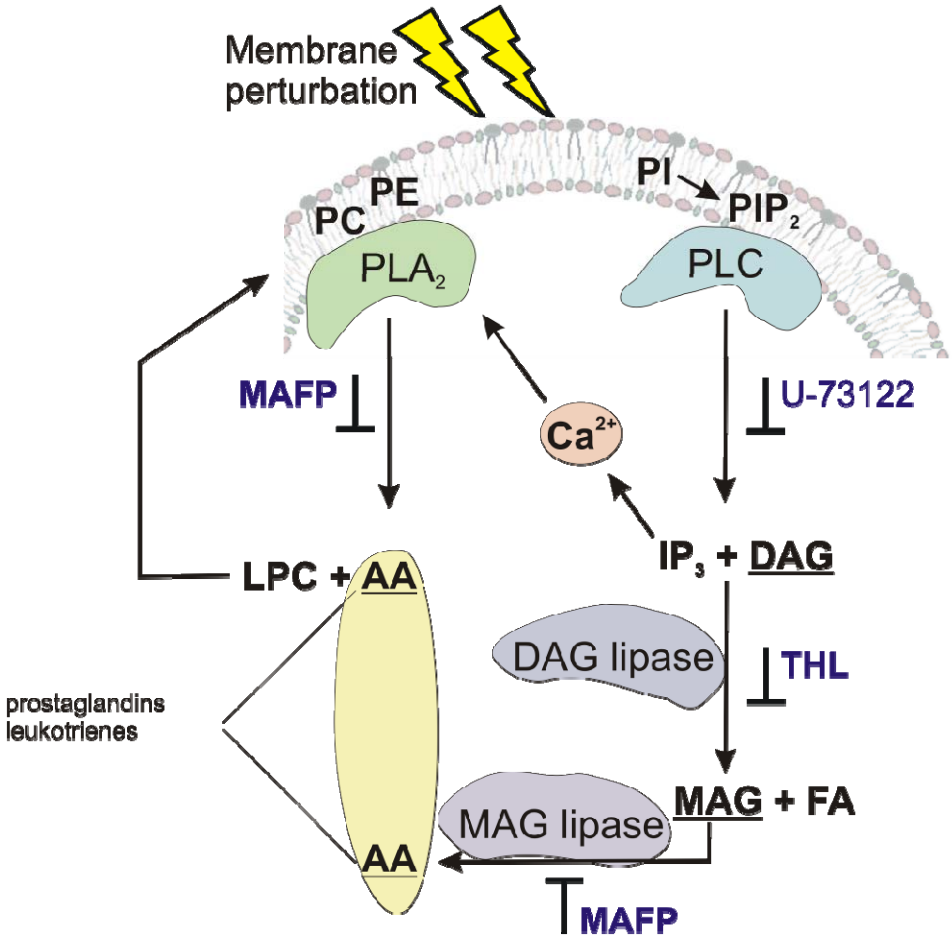

Figure 4.12. Overview of the potential AA producing pathways, applied inhibitors and analysed lipid metabolites (underlined). Note that DAG, AA and Ca^{2+} are known Hsp modulators.

Different types of inhibitors were selected: U-73122, an effective PLC inhibitor (Shimizu et al., 2007; Tang et al., 2006), THL, a selective DAG lipase inhibitor

(Bisogno et al., 2003; Bisogno et al., 2006) and MAFP, a pluripotent inhibitor with dual activity against $cPLA_2$/$iPLA_2$ (Balsinde and Dennis, 1996; Balsinde et al., 1999; Ghomashchi et al., 1999; Huang et al., 1996). In addition, MAFP was reported to be very potent as a fatty acid amide hydrolase (FAAH) and MAG lipase inhibitor (Goparaju et al., 1999; Shimizu and Yokotani, 2008).

Following a 20-min preincubation period with the inhibitors at 37 °C, the samples were exposed to stress treatments (43 °C or 40 mM BA) for 1 h. Ethanol was used as solvent for inhibitors; its final concentration did not exceed 0.1 %. This concentration had no measurable effect on lipid mediator levels compared to the solvent-free controls (Table 4.3).

Without inhibitors, the AA amount enhanced after treatment as noted above (Figure 4.11). The 20:4-DAG level altered no significantly upon HS at 43 °C, but revealed a 6-fold elevation following the addition of BA. The 20:4-MAG level was very remarkably risen by both stresses, as demonstrated by a 10-fold increase after HS and a 60-fold elevation upon BA treatment (insert in Figure 4.13).

Although the PLC inhibitor U-73122 (5 μM) was expected to diminish the amount of all measured intermediates on the PLC pathway by acting upstream, it failed to do so (Table 4.3). It occurred probably due to the presence of B16-specific multidrug resistant (MDR) transporter proteins which can effectively pump out hydrophobic molecules from cells (see Discussion).

The DAG lipase inhibitor THL (30 μM) was supposed to influence the PLC pathway by increasing 20:4-DAG and decreasing AA levels. 20:4-MAG amounts were no essentially altered by HS but reduced slightly after BA challenge in the presence of THL (Figure 5.13).

MAFP (10 μM) as a combined PLA_2 and MAG lipase inhibitor was expected to decrease the free AA level. In parallel, it was supposed to elevate 20:4-MAG amounts, due to its MAG lipase inhibitory potency. As depicted in Figure 4.13, MAFP resulted in ca. 50 % reduction in AA levels in both heat-shocked and BA-treated cells. Furthermore, it caused a spectacular (ca. 50-fold) increase in the level of 20:4-MAG for all conditions tested (37 °C, 43 °C, BA) compared to the inhibitor-free experiments. Unexpectedly, 20:4-DAG level was also slightly increased at 43 °C and 1.5-fold with BA due to MAFP addition. It could be a result of DAG lipase feed-back inhibition by 20:4-MAG, the reaction product of this enzyme.

In the following MAFP and THL were used in combination in order to decide which inhibitor property of MAFP played determining role in the B16 cell system. The

co-application of the two inhibitors caused no further changes in the AA level, but led to a striking drop in 20:4-MAG level (70 % at 43 ºC and 95 % with BA) as compared to MAFP treatment alone. These findings revealed that MAFP acted exclusively as a MAG lipase inhibitor and that the PLC pathway generated about half of the total AA produced.

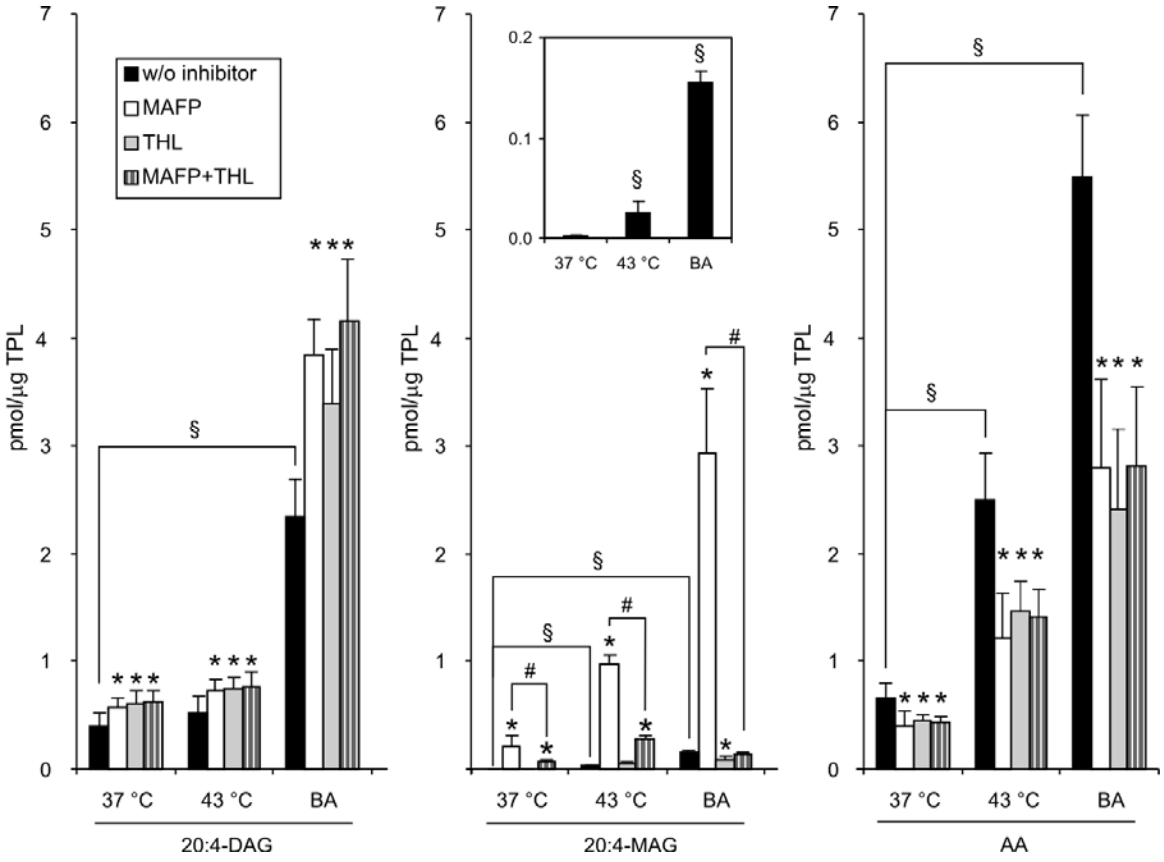

Figure 4.13. Effect of inhibitors on the levels of 20:4-DAG, 20:4-MAG and AA. B16 cells were preincubated without (w/o) or with inhibitor (MAFP 10 µM, THL 30 µM) for 20 min. Then they were left untreated at 37 °C, treated at 43 °C or with 40 mM BA for 1 h. Lipid intermediates were quantified by GC-MS and expressed in pmol/µg TPL as means ± SD (n = 5), $p < 0.05$ (Student's *t*-test with the Bonferroni correction), * w/o vs. with inhibitor, # MAFP vs. MAFP+THL, § w/o inhibitor at 37 °C vs. w/o inhibitor upon treatment.

Table 4.3. Percentage composition of major FAs in B16 cells

		DAG	MAG	AA	
Solvent-free	37	0.410 ± 0.110	0.003 ± 0.001	0.623 ± 0.015	
	43	0.515 ± 0.150	0.030 ± 0.015	2.480 ± 0.400	
	BA	2.413 ± 0.300	0.155 ± 0.012	5.611 ± 0.540	
Ethanol only	37	0.400 ± 0.124	0.003 ± 0.001	0.650 ± 0.140	n.s.*
(w/o inhibitor)	43	0.520 ± 0.154	0.026 ± 0.011	2.500 ± 0.430	n.s.*
	BA	2.345 ± 0.340	0.156 ± 0.010	5.500 ± 0.566	n.s.*
U-73122	37	0.391 ± 0.102	0.003 ± 0.001	0.609 ± 0.014	n.s.$
	43	0.528 ± 0.149	0.021 ± 0.012	2.590 ± 0.520	n.s.$
	BA	2.477 ± 0.260	0.160 ± 0.015	5.443 ± 0.630	n.s.$

B16 cells were incubated without (solvent-free) and with 0.1 % ethanol for 20 min. In further experiments they were preincubated without (ethanol only, i.e. w/o inhibitor) or with inhibitor (U-73122 5 μM) for 20 min. Then they were left untreated at 37 °C, treated at 43 °C or with 40 mM BA for 1 h. Lipid intermediates were quantified by GC-MS and expressed in pmol/μg TPL as means ± SD (n = 2 for ethanol vs. solvent-free, n = 3 for U-73122 vs. ethanol (w/o inhibitor)), $p < 0.05$ (Student's *t*-test), *ethanol-containing vs. solvent-free, $U-73122 vs. w/o inhibitor (i.e. ethanol only), n.s. not significant.

To find out why the PLC inhibitor U-73122 failed to exert any effect and why the potency of MAFP against cPLA$_2$ could not be predominated, it was suggested that they did not achieve effective inhibitory concentrations in the cell. It is noted that these agents are highly hydrophobic and, therefore, may serve as ligands for MDR transporters, which could extrude them from the cell. To prove this idea, the calcein assay developed by (Homolya et al., 1996) was applied (see Section xx). It revealed a very high MDR activity factor in B16 cells (MAF = 0.81, Figure 4.14). Thus, it is conceivable that a functional MDR in the cell membrane could be responsible for decreasing intracellular levels and, consequently, the effectiveness of the inhibitors. Indeed, in this study the inhibitors were used at 1-3x10^{-5} M concentrations. Those agents where the documented IC$_{50}$ values fell also in the μM range, i.e. U-73122 and MAFP as a PLA$_2$ inhibitor (IC$_{50}$~0.5 μM), did not display inhibitory effect. However, in cases when the documented IC$_{50}$ values were 2-3 orders of magnitude lower (such as for MAFP as a MAG lipase inhibitor (IC$_{50}$~2-3 nM) and for THL as DAG-lipase inhibitor (IC$_{50}$~60 nM)), significant inhibition was observed.

To confirm the potency of MAFP as a PLA$_2$ inhibitor, the supernatant of lysed B16 cells were assayed for PLA$_2$ activity. The assay revealed 85 % inhibition in the presence of MAFP (10 μM), thereby unambiguously indicated the efficacy of MAFP against B16 cell PLA$_2$ enzymes under *in vitro* condition (Figure 4.15).

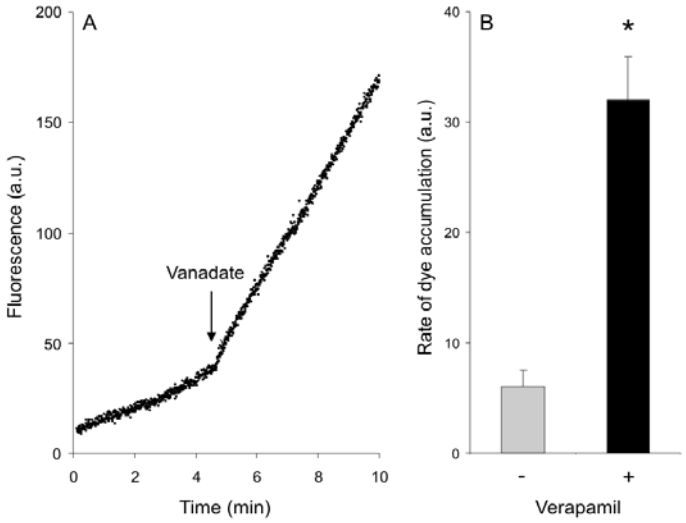

Figure 4.14. Measurement of MDR activity. Panel A, representative trace of calcein accumulation in B16(F10) cells. The cells were incubated in the presence of 0.25 μM calcein AM and fluorescence was monitored by spectrofluorometry (values in arbitrary units, a.u.). After 5 min of incubation, sodium orthovanadate as a MDR inhibitor (final concentration 500 μM) was added to the medium. Panel B, effect of the MDR inhibitor verapamil (100 μM) on calcein AM uptake into B16(F10) cells. The incubation media contained 0.25 μM calcein AM and the dye accumulation was recorded for 5 min at 37 °C in the presence or absence of the inhibitor (as indicated). The rates were calculated by linear regression and presented as means ± SD (n = 4), *$p < 0.05$.

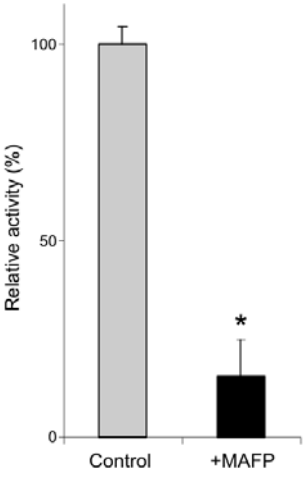

Figure 4.15. Effect of PLA_2 inhibitor on PLA_2 activity in soluble fractions from B16 cells. MAFP was added in 10 μM final concentration. Enzymatic activity (high speed supernatant) was measured as described in Materials and methods. Data are expressed as relative % and presented as means ± SD (n = 3), *$p < 0.05$.

4.3. DISCUSSION

In addition to their roles in the structural organization of membranes, different membrane lipids can be metabolized and generate numerous signalling molecules in response to stimuli (such as sphingolipids or products of PLA_2 activation). Growing evidence links such signalling processes also to membrane microdomains. In turn, the lipid signalling molecules can modify gene expression and, therefore, couple environmental stress or other stimuli to energy metabolism, cellular aging, etc.

To observe lipid alterations due to HS and membrane fluidity modulation the ESI-MS/MS molecular species results were evaluated using a data-mining PCA method which revealed a clear distinction of the experiments into four non-overlapping clusters according to the different stresses. The first component, accounted for almost 60 % of variance, clearly distinguished the untreated and stress conditions raising the possibility that common lipid metabolic pathways are involved in the stress-mediated lipid changes. The second and third components displayed differences for the mild or severe heat and the BA-induced membrane stresses, pointing to specific alterations in the lipidome due to these membrane perturbations.

A key characteristic of the lipid remodelling after heat (both mild and severe) or BA stress was the accumulation of Chol, Cer, saturated PC and PE-P species in B16 cells. These lipid species may support the generation of tightly-packed subdomains that correspond to liquid-ordered phases biophysically characterized in raft domains in cells and in model membranes (Mukherjee and Maxfield, 2004). It is known that elevated Cer levels can displace Chol from membrane/lipid “Chol-rafts” and form large, Cer-enriched membrane platforms “Cer-rafts” (Grassme et al., 2007; Patra, 2008). Since both Chol and Cer - besides other raft-component lipids - piled up during stress in whole B16 cells, it is conceivable that rafts are rearranged and contain different protein components, thereby altering various signalling pathways, (such as phosphatidylinositol 3-kinase, Akt and glycogen synthase kinase 3) which may, in turn, transmit the stress signal from the PM to the nucleus (Vigh et al., 2005; Vigh et al., 2007a). These findings may explain the previous observations concerning heat- or BA-induced Chol-rich PM microdomain condensation observed by fluorescence microscopy in B16 cells (Nagy et al., 2007). The elevation in saturated lipids and the concomitant decrease in polyenes was another clear consequence of stress. This may highlight common metabolic processes which are involved in stress responses, while the lipid species- or lipid class-dependent alterations may indicate stressor-specific changes.

In line with the commonly-accepted view in the literature (Balboa and Balsinde, 2006; Balsinde et al., 1999; Balsinde et al., 2002; Hirabayashi et al., 2004) it was suggested that the depletion of PUFA-containing lipids (with special emphasis on 20:4-containing species) following heat and BA treatments was a results of phospholipase actions. Such enzymatic activity is thought to be affected by membrane microheterogeneity and/or fluidity for both PLA_2 (Hønger et al., 1996) and PLC (Ahyayauch et al., 2005). These phospholipases can also be stimulated by HS and chemical stressors (Calderwood and Stevenson, 1993; Samples et al., 1999).

The increased amount of LPC after the addition of BA, as observed by ESI-MS in this study, supported the involvement of a PLA_2 enzyme. Because AA can almost exclusively be found in the *sn*-2 position, the decrease in PC(36:4) is consistent with the elevation of the main LPC species LPC(16:0).

The lipid most altered by PUFA depletion was PI(38:4). PI can be metabolized mainly by PLC or PI-specific PLA_2 (Corda et al., 2009). The former hydrolyzes PIP2, thereby releasing two second messengers, IP_3 and DAG (Wymann and Schneiter, 2008). Upon binding to IP_3 receptors IP_3 rapidly induces the release of Ca^{2+} from the endoplasmic reticulum. Importantly, it has been published that heat induces IP_3 production and polyphosphoinositide turnover in the initial stage of hyperthermia (Calderwood et al., 1987). Furthermore, several publications report that HS leads to a fast elevation in $[Ca^{2+}]_i$ from internal stores and a massive Ca^{2+} influx from the extracellular medium. Cell calcium seems to be critical for the transcriptional activation of *hs* genes in B16 (Nagy et al., 2007) and other cell lines (Kiang and Tsokos, 1998) and references therein).

Enhanced activity of phosphoinositide-specific PLC causes the formation of DAG which is highly enriched in AA and therefore may act as second messenger (Wakelam, 1998). For example, it could increase, the membrane activation and association of various isoforms of PKC which have been reported to drive the phosphorylation of HSFs (Vigh et al., 2007a). This is in agreement with the Hsp70 induction that occurred upon activation of PKC (Vigh et al., 2005). Additionally, the BA-induced increase in DAG and the heat-induced enhancement of PS, recorded in the present study, may have a positive regulatory role in PKC activation, because both DAG and PS are essential cofactors of PKC (Escribá et al., 2008; Griner and Kazanietz, 2007), but can be differently influenced by the different treatments.

The released 20:4-DAG can be further metabolized by DAG lipase to 20:4-MAG (Shimizu and Yokotani, 2008; Tang et al., 2006). Subsequently, from 20:4-MAG AA

can be generated through the action of MAG lipase or FAAH (Chau and Tai, 1981). AA produced by both PLA_2 and PLC-mediated pathways can transmit signals, it can be recycled via the Lands pathway, but a portion can be lost to β-oxidation. The Hsp modulator ability of AA was proven by treatment of HeLa cells with AA which stimulated HSF1–DNA binding, enhanced HSF1 phosphorylation and upregulated transcription of the *Hsp70* gene (Jurivich et al., 1996).

The time-course study of AA amounts displayed a pronounced increase after 1 h treatment either with 40 mM BA or at 43 °C. Thus, the loss in 20:4-containing lipids was accompanied by the liberation of a sizable portion of AA after severe stresses. However, as demonstrated by the elevated level of PI(36:4) upon both heat stresses, a portion of the AA probably went through reacylation, showing again that the distinct stresses can be distinguished by subtly altered species of the same lipid class or even by modulation of a single lipid species in a stressor-dependent manner. Finally, it is possible that a portion of the released AA may undergo oxidative metabolism by several enzymes such as lipoxygenases and cyclooxygenases whose products are also potent Hsp inducers (Köller and König, 1991; Santoro, 2000).

The accumulation of 20:4-DAG with BA and 20:4-MAG after both 43 °C and BA treatments (vs. 37 °C) clearly demonstrated the participation of the PLC pathway in the stress-induced lipid remodelling and AA generation. In addition, by far the highest rise in all three possible intermediates (20:4-DAG, 20:4-MAG and AA) was observed following BA treatment. This result is in accordance with literature data that phospholipases can be controlled by membrane microviscosity (Ahyayauch et al., 2005).

To determine the involvement of the possible phospholipases in AA release, different inhibitors were used. The application of MAFP (applied at 10 μM), which is widely considered in the literature as combined $cPLA_2$/$iPLA_2$ inhibitor (IC_{50}~0.5 μM), resulted in a marked decline in AA release after both 43 °C and BA stresses. Importantly, MAFP has also been reported to be able to more efficiently inhibit FAAH and MAG-lipase activities (IC_{50}~2-3 nM) (Goparaju et al., 1999). This latter could account for the elevated amounts of 20:4-MAG not only upon stresses but also under non-stressed conditions at 37 °C (Figure 4.9). It indicates a high basal MAG lipase activity in B16(F10), a cancer cell with strong metastatic capacity. It was reported recently that MAG lipase is highly enhanced in aggressive tumour cells from multiple tissues of origin (Nomura et al., 2010). The authors demonstrated that MAG lipase regulates FFA levels in such cells. The induced MAG lipase−FFA pathway feeds into a

complex lipid network full with pro-tumourigenic signalling molecules and also promotes survival, migration, and *in vivo* tumour growth. In this way aggressive tumour cells couple lipogenesis with high lipolytic activity to produce a set of pro-tumourigenic signals that support their malignant behaviour.

The DAG-lipase inhibitor THL (30 μM, IC_{50}~60 nM) resulted in a significant drop in 20:4-MAG level elevated by the MAG lipase inhibitor MAFP. These findings proved the role of the PLC–DAG lipase–MAG lipase pathway in AA formation and allowed some estimates for its quantitative contribution. Because both MAFP and THL alone or in combination showed similar (ca. 40-50 %) inhibition in the level of AA, it looks likely that, in our system, MAFP functioned exclusively as a MAG lipase inhibitor and the PLC pathway released about half of the AA. It is conceivable to suggest that the PLA_2 pathway accounted for the other half as revealed by the decrease in 20:4-containing PC and PE species and LPC elevation.

Recently, the question of how the membrane structural changes can be coupled to the Janus-like characteristics of hyperthermia in cancer therapy (Calderwood and Ciocca, 2008) was addressed in several publications (see e.g. (Grimm et al., 2009). The findings with the B16(F10) cancer cell line showed the accumulation of lipids with raft-forming properties. Mild hyperthermia (≤41 °C), which induces Hsps only to moderate levels (Nagy et al., 2007), also displayed this membrane feature, which is known to be linked to sensitivity to γ-irradiation (Bionda et al., 2007). Thus, these results may facilitate the understanding how mild hyperthermia can be applied as an adjuvant for chemotherapy, immunotherapy and radiotherapy by influencing membrane microdomain organization. In contrast, severe stress, elicited by 43 °C or BA, harshly activated phospholipases through robust membrane perturbation rendering the membranes more saturated and resulting in the production of lipid mediators which may contribute to Hsp synthesis. This membrane reorganization and the increased elevated Hsp levels ultimately may cause tolerance against heat, chemo- or radiotherapy.

In summary, the above experiments indicate that alterations in membrane fluidity and/or microheterogeneity after heat- or a fluidizing agent-induced stress resulted in significant and highly-specific changes in membrane lipid composition. The elevated amount of lipids with raft-forming properties (saturated lipid species, Chol and Cer) under both mild and severe stress conditions may explain the condensation of ordered PM domains previously observed by fluorescence microscopy (Nagy et al., 2007). The depletion of PUFA-containing lipid molecular species with a parallel enhancement in saturated species was found to be a result of the activation of phospholipases (mainly

PLA_2 and PLC). Furthermore, the phospholipase C–DAG lipase–MAG lipase pathway was identified in B16 cells. It contributed significantly to the release of several lipid mediators (including the potent HS modulator AA) following stress. Because different stresses were found to lead to unique alterations in the lipid profile of B16 cells, this work demonstrate that there are delicate perception mechanisms which can be operational for individual stresses.

Table 4.2. Molecular species alterations of lipid classes after stress treatments in B16 cells

	37°C			41°C			43°C			BA		
PC(30:0)	1.52	±	0.07	1.61	±	0.08	1.77	±	0.08*	1.92	±	0.05*
PC(30:1)	0.47	±	0.08	0.39	±	0.02	0.41	±	0.04	0.45	±	0.02
PC(32:0)	1.58	±	0.02	1.99	±	0.14*	2.56	±	0.20*	2.35	±	0.16*
PC(32:1)	6.14	±	0.25	5.93	±	0.18	5.69	±	0.27	6.27	±	0.17
PC(32:2)	0.49	±	0.02	0.51	±	0.06	0.48	±	0.02	0.52	±	0.02
PC(34:1)	12.10	±	0.47	11.46	±	0.19	11.35	±	0.31	11.99	±	0.27
PC(34:2)	2.81	±	0.06	2.56	±	0.07*	2.48	±	0.05*	2.79	±	0.09
PC(36:1)	1.71	±	0.05	1.57	±	0.14	1.69	±	0.19	1.76	±	0.20
PC(36:2)	3.88	±	0.10	3.66	±	0.21	3.58	±	0.33	3.88	±	0.11
PC(36:3)	1.39	±	0.05	1.14	±	0.05*	1.16	±	0.05*	1.20	±	0.08*
PC(36:4)	1.10	±	0.10	0.96	±	0.04	0.89	±	0.05*	0.84	±	0.05*
PC(38:5)	0.73	±	0.07	0.71	±	0.08	0.68	±	0.07	0.64	±	0.03
PC(38:6)	0.81	±	0.06	0.66	±	0.03*	0.75	±	0.10	0.65	±	0.06*
PC	**34.73**	**±**	**1.13**	**33.17**	**±**	**0.83**	**33.50**	**±**	**1.35**	**35.28**	**±**	**1.13**
PC(O-30:0)	0.16	±	0.02	0.16	±	0.02	0.20	±	0.02	0.18	±	0.03
PC(O-32:0)	0.72	±	0.06	0.68	±	0.07	0.76	±	0.03	0.76	±	0.04
PC(O-32:1)	0.82	±	0.12	0.81	±	0.03	0.78	±	0.04	0.88	±	0.05
PC(O-32:2)	0.14	±	0.01	0.14	±	0.01	0.14	±	0.01	0.15	±	0.02
PC(O-34:0)	0.26	±	0.03	0.26	±	0.06	0.29	±	0.07	0.31	±	0.05
PC(O-34:1)	2.28	±	0.07	2.20	±	0.08	2.27	±	0.11	2.36	±	0.17
PC(O-34:2)	0.69	±	0.04	0.65	±	0.02	0.63	±	0.06	0.63	±	0.03
PC(O-34:3)	0.08	±	0.02	0.07	±	0.01	0.07	±	0.04	0.07	±	0.02
PC(O-36:1)	0.51	±	0.07	0.47	±	0.04	0.47	±	0.06	0.51	±	0.02
PC(O-36:2)	0.60	±	0.04	0.67	±	0.04	0.63	±	0.20	0.66	±	0.08
PC(O-36:3)	0.28	±	0.02	0.23	±	0.03	0.24	±	0.01*	0.23	±	0.00*
PC(O-36:4)	0.17	±	0.03	0.13	±	0.07	0.16	±	0.01	0.13	±	0.02
PC(O-36:5)	0.12	±	0.02	0.09	±	0.01*	0.08	±	0.03	0.10	±	0.01
PC(O-38:2)	0.09	±	0.01	0.11	±	0.03	0.08	±	0.03	0.12	±	0.01*
PC(O-38:3)	0.09	±	0.01	0.09	±	0.01	0.09	±	0.01	0.08	±	0.01
PC(O-38:4)	0.14	±	0.01	0.09	±	0.00*	0.13	±	0.02	0.10	±	0.02
PC(O-38:5)	0.28	±	0.03	0.22	±	0.02*	0.20	±	0.01*	0.25	±	0.03
PC(O-40:6)	0.11	±	0.04	0.10	±	0.01	0.09	±	0.02	0.10	±	0.03
PC-O	**7.54**	**±**	**0.37**	**7.19**	**±**	**0.12**	**7.31**	**±**	**0.41**	**7.64**	**±**	**0.37**
PE(32:1)	0.33	±	0.02	0.33	±	0.00	0.34	±	0.02	0.35	±	0.02
PE(34:2)	0.56	±	0.03	0.54	±	0.02	0.57	±	0.02	0.53	±	0.02
PE(34:1)	1.53	±	0.05	1.53	±	0.06	1.57	±	0.05	1.63	±	0.06
PE(36:1)	1.23	±	0.05	1.25	±	0.02	1.27	±	0.05	1.34	±	0.06
PE(36:2)	2.06	±	0.05	2.04	±	0.03	2.13	±	0.06	2.02	±	0.06
PE(36:3)	0.39	±	0.02	0.39	±	0.01	0.45	±	0.01*	0.39	±	0.01
PE(36:4)	0.39	±	0.02	0.38	±	0.01	0.39	±	0.02	0.36	±	0.01

PE(38:2)	0.39	±	0.01	0.41	±	0.03	0.42	±	0.01*	0.41	±	0.02
PE(38:3)	0.84	±	0.00	0.82	±	0.02	0.87	±	0.07	0.81	±	0.05
PE(38:4)	1.19	±	0.01	1.16	±	0.04	1.23	±	0.01*	1.19	±	0.03
PE(38:5)	1.13	±	0.08	1.08	±	0.05	1.09	±	0.05	0.98	±	0.02*
PE(38:6)	0.83	±	0.03	0.78	±	0.02	0.75	±	0.06	0.74	±	0.01*
PE(40:5)	0.60	±	0.03	0.53	±	0.04	0.54	±	0.01	0.57	±	0.00
PE(40:6)	1.24	±	0.02	1.15	±	0.07	1.16	±	0.05	1.30	±	0.04
PE	**12.73**	**±**	**0.32**	**12.41**	**±**	**0.07**	**12.79**	**±**	**0.40**	**12.64**	**±**	**0.35**
PE(P-16:0/16:0)	0.10	±	0.00	0.13	±	0.01*	0.16	±	0.01*	0.13	±	0.01*
PE(P-16:0/16:1)	0.16	±	0.03	0.17	±	0.02	0.16	±	0.01	0.17	±	0.01
PE(P-16:0/18:1)	1.15	±	0.03	1.11	±	0.04	1.12	±	0.04	1.06	±	0.04*
PE(P-16:0/18:2)	0.09	±	0.00	0.10	±	0.01	0.09	±	0.00	0.09	±	0.01
PE(P-16:0/18:3)	0.03	±	0.00	0.03	±	0.00	0.02	±	0.00	0.03	±	0.01
PE(P-16:0/20:3)	0.47	±	0.02	0.47	±	0.02	0.48	±	0.02	0.45	±	0.02
PE(P-16:0/20:4)	0.84	±	0.01	0.79	±	0.03	0.79	±	0.01*	0.74	±	0.01*
PE(P-16:0/20:5)	0.29	±	0.03	0.27	±	0.04	0.26	±	0.03	0.25	±	0.01
PE(P-16:0/22:3)	0.07	±	0.01	0.08	±	0.00	0.08	±	0.01	0.08	±	0.00
PE(P-16:0/22:4)	0.09	±	0.01	0.10	±	0.01	0.09	±	0.01	0.09	±	0.00
PE(P-16:0/22:5)	0.76	±	0.02	0.75	±	0.03	0.74	±	0.03	0.68	±	0.02*
PE(P-16:0/22:6)	0.75	±	0.00	0.72	±	0.02	0.66	±	0.02*	0.66	±	0.03*
PE(P-18:0/16:1)	0.11	±	0.01	0.12	±	0.01	0.12	±	0.01	0.12	±	0.01
PE(P-18:0/16:0)	0.10	±	0.01	0.14	±	0.01*	0.15	±	0.01*	0.12	±	0.02
PE(P-18:0/18:2)	0.04	±	0.01	0.04	±	0.01	0.04	±	0.00	0.04	±	0.00
PE(P-18:0/18:1)	0.44	±	0.02	0.47	±	0.01	0.46	±	0.03	0.43	±	0.01
PE(P-18:0/20:5)	0.11	±	0.01	0.11	±	0.00	0.11	±	0.01	0.11	±	0.01
PE(P-18:0/20:4)	0.37	±	0.03	0.36	±	0.02	0.37	±	0.00	0.34	±	0.01
PE(P-18:0/20:3)	0.20	±	0.02	0.19	±	0.01	0.21	±	0.01	0.21	±	0.01
PE(P-18:0/22:6)	0.30	±	0.01	0.28	±	0.02	0.26	±	0.03	0.28	±	0.01*
PE(P-18:0/22:5)	0.26	±	0.02	0.28	±	0.02	0.26	±	0.01	0.26	±	0.00
PE(P-18:0/22:4)	0.03	±	0.01	0.03	±	0.00	0.02	±	0.01	0.02	±	0.00
PE(P-18:0/22:3)	0.02	±	0.00	0.01	±	0.00*	0.02	±	0.00	0.02	±	0.01
PE(P-18:1/16:0)	0.69	±	0.02	0.77	±	0.03*	0.80	±	0.01*	0.74	±	0.02
PE(P-18:1/16:1)	0.21	±	0.01	0.21	±	0.01	0.21	±	0.01	0.21	±	0.03
PE(P-18:1/18:1)	0.67	±	0.04	0.66	±	0.02	0.65	±	0.01	0.63	±	0.02
PE(P-18:1/18:2)	0.06	±	0.01	0.05	±	0.01	0.05	±	0.01	0.05	±	0.00
PE(P-18:1/18:3)	0.02	±	0.01	0.01	±	0.00	0.02	±	0.01	0.01	±	0.00
PE(P-18:1/20:3)	0.25	±	0.01	0.24	±	0.02	0.24	±	0.03	0.24	±	0.01
PE(P-18:1/20:4)	0.46	±	0.05	0.45	±	0.01	0.44	±	0.03	0.40	±	0.03
PE(P-18:1/20:5)	0.14	±	0.01	0.14	±	0.00	0.14	±	0.01	0.13	±	0.01
PE(P-18:1/22:3)	0.02	±	0.00	0.02	±	0.00*	0.03	±	0.01	0.02	±	0.00
PE(P-18:1/22:4)	0.03	±	0.00	0.03	±	0.00	0.03	±	0.00	0.03	±	0.01
PE(P-18:1/22:5)	0.31	±	0.01	0.32	±	0.01	0.33	±	0.03	0.30	±	0.02
PE(P-18:1/22:6)	0.36	±	0.01	0.35	±	0.02	0.35	±	0.01	0.33	±	0.02
PE-P	**9.99**	**±**	**0.22**	**10.01**	**±**	**0.30**	**9.99**	**±**	**0.21**	**9.48**	**±**	**0.08***
PS(32:1)	0.04	±	0.00	0.06	±	0.00*	0.04	±	0.00*	0.03	±	0.00
PS(34:1)	0.36	±	0.02	0.41	±	0.02*	0.40	±	0.01	0.30	±	0.02*
PS(36:1)	1.35	±	0.04	1.63	±	0.09*	1.53	±	0.09*	1.31	±	0.09
PS(36:2)	0.33	±	0.02	0.41	±	0.01*	0.39	±	0.04	0.27	±	0.04
PS(38:1)	0.14	±	0.01	0.17	±	0.01*	0.15	±	0.01	0.14	±	0.01
PS(38:2)	0.22	±	0.01	0.26	±	0.01*	0.24	±	0.02	0.22	±	0.03
PS(38:3)	0.23	±	0.01	0.30	±	0.02*	0.26	±	0.01*	0.22	±	0.01
PS(38:4)	0.08	±	0.01	0.09	±	0.01	0.10	±	0.01	0.05	±	0.00*
PS(38:5)	0.05	±	0.01	0.05	±	0.00	0.04	±	0.01	0.04	±	0.00
PS(38:6)	0.05	±	0.01	0.04	±	0.01	0.03	±	0.00*	0.03	±	0.00*
PS(40:3)	0.05	±	0.01	0.06	±	0.00	0.06	±	0.01	0.05	±	0.00

PS(40:4)	0.08	±	0.01	0.08	±	0.02	0.08	±	0.01	0.08	±	0.02
PS(40:5)	0.45	±	0.04	0.52	±	0.05	0.52	±	0.06	0.45	±	0.06
PS(40:6)	0.62	±	0.04	0.72	±	0.05	0.68	±	0.06	0.56	±	0.02
PS(40:7)	0.19	±	0.02	0.21	±	0.04	0.26	±	0.01*	0.19	±	0.03
PS	**4.22**	**±**	**0.14**	**5.00**	**±**	**0.13***	**4.78**	**±**	**0.22***	**3.93**	**±**	**0.33**
PI(32:1)	0.11	±	0.01	0.13	±	0.03	0.12	±	0.02	0.23	±	0.03*
PI(34:1)	0.62	±	0.03	0.71	±	0.07	0.64	±	0.08	0.87	±	0.03*
PI(34:2)	0.39	±	0.03	0.38	±	0.03	0.30	±	0.01*	0.39	±	0.08
PI(36:1)	0.71	±	0.02	0.74	±	0.07	0.58	±	0.04*	0.63	±	0.07
PI(36:2)	1.73	±	0.07	1.71	±	0.02	1.41	±	0.11*	1.38	±	0.12*
PI(36:3)	0.32	±	0.03	0.36	±	0.03	0.30	±	0.02	0.33	±	0.02
PI(36:4)	0.46	±	0.04	0.56	±	0.02*	0.57	±	0.02*	0.44	±	0.04
PI(38:2)	0.34	±	0.08	0.28	±	0.03	0.24	±	0.02	0.21	±	0.04
PI(38:3)	1.16	±	0.06	1.08	±	0.02	0.90	±	0.01*	0.84	±	0.03*
PI(38:4)	3.16	±	0.10	3.39	±	0.20	2.86	±	0.10*	2.26	±	0.12*
PI(38:5)	1.06	±	0.11	1.20	±	0.10	1.27	±	0.10	0.88	±	0.03
PI(38:6)	0.09	±	0.03	0.11	±	0.01	0.10	±	0.01	0.09	±	0.04
PI(40:5)	0.13	±	0.03	0.12	±	0.02	0.07	±	0.04	0.09	±	0.01
PI(40:6)	0.12	±	0.02	0.07	±	0.02*	0.03	±	0.04*	0.07	±	0.03
PI	**10.41**	**±**	**0.36**	**10.84**	**±**	**0.49**	**9.38**	**±**	**0.24***	**8.71**	**±**	**0.48***
PG(34:0)	0.19	±	0.03	0.23	±	0.01	0.19	±	0.05	0.23	±	0.04
PG(34:1)	0.60	±	0.06	0.52	±	0.01	0.54	±	0.03	0.65	±	0.06
PG(34:2)	0.18	±	0.00	0.15	±	0.02*	0.21	±	0.02	0.17	±	0.03
PG(36:1)	0.28	±	0.04	0.26	±	0.06	0.28	±	0.06	0.34	±	0.04
PG(36:2)	0.37	±	0.03	0.40	±	0.04	0.33	±	0.04	0.47	±	0.03*
PG	**1.63**	**±**	**0.12**	**1.56**	**±**	**0.05**	**1.55**	**±**	**0.11**	**1.86**	**±**	**0.15**
CL68:4	0.26	±	0.09	0.21	±	0.02	0.11	±	0.06	0.23	±	0.03
CL70:4	0.20	±	0.03	0.24	±	0.09	0.17	±	0.04	0.23	±	0.03
CL70:5	0.28	±	0.05	0.18	±	0.05	0.15	±	0.08	0.34	±	0.02
CL	**0.74**	**±**	**0.14**	**0.63**	**±**	**0.06**	**0.43**	**±**	**0.11***	**0.79**	**±**	**0.07**
SM(d18:1/14:0)	0.04	±	0.02	0.03	±	0.01	0.02	±	0.01	0.02	±	0.01
SM(d18:0/16:0)	0.08	±	0.04	0.05	±	0.04	0.05	±	0.02	0.05	±	0.04
SM(d18:1/16:0)	0.76	±	0.10	0.85	±	0.13	0.80	±	0.01	0.81	±	0.09
SM(d18:1/16:1)	0.05	±	0.03	0.04	±	0.03	0.08	±	0.03	0.05	±	0.01
SM(d18:1/17:0)	0.03	±	0.02	0.03	±	0.01	0.00	±	0.01	0.02	±	0.01
SM(d18:1/18:0)	0.18	±	0.05	0.13	±	0.05	0.16	±	0.04	0.11	±	0.06
SM(d18:1/20:0)	0.20	±	0.06	0.09	±	0.02*	0.06	±	0.05*	0.06	±	0.05*
SM(d18:1/22:1)	0.06	±	0.03	0.05	±	0.03	0.05	±	0.01	0.10	±	0.02
SM(d18:1/22:0)	0.24	±	0.06	0.08	±	0.05*	0.20	±	0.15	0.17	±	0.09
SM(d18:1/24:0)	0.08	±	0.01	0.10	±	0.03	0.11	±	0.03	0.12	±	0.04
SM(d18:1/24:1)	0.35	±	0.01	0.26	±	0.04*	0.33	±	0.04	0.35	±	0.03
SM	**2.06**	**±**	**0.07**	**1.70**	**±**	**0.31**	**1.87**	**±**	**0.16**	**1.86**	**±**	**0.30**
LPC(16:0)	0.41	±	0.01	0.47	±	0.04	0.36	±	0.05	0.57	±	0.05*
LPC(16:1)	0.05	±	0.01	0.05	±	0.00	0.04	±	0.01	0.06	±	0.01
LPC(18:0)	0.12	±	0.02	0.14	±	0.02	0.14	±	0.01	0.24	±	0.02*
LPC(18:1)	0.15	±	0.01	0.13	±	0.01	0.13	±	0.01	0.20	±	0.02*
LPC(18:2)	0.01	±	0.00	0.00	±	0.00*	0.01	±	0.01	0.01	±	0.00
LPC	**0.74**	**±**	**0.03**	**0.80**	**±**	**0.08**	**0.67**	**±**	**0.08**	**1.08**	**±**	**0.09***
Cer(d18:1/16:0)	0.14	±	0.00	0.16	±	0.00*	0.17	±	0.01*	0.17	±	0.01*
Cer(d18:1/18:0)	0.04	±	0.00	0.05	±	0.01	0.06	±	0.00*	0.05	±	0.00
Cer(d18:1/20:0)	0.04	±	0.00	0.04	±	0.00	0.05	±	0.00*	0.04	±	0.00

Cer(d18:1/22:0)	0.07	±	0.01	0.09	±	0.00*	0.11	±	0.01*	0.09	±	0.01
Cer(d18:1/23:0)	0.01	±	0.00	0.01	±	0.00	0.01	±	0.00	0.01	±	0.00
Cer(d18:1/24:0)	0.15	±	0.00	0.17	±	0.01*	0.21	±	0.02*	0.19	±	0.01*
Cer(d18:1/24:1)	0.13	±	0.01	0.15	±	0.01*	0.16	±	0.01*	0.16	±	0.01*
GluCer(d18:1/16:0)	0.14	±	0.01	0.17	±	0.00*	0.18	±	0.02*	0.17	±	0.01*
GluCer(d18:1/24:1)	0.19	±	0.01	0.20	±	0.01	0.20	±	0.02	0.20	±	0.01
Cer	**0.93**	**±**	**0.03**	**1.06**	**±**	**0.04***	**1.16**	**±**	**0.08***	**1.08**	**±**	**0.06***
CE14:0	0.02	±	0.00	0.02	±	0.00	0.02	±	0.00	0.02	±	0.00
CE15:0	0.01	±	0.00	0.01	±	0.00	0.01	±	0.01	0.01	±	0.00
CE16:0	0.11	±	0.02	0.10	±	0.02	0.10	±	0.00	0.13	±	0.01
CE16:1	0.04	±	0.00	0.04	±	0.01	0.04	±	0.01	0.04	±	0.00
CE18:0	0.03	±	0.00	0.03	±	0.00	0.03	±	0.00	0.03	±	0.00
CE18:1	0.09	±	0.00	0.07	±	0.01*	0.08	±	0.01	0.10	±	0.00*
CE18:2	0.01	±	0.00	0.01	±	0.00	0.01	±	0.00	0.02	±	0.00*
CE18:3	0.01	±	0.00	0.00	±	0.00	0.00	±	0.00	0.00	±	0.00
CE20:0	0.03	±	0.00	0.03	±	0.00	0.04	±	0.00	0.03	±	0.01
CE20:1	0.00	±	0.00	0.00	±	0.00	0.00	±	0.00	0.00	±	0.00
CE20:4	0.01	±	0.00	0.01	±	0.00	0.01	±	0.00	0.02	±	0.00
CE20:5	0.00	±	0.00	0.00	±	0.00	0.00	±	0.00*	0.00	±	0.00
CE22:1	0.01	±	0.00	0.00	±	0.00	0.01	±	0.00	0.00	±	0.00
CE22:6	0.01	±	0.00	0.01	±	0.00	0.00	±	0.00*	0.01	±	0.00
CE	**0.38**	**±**	**0.03**	**0.35**	**±**	**0.02**	**0.35**	**±**	**0.03**	**0.41**	**±**	**0.01**
Chol	**13.56**	**±**	**0.04**	**14.93**	**±**	**0.39***	**15.77**	**±**	**0.51***	**14.84**	**±**	**0.42***

B16 cells were left untreated at 37 °C, treated at 41 °C, 43 °C or with 40 mM BA for 1 h. Lipids were quantified by ESI-MS/MS. Data are expressed as mol % of analyzed lipids and presented as means ± SD (n = 4), *q < 0.025 compared to 37 °C. q < 0.025 corresponds ca. p < 0.015 and predicts 1 false positive result out of 40 significant as shown in Figure 4.16. It means that with 116 statistically-significant results, the expected number of false positive discoveries were less than 3. For further details of statistic see Materials and methods.

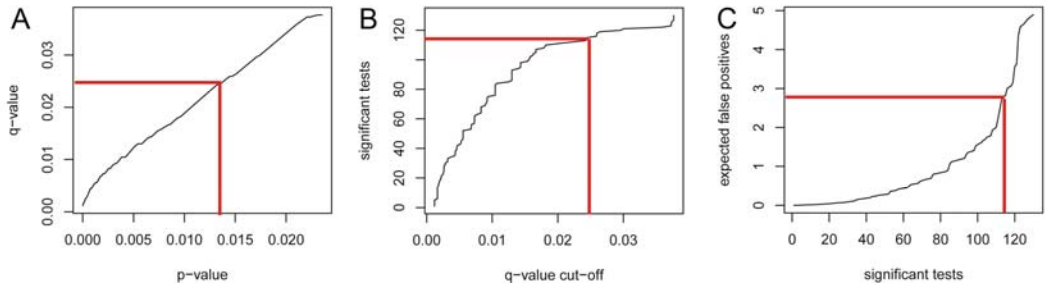

Figure 4.16. Statistical relationships between (**A**) p value and q value, (**B**) q value cut-off and number of significant tests and (**C**) significant tests and expected false positive results. The plots were generated by Q-value RGui in R statistical program (www.r-project.org). The red lines depict the given p value, the number of significant tests and the number of expected false positive results at q = 0.025.

CHAPTER 5. HEAT STRESS CAUSES SPATIALLY-DISTINCT MEMBRANE RE-MODELLING IN K562 LEUKEMIA CELLS

All experiments, evaluation and statistical analysis were performed by myself, with the following exceptions: DPH lifetime and Laurdan two-photon microscopy analyses were performed in collaboration with Tiziana Parasassi and Giuseppe Maulucci, respectively, in different laboratories in Rome. EPR spectroscopy measurements were run together with Elfrieda Fodor, while DPH and LD540 microscopy were done together with Imre Gombos. Data evaluations were performed in collaboration with Tiziana Parasassi, Elfrieda Fodor and Giuseppe Maulucci. Zsolt Török, Sándor Benkő, Ibolya Horváth, Tibor Páli, Mária Péter and Marco De Spirito took valuable part in the interpretation of results. The paper published from this research was written by myself, Mária Péter, Ibolya Horváth, Tiziana Parasassi and Tibor Páli, and critically reviewed by László Vígh, Ibolya Horváth, Tiziana Parasassi and John L. Harwood. The contribution of all co-authors is gratefully acknowledged.

Recently, there has been considerable interest in the application of hyperthermia in cancer treatment. This is a promising therapy modality for tumours, especially in combination with radiotherapy, because various tumours are often more thermally sensitive than normal tissues (Grimm et al., 2009). However, the primary target of cellular heat killing is still unknown. More than 30 years ago it was proposed that tumour cell membranes are the primary targets for heat treatment and that the effectiveness of hyperthermic cell killing is influenced strongly by the fluidity of membranes (Yatvin et al., 1979). In agreement with this idea, the use of membrane fluidizing agents (such as local anaesthetics) was shown to potentiate the therapeutic effect of hyperthermia (Yatvin et al., 1979).

It has also been noticed that, cells exposed to non-lethal increased temperatures or treated with a variety of compounds targeting membranes develop a stronger resistance to a subsequent severe HS (Vigh et al., 2005) – a process known as acquired thermotolerance. A major obstacle for many types of antitumour treatment is that they induce a HSR thus causing tumours to be more resistant to later treatments. Amongst other effects, the HSR restores the normal protein folding environment by upregulating Hsps and altering their subcellular locations (Dempsey et al., 2010; Horváth et al., 2008; Kirkegaard et al., 2010; Multhoff, 2007). This changes the pathways regulating cell growth, metabolism and survival.

Several reviews recently have considered the question as to how membrane structural alterations can be linked to the Janus-like properties of hyperthermia in cancer

therapy has been addressed in recent reviews (Calderwood and Ciocca, 2008; Grimm et al., 2009). In addition, cellular membranes have been implicated as the primary heat sensors (Vigh et al., 2007a; Vigh et al., 2007b) as well as in the decision-making for thermal cell killing (Grimm et al., 2009; Moulin et al., 2007).

In earlier research it was demonstrated that membrane hyperfluidization acts as a primary signal to initiate the Hsp response in prokaryotes (Horváth et al., 1998; Shigapova et al., 2005), yeast (Carratù et al., 1996), K562 leukemia (Balogh et al., 2005) and B16 melanoma cells (Nagy et al., 2007). In a similar fashion to HS, exposing K562 cells to BA, which is a known membrane fluidizing agent (Kitagawa and Hirata, 1992; Maula et al., 2009), caused very similar increases in cytosolic Ca^{2+} concentration, Hsp70 synthesis and mitochondrial hyperpolarization (Balogh et al., 2005). In addition, the microdomain organization of PMs was revealed to be an important factor in the detection and transduction of heat- or non-proteotoxic chemical agent-induced membrane stress into signals that give rise to the transcriptional activation of *hs* genes in B16 melanoma cells (Nagy et al., 2007). In recent reviews, the temporal and spatial regulation of the membrane hyperfine structure have been discussed as being a hallmark of sensing and signalling events following cellular stress (Horváth et al., 2008; Vigh et al., 2007a).

An alteration in the physical state of membranes is caused in the post-heat phase of HS (Dynlacht and Fox, 1992a; Dynlacht and Fox, 1992b; Revathi et al., 1994). Furthermore, it is well known that phospholipases and sphingomyelinases are activated during various stresses, therefore hydrolysing existing membrane lipids and giving rise to lipid mediators (Balogh et al., 2010; Calderwood and Stevenson, 1993; Calderwood et al., 1993; Escribá et al., 2008; Moulin et al., 2007). The metabolites which are produced, such as lysoPLs, FFA, DAG, MAG or Cer, together with newly synthesized lipid molecular species, may be produced at different membrane positions causing formation, segregation or rearrangement of membrane microdomains. Moreover, recently it was reported that alterations in membrane fluidity and/or microheterogeneity achieved either by heat or a fluidizing agent caused marked and highly-specific changes in the membrane lipid composition of B16 cells (Balogh et al., 2010). In addition, it can be assumed that, together with the retailoring of certain lipid molecular species and changes in lipases or certain members of PKC family (Escribá et al., 2008), some preexisting subpopulations of Hsps may also become associated with membranes in cells that had been exposed to hyperfluidization stress. Some Hsps are known to be associated with the surface or located within intracellular membranes (Horváth et al.,

2008; Multhoff, 2009; Vigh et al., 2005; Vigh et al., 2007a; Vigh et al., 2007b) possibly associated with ordered microdomains ("rafts") (Broquet et al., 2003; Dempsey et al., 2010; Stangl et al., 2011). In addition, Hsps have been shown to alter major properties of the membrane lipid phase state such as the fluidity, permeability, or non-bilayer propensity because of their specific interactions with membrane lipids (Tsvetkova et al., 2002; Török et al., 1997).

In order to gain further information about the role of membranes during hyperfluidization-induced stress, K562 cells were used. These were stressed by increased heat and the resultant membrane organisation changes were monitored by Laurdan, which can be regarded as the ideal probe to examine lateral structure of membranes in living cells by two-photon excitation fluorescence microscopy (Parasassi et al., 1997). Laurdan's even distribution in membranes, and its lipid phase-dependent emission spectral shift allowed the possibility of accumulating novel results compared to those produced using fluorescent probes which mainly partition into specific membrane regions but whose fluorescence intensities and spectral maxima are not usually sensitive to the lipid phase state (Bagatolli, 2006). By using Laurdan-labelled K562 cells, membrane lateral packing could be spatially resolved and/or domain information could be directly accumulated from the fluorescent images. I compared these results with those produced by "classical" approaches, which provide "bulk" information such as anisotropy or fluorescence lifetime measurements using DPH analogues and electron paramagnetic resonance (EPR) measurements with spin-labelled probes. By using these methods in heat-primed vs. non-stressed cells or isolated PMs I was able to gain important new insights about the various types of surface and intracellular membrane events initiated by HS.

5.1. MATERIALS AND METHODS

5.1.1. Materials

DPH, TMA-DPH, DPH-PA and 6-dodecanoyl-2-dimethylaminonaphthalene (Laurdan) were from Molecular Probes, Inc. (Eugene, Oregon, USA). RPMI-1640 medium and 5- and 16-(4',4'-dimethyloxazolidine-*N*-oxyl) stearic acid spin labels (5- and 16-SASL) were purchased from Sigma (Steinheim, Germany). BA of analytical grade was from Merck (Darmstadt, Germany). The LD-specific dye LD540 was a generous gift from

Professor Christoph Thiele (Bonn, Germany). All other chemicals were purchased from Sigma and were of the best available grade.

5.1.2. Cell culture

K562 cells (ATCC: CCL-243) were cultured in RPMI-1640 medium, supplemented with 10 % FCS and 2 mM glutamine in a humidified 5 % CO_2, 95 % air atmosphere at 37 °C and routinely subcultured in every three days for maximum four passages.

5.1.3. Fluorescence anisotropy

The PM fraction of K562 cells was isolated, labelled and membrane fluidity was measured as detailed in Chapter 2.5. Isolated PMs were labelled with 0.2 μM DPH or its derivatives, TMA-DPH and DPH-PA at a molar ratio of about 1:200 probe/phospholipid for 5 min. For *in vivo* fluidity measurements, K562 cells were labelled with 0.2 μm DPH for 30 min, or with DPH-PA and TMA-DPH for 5 min. Steady-state fluorescence anisotropy was measured in a PTI spectrofluorometer.

In order to follow the temperature dependence of fluidity, the temperature was maintained at 37 °C for 5 min, programmed at 0.4 °C/min from 37 °C to 42 °C, maintained isothermally for 1 h, cooled down gradually (0.4 °C/min) to 37 °C and held for 5 min. The time course of the fluorescence anisotropy upon addition of BA was performed as follows: cells were incubated at 37 °C for 5 min and BA (30 mM) was introduced into the cuvette. Anisotropy results were collected every 30 s for temperature dependence for 120 and for 50 min in the case of BA treatment.

5.1.4. DPH lifetime distribution studies

Labelling of K562 cells was with 0.2 μM DPH for 30 min. Time-resolved emission was measured using the K2 phase fluorometer (ISS Inc., Champaign, Illinois, USA) (Gratton and Limkeman, 1983). The excitation source was a He-Cd laser (λ = 325 nm). Phase and modulation data were collected using 9 modulation frequencies ranging from 2 to 180 MHz. Lifetime measurements were performed using a reference solution of 1,4-bis(5-phenyloxazol-2-yl)benzene in ethanol (τ = 1.35 ns). Emission was observed through a KV370 cutoff filter (Schott Glass Technologies Inc., Duryea, PA). Data were

analyzed using the Globals Unlimited software (Laboratory for Fluorescence Dynamics, University of California at Irvine, USA).

5.1.5. EPR studies

EPR spectroscopy is a sensitive tool for the detection of paramagnetic species (e.g. free radicals, transition metal ions). Except for rare cases, biomembranes are transparent to EPR measurements unless stable free radicals are introduced (Berliner, 1976). Spin-labelling is a technique of introducing stable nitroxide radicals into biological samples at low, non-perturbing concentrations; in this study stearic acid spin labels (5- and 16-SASL) were used. Spin-label EPR spectroscopy has become a very useful technique for examining biological membranes, because it has an optimal time scale to study membrane dynamics (Marsh and Horvath, 1989). The time window of conventional EPR spectroscopy – when the spectrometer works in the so-called X-band (9 GHz) region – is determined by the spectral anisotropy of the nitroxide group of the spin-label and ranges between 10^{-11}–10^{-7} s, which optimally matches the time scale of the rotational motions of the lipids in membranes. The EPR spectra of these probes comprises three hyperfine lines (assigned as high-field, center-field, and low-field peaks). The hyperfine splitting results from the coupling of the nitrogen unpaired electron spin with the nitrogen nuclear spin (see Figure 5.9). The spectra are sensitive – among other factors – to molecular motions, and also to the nature of the medium in which the probe is dissolved. Thus, information can be obtained regarding the physical state and dynamic properties of the membrane and membrane constituents (e.g. mobility, lipid order, polarity) (Boggs and Mason, 1986; Marsh, 2001). The sensitivity of spin-label EPR spectroscopy to membrane dynamics has an additional valuable consequence. In natural membranes or in lipid–protein complexes, two-component EPR spectra are usually obtained indicating the presence of two lipid populations with different mobilities (Marsh and Horvath, 1989). The lipids at the interface of the proteins are immobilized, thus the corresponding bulk and protein-associated components are well resolved in the EPR spectrum. Therefore, it is possible to quantitate both the stoichiometry and the selectivity of the interactions of different spin-labelled lipids with the protein, and to study the dynamics of the protein-associated lipids (Horváth, 1994; Marsh and Horváth, 1998).

Cells were kept at 37 °C (control) or heat-shocked at 42 °C for 1 h and pelleted by centrifugation at 400 *g* for 5 min and subsequently washed twice in excess volume of

phosphate buffered saline pH = 7.4 (PBS) at 37 °C. The final cell pellets were resuspended in PBS at a concentration of 1.2 x 10^7 cells/ml. For membrane samples, the spin-labelled lipid probe is usually added exogenously to the aqueous membrane dispersion as a small volume of concentrated solution in organic solvent (that is harmless to the biomembrane). Ethanol-mediated labelling has the advantage that it can be controlled very conveniently and quantitatively. Accordingly, for EPR measurements 2.5 μL of 5-SASL (2.5 mg/ml in ethanol) or 5 μL of 16-SASL (1 mg/ml in ethanol) spin label was added to an aliquot of 400 μL cell suspension, the mixture was kept for 5 min at room temperature and occasionally vortexed. In order to free the sample from unincorporated spin label and the organic solvent, cells were pelleted by centrifugation at 400 *g* for 5 min and the pellet introduced into 1 mm diameter EPR glass capillary. Glass capillaries have the advantage that they can be easily flame-sealed, and their background signal is usually very weak and broad, and does not disturb the spin label spectrum. After sealing, the capillaries were further centrifuged in a bench top centrifuge (400 *g*, 5 min) and the excess supernatant was removed to obtain a sample length of 5 mm in each capillary. This was important, because water absorbs microwave thereby leading to a weaker signal. In addition, in the case of single-chain spin-labelled lipids, e.g. FAs, removal of excess supernatant is especially important, because these type of labels, due to their partial solubility in water, may establish a partition equilibrium. EPR spectra were measured in a Bruker (Rheinstetten, Germany) ECS 106 X-band spectrometer equipped with a TE102 cavity and a nitrogen gas flow temperature regulator at 37 °C or 42 °C. Microwave power was 2 mW and 100 kHz field modulation with an amplitude of 0.1 mT was used for first-harmonic detection. Spectra were centred around 335 mT and scanned over a field width of 10 mT. For each sample, two spectra were accumulated with 20.5 ms averaging at each of the 1024 field steps. The time elapsed from labelling the sample and recording the spectra was marked and comparisons were made between spectra recorded at the same time intervals, to avoid any mismatch between the redistribution of the spin probe with time in the live cells. The spectra were recorded within the time interval where the rate of reduction of the doxylstearate due to internalization followed by mitochondrial reduction of the probe was negligible (Duda et al., 1994). Peak heights and positions were measured using the corresponding routines in the Bruker software as well as the numerical integration of the spectra after baseline correction.

5.1.6. Laurdan two-photon microscopy

Laurdan displays a lipid phase-dependent emission spectral shift. This red shift due to altered water penetration into the lipid bilayer allows the estimation of lipid packing orders within the membranes of intact and living cells (Gaus et al., 2003). Originally, the generalized polarization GP was defined analogous to the classical fluorescence polarization $P=(I_1-I_2)/I_1+I_2)$ where I_1 and I_2 represent two different (perpendicular) orientations of the observation polarizer. For phospholipid vesicles Laurdan emission wavelengths of 440 and 500 nm correspond to the emission maxima in the gel and in the liquid crystalline phases, respectively; $GP=(I_{440}-I_{500})/I_{440}+I_{500})$ (Parasassi et al., 1990). In two-photon fluorescence microscopy (excitation at 800 nm) the two intensity images between 400–460 nm and 470−530 nm are collected simultaneously. Thus, GP defined as

$$GP = \frac{I_{(400-460)} - G\, I_{(470-880)}}{I_{(400-460)} + G\, I_{(470-880)}}$$

, where G is a calibration factor for the instrument response.

In order to study the membranes properties of K562 cells by Laurdan two-photon microscopy the cells were labelled directly in the cell culture media. The stock Laurdan solution concentration was 1 mM in dimethyl sulfoxide (DMSO), and it was replaced every three weeks. 10 μL of Laurdan stock solution was added per mL of RPMI medium. After 30 min of incubation in the dark at room temperature or at 42 °C, the cells were centrifuged, resuspended in RPMI medium at 22 °C and mounted upon a microscope slide.

An inverted confocal microscope (DMIRE2, Leica Microsystems, Germany) with a 63X oil immersion objective (NA 1.4) under excitation at 800 nm with a mode-locked Titanium-Sapphire laser (Chamaleon, Coherent, Santa Clara, California, USA) was used to obtain Laurdan intensity images. Internal photon multiplier tubes collected images in an eight bit, unsigned images at a 400 Hz scan speed. Simultaneous recordings with emission in the range of 400–460 nm and 470–530 nm and imaging was performed at 22 °C to obtain the Laurdan intensity images. GP images was calculated for each pixel using the intensity images. G was obtained from the measurement of GP values of Laurdan solution in DMSO at 22 °C (GP_{exp}) calculating with a known GP value of $GP_{DMSO} = 0.207$ as follows:

$$G = (GP_{DMSO} + GP_{DMSO}GP_{exp} - 1 - GP_{exp})/(GP_{DMSO}GP_{exp} - GP_{DMSO} + GP_{exp} - 1).$$

The G factor had ~2 % variation across the imaging area. GP images (as eight-bit unsigned images) were pseudocoloured in ImageJ. Background was determined from areas without cells (it corresponded to intensities below 7 % of the maximum intensity), were set to zero and coloured black. The histogram values for GP were determined within multiple circular Regions-of-Interest (ROI) with 20 pixel diameter (Area 316 pixel) for different membrane regions. The ROI for PM were chosen along the contour profile of the cell, the perinuclear ROI along the contour profiles of the nuclei, the ROI for internal membranes (except the perinuclear region) in the rest of the cell. n = 10 ROI were measured for each membrane region within one cell. 3 control and 3 heat-stressed cells were analysed.

Analysis and line profiles of acquired images were performed with ImageJ (http://rsbweb.nih.gov/ij/).

5.1.7. Fluorescence microscopy

Using suspensions of K562 cells in PBS, labelling was with 2 μM DPH-PA, TMA-DPH or DPH for 5 min or 30 min at 37 °C or 42 °C as indicated. For experiments with double-labelling, cells were labelled with a mixture containing 2 μM DPH and 30 nM LD540 for 30 min. Images were taken with a CytoScout fluorescent microscope (Upper Austrian Research GmbH, Linz, Austria) using a 100x objective, D365/10 and D405/30 filter for excitation and emission of DPH and HQ532/70 and HQ 600/40 filters for excitation and emission of the LD540 probe.

5.1.8. Statistics

Results are presented as means ± SD and compared for significance using Student's *t*-test (paired or unpaired; details are given in the Figures).

5.2. RESULTS

5.2.1. Laurdan two-photon microscopy shows that heat stress gives rise to spatially-distinct membrane re-organisation in vivo

In order to examine alterations in the physical state of cell membranes following a short HS (42 °C, 1 h), Laurdan fluorescence using two-photon microscopy were measured. Laurdan is an environmentally-sensitive fluorescence probe that gives a spectral shift of emission which depends on the lipid phase state, i.e., bluish in ordered, gel phases and greenish in disordered, liquid-crystalline phases. The probe distributes itself equally in lipid phases and does not associate preferentially with phospholipid headgroups or specific fatty acids. As a normalized ratio of the intensity at the two emission wavelengths regions, the generalized polarization (GP) provides a measure of membrane order, in the range between +1 (gel) and −1 (liquid-crystalline) (Bagatolli, 2006; Parasassi et al., 1991).

GP images of Laurdan-labelled K562 cells revealed high-GP regions at the PM while low-GP regions were mainly found at perinuclear and internal membranes (Figure 5.1A). This was in agreement with previous findings using various cell types (Yu et al., 1996). When cells were treated at 42 °C for 1 h and afterwards cooled down to 22 °C for the fluorescence analysis, in general the membranes showed more disorder than in the non-stressed controls (Figure 5.1B). This caused an average shift towards lower GP values (Figure 5.1C).

Detailed examination also revealed that the endomembranes and the PM of the K562 cells subjected to HS displayed contrasting behaviour. Moreover, the findings by Region-of-Interest (ROI) analysis showed that the PM became more rigid, while the internal membranes, especially the perinuclear region became more fluid following HS. The GP profiles of high resolution pictures clearly show the condensed cell surface and disordered inner membrane region in post-heat cells when compared to non-stressed cells (Figure 5.2).

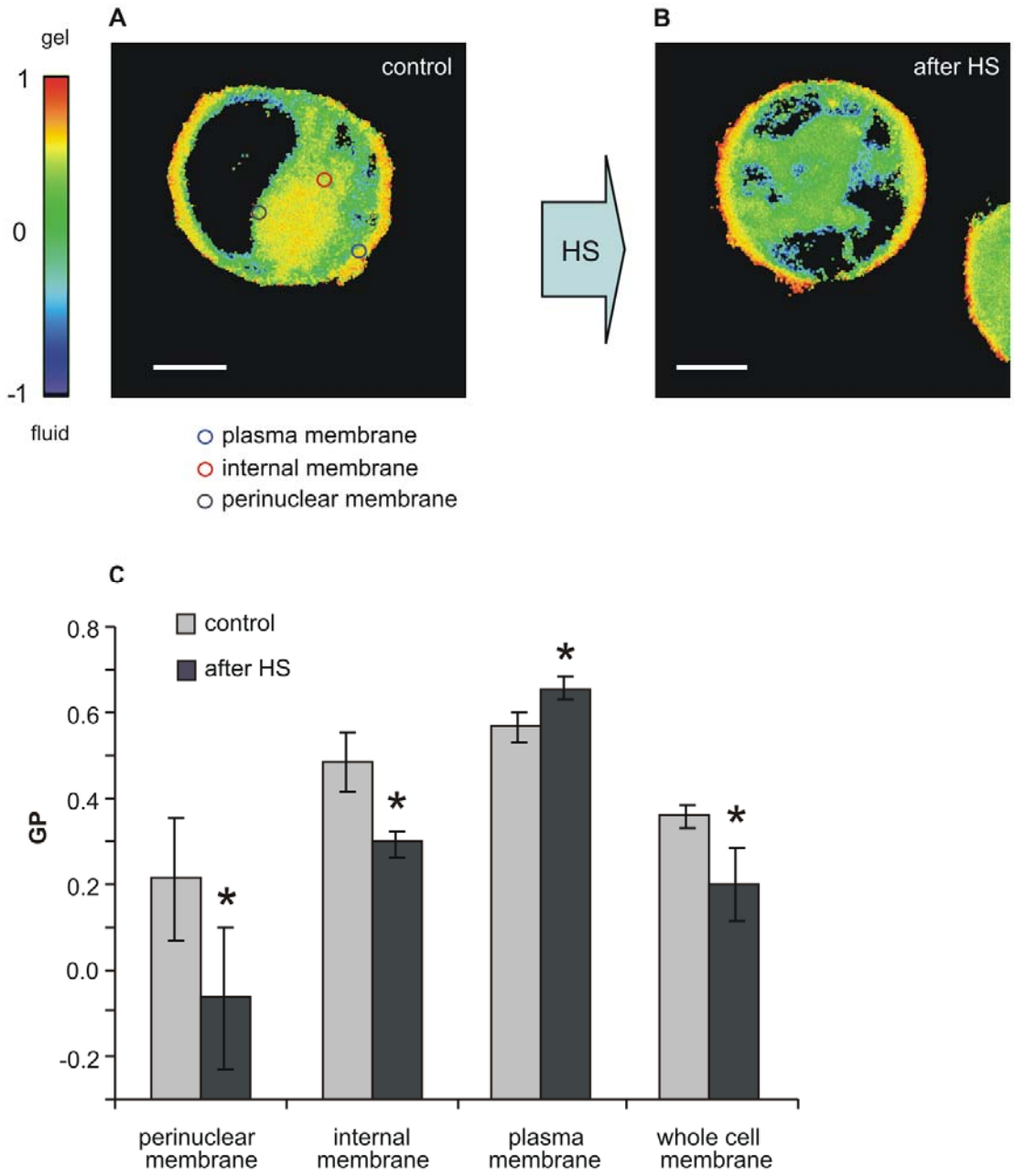

Figure 5.1. Heat shock induces membrane changes as visualised by Laurdan two-photon microscopy. K562 cells in RPMI medium were treated at 42 °C for 1 h and imaged (**A**) before and (**B**) after HS at room temperature (21 °C). The colour chart in Panel A represents Laurdan GP values as indicated. Bars in A and B, 6 μm. (**C**) Histogram of GP changes observed in whole cell and in subcellular (perinuclear, internal and plasma membrane) regions. An example set of ROIs used for quantification of subcellular GP distribution is given in panel A. Data are expressed as means ± SD, n = 30, *p<0.05 compared to the control, unpaired t-test.

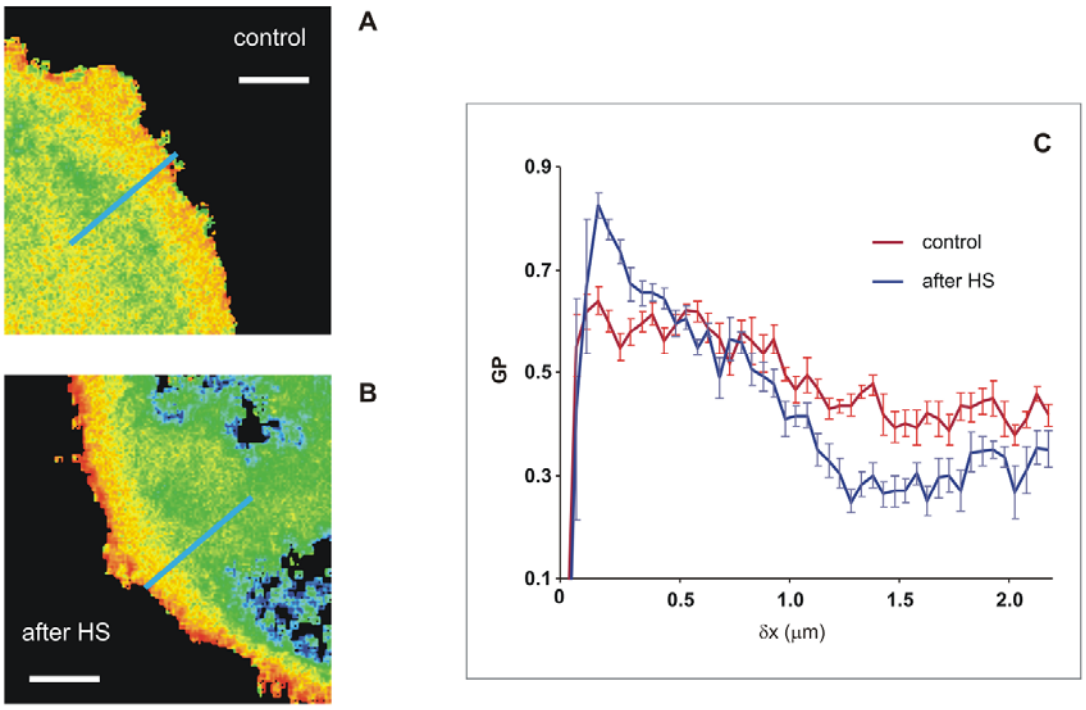

Figure 5.2. High resolution images of the cell border showing the general polarisation distribution. K562 cells in RPMI medium were treated at 42 °C for 1 h and imaged (**A**) before and (**B**) after HS at room temperature (21 °C). Bars in A and B, 1 μm. (**C**) GP profile along blue lines shown in panels A and B. For other details see Figure 5.1.

5.2.2. Fluorescent polarisation revealed the usual fluidity changes in isolated membranes but unusual alterations in cells

Different probes were used in order to examine the heat-induced membrane rearrangements in more detail. DPH fluorescent probes with negatively or positively charged surface anchors (DPH-PA or TMA-DPH, respectively) as well as DPH itself were employed. K562 cells were treated for 1 h at 42 °C. After harvesting, they were labelled at 37 °C for 30 min (DPH) or 5 min (TMA-DPH, DPH-PA). These times had been shown to be appropriate for the individual probes (Balogh et al., 2005). Alterations in fluorescence anisotropy revealed a fluidity decrease with DPH-PA as well as with DPH. However, a fluidity increase was found with TMA-DPH (Figure 5.3).

The time course of heat-induced membrane rearrangements was followed by measuring alterations in membrane fluidity in living cells. These were compared with results from PM isolates which represented non-responding controls. In both cases a heating/cooling cycle was used. For isolated PMs, as expected, a fluidity increase

during the heating period was found with all three labels. The fluidity returned completely to its starting value on return to 37 °C (Figure 5.4).

A different pattern was found with cells. In contrast to the "normal" fluidity–temperature profile of PMs, membrane fluidity measurements conducted on living cells displayed an anomalous response to HS. The negatively charged probe DPH-PA did not detect any change in lipid order during heating. However, an anisotropy increase was found as soon as the temperature was returned back to 37 ºC when it became constant. When TMA-DPH was used it revealed a strong membrane fluidization upon temperature increase and a further slow, steady increase of membrane disordering during 1 h exposure to 42 °C. When cells were returned to normal (37 °C) growth temperature an ordering effect was observed, although anisotropy did not reach the initial value. A prompt fluidization following shift to 42 °C was found for the DPH probe after which a slight rigidization took place gradually at this temperature. The DPH anisotropy value detected in cells on restoration of the normal 37 °C growth temperature was higher than that measured prior to treatment (Figure 5.4).

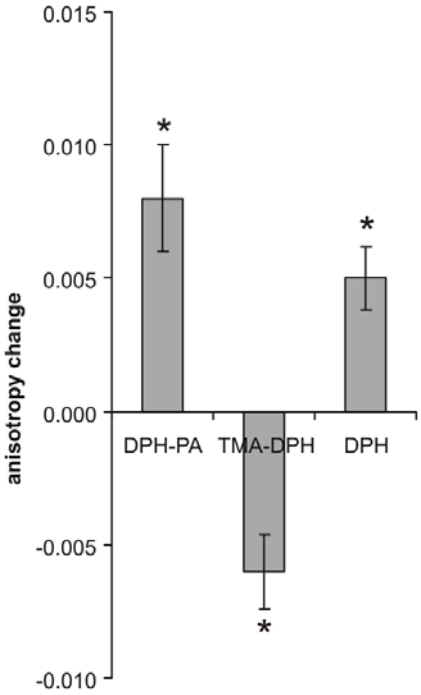

Figure 5.3. Alterations in anisotropy as revealed by different fluorescent probes. K562 cells in RPMI medium were heat-treated at 42 °C for 1 h or left at 37 °C, harvested and labelled with DPH-PA, TMA-DPH or DPH. The fluorescence steady-state anisotropy measurement was performed at 37 °C and 5 min of trace was averaged. The anisotropy differences were calculated relative to the 37 °C control values. Data are represented as means ± SD, n = 4, *$p < 0.05$, paired *t*-test.

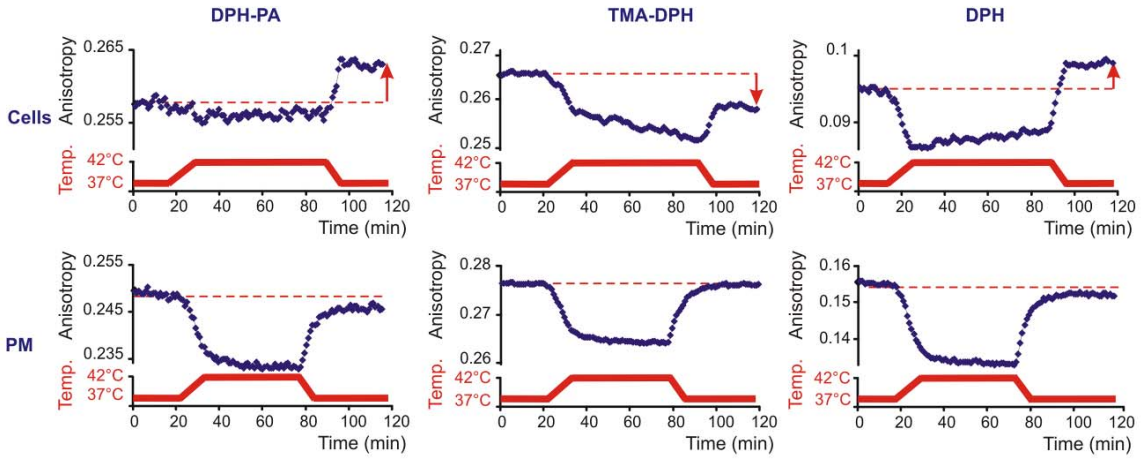

Figure 5.4. Fluorescence changes during heat treatment are different in isolated PMs compared to intact cells. K562 cells or PM fractions isolated from untreated cells were labelled with DPH-PA, TMA-DPH or DPH and the fluorescence steady-state anisotropy (blue) was followed (representative traces are shown from n = 4 independent experiments). Cyclic temperature shift was applied (red). The arrows indicate the anisotropy difference at 37 °C before and after 42 °C HS.

5.2.3. Benzyl alcohol-induced fluidization also shows distinct differences between isolated plasma membranes and cells in vivo

In order to learn more about the kinetics of hyperfluidization-induced membrane rearrangements, the action of the chemical membrane fluidizer BA was studied. This was used at a previously selected concentration (30 mM), which showed various effects that were found for 42 °C heat treatment (Balogh et al., 2005). Temporary fluidization was observed in living cells as a result of BA addition. This was followed by an exponential compensatory decay observed with DPH-PA and, to much smaller extent, by DPH. When TMA-DPH was used as a probe only fluidization was detected and this was almost stable after about 20 min. For isolated PMs, BA addition caused a very pronounced fluidization, as expected, with all three probes (Figure 5.5).

Importantly, the *in vivo* heat cycling experiments using DPH and its analogues were repeated using B16 mouse melanoma, L929 mouse fibroblastoid, WEHI164 mouse fibrosarcoma, HeLa human epithelial carcinoma and freshly isolated mouse spleen cells with strikingly similar changes in the fluidity profiles observed upon heat or

BA treatment (Table 5.1). This indicates that the data with K562 cells can be applied to other cell types.

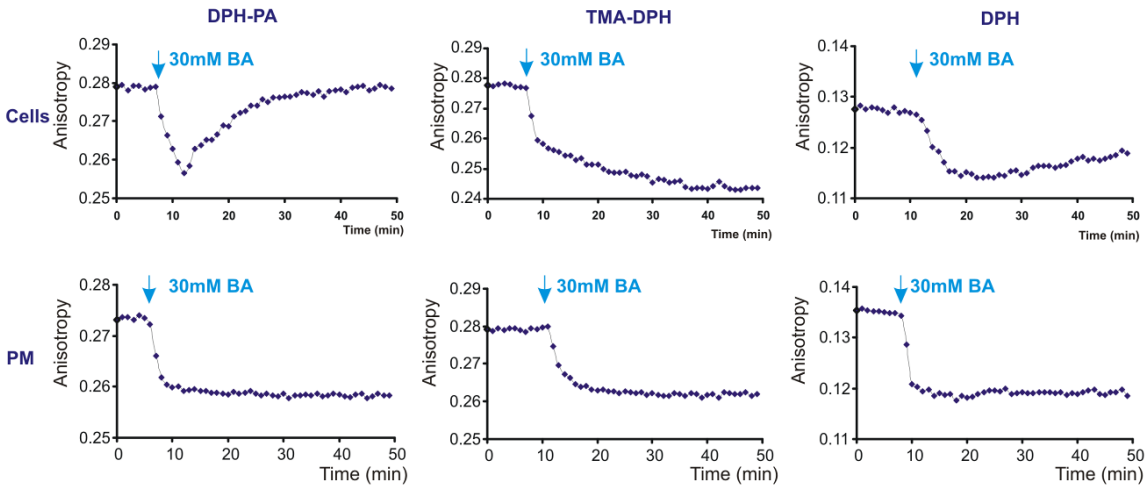

Figure 5.5. Cells and isolated PMs show different changes in anisotropy upon benzyl alcohol addition. K562 cells or PM fractions isolated from untreated cells were labelled with DPH-PA, TMA-DPH or DPH and the fluorescence steady-state anisotropy was followed at 37°C (representative traces are shown from n = 4 independent experiments). BA was administered as indicated (blue arrows).

Table 5.1. Fluorescence anisotropy changes during and after HS in different cell lines.

	DPH-PA		TMA-DPH		DPH	
	HS 1h	Post heat	HS 1h	Post heat	HS 1h	Post heat
B16 n=2	-0.001 ±0.0006	0.005 ±0.0017	-0.012 ±0.0043	-0.003 ±0.0014	-0.017 ±0.006	0.003 ±0.0017
L929 n=5	0.018 ±0.0022	0.025 ±0.0043	-0.011 ±0.0021	-0.004 ±0.0017	-0.013 ±0.0018	0.002 ±0.0016
WEHI164 n=2	-0.004 ±0.0019	0.002 ±0.0014	-0.009 ±0.0033	-0.003 ±0.0024	-0.006 ±0.0018	-0.004 ±0.0014
HeLa n=2	0.002 ±0.0008	0.008 ±0.0011	-0.013 ±0.0037	-0.006 ±0.0031	-0.008 ±0.0023	0.006 ±0.0023
mouse spleen cells n=2	0.009 ±0.0026	0.017 ±0.0033	-0.023 ±0.0061	-0.008 ±0.0047	0.002 ±0.0014	0.011 ±0.0048

B16, L929, WEHI169 and HeLa cells were cultured in DMEM supplemented with 10 % FCS, harvested by trypsinisation, washed twice and labelled as described in chapter 2.5. Freshly isolated mouse spleen cells were a generous gift from Duda laboratory BRC Szeged. HS was followed as in Figure 5.4. The anisotropy values were measured for 1 h at 42 °C for B16, L929, WEHI169 and HeLa cells and at 40 °C for mouse spleen cells (in order to keep the viability of spleen cells over 90 %). Thereafter the cuvette was cooled to 37 °C and after 5 min the post heat values were recorded. The anisotropy differences were calculated relative to the 37 °C control values. All measurements are expressed as the average of 5 min trace and presented as mean ± SD.

5.2.4. Changes in membrane heterogeneity, as detected by lifetime distribution, are caused by heat stress

The membrane's physical state can be evaluated by the DPH lifetime value, because the membrane's state causes a change in the dielectric constant of the probe's environment itself. Moreover, the dielectric constant is the particular property to which DPH fluorescence lifetime responds (Parasassi et al., 1992). In a continuous distribution of DPH lifetime values, the centre value gives information about the average polarity of the entire fluorophore environment, while the full width at half maximum (abbreviated to 'width', in the following text) yields a measure of the heterogeneity of this environment. The DPH lifetime distribution was measured before, during and after 1 h of HS at 42 °C in K562 cells (Figure 5.6).

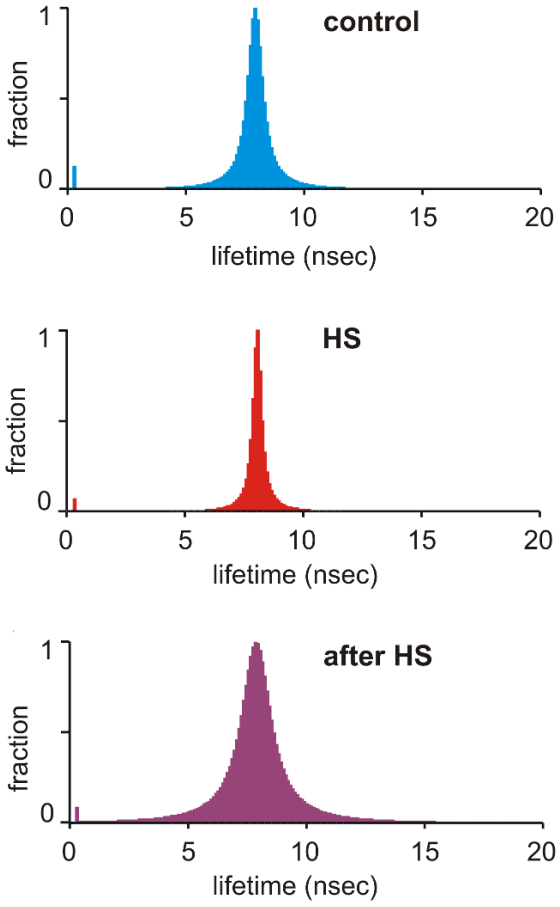

Figure 5.6. DPH lifetime distribution in K562 cells reveals heat-induced membrane heterogeneity changes. Cells were labelled with DPH. Phase and modulation data were collected using 9 modulation frequencies ranging from 2 to 180 MHz. Measurements were performed at 37 °C, during 1 h HS at 42 °C and in the post-heat phase after returning to 37 °C (representative results are shown from two independent experiments).

While the centre values remained constant during the heating/cooling cycle, the width altered with the different conditions when compared to the starting values. Thus, the width decreased with heating, but increased, to values higher than initial ones, in the post-heating phase (cells at 37 °C after HS). These data indicate a temporary relative decrease in membrane heterogeneity during HS, followed by a return to a significantly higher membrane heterogeneity in the post-heating phase.

5.2.5. DPH analogues distribute differently within cells

Information about the subcellular distribution of the probes is somewhat controversial in the literature (see Discussion). Thus, in order to determine which subcellular compartments were labelled by the probes, a fluorescence microscopic study was carried out. After 5 and 30 min labelling periods at different temperatures with DPH and its derivatives images were collected (Figure 5.7). It can be concluded from these results that individual DPH analogues label different cellular compartments to varying extents. DPH-PA showed a bright PM staining, but the nuclear membrane and an internal lamellar structure (probably ER) were labelled as well. The fluorescence signal for the PM was the most distinct with TMA-DPH which also revealed fainter, diffuse and vesicular internal structures. Labelling was less intense with DPH for all the cellular membranes which was unexpected. In fact, the brightest signals originated from discrete spots, which were assumed to be lipid droplets (LD). The latter conclusion was tested by a colabelling experiment. Cells were labelled with a LD-specific dye LD540 (Spandl et al., 2009) and with DPH. Merging of the images showed that the spots stained with DPH were almost completely colocalized with LDs stained with LD540 (Figure 5.8). this provided conformation that the structures were most probably LDs.

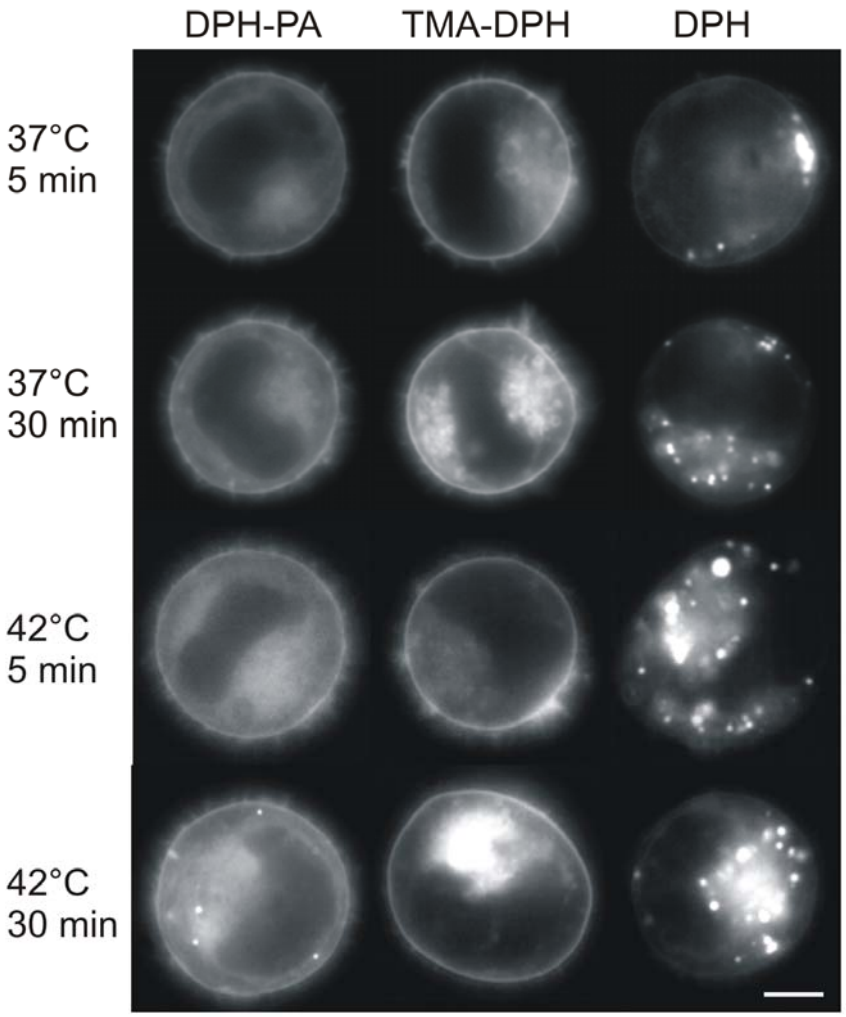

Figure 5.7. Different fluorescent probes show different patterns of localization in K562 cells. Cells were incubated with different DPH analogues at 37 °C or 42 °C for 5 or 30 min as indicated. Fluorescence video microscopic images were recorded within 2 min following the incubation (similar results were found in 3 independent experiments). Bar, 6 μm.

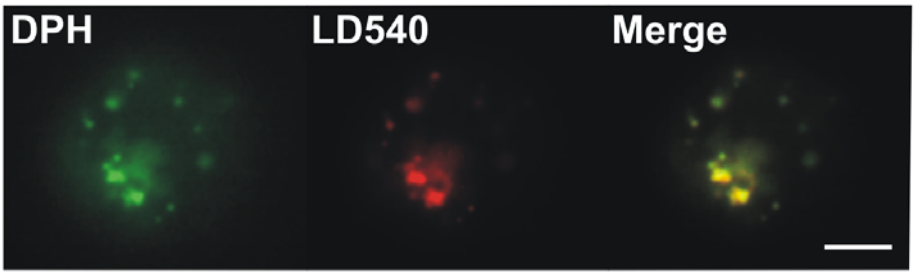

Figure 5.8. Colocalization of DPH with lipid droplets in K562 cells. Cells were double-stained with DPH and LD540 (which stains LDs) and examined with a CytoScout fluorescence microscope. Bar, 6 μm.

5.2.6. EPR studies provide confirmation that heat stress causes re-arrangements of membrane structure

Spin-label EPR spectra can provide data on the membrane environment of nitroxide-labelled stearic acids (Marsh, 1981; Páli et al., 2003). The stearic acid spin labels (5- and 16-SASL) partition from the aqueous phase into membranes with high affinity with their paramagnetic nitroxyl group located close to the lipid headgroup and near the centre of the bilayer, respectively (see e.g., Páli et al., 1999). EPR spectra of K562 cells labelled with 5- or 16-SASL were measured before, during and after HS (Figure 5.9). These were then compared.

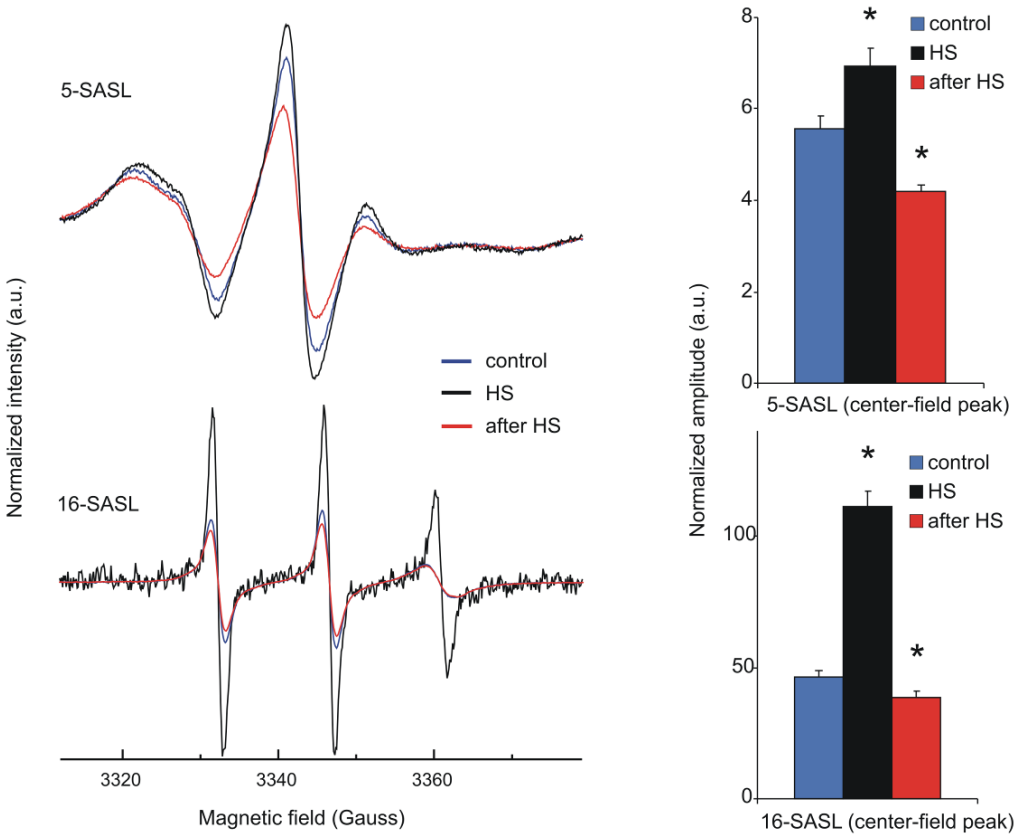

Figure 5.9. Spin-labelling of K562 cells reveals changes in membrane rigidization following HS. EPR spectra of K562 cells labelled with 5- (top) and 16-SASL (bottom) are shown. Spectra were recorded at 37 °C (blue lines, control), during 1 h HS at 42 °C (black lines, HS) and after returning to 37 °C (red lines, after HS). The spectra are normalised so that they represent the same number of spins. Total scan range is 10 mT. The corresponding bar graphs show the normalized amplitudes of the center-field ^{14}N hyperfine EPR lines ($m_I = 0$). Data are expressed as means ± SD, n = 3 (independent preparations), *$p < 0.05$ compared to 37 °C control, unpaired *t*-test.

There were no large alterations in hyperfine splitting, but significant alterations in the line widths at both vertical locations, probed by 5- and 16-SASL, respectively were observed (Figure 5.9). Increasing the temperature from 37 °C (blue lines) to 42 °C (black lines) increased the amplitude of the EPR lines in a depth-dependent manner due to motional line-narrowing (Figure 5.9). In the post-heat state when, after 1 h HS at 42 °C the measurements were carried out at 37 °C (red lines), however, a line-broadening effect and a decrease in the line heights, indicating rigidization, compared to the pre-heat state for both 5- and 16-SASL spin labels were found. To have an estimate of this line broadening, the normalized amplitude values (maximum line height normalised to the total spin label intensity, Dixon et al., 2004) were calculated and a similar relative change was found between the pre- and post-heat state for both labels (ratios of 0.76 and of 0.83 for 5- and 16-SASL (pre-heat:post-heat) center-field peaks, respectively, Figure 6.9, bar graphs).

5.3. DISCUSSION

5.3.1. Different probes reveal different aspects of membrane organisation

It had been shown previously that non-proteotoxic membrane perturbants are able to lower the temperature threshold for the HSR, i.e. to increase the expression of the Hsps in mammalian cells (Balogh et al., 2005; Nagy et al., 2007). To examine membrane alterations as a consequence of hyperfluidization stress, changes in membrane organisation were followed by different methods. Each of the fluorescence and paramagnetic probes used in this study were able to reveal membrane changes upon heat and/or BA stress. However, it is intriguing to question why the membrane order imaged by Laurdan and the membrane fluidity detected by different DPH analogues or spin-labelled probes were rather different (Table 5.2). One can suggest many reasons for environmental heterogeneity in relation to the properties of probes in specific environments. For example, the distribution of probes among cellular membranes and LDs, preference for the different leaflets of the PM, localization in a defined position (depth), attraction to or repulsion from charged environments or partition into specific lipid-lipid or lipid-protein organizations (domains or clusters) (Sklar, 1984). Thus, any conclusions from experiments in which only a single probe has been utilised must be

made with great care and, indeed, general interpretations of membrane fluidity should not be drawn.

Table 5.2. Characteristics of different probes used

	Membrane localization	Charge	Effect seen at post-stress state*
Laurdan	PM (confocal microscopy)	no	rigidization
Laurdan	endomembranes (confocal microscopy)	no	fluidization
Laurdan	whole cell membrane	no	overall fluidization
DPH	mainly LDs	no	rigidization
TMA-DPH	PM and PM-like endocytic compartments	positive	fluidization
DPH-PA	PM and endomembranes	negative	rigidization
5-SASL	PM endomembranes? (not in mitochondria)	negative	rigidization
16-SASL	PM endomembranes? (not in mitochondria)	negative	rigidization

* compared to the initial pre-stress state (control at 37 ºC). PM, plasma membrane; LD, lipid droplet.

5.3.2. Contrasting temperature-induced alterations in fluidity in different cellular membranes were shown with Laurdan

Laurdan two-photon microscopy revealed clearly an increased order (or a decreased fluidity) in PMs. This contrasted with a decreased membrane order (or an increased fluidity) in the intracellular membranes (particularly perinuclear) when cells were pre-exposed to HS. This conclusion was made possible because of the spatial resolution of Laurdan GP microscopy images. Moreover, in whole cells, when the GP values were averaged over all cell membrane compartments, a decreased order was obtained. This overall fluidization effect after HS clearly did not reveal the subtle nature of the subcellular alterations.

5.3.3. Depending on their chemical structure DPH analogues distribute differently in cells

The intramembrane and subcellular localization of DPH analogues has been widely studied. It has been proposed that they report, at least in part, from the PM (Revathi et al., 1994). Thus, TMA-DPH strongly incorporates into PM within 5 min (Figure 5.7). The internalization of this probe may be indicative of endocytosis, because the absence of TMA-DPH from non-endocytic compartments has been reported (Coupin et al., 1999). Moreover, using TMA-DPH fluorescence anisotropy assays it was concluded that membrane fluidity remains the same in the endocytic and the PM compartments (Illinger et al., 1995). When the microscopic images obtained were compared with those from the Kuhry-group and bearing in mind the constant nature of the anisotropy during the first 20 min trace at 37 °C (Figure 5.4), the above-mentioned view could be corroborated. The data obtained with TMA-DPH showed an increased fluidity in PM (and PM-like endocytic compartments) after HS. Post-heat fluidization of PM as monitored with TMA-DPH was also found in liver cells after 42 °C heating by (Revathi et al., 1994) and in several other cell lines following a severe 45 °C thermal challenge (Dynlacht and Fox, 1992b). The negatively charged DPH-PA reporting from PM and endomembranes (including the perinuclear region as well) (Figure 5.7) displayed a less fluid environment after HS (Figures 5.3, 5.4) compared to TMA-DPH. Interestingly, the anisotropy values in the post-stress relaxation period at 37 °C (Figure 5.4) showed the same characteristics as were found with post-heat labelling (Figure 5.3). Thus, anisotropy increased with DPH-PA and decreased with TMA-DPH. Therefore, it seems that the different labelling periods (short - 5 min or long - 60 min) did not influence the outcome of anisotropy values with these probes.

In addition to their different localization, positively or negatively charged probes are thought to show leaflet specificity. However, several partly conflicting conclusions are reported in the literature. Kitagawa et al. (1991) concluded that the quaternary ammonium cation TMA-DPH binds first to the outer leaflet of the PM and then gradually moves into the cytoplasmic side, distributing in both membrane leaflets but mainly to the inner leaflet. In contrast, the fluorescence anisotropy of anionic DPH-PA, according to these authors, reflects the fluidity of outer leaflet of the PM because of electric repulsion from the region, due to the presence of acidic phospholipids. On the other hand, the Schroeder group drew the opposite conclusion to explain their findings by the “charge similarity” principle: TMA-DPH appears to selectively localize in the

outer leaflet, while the negatively charged DPH-PA appears to localize to the inner leaflet of the PM (Gallegos et al., 2004). The Kurhy group (Coupin et al., 1999) reported that TMA-DPH, once incorporated into the peripheral membranes, was retained in the external leaflet of the bilayer. It is certainly possible, whatever the leaflet specificity of these probes is, that they prefer different lipid microenvironments due to their electric charge. In this vein, the FFA derivative (i.e. negatively charged) EPR probes may partition in a similar fashion to DPH-PA in membranes reporting most probably from the same charge-specific microenvironments. The localization of EPR probes cannot be studied directly but the observed line broadening effects were not dependent on the depth of the reporter moiety because it was seen that a similar relative change in the normalised amplitude as a result of HS for both spin labels (Figure 5.9). The line broadening was too small to determine which possible factors (e.g. changes in rotational dynamics or spin-spin interaction) contributed significantly, but some structural rearrangements, such as lateral reorganisation of membrane domains or an overall decrease in membrane fluidity (Kota et al., 2002) could explain the observed spectral effects. To summarise, I conclude that, the negatively charged fluorescent and EPR probes (regardless of their vertical localization in the bilayer) reported a less fluid environment in the post-heat state.

5.3.4. DPH itself partitions into lipid droplets

DPH was not strictly localized in the cellular membranes unlike its analogues. Instead it appeared to partition into LDs with high efficacy as well (Figures 5.7 and 5.8). This finding has been largely ignored in other studies reported in the literature despite some data showing the masking effect of TAGs on whole cell membrane anisotropy measurements with DPH (Collard and De Wildt, 1978; Pessin et al., 1978; Rodes et al., 1995; Storch et al., 1989). Up until recently, LDs, which occur in most mammalian cells, were considered inert storage sites for energy rich fats. However, LDs are increasingly considered nowadays as dynamic functional organelles involved in many intracellular processes like lipid metabolism, cell signalling, and vesicle trafficking (Meex et al., 2009). DPH revealed a fluidity decrease in the post-heat state of K562 cells (Figure 5.4) in agreement with the results of Revathi et al. (1994) using liver cells. However, I suggest that this is not attributable to the PM changes, but rather to the rearrangement of intracellular membranes and/or LDs. Examination of the DPH fluorescence lifetime measurement did not reveal any change in the center value.

Therefore, the average polarity of the entire fluorophore environment remained unaltered by HS. In contrast, a much broadened lifetime distribution was found in samples derived from the post-heating phase which suggested a more heterogeneous microenvironment for the probe. The data suggest that LDs may also undergo heat-induced remodelling.

5.3.5. Cells modify the fluidization seen in isolated membranes

In addition to the heat-induced membrane rearrangements detected in the post-heat state by DPH and its analogues, the time course of the reorganization revealed anomalous (and probe-dependent) responses of K562 cells to hyperfluidity stress. As well as the unchanged fluidity observed by DPH-PA upon HS, addition of the chemical fluidizer BA showed two-phase kinetics consisting of a rapid fluidization followed by an exponential fluidity compensation. This indicates that BA enters the membranes rapidly, while warming the cuvette takes a longer time which is long enough to maintain the anisotropy constant by continuous compensation during heating. Changes revealed by TMA-DPH showed an instantaneous membrane disordering upon both BA and heat stresses followed by a further decrease in anisotropy. A similar time-dependent gradual reduction in the TMA-DPH anisotropy was found during heat or alcohol treatment of Jurcat cells (Moulin et al., 2007). The different behaviour of living cells is in sharp contrast to the fluidity–temperature profile of isolated PM. This strongly indicates an active process, such as upregulated lipid enzyme function and/or protein translocation or transport for the membranes in live cells. In addition, the very similar alterations in the fluidity profiles following hyperfluidity treatment which were observed in several other cell lines *in vivo* suggest that the membrane rearrangement induced by a rapid membrane perturbation is a general phenomenon. This may, therefore, allow discussion and interpretation associated biochemical and biophysical phenomena to be placed in a more general context.

5.3.6. The probes detect stress-induced changes in membrane rafts

Laurdan microscopy has been shown by various laboratories to be capable of visualizing lipid structure and raft domains in living cells (Gaus et al., 2003) and showing the coalescence of ordered domains in specific membrane morphologies, such as macrophage filopodia (Gaus et al., 2003), neutrophil lamellipodia (Kindzelskii et al., 2004) or immunological synapses in T lymphocytes (Gaus et al., 2005). Moreover, the higher GP values reported from PM of K562 cells in my thesis can be attributed to coalescence and/or de novo production of ordered, raft-like domains as a result of stress. The data are in full agreement with previous data obtained in B16 cells using fPEG-Chol, which specifically recognizes sterol-rich membrane domains and colocalizes with various raft markers. When B16 cells were exposed to heat or BA treatment, the Chol-rich surface membrane microdomains fused into larger platforms following both treatments and this alteration persisted for hours after ceasing the stress (Nagy et al., 2007). Moreover, Ca^{2+} loading of erythrocytes has been reported to be coupled to an elevated lipid order (Vest et al., 2006). It was demonstrated previously in K562 cells (Balogh et al., 2005), that the intracellular Ca^{2+} level was ubiquitously upregulated as it was generally in heat-stressed cells (Kiang and Tsokos, 1998). Therefore, intracellular Ca^{2+}-rise may play a role in the ordering of PM as shown by Laurdan in response to HS (Figure 5.1).

It has been shown that elevated Cer levels can rapidly displace Chol from membrane/lipid "Chol-rafts" to form "Cer-rafts" (Grassme et al., 2007; Gulbins and Kolesnick, 2003; Patra, 2008). Increased Cer production was reported by Moulin et al. (2007) in a variety of cell types (HL60, U937, Jurkat and Jurkat A3 cells). Moreover, a key feature of the lipid remodelling due to heat or BA-induced membrane perturbation was also the increase in Cer in B16 cells (Chapter 4). Moreover, Al-Makdissy et al. (2003) measured DPH and TMA-DPH anisotropy during the sphingomyelinase treatment of PM. They reported that DPH and TMA-DPH anisotropy was reduced when Cer was produced. Thus, the probes was present in a more disordered lipid environment following Cer generation. Megha and London (2004) showed that this reduction in anisotropy was due to displacement of DPH, and probably TMA-DPH, from the ordered ceramide-rich rafts to the disordered lipid regions of the bilayer. The fluidity of PM and detergent-free raft fractions isolated from murine L-cells were compared using TMA-DPH and DPH-PA probes (Gallegos et al., 2004). Interestingly, TMA-DPH reported the

isolated raft to be more fluid than the PM, while DPH-PA suggested the opposite. In this thesis I have shown unambiguously that the microenvironmental changes may be sensed in a different way or even oppositely by structurally different probes, i.e. fluidization of PM was measured by TMA-DPH as opposed to the increased packing observed by Laurdan. However, the two phenomena could be linked to the extrusion of TMA-DPH from the newly formed or restructured ordered PM domains with stress, resulting in an overall increase in TMA-DPH fluidity. DPH-PA and the EPR probes, despite the differences in the depth of the probe location, reported an overall rigidization of the cellular membranes after HS, while Laurdan displayed an average fluidization. One explanation could be that the negatively charged probes are more sensitive to a rigidization which comes from the stress-induced ordered domain formation. This idea is supported by the fact that the acidic derivative of Laurdan, C-laurdan has been suggested to be a better sensor of membrane compared to Laurdan itself (Kaiser et al., 2009; Kim et al., 2007).

5.3.7. Thermosensitivity or tolerance can be influenced by membrane heterogeneity

The membrane changes described in this chapter can also be interpreted in relation to thermosensitivity or thermotolerance. Thus, in a comparative study heat-resistant and -sensitive mutants of CHO cells, mouse fibrosarcoma variants and Crandall feline kidney cells were stressed at 45 °C (Dynlacht and Fox, 1992b). They found that the level of post-heat fluidization as detected by TMA-DPH could be a marker to evaluate the heat sensitivity of the cells.

Cell membranes can be rapidly remodelled following mild membrane fluidization and this can directly contribute to the acquisition of stress tolerance (Shigapova et al., 2005) or indirectly can be involved in the upregulation of Hsp synthesis (Chapter 4 and (Nagy et al., 2007). The increased formation of rigid domains in surface membranes and the simultaneous increase in molecular disorder within the internal membranes, as shown in this chapter for K562 cells preexposed to mild HS, is also known to be accompanied by a massive formation of Hsps without any detectable loss of cell survival (Chapter 3). The localization of Hsp72 and Hsp60 was also affected by certain membrane fluidizing and HS treatments, thus causing a decrease in intracellular Hsps with a simultaneous increase in surface-located Hsps as reported recently by Dempsey et al. (2010). In addition, it was shown that membrane fluidizing treatments, like

hyperthermia can either increase or reduce the cytotoxicity of specific apoptosis inducers depending on cell used, type of drug or the stage of drug treatment at which the fluidizing treatment is applied (Dempsey et al., 2010). Therefore, decision-making between cell protection and cell death may involve similar processes. However, the contribution of individual elements can differ in these two phenomena thus leading to the reorganisation of plasma and intracellular membranes to different extents. Microscopic imaging of fluidization-induced membrane remodelling together with simultaneous measurement of signal transduction events originating from membranes, Hsp synthesis and protein translocation has broad application in the understanding of the molecular mechanisms of cell killing and survival. In turn, this could have an important application in developing better therapies for the medical treatment of diseases such as cancer.

CHAPTER 6. GENERAL DISCUSSION

Both acute and chronic stresses are able to disturb cellular homeostasis and to cause deleterious effects on cellular infrastructure. Therefore, organisms have developed a number of adaptive cellular response pathways. The cellular stress response is a universal mechanism of extraordinary physiological/pathophysiological significance.

The HSR, an important subclass of CSR, can be activated by diverse environmental and physiological stressors that result in the immediate induction of stress genes encoding molecular chaperones, proteases, and other proteins (Kültz, 2005). According to the *denatured protein sensor* hypothesis, a common cell sensory element might be misfolded or aggregated proteins disturbing the protein homeostasis (Morimoto, 1998). However, earlier studies on prokaryotes and yeast, as detailed in Chapter 1, clearly suggested that, during abrupt temperature fluctuations, membranes represent the most thermally sensitive macromolecular structures. These studies led to the formulation of the *membrane sensor hypothesis* which postulates that membranes can sense environmental changes and, as a consequence of changes in their phase state and microdomain organisation, transmit HS signals that activate *hsp* transcription (Vigh et al., 1998).

In this thesis I aimed to probe the validity of the membrane sensor theory in mammalian cells and to explore the mechanisms behind lipid signals and membrane lipid structural reorganizations leading to HSR and adaptation.

In Chapter 3 two structurally distinct membrane fluidizers, the local anaesthetic BA and HE were applied (see Balogh et al., 2005). These were used at concentrations so that their addition to K562 erythroleukemic cells caused similar increases in the level of PM fluidity as tested by DPH anisotropy. Thus, the level of membrane fluidization induced by the chemical agents on isolated membranes at such concentrations corresponded to the membrane fluidity increase seen during a thermal shift to 42 °C. The formation of isofluid membrane states in response to the administration of BA or HE resulted in an increase in the expression of Hsp70 at the physiological temperature and almost identical downshifts in the temperature thresholds of the HSR. Similarly to HS, the exposure of the cells to such membrane fluidizers elicited nearly identical increases of cytosolic Ca^{2+} concentration in both Ca^{2+}-containing and Ca^{2+}-free media and also closely similar increases in mitochondrial hyperpolarization. Very importantly, evidence was obtained that the activation of Hsp expression by membrane fluidizers was not induced by a protein unfolding signal.

In line with these results, the membrane sensor hypothesis was extended to B16(F10) mouse melanoma cells by applying BA and heat as stressors (Nagy et al., 2007). From these experiments it was concluded that a subset of *hsp* genes was upregulated as a result of stress. Moreover, through the *in vivo* labelling of melanoma cells with fPEG-Chol that inserts into Chol-rich membrane domains, it was found that similarly to HS, BA initiates profound redistribution of Chol-rich PM domains by increasing the number of larger, while decreasing the number of smaller domains.

In Chapter 4 I then went on to explore heat- and BA-induced stresses further by characterizing stress-induced membrane lipid changes in B16(F10) cells (see Balogh et al. 2010). Lipidomic fingerprints revealed that membrane stress achieved either by heat or BA resulted in pronounced and highly specific alterations in lipid composition. The loss in polyenes with the concomitant increase in saturated lipid species was shown to be a consequence of the activation of phospholipases (mainly PLA_2 and PLC). A PLC–DAG lipase–MAG lipase pathway was identified in B16(F10) cells and contributed significantly to the production of several lipid mediators upon stress including the potent HS modulator AA. Additionally, the accumulation of Chol, Cer and saturated PL species with raft-forming properties was observed upon both heat and BA treatments.

In Chapter 5 (see Balogh et al., 2011) heat-induced membrane changes were examined in more detail using several visualisation methods. With Laurdan two-photon microscopy it could be shown that, in contrast to the enhanced formation of ordered domains in surface membranes, the molecular disorder is significantly elevated within the internal membranes of cells preexposed to mild HS. These results were compared with those obtained by anisotropy, fluorescence lifetime and electron paramagnetic resonance measurements. All probes detected membrane changes upon HS. However, the structurally different probes revealed substantially distinct alterations in membrane heterogeneity. These data call attention to the careful interpretation of results obtained with only a single label.

Taken together, the accumulation of Chol, Cer and saturated PL species with raft-forming properties (Chapter 4) may explain the condensation of ordered PM domains in the B16(F10) melanoma model (Nagy et al., 2007) and presumably a similar mechanism can be responsible for PM ordering in K562 cells (Chapter 5). Additionally, these raft formations can be coupled with a modulation of the activities of certain *hsp* genes (Nagy et al., 2007). Thus, it has been shown that the membrane sensor hypothesis has a strong rationale. Ongoing studies further support this theory. Lipidomic analysis of B16(F10) cells cultured with different initial cell densities or with variant serum content

was carried out (Peter et al., 2012). Profound losses of polyene-containing lipid molecular species with a concomitant monoene production were found in conjunction with increasing cell number or decreasing serum content. AA content of PLs was 7.5 % and 3.4 % at 0.75 and 6 million cells/10 cm plate, respectively. Parallel investigations on the induction of selected *hsp* genes revealed that the lipid molecular species remodelling, initiated by variation in cell culture conditions, refines both the amplitude and profile of Hsp response upon HS, i.e. positive correlation was found between HSR (42 °C, 1 h) and cellular AA content (Peter et al., 2012). Importantly, parallel with the reduction of HSR, the total membrane area covered by fPEG-Chol-positive raft domains in high cell number cultures decreased by more than 50 % compared with those measured in low cell number counterparts (Gombos et al., 2011). It was demonstrated previously that membrane Chol profoundly affects the targeting of the small GTP-binding protein Rac1 to membranes (del Pozo et al., 2004). It was also suggested, that stress-stimulated, PI3K-driven conversion of PIP2 to PIP3 activates Rac1 under mild, non-denaturing HS conditions (Kültz, 2005), and Rac 1 may be required in HS-induced Hsp expression (Han et al., 2001). Therefore, the redistribution of Chol-rich membrane domains (also documented in Chapter 4) may alter the stress response via Rac1-dependent mechanism. Indeed, Rac1 inhibition by a specific inhibitor (NSC233766) diminished HS-induced *hsp25* expression by approximately 50 % at 41.5 °C (Gombos et al., 2011).

On the whole, by the results shown above, strong evidence has been provided for the membrane sensor hypothesis in mammalian cells. Combining my own data with literature findings allowed me to summarise the membrane-originated/associated lipid signals in the context of stress responses as depicted in Figure 6.1. This figure is a combination and extension of previous figures in Chapter 1 and 4, originally based on (Akhavan et al., 2010; Balogh et al., 2010; Escribá et al., 2008; Park et al., 2005; Vigh et al., 2005). The evidence for the summary diagram is as follows:

An early study by Calderwood et al. emphasized the importance of inositol lipid metabolism in HS, when the heat-induced initial falls in PIP2 and PIP levels were shown to be due to the action of PLC enzyme(s) (Calderwood et al., 1987). It is known that the different families of mammalian PLCs can be activated by several stimuli. During activation, interactions with regulatory proteins (receptor and non-receptor tyrosine kinases, subunits of heterotrimeric G proteins or small GTPases from the Ras and Rho family) could influence PLC conformation directly or, as suggested by recent

studies, bring PLC molecules within proximity of the membrane where the local environment could lead to interfacial activation (Bunney and Katan, 2011).

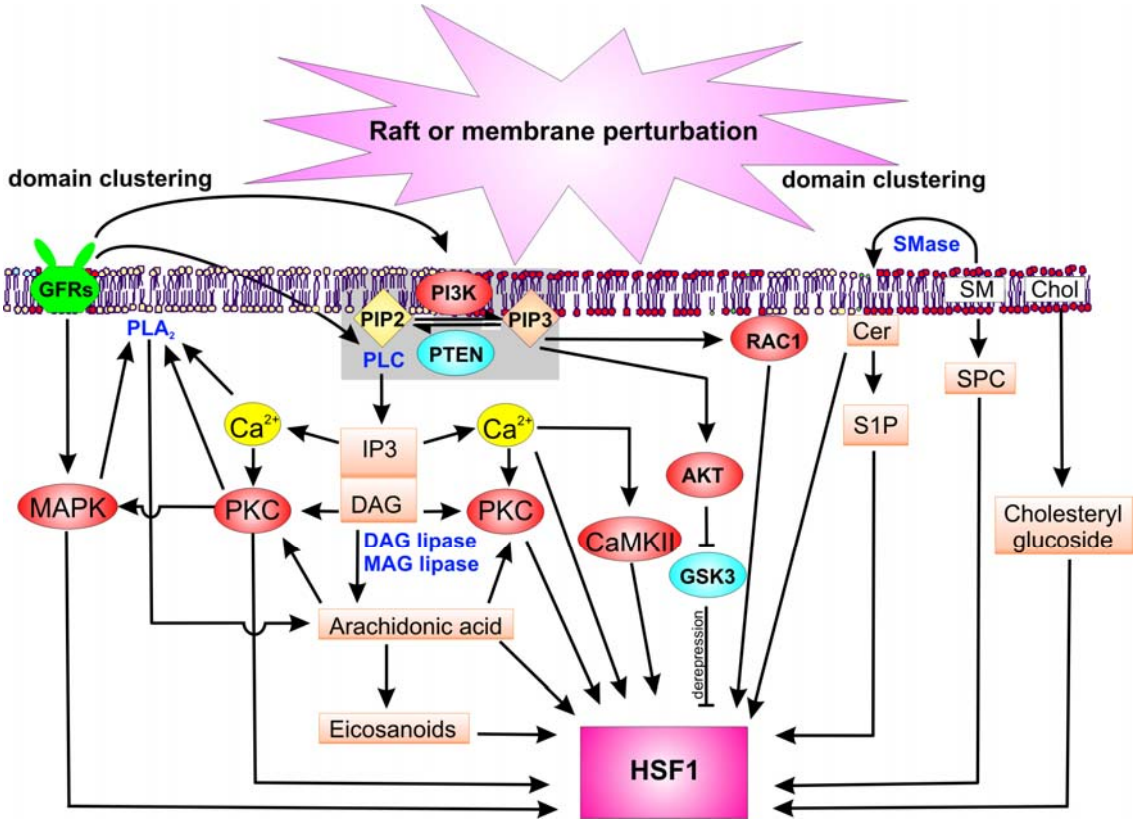

Figure 6.1. Membrane-controlled signal pathways in stress response. Akt, protein kinase B; CaMKII, calcium/calmodulin-dependent protein kinase II; Cer, ceramide; Chol, cholesterol; DAG lipase, diacylglycerol lipase; DAG, diacylglycerol; GFR, growth factor receptor; GSK3, glycogen synthase kinase-3; HSF1, heat shock factor 1; IP3, inositol triphosphate; MAG lipase, monoacylglycerol lipase; MAPK, mitogen-activated protein kinase; PI3K, phosphoinositide 3-kinase; PIP2, phosphatidylinositol-4,5-biphosphate; PIP3, phosphatidylinositol-3,4,5-triphosphate; PKC, protein kinase C; PLA2, phospholipase A2; PLC, phospholipase C; PTEN, phosphatase and tensin homologue protein; Rac1, Ras-related C3 botulinum toxin substrate 1; S1P, sphingosine-1-phosphate; SM, sphingomyelin; SMase, sphingomyelinase; SPC, sphingosyl phosphorylcholine. The figure is not intended to show the exact localisation of all components.

It is therefore conceivable that, in response to HS, the ligand-independent activation of growth factor receptors (Lambert et al., 2006) or the activation of small GTPases (e.g. Rac1) (together with membrane lipid environmental changes) lead to the initiation of PLC action. The best documented consequence of this reaction, and a major cell signalling response, is the generation of two second messengers: IP_3, a common Ca^{2+}-mobilizing second messenger, and DAG, an activator of several types of effector proteins including PKC isoforms (Bunney and Katan, 2011). HS is known to stimulate

rapid release of inositol phosphates (Calderwood et al., 1987). These results showed that inositol phosphate signals were generated within minutes and their turnover was very rapid. The concomitantly fast Ca^{2+}-rise (Chapter 3) is a prerequisite for the *hsp* transcription (Price and Calderwood, 1991). In addition, CaMKII mediates the HS response triggered by increases in $[Ca^{2+}]_i$, activation by the binding of Ca^{2+}/calmodulin and through the ability to undergo autophosphorylation (Holmberg et al., 2001). DAG can be further metabolised by DAG lipase–MAG lipase producing AA. AA together with lysoPLs can also be generated by PLA_2 enzymes. Elevations in $[Ca^{2+}]_i$, PKC phosphorylation, or protein–protein interactions (e.g. calmodulin) can regulate PLA_2 activity (van Rossum and Patterson, 2009). Moreover, the generation of *cis*-unsaturated FAs by PLA_2 is key to the activation of PKC, and may stabilize PKC in an activated state (Huang et al., 1997). It has been proposed that AA may serve to direct Ca^{2+}-sensitive and Ca^{2+}-insensitive PKC isoforms to proper membrane targets and feedback modulation of Ca^{2+} signals (O'Flaherty et al., 2001).

The above-mentioned Ca^{2+} signalling network is very complex. Based on a mathematical simulation, the EGFR signal flows through two interconnected pathways, the PLC–PKC pathway and the MAPK pathway which interact at two points. PKC activates MAPK, while MAPK can phosphorylate and activate $cPLA_2$. After this, the AA produced by $cPLA_2$ acts synergistically with DAG to activate PKC (Bhalla and Iyengar, 1999). AA can be further metabolized to eicosanoids, which can act through G protein coupled receptors. They can cross cell membranes to act on neighbouring cells or act within the cell and they function to stimulate enzymes such as PKC (van Rossum and Patterson, 2009). Certain eicosanoids and also the precursor AA alone are also able to induce HSR (Santoro, 2000).

PIP2 is a substrate of PI3K to produce PIP3, which is another lipid with key signalling functions and a major role in the control of cell survival (e.g. stress response), growth and proliferation. The components of the PI3K pathway include upstream regulators of PI3K enzymes (such as EGFR and Ras), PTEN, and several Ser/Thr kinases and transcription factors (Bunney and Katan, 2010). Several proteins propagate different cellular signals following binding to PIP3, and these include Akt and Rac1 (see above), important players of membrane-derived stress signal pathways. Moreover, it has been demonstrated that depolarization of myotubes increased the expression for Hsp70. In this model inhibition of IP_3-dependent Ca^{2+} signals or Ca^{2+}-dependent PKC and importantly, inhibition of PI3K activity all decreased Hsp70 induction (Jorquera et al., 2009).

Besides Hsp generation driven by the signal pathways in Figure 6.1, other membrane-protecting defence mechanisms should be taken into account. The increased formation of rigid domains in surface membranes and the parallel elevation of molecular disorder within the internal membranes, demonstrated in Chapter 6 for K562 cells pre-exposed to mild HS, strongly indicate an active process, e.g. upregulated lipid enzyme function and/or protein translocation or transport targeting the membranes in intact cells. The question arises as to whether these processes can contribute to cell survival. It has been documented that a subpopulation of Hsps is present either on the surface or within cellular membranes and certain Hsps remodel the pre-existing architecture and physical order of membranes (Horváth et al., 2008; Nakamoto and Vigh, 2007; Vigh et al., 2005; Vigh et al., 2007c). The roles of sHsps in controlling the physical state, bilayer stability and integrity of membranes via specific lipid interactions have basically been established in the case of the sHsp from *Synechocystis* PCC 6803, where most of the heat-induced Hsp17 is associated with thylakoid membranes (Horváth et al., 1998). The interactions between purified Hsp17 and large unilamellar vesicles consisting of synthetic or cyanobacterial lipids strongly increase the membrane microviscosity (Török et al., 2001). GroEL chaperonin also associates with thylakoid and lipid membranes (Kovacs et al., 1994; Török et al., 1997) increasing the membrane physical order, especially in the polar headgroup region of the lipid. Therefore, GroEL chaperonins are not only able to assist the folding of both soluble and membrane-associated proteins, but also to rigidify and therefore stabilize lipid membranes during HS (Török et al., 1997). In mammalian cells most of the Hsp60 is localized in the matrix compartment of the mitochondria. A membrane localization for Hsp70, the major stress-inducible chaperon of mammalian cells, and Hsp60 was induced by certain membrane fluidizing and HS treatments (Dempsey et al., 2010). Moreover, it was earlier suggested that Hsp70 might associate directly with PM lipids (Hightower and Guidon, 1989). Furthermore, different Hsps have been found to associate to a variable extent with detergent-resistant microdomains, and the association of the Hsps with these microdomains can be modulated by stress (Broquet et al., 2003). In conclusion, besides other proteins, such as members of Ras/Rac small GTPases, which become prenylated and membrane-associated during stress (see above and in (Escribá et al., 2008; Vigh et al., 2005), the pre-existing Hsps could be important for the general membrane defence mechanism. On the other hand, a key feature of the lipid remodelling due to heat- (both mild and severe) or BA-induced membrane perturbation was the accumulation of Chol, Cer, saturated PC and PE-P species in B16(F10) cells. These lipid species support the

formation of tightly-packed subdomains in model membranes and raft domains in cells. In addition, the lipid chain saturation itself or the elevated Chol level are able to stabilize the membranes during HS (Quinn et al., 1989).

Membrane alterations, signal pathways from membranes to *hsp* genes and Hsps themselves play fundamental roles in the aetiology of several human diseases, such as cancer or type 2 diabetes (Escribá et al., 2008). Insulin and the insulin-like growth factors (IGFs) control many aspects of metabolism, growth and survival in a wide range of mammalian tissues. Insulin/IGF signalling also contributes to regulation of lifespan (Narasimhan et al., 2009), while dysregulation of signalling has been implicated in cancer (Pollak, 2008). Although insulin and IGFs play distinct physiological roles, they utilise the same signalling pathways, involving PI3K and Akt or Ras and MAPK, which mediate responses to many other cellular stimuli (Siddle, 2011). Activation of Akt mediates insulin-stimulated translocation of GLUT4 glucose transporters to PM in muscle and adipose tissue (Whiteman et al., 2002), while downregulation of this pathway may contribute to diabetes-associated insulin resistance. On the other hand, several human tumours have mutations that elevate signalling through PI3K pathway that is induced by insulin and a number of growth factors (Pollak, 2008). In addition, the MAG lipase–FFA network regulates a host of secondary lipid metabolites that include key signalling molecules, such as LPA and PGE2, known to support cancer malignancy. Therefore, MAG lipase serves as key metabolic hub in aggressive cancer cells, where the enzyme regulates a FA network that feeds into a number of pro-tumourigenic signalling pathways (Nomura et al., 2010). Moreover, the aberrant function of the above-mentioned pathways in disease states leads to downregulated or enhanced Hsp formation. Decreased expression of stress proteins in patients with type 2 diabetes correlates with reduced insulin sensitivity; activation of Hsp70 with heat therapy is known to improve clinical parameters in these patients (Chung et al., 2008; Hooper and Hooper, 2005). Conversely, aberrantly high levels of either the overall array of Hsps or certain Hsp classes are characteristic of different cancer cells (Escribá et al., 2008).

Collectively, the presented data in this thesis point beyond the initial goal of the thesis. The integrated view of lipid-controlled signalling pathways in Figure 6.1 may help to better understand the complex network of lipids and regulatory proteins and their roles in stress response. It should be noted, however, that the mechanism(s) for the transmission of a stress signal from the cell surface to *hs* genes with the involvement of the activation of lipases, receptors or receptor-like molecules is far from clear. Further investigations of the network of these pathways that trigger or attenuate survival,

proliferation or energy metabolism, is essential in order to understand the pathomechanism of numerous diseases and for identifying of new therapeutic targets.

Although Selye's vision on the protective nature of stress responses in diseases was formulated more than 60 years ago, his legacy of empiric research remains extremely influential today: "Disease consists of two components-damage and defence. Up to now medicine attempted to attack almost only the damaging pathogen (to kill the germs, to excise tumours, to neutralize poisons). As regards defence, hitherto medicine limited itself to such vague advice as the usefulness of rest, wholesome food, etc. A study of the general adaptation syndrome suggests that henceforth we will be able to rely upon much more effective means of aiding adaptation to non-specific local or systemic injury by supplementing the natural defensive measures of the general adaptation syndrome whenever these are suboptimal." (Selye, 1950).

BIBLIOGRAPHY

Ahn S, Thiele DJ (2003) Redox regulation of mammalian heat shock factor 1 is essential for Hsp gene activation and protection from stress. Genes Dev 17: 516-528.

Ahyayauch H, Villar AV, Alonso A, Goñi FM (2005) Modulation of PI-specific phospholipase C by membrane curvature and molecular order. Biochemistry 44: 11592-11600.

Akerfelt M, Morimoto RI, Sistonen L (2010) Heat shock factors: integrators of cell stress, development and lifespan. Nat Rev Mol Cell Biol 11: 545-555.

Akhavan D, Cloughesy TF, Mischel PS (2010) mTOR signaling in glioblastoma: lessons learned from bench to bedside. Neuro Oncol 12: 882-889.

Al-Makdissy N, Younsi M, Pierre S, Ziegler O, Donner M (2003) Sphingomyelin/cholesterol ratio: an important determinant of glucose transport mediated by GLUT-1 in 3T3-L1 preadipocytes. Cell Signal 15: 1019-1030.

Alanko SMK, Halling KK, Maunula S, Slotte JP, Ramstedt B (2005) Displacement of sterols from sterol/sphingomyelin domains in fluid bilayer membranes by competing molecules. Biochim Biophys Acta 1715: 111-121.

Amici C, Palamara AT, Santoro MG (1993) Induction of thermotolerance by prostaglandin A in human cells. Exp Cell Res 207: 230-234.

Amici C, Sistonen L, Santoro MG, Morimoto RI (1992) Antiproliferative prostaglandins activate heat shock transcription factor. Proc Natl Acad Sci U S A 89: 6227-6231.

Ananthan J, Goldberg AL, Voellmy R (1986) Abnormal proteins serve as eukaryotic stress signals and trigger the activation of heat shock genes. Science 232: 522-524.

Anckar J, Sistonen L (2011) Regulation of HSF1 function in the heat stress response: implications in aging and disease. Annu Rev Biochem 80: 1089-1115.

Azem A, Diamant S, Kessel M, Weiss C, Goloubinoff P (1995) The protein-folding activity of chaperonins correlates with the symmetric GroEL14(GroES7)2 heterooligomer. Proc Natl Acad Sci U S A 92: 12021-12025.

Bagatolli LA (2006) To see or not to see: lateral organization of biological membranes and fluorescence microscopy. Biochim Biophys Acta 1758: 1541-1556.

Baginski ES, Foà PP, Zak B (1967) Microdetermination of inorganic phosphate, phospholipids, and total phosphate in biologic materials. Clin Chem 13: 326-332.

Balboa MA, Balsinde J (2006) Oxidative stress and arachidonic acid mobilization. Biochim Biophys Acta 1761: 385-391.

Balogh G, Horváth I, Nagy E, Hoyk Z, Benkõ S, et al. (2005) The hyperfluidization of mammalian cell membranes acts as a signal to initiate the heat shock protein response. FEBS J 272: 6077-6086.

Balogh G, Maulucci G, Gombos I, Horváth I, Török Z, et al. (2011) Heat stress causes spatially-distinct membrane re-modelling in K562 leukemia cells. PLoS One 6: e21182.

Balogh G, Péter M, Liebisch G, Horváth I, Török Z, et al. (2010) Lipidomics reveals membrane lipid remodelling and release of potential lipid mediators during early stress responses in a murine melanoma cell line. Biochim Biophys Acta 1801: 1036-1047.

Balsinde J, Balboa MA, Insel PA, Dennis EA (1999) Regulation and inhibition of phospholipase A2. Annu Rev Pharmacol Toxicol 39: 175-189.

Balsinde J, Dennis EA (1996) Distinct roles in signal transduction for each of the phospholipase A2 enzymes present in P388D1 macrophages. J Biol Chem 271: 6758-6765.

Balsinde J, Winstead MV, Dennis EA (2002) Phospholipase A(2) regulation of arachidonic acid mobilization. FEBS Lett 531: 2-6.

Bang OS, Ha BG, Park EK, Kang SS (2000) Activation of Akt is induced by heat shock and involved in suppression of heat-shock-induced apoptosis of NIH3T3 cells. Biochem Biophys Res Commun 278: 306-311.

Baritaki S, Apostolakis S, Kanellou P, Dimanche-Boitrel M, Spandidos DA, et al. (2007) Reversal of tumor resistance to apoptotic stimuli by alteration of membrane fluidity: therapeutic implications. Adv Cancer Res 98: 149-190.

Berliner L (1976) Spin Labeling: Theory and Applications, Academic Press, New York.

Bevers EM, Williamson PL (2010) Phospholipid scramblase: an update. FEBS Lett 584: 2724-2730.

Bhalla US, Iyengar R (1999) Emergent properties of networks of biological signaling pathways. Science 283: 381-387.

Bijur GN, Jope RS (2000) Opposing actions of phosphatidylinositol 3-kinase and glycogen synthase kinase-3beta in the regulation of HSF-1 activity. J Neurochem 75: 2401-2408.

Bionda C, Hadchity E, Alphonse G, Chapet O, Rousson R, et al. (2007) Radioresistance of human carcinoma cells is correlated to a defect in raft membrane clustering. Free Radic Biol Med 43: 681-694.

Bisogno T, Cascio MG, Saha B, Mahadevan A, Urbani P, et al. (2006) Development of the first potent and specific inhibitors of endocannabinoid biosynthesis. Biochim Biophys Acta 1761: 205-212.

Bisogno T, Howell F, Williams G, Minassi A, Cascio MG, et al. (2003) Cloning of the first sn1-DAG lipases points to the spatial and temporal regulation of endocannabinoid signaling in the brain. J Cell Biol 163: 463-468.

Björk JK, Sistonen L (2010) Regulation of the members of the mammalian heat shock factor family. FEBS J 277: 4126-4139.

Boggs JM, Mason JT (1986) Calorimetric and fatty acid spin label study of subgel and interdigitated gel phases formed by asymmetric phosphatidylcholines. Biochim Biophys Acta 863: 231-242.

Boon JM, Smith BD (2002) Chemical control of phospholipid distribution across bilayer membranes. Med Res Rev 22: 251-281.

Borkan SC, Gullans SR (2002) Molecular chaperones in the kidney. Annu Rev Physiol 64: 503-527.

Bosco EE, Mulloy JC, Zheng Y (2009) Rac1 GTPase: a "Rac" of all trades. Cell Mol Life Sci 66: 370-374.

Brameshuber M, Weghuber J, Ruprecht V, Gombos I, Horváth I, et al. (2010) Imaging of mobile long-lived nanoplatforms in the live cell plasma membrane. J Biol Chem 285: 41765-41771.

Bretscher MS (1971) The proteins of erythrocyte membranes: where are they?. Biochem J 122: 40P.

Brites P, Waterham HR, Wanders RJA (2004) Functions and biosynthesis of plasmalogens in health and disease. Biochim Biophys Acta 1636: 219-231.

Broquet AH, Thomas G, Masliah J, Trugnan G, Bachelet M (2003) Expression of the molecular chaperone Hsp70 in detergent-resistant microdomains correlates with its membrane delivery and release. J Biol Chem 278: 21601-21606.

Brown DA, Rose JK (1992) Sorting of GPI-anchored proteins to glycolipid-enriched membrane subdomains during transport to the apical cell surface. Cell 68: 533-544.

Brügger B, Erben G, Sandhoff R, Wieland FT, Lehmann WD (1997) Quantitative analysis of biological membrane lipids at the low picomole level by nano-electrospray ionization tandem mass spectrometry. Proc Natl Acad Sci U S A 94: 2339-2344.

Buchan JR, Parker R (2009) Eukaryotic stress granules: the ins and outs of translation. Mol Cell 36: 932-941.

Bukau B, Horwich AL (1998) The Hsp70 and Hsp60 chaperone machines. Cell 92: 351-366.

Bunney TD, Katan M (2010) Phosphoinositide signalling in cancer: beyond PI3K and PTEN. Nat Rev Cancer 10: 342-352.

Bunney TD, Katan M (2011) PLC regulation: emerging pictures for molecular mechanisms. Trends Biochem Sci 36: 88-96.

Burke JE, Dennis EA (2009) Phospholipase A2 structure/function, mechanism, and signaling. J Lipid Res 50 Suppl: S237-42.

Butler PJ, Tsou T, Li JY, Usami S, Chien S (2002) Rate sensitivity of shear-induced changes in the lateral diffusion of endothelial cell membrane lipids: a role for membrane perturbation in shear-induced MAPK activation. FASEB J 16: 216-218.

Calderwood SK, Bornstein B, Farnum EK, Stevenson MA (1989) Heat shock stimulates the release of arachidonic acid and the synthesis of prostaglandins and leukotriene B4 in mammalian cells. J Cell Physiol 141: 325-333.

Calderwood SK, Ciocca DR (2008) Heat shock proteins: stress proteins with Janus-like properties in cancer. Int J Hyperthermia 24: 31-39.

Calderwood SK, Stevenson MA (1993) Inducers of the heat shock response stimulate phospholipase C and phospholipase A2 activity in mammalian cells. J Cell Physiol 155: 248-256.

Calderwood SK, Stevenson MA, Hahn GM (1987) Heat stress stimulates inositol trisphosphate release and phosphorylation of phosphoinositides in CHO and Balb C 3T3 cells. J Cell Physiol 130: 369-376.

Calderwood SK, Stevenson MA, Hahn GM (1988) Effects of heat on cell calcium and inositol lipid metabolism. Radiat Res 113: 414-425.

Calderwood SK, Stevenson MA, Price BD (1993) Activation of phospholipase C by heat shock requires GTP analogs and is resistant to pertussis toxin. J Cell Physiol 156: 153-159.

Calderwood SK, Xie Y, Wang X, Khaleque MA, Chou SD, et al. (2010) Signal transduction pathways leading to heat shock transcription. Sign Transduct Insights 2: 13-24.

Carrasco S, Mérida I (2007) Diacylglycerol, when simplicity becomes complex. Trends Biochem Sci 32: 27-36.

Carratù L, Franceschelli S, Pardini CL, Kobayashi GS, Horvath I, et al. (1996) Membrane lipid perturbation modifies the set point of the temperature of heat shock response in yeast. Proc Natl Acad Sci U S A 93: 3870-3875.

Catalá A (2010) A synopsis of the process of lipid peroxidation since the discovery of the essential fatty acids. Biochem Biophys Res Commun 399: 318-323.

Chang Y, Abe A, Shayman JA (1995) Ceramide formation during heat shock: a potential mediator of alpha B-crystallin transcription. Proc Natl Acad Sci U S A 92: 12275-12279.

Chau LY, Tai HH (1981) Release of arachidonate from diglyceride in human platelets requires the sequential action of a diglyceride lipase and a monoglyceride lipase. Biochem Biophys Res Commun 100: 1688-1695.

Cheng JZ, Sharma R, Yang Y, Singhal SS, Sharma A, et al. (2001) Accelerated metabolism and exclusion of 4-hydroxynonenal through induction of RLIP76 and hGST5.8 is an early adaptive response of cells to heat and oxidative stress. J Biol Chem 276: 41213-41223.

Christie WW, Han X (2010) Lipid analysis - Isolation, Separation, Identification and Lipidomic Analysis, The Oily Press, Bridgwater.

Chung J, Nguyen A, Henstridge DC, Holmes AG, Chan MHS, et al. (2008) HSP72 protects against obesity-induced insulin resistance. Proc Natl Acad Sci U S A 105: 1739-1744.

Collard JG, De Wildt A (1978) Localization of the lipid probe 1,6-diphenyl-1,3,5 hexatriene (DPH) in intact cells by fluorescence microscopy. Exp Cell Res 116: 447-450.

Cook H, McMaster C (2004) Fatty acid desaturation and chain elongation in eukaryotes. In: Vance D and Vance J (Eds.), Biochemistry of Lipids, Lipoproteins and Membranes. Elsevier, Amsterdam. pp 181-204.

Corda D, Zizza P, Varone A, Filippi BM, Mariggiò S (2009) The glycerophosphoinositols: cellular metabolism and biological functions. Cell Mol Life Sci 66: 3449-3467.

Cottet-Rousselle C, Ronot X, Leverve X, Mayol J (2011) Cytometric assessment of mitochondria using fluorescent probes. Cytometry A 79: 405-425.

Coupin GT, Muller CD, Rémy-Kristensen A, Kuhry JG (1999) Cell surface membrane homeostasis and intracellular membrane traffic balance in mouse L929 cells. J Cell Sci 112 (Pt 14): 2431-2440.

Csermely P, Schnaider T, Soti C, Prohászka Z, Nardai G (1998) The 90-kDa molecular chaperone family: structure, function, and clinical applications. A comprehensive review. Pharmacol Ther 79: 129-168.

Csont T, Balogh G, Csonka C, Boros I, Horváth I, et al. (2002) Hyperlipidemia induced by high cholesterol diet inhibits heat shock response in rat hearts. Biochem Biophys Res Commun 290: 1535-1538.

Curran BP, Khalawan SA (1994) Alcohols lower the threshold temperature for the maximal activation of a heat shock expression vector in the yeast Saccharomyces cerevisiae. Microbiology 140: 2225-2228.

de Marco A, Vigh L, Diamant S, Goloubinoff P (2005) Native folding of aggregation-prone recombinant proteins in Escherichia coli by osmolytes, plasmid- or benzyl alcohol-overexpressed molecular chaperones. Cell Stress Chaperones 10: 329-339.

Demchenko AP, Mély Y, Duportail G, Klymchenko AS (2009) Monitoring biophysical properties of lipid membranes by environment-sensitive fluorescent probes. Biophys J 96: 3461-3470.

Dempsey NC, Ireland HE, Smith CM, Hoyle CF, Williams JHH (2010) Heat shock protein translocation induced by membrane fluidization increases tumor-cell sensitivity to chemotherapeutic drugs. Cancer Lett 296: 257-267.

del Pozo MA, Alderson NB, Kiosses WB, Chiang H, Anderson RGW, et al. (2004) Integrins regulate Rac targeting by internalization of membrane domains. Science 303: 839-842.

Dietz TJ, Somero GN (1992) The threshold induction temperature of the 90-kDa heat shock protein is subject to acclimatization in eurythermal goby fishes (genus Gillichthys). Proc Natl Acad Sci U S A 89: 3389-3393.

Ding XZ, Smallridge RC, Galloway RJ, Kiang JG (1996) Increases in HSF1 translocation and synthesis in human epidermoid A-431 cells: role of protein kinase C and [Ca2+]i. J Investig Med 44: 144-153.

Dixon N, Pali T, Kee TP, Marsh D (2004) Spin-labelled vacuolar-ATPase inhibitors in lipid membranes. Biochim Biophys Acta 1665: 177-183.

Dragovic Z, Broadley SA, Shomura Y, Bracher A, Hartl FU (2006) Molecular chaperones of the Hsp110 family act as nucleotide exchange factors of Hsp70s. EMBO J 25: 2519-2528.

Duda E, Benko S, Galiba E, Horvath I, Pali T, et al. (1994) Lipid saturation in the target cells plasma membrane blocks tumor necrosis factor mediated cell killing. In: Berczi, I. and Szelenyi, J. (Eds.), Advances in Psychoneuroimmunology. Plenum Press, New York. pp 181-190.

Dynlacht JR, Fox MH (1992a) Heat-induced changes in the membrane fluidity of Chinese hamster ovary cells measured by flow cytometry. Radiat Res 130: 48-54.

Dynlacht JR, Fox MH (1992b) The effect of 45 degrees C hyperthermia on the membrane fluidity of cells of several lines. Radiat Res 130: 55-60.

Elmquist JK, Scammell TE, Saper CB (1997) Mechanisms of CNS response to systemic immune challenge: the febrile response. Trends Neurosci 20: 565-570.

Engblom D, Ek M, Saha S, Ericsson-Dahlstrand A, Jakobsson P, et al. (2002) Prostaglandins as inflammatory messengers across the blood-brain barrier. J Mol Med (Berl) 80: 5-15.

Escribá PV, González-Ros JM, Goñi FM, Kinnunen PKJ, Vigh L, et al. (2008) Membranes: a meeting point for lipids, proteins and therapies. J Cell Mol Med 12: 829-875.

Escribá PV, Sánchez-Dominguez JM, Alemany R, Perona JS, Ruiz-Gutiérrez V (2003) Alteration of lipids, G proteins, and PKC in cell membranes of elderly hypertensives. Hypertension 41: 176-182.

Fadeel B, Xue D (2009) The ins and outs of phospholipid asymmetry in the plasma membrane: roles in health and disease. Crit Rev Biochem Mol Biol 44: 264-277.

Fahy E, Subramaniam S, Brown HA, Glass CK, Merrill AHJ, et al. (2005) A comprehensive classification system for lipids. J Lipid Res 46: 839-861.

Fahy E, Subramaniam S, Murphy RC, Nishijima M, Raetz CRH, et al. (2009) Update of the LIPID MAPS comprehensive classification system for lipids. J Lipid Res 50 Suppl: S9-14.

Farrer BT, Pecoraro VL (2002) Heavy-metal complexation by de novo peptide design. Curr Opin Drug Discov Devel 5: 937-943.

Finka A, Mattoo RUH, Goloubinoff P (2011) Meta-analysis of heat- and chemically upregulated chaperone genes in plant and human cells. Cell Stress Chaperones 16: 15-31.

Folch J, Lees M, Sloane Stanley GH (1957) A simple method for the isolation and purification of total lipides from animal tissues. J Biol Chem 226: 497-509.

Futai M, Sternweis PC, Heppel LA (1974) Purification and properties of reconstitutively active and inactive adenosinetriphosphatase from Escherichia coli. Proc Natl Acad Sci U S A 71: 2725-2729.

Gallegos AM, McIntosh AL, Atshaves BP, Schroeder F (2004) Structure and cholesterol domain dynamics of an enriched caveolae/raft isolate. Biochem J 382: 451-461.

Galloway SM, Deasy DA, Bean CL, Kraynak AR, Armstrong MJ, et al. (1987) Effects of high osmotic strength on chromosome aberrations, sister-chromatid exchanges and DNA strand breaks, and the relation to toxicity. Mutat Res 189: 15-25.

Garbe TR, Yukawa H (2001) Common solvent toxicity: autoxidation of respiratory redox-cyclers enforced by membrane derangement. Z Naturforsch C 56: 483-491.

Gaus K, Chklovskaia E, Fazekas de St Groth B, Jessup W, Harder T (2005) Condensation of the plasma membrane at the site of T lymphocyte activation. J Cell Biol 171: 121-131.

Gaus K, Gratton E, Kable EPW, Jones AS, Gelissen I, et al. (2003) Visualizing lipid structure and raft domains in living cells with two-photon microscopy. Proc Natl Acad Sci U S A 100: 15554-15559.

Ghomashchi F, Loo R, Balsinde J, Bartoli F, Apitz-Castro R, et al. (1999) Trifluoromethyl ketones and methyl fluorophosphonates as inhibitors of group IV and VI phospholipases A(2): structure-function studies with vesicle, micelle, and membrane assays. Biochim Biophys Acta 1420: 45-56.

Goloubinoff P, Christeller JT, Gatenby AA, Lorimer GH (1989) Reconstitution of active dimeric ribulose bisphosphate carboxylase from an unfoleded state depends on two chaperonin proteins and Mg-ATP. Nature 342: 884-889.

Gombos I, Crul T, Piotto S, Güngör B, Török Z, et al. (2011) Membrane-lipid therapy in operation: The HSP co-inducer BGP-15 activates stress signal transduction pathways by remodeling plasma membrane rafts. Plos One accepted: .

Gomez-Cambronero J (2010) New concepts in phospholipase D signaling in inflammation and cancer. ScientificWorldJournal 10: 1356-1369.

Goparaju SK, Ueda N, Taniguchi K, Yamamoto S (1999) Enzymes of porcine brain hydrolyzing 2-arachidonoylglycerol, an endogenous ligand of cannabinoid receptors. Biochem Pharmacol 57: 417-423.

Grant RL, Acosta DJ (1994) A digitized fluorescence imaging study on the effects of local anesthetics on cytosolic calcium and mitochondrial membrane potential in cultured rabbit corneal epithelial cells. Toxicol Appl Pharmacol 129: 23-35.

Grassme H, Riethmuller J, Gulbins E (2007) Biological aspects of ceramide-enriched membrane domains. Prog Lipid Res 46: 161-170.

Gratton E, Limkeman M (1983) A continuously variable frequency cross-correlation phase fluorometer with picosecond resolution. Biophys J 44: 315-324.

Grimm MJ, Zynda ER, Repasky EA (2009) Temperature matters: cellular targets of hyperthermia in cancer biology and immunology. In: Pockley AG, Calderwood SK and Santoro MG (Eds.), Prokaryotic and Eukaryotic Heat Shock Proteins in Infectious Disease. Springer, Dordrecht. pp 267-306.

Griner EM, Kazanietz MG (2007) Protein kinase C and other diacylglycerol effectors in cancer. Nat Rev Cancer 7: 281-294.

Grynkiewicz G, Poenie M, Tsien RY (1985) A new generation of Ca2+ indicators with greatly improved fluorescence properties. J Biol Chem 260: 3440-3450.

Gudi S, Nolan JP, Frangos JA (1998) Modulation of GTPase activity of G proteins by fluid shear stress and phospholipid composition. Proc Natl Acad Sci U S A 95: 2515-2519.

Gulbins E, Kolesnick R (2003) Raft ceramide in molecular medicine. Oncogene 22: 7070-7077.

Gupta SC, Sharma A, Mishra M, Mishra RK, Chowdhuri DK (2010) Heat shock proteins in toxicology: how close and how far? Life Sci 86: 377-384.

Gurr MI, Harwood JL, Frayn KN (2002) Lipid Biochemistry, Blackwell Science, Oxford.

Guschina IA, Harwood JL (2006) Mechanisms of temperature adaptation in poikilotherms. FEBS Lett 580: 5477-5483.

Guyton KZ, Gorospe M, Wang X, Mock YD, Kokkonen GC, et al. (1998) Age-related changes in activation of mitogen-activated protein kinase cascades by oxidative stress. J Investig Dermatol Symp Proc 3: 23-27.

Hahn J (2009) The Hsp90 chaperone machinery: from structure to drug development. BMB Rep 42: 623-630.

Hammer Ø, Harper DA, Ryan PD (2001) PAST: paleontological statistics software package for education and data analysis. Palaeontologia Electronica 4: 9pp.

Han SI, Oh SY, Jeon WJ, Kim JM, Lee JH, et al. (2002) Mild heat shock induces cyclin D1 synthesis through multiple Ras signal pathways. FEBS Lett 515: 141-145.

Han SI, Oh SY, Woo SH, Kim KH, Kim JH, et al. (2001) Implication of a small GTPase Rac1 in the activation of c-Jun N-terminal kinase and heat shock factor in response to heat shock. J Biol Chem 276: 1889-1895.

Hannun YA, Obeid LM (2008) Principles of bioactive lipid signalling: lessons from sphingolipids. Nat Rev Mol Cell Biol 9: 139-150.

Hargitai J, Lewis H, Boros I, Rácz T, Fiser A, et al. (2003) Bimoclomol, a heat shock protein co-inducer, acts by the prolonged activation of heat shock factor-1. Biochem Biophys Res Commun 307: 689-695.

Hartl FU (1996) Molecular chaperones in cellular protein folding. Nature 381: 571-579.

Harwood J, Evans M, Ramji D, Murphy D, Dodds P (2007) Medical and agricultural aspects of lipids. In: Gunstone F, Harwood J and Dijkstra A (Eds.), The Lipid Handbook. CRC Press, Boca Raton. pp 703-782.

Hasday JD, Singh IS (2000) Fever and the heat shock response: distinct, partially overlapping processes. Cell Stress Chaperones 5: 471-480.

Hayakawa M, Ishida N, Takeuchi K, Shibamoto S, Hori T, et al. (1993) Arachidonic acid-selective cytosolic phospholipase A2 is crucial in the cytotoxic action of tumor necrosis factor. J Biol Chem 268: 11290-11295.

Heads RJ, Yellon DM, Latchman DS (1995) Differential cytoprotection against heat stress or hypoxia following expression of specific stress protein genes in myogenic cells. J Mol Cell Cardiol 27: 1669-1678.

Hexeberg S, Willumsen N, Rotevatn S, Hexeberg E, Berge RK (1993) Cholesterol induced lipid accumulation in myocardial cells of rats. Cardiovasc Res 27: 442-446.

Heyn MP (1979) Determination of lipid order parameters and rotational correlation times from fluorescence depolarization experiments. FEBS Lett 108: 359-364.

Hightower LE, Guidon PTJ (1989) Selective release from cultured mammalian cells of heat-shock (stress) proteins that resemble glia-axon transfer proteins. J Cell Physiol 138: 257-266.

Hightower LE, White FP (1981) Cellular responses to stress: comparison of a family of 71--73-kilodalton proteins rapidly synthesized in rat tissue slices and canavanine-treated cells in culture. J Cell Physiol 108: 261-275.

Hino Y, Minakami S (1982) Hexose-6-phosphate dehydrogenase of rat liver microsomes. Isolation by affinity chromatography and properties. J Biol Chem 257: 2563-2568.

Hirabayashi T, Murayama T, Shimizu T (2004) Regulatory mechanism and physiological role of cytosolic phospholipase A2. Biol Pharm Bull 27: 1168-1173.

Hochachka P, Somero G (2002) Biochemical Adaptation: Mechanism and Process in Physiological Evolution, University Press, Oxford.

Holmberg CI, Hietakangas V, Mikhailov A, Rantanen JO, Kallio M, et al. (2001) Phosphorylation of serine 230 promotes inducible transcriptional activity of heat shock factor 1. EMBO J 20: 3800-3810.

Homolya L, Holló M, Müller M, Mechetner EB, Sarkadi B (1996) A new method for a quantitative assessment of P-glycoprotein-related multidrug resistance in tumour cells. Br J Cancer 73: 849-855.

Homolya L, Holló Z, Germann UA, Pastan I, Gottesman MM, et al. (1993) Fluorescent cellular indicators are extruded by the multidrug resistance protein. J Biol Chem 268: 21493-21496.

Hooper PL, Hooper JJ (2005) Loss of defense against stress: diabetes and heat shock proteins. Diabetes Technol Ther 7: 204-208.

Horváth I, Glatz A, Varvasovszki V, Török Z, Páli T, et al. (1998) Membrane physical state controls the signaling mechanism of the heat shock response in Synechocystis PCC 6803: identification of hsp17 as a "fluidity gene". Proc Natl Acad Sci U S A 95: 3513-3518.

Horváth I, Multhoff G, Sonnleitner A, Vígh L (2008) Membrane-associated stress proteins: more than simply chaperones. Biochim Biophys Acta 1778: 1653-1664.

Horváth LI (1994) Spin-label ESR study of molecular dynamics of lipid/protein association in membranes. Subcell Biochem 23: 205-245.

Huang XP, Pi Y, Lokuta AJ, Greaser ML, Walker JW (1997) Arachidonic acid stimulates protein kinase C-epsilon redistribution in heart cells. J Cell Sci 110 (Pt 14): 1625-1634.

Huang Z, Payette P, Abdullah K, Cromlish WA, Kennedy BP (1996) Functional identification of the active-site nucleophile of the human 85-kDa cytosolic phospholipase A2. Biochemistry 35: 3712-3721.

Hønger T, Jørgensen K, Biltonen RL, Mouritsen OG (1996) Systematic relationship between phospholipase A2 activity and dynamic lipid bilayer microheterogeneity. Biochemistry 35: 9003-9006.

Ianaro A, Ialenti A, Maffia P, Di Meglio P, Di Rosa M, et al. (2003) Anti-inflammatory activity of 15-deoxy-delta12,14-PGJ2 and 2-cyclopenten-1-one: role of the heat shock response. Mol Pharmacol 64: 85-93.

Illinger D, Duportail G, Mely Y, Poirel-Morales N, Gerard D, et al. (1995) A comparison of the fluorescence properties of TMA-DPH as a probe for plasma membrane and for endocytic membrane. Biochim Biophys Acta 1239: 58-66.

Ishikura S, Koshkina A, Klip A (2008) Small G proteins in insulin action: Rab and Rho families at the crossroads of signal transduction and GLUT4 vesicle traffic. Acta Physiol (Oxf) 192: 61-74.

Isidorov VA, Rusak M, Szczepaniak L, Witkowski S (2007) Gas chromatographic retention indices of trimethylsilyl derivatives of mono- and diglycerides on capillary columns with non-polar stationary phases. J Chromatogr A 1166: 207-211.

Israelachvili JN (1978) The packing of lipids and proteins in membranes. In: Deamer DW (Eds.), Light Transducing Membranes: Structure, Function and Evolution. Academic Press, New York. pp 91-107.

Issels RD (2008) Hyperthermia adds to chemotherapy. Eur J Cancer 44: 2546-2554.

Ivanov AI, Romanovsky AA (2004) Prostaglandin E2 as a mediator of fever: synthesis and catabolism. Front Biosci 9: 1977-1993.

Jacobson K, Sheets ED, Simson R (1995) Revisiting the fluid mosaic model of membranes. Science 268: 1441-1442.

Jean-Louis S, Akare S, Ali MA, Mash EAJ, Meuillet E, et al. (2006) Deoxycholic acid induces intracellular signaling through membrane perturbations. J Biol Chem 281: 14948-14960.

Jednákovits A, Ferdinándy P, Jaszlits L, Bányász T, Magyar J, et al. (2000) In vivo and in vitro acute cardiovascular effects of bimoclomol. Gen Pharmacol 34: 363-369.

Jenkins GM, Cowart LA, Signorelli P, Pettus BJ, Chalfant CE, et al. (2002) Acute activation of de novo sphingolipid biosynthesis upon heat shock causes an accumulation of ceramide and subsequent dephosphorylation of SR proteins. J Biol Chem 277: 42572-42578.

Johansson J, Mandin P, Renzoni A, Chiaruttini C, Springer M, et al. (2002) An RNA thermosensor controls expression of virulence genes in Listeria monocytogenes. Cell 110: 551-561.

Johnson FH, Eyring H, Steblay R, Chaplin H, Huber C, et al. (1945) The nature and control of reactions in bioluminescence: with special reference to the mechanism of

reversible and irreversible inhibitions by hydrogen and hydroxyl ions, temperature, pressure, alcohol, urethane, and sulfanilamide in bacteria. J Gen Physiol 28: 463-537.

Jorquera G, Juretić N, Jaimovich E, Riveros N (2009) Membrane depolarization induces calcium-dependent upregulation of Hsp70 and Hmox-1 in skeletal muscle cells. Am J Physiol Cell Physiol 297: C581-90.

Jurivich DA, Pangas S, Qiu L, Welk JF (1996) Phospholipase A2 triggers the first phase of the thermal stress response and exhibits cell-type specificity. J Immunol 157: 1669-1677.

Jurivich DA, Sistonen L, Kroes RA, Morimoto RI (1992) Effect of sodium salicylate on the human heat shock response. Science 255: 1243-1245.

Jurivich DA, Sistonen L, Sarge KD, Morimoto RI (1994) Arachidonate is a potent modulator of human heat shock gene transcription. Proc Natl Acad Sci U S A 91: 2280-2284.

Kabayama K, Sato T, Saito K, Loberto N, Prinetti A, et al. (2007) Dissociation of the insulin receptor and caveolin-1 complex by ganglioside GM3 in the state of insulin resistance. Proc Natl Acad Sci U S A 104: 13678-13683.

Kaiser H, Lingwood D, Levental I, Sampaio JL, Kalvodova L, et al. (2009) Order of lipid phases in model and plasma membranes. Proc Natl Acad Sci U S A 106: 16645-16650.

Kampinga HH, Craig EA (2010) The HSP70 chaperone machinery: J proteins as drivers of functional specificity. Nat Rev Mol Cell Biol 11: 579-592.

Kampinga HH, Hageman J, Vos MJ, Kubota H, Tanguay RM, et al. (2009) Guidelines for the nomenclature of the human heat shock proteins. Cell Stress Chaperones 14: 105-111.

Kasprzak KS (2002) Oxidative DNA and protein damage in metal-induced toxicity and carcinogenesis. Free Radic Biol Med 32: 958-967.

Kempner ES (1993) Damage to proteins due to the direct action of ionizing radiation. Q Rev Biophys 26: 27-48.

Khaled AR, Reynolds DA, Young HA, Thompson CB, Muegge K, et al. (2001) Interleukin-3 withdrawal induces an early increase in mitochondrial membrane potential unrelated to the Bcl-2 family. Roles of intracellular pH, ADP transport, and F(0)F(1)-ATPase. J Biol Chem 276: 6453-6462.

Khaleque MA, Bharti A, Sawyer D, Gong J, Benjamin IJ, et al. (2005) Induction of heat shock proteins by heregulin beta1 leads to protection from apoptosis and anchorage-independent growth. Oncogene 24: 6564-6573.

Khanna A, Aten RF, Behrman HR (1995) Physiological and pharmacological inhibitors of luteinizing hormone-dependent steroidogenesis induce heat shock protein-70 in rat luteal cells. Endocrinology 136: 1775-1781.

Kiang JG, Carr FE, Burns MR, McClain DE (1994) HSP-72 synthesis is promoted by increase in [Ca2+]i or activation of G proteins but not pHi or cAMP. Am J Physiol 267: C104-14.

Kiang JG, Ding XZ, McClain DE (1998) Overexpression of HSP-70 attenuates increases in [Ca2+]i and protects human epidermoid A-431 cells after chemical hypoxia. Toxicol Appl Pharmacol 149: 185-194.

Kiang JG, Koenig ML, Smallridge RC (1992) Heat shock increases cytosolic free Ca2+ concentration via Na(+)-Ca2+ exchange in human epidermoid A 431 cells. Am J Physiol 263: C30-8.

Kiang JG, McClain DE (1993) Effect of heat shock, [Ca2+]i, and cAMP on inositol trisphosphate in human epidermoid A-431 cells. Am J Physiol 264: C1561-9.

Kiang JG, Tsokos GC (1998) Heat shock protein 70 kDa: molecular biology, biochemistry, and physiology. Pharmacol Ther 80: 183-201.

Kieran D, Kalmar B, Dick JRT, Riddoch-Contreras J, Burnstock G, et al. (2004) Treatment with arimoclomol, a coinducer of heat shock proteins, delays disease progression in ALS mice. Nat Med 10: 402-405.

Kim HM, Choo H, Jung S, Ko Y, Park W, et al. (2007) A two-photon fluorescent probe for lipid raft imaging: C-laurdan. Chembiochem 8: 553-559.

Kimelberg HK, Papahadjopoulos D (1974) Effects of phospholipid acyl chain fluidity, phase transitions, and cholesterol on (Na+ + K+)-stimulated adenosine triphosphatase. J Biol Chem 249: 1071-1080.

Kindzelskii AL, Sitrin RG, Petty HR (2004) Cutting edge: optical microspectrophotometry supports the existence of gel phase lipid rafts at the lamellipodium of neutrophils: apparent role in calcium signaling. J Immunol 172: 4681-4685.

Kirkegaard T, Roth AG, Petersen NHT, Mahalka AK, Olsen OD, et al. (2010) Hsp70 stabilizes lysosomes and reverts Niemann-Pick disease-associated lysosomal pathology. Nature 463: 549-553.

Kitagawa S, Hirata H (1992) Effects of alcohols on fluorescence anisotropies of diphenylhexatriene and its derivatives in bovine blood platelets: relationships of the depth-dependent change in membrane fluidity by alcohols with their effects on platelet aggregation and adenylate cyclase activity. Biochim Biophys Acta 1112: 14-18.

Kitagawa S, Matsubayashi M, Kotani K, Usui K, Kametani F (1991) Asymmetry of membrane fluidity in the lipid bilayer of blood platelets: fluorescence study with diphenylhexatriene and analogs. J Membr Biol 119: 221-227.

Kota Z, Horvath LI, Droppa M, Horvath G, Farkas T, et al. (2002) Protein assembly and heat stability in developing thylakoid membranes during greening. Proc Natl Acad Sci U S A 99: 12149-12154.

Kovacs E, Torok Z, Horvath I, Vigh L (1994) Heat-stress induces association of the groel-analog chaperonin with thylakoid membranes in cyanobacterium, Synechocystis PCC-6803. Plant Physiol Biochem 32: 285-293.

Kozawa O, Niwa M, Matsuno H, Tokuda H, Miwa M, et al. (1999b) Sphingosine 1-phosphate induces heat shock protein 27 via p38 mitogen-activated protein kinase activation in osteoblasts. J Bone Miner Res 14: 1761-1767.

Kozawa O, Tanabe K, Ito H, Matsuno H, Niwa M, et al. (1999a) Sphingosine 1-phosphate regulates heat shock protein 27 induction by a p38 MAP kinase-dependent mechanism in aortic smooth muscle cells. Exp Cell Res 250: 376-380.

Kunimoto S, Kobayashi T, Kobayashi S, Murakami-Murofushi K (2000) Expression of cholesteryl glucoside by heat shock in human fibroblasts. Cell Stress Chaperones 5: 3-7.

Kunimoto S, Murofushi W, Kai H, Ishida Y, Uchiyama A, et al. (2002) Steryl glucoside is a lipid mediator in stress-responsive signal transduction. Cell Struct Funct 27: 157-162.

Kyriakis JM, Avruch J (2001) Mammalian mitogen-activated protein kinase signal transduction pathways activated by stress and inflammation. Physiol Rev 81: 807-869.

Köller M, König W (1991) 12-Hydroxyeicosatetraenoic acid (12-HETE) induces heat shock proteins in human leukocytes. Biochem Biophys Res Commun 175: 804-809.

Königshofer H, Tromballa H, Löppert H (2008) Early events in signalling high-temperature stress in tobacco BY2 cells involve alterations in membrane fluidity and enhanced hydrogen peroxide production. Plant Cell Environ 31: 1771-1780.

Kültz D (2003) Evolution of the cellular stress proteome: from monophyletic origin to ubiquitous function. J Exp Biol 206: 3119-3124.

Kültz D (2005) Molecular and evolutionary basis of the cellular stress response. Annu Rev Physiol 67: 225-257.

Kültz D, Chakravarty D (2001) Maintenance of genomic integrity in mammalian kidney cells exposed to hyperosmotic stress. Comp Biochem Physiol A Mol Integr Physiol 130: 421-428.

Kürthy M, Mogyorósi T, Nagy K, Kukorelli T, Jednákovits A, et al. (2002) Effect of BRX-220 against peripheral neuropathy and insulin resistance in diabetic rat models. Ann N Y Acad Sci 967: 482-489.

Lakowicz J (2006) Fluorescence anisotropy. In: Lakowicz J, Principles of Fluorescence Spectroscopy. Springer, New York. pp 353-382.

Lambert S, Vind-Kezunovic D, Karvinen S, Gniadecki R (2006) Ligand-independent activation of the EGFR by lipid raft disruption. J Invest Dermatol 126: 954-962.

Lee BS, Chen J, Angelidis C, Jurivich DA, Morimoto RI (1995) Pharmacological modulation of heat shock factor 1 by antiinflammatory drugs results in protection against stress-induced cellular damage. Proc Natl Acad Sci U S A 92: 7207-7211.

Leidl K, Liebisch G, Richter D, Schmitz G (2008) Mass spectrometric analysis of lipid species of human circulating blood cells. Biochim Biophys Acta 1781: 655-664.

Lepore DA, Knight KR, Anderson RL, Morrison WA (2001) Role of priming stresses and Hsp70 in protection from ischemia-reperfusion injury in cardiac and skeletal muscle. Cell Stress Chaperones 6: 93-96.

Liebisch G, Binder M, Schifferer R, Langmann T, Schulz B, et al. (2006) High throughput quantification of cholesterol and cholesteryl ester by electrospray ionization tandem mass spectrometry (ESI-MS/MS). Biochim Biophys Acta 1761: 121-128.

Liebisch G, Drobnik W, Lieser B, Schmitz G (2002) High-throughput quantification of lysophosphatidylcholine by electrospray ionization tandem mass spectrometry. Clin Chem 48: 2217-2224.

Liebisch G, Drobnik W, Reil M, Trümbach B, Arnecke R, et al. (1999) Quantitative measurement of different ceramide species from crude cellular extracts by electrospray ionization tandem mass spectrometry (ESI-MS/MS). J Lipid Res 40: 1539-1546.

Liebisch G, Lieser B, Rathenberg J, Drobnik W, Schmitz G (2004) High-throughput quantification of phosphatidylcholine and sphingomyelin by electrospray ionization tandem mass spectrometry coupled with isotope correction algorithm. Biochim Biophys Acta 1686: 108-117.

Lin RZ, Hu ZW, Chin JH, Hoffman BB (1997) Heat shock activates c-Src tyrosine kinases and phosphatidylinositol 3-kinase in NIH3T3 fibroblasts. J Biol Chem 272: 31196-31202.

Lindquist S (1986) The heat-shock response. Annu Rev Biochem 55: 1151-1191.

Lingwood D, Ries J, Schwille P, Simons K (2008) Plasma membranes are poised for activation of raft phase coalescence at physiological temperature. Proc Natl Acad Sci U S A 105: 10005-10010.

Lingwood D, Simons K (2010) Lipid rafts as a membrane-organizing principle. Science 327: 46-50.

Liscum L (2004) Cholesterol bisynthesis. In: Vance D and Vance JE (Eds.), Biochemistry of Lipids, Lipoproteins and Membranes. Elsevier, Amsterdam. pp 409-432.

Liu PK (2001) DNA damage and repair in the brain after cerebral ischemia. Curr Top Med Chem 1: 483-495.

Maeda M, Doi O, Akamatsu Y (1980) Behavior of vesicular stomatitis virus glycoprotein in mouse LM cells with modified membrane-phospholipids. Biochim Biophys Acta 597: 552-563.

Maroni P, Bendinelli P, Zuccorononno C, Schiaffonati L, Piccoletti R (2000) Cellular signalling after in vivo heat shock in the liver. Cell Biol Int 24: 145-152.

Marsh D (1981) Electron spin resonance: spin labels. Mol Biol Biochem Biophys 31: 51-142.

Marsh D (2001) Polarity and permeation profiles in lipid membranes. Proc Natl Acad Sci U S A 98: 7777-7782.

Marsh D, Horvath L (1989) Spin label studies of the structure and dynamics of lipids and proteins in membranes. In: Hoff A (Eds.), Advanced EPR. Applications in Biology and Biochemistry. Elsevier, Amsterdam. pp 707-752.

Marsh D, Horváth LI (1998) Structure, dynamics and composition of the lipid-protein interface. Perspectives from spin-labelling. Biochim Biophys Acta 1376: 267-296.

Mathieson FA, Nixon GF (2006) Sphingolipids differentially regulate mitogen-activated protein kinases and intracellular Ca2+ in vascular smooth muscle: effects on CREB activation. Br J Pharmacol 147: 351-359.

Matyash V, Liebisch G, Kurzchalia TV, Shevchenko A, Schwudke D (2008) Lipid extraction by methyl-tert-butyl ether for high-throughput lipidomics. J Lipid Res 49: 1137-1146.

Maula T, Westerlund B, Slotte JP (2009) Differential ability of cholesterol-enriched and gel phase domains to resist benzyl alcohol-induced fluidization in multilamellar lipid vesicles. Biochim Biophys Acta 1788: 2454-2461.

Maxfield FR, van Meer G (2010) Cholesterol, the central lipid of mammalian cells. Curr Opin Cell Biol 22: 422-429.

Mayer MP, Bukau B (2005) Hsp70 chaperones: cellular functions and molecular mechanism. Cell Mol Life Sci 62: 670-684.

Meex RCR, Schrauwen P, Hesselink MKC (2009) Modulation of myocellular fat stores: lipid droplet dynamics in health and disease. Am J Physiol Regul Integr Comp Physiol 297: R913-24.

Megha, London E (2004) Ceramide selectively displaces cholesterol from ordered lipid domains (rafts): implications for lipid raft structure and function. J Biol Chem 279: 9997-10004.

Merrill A (2008) Sphingolipids. In: Vance D and Vance JE (Eds.), Biochemistry of Lipids, Lipoproteins and Membranes. Elsevier, Amsterdam. pp 363-397.

Milton AS, Wendlandt S (1970) A possible role for prostaglandin E1 as a modulator for temperature regulation in the central nervous system of the cat. J Physiol 207: 76P-77P.

Mondal M, Mesmin B, Mukherjee S, Maxfield FR (2009) Sterols are mainly in the cytoplasmic leaflet of the plasma membrane and the endocytic recycling compartment in CHO cells. Mol Biol Cell 20: 581-588.

Morenilla-Palao C, Pertusa M, Meseguer V, Cabedo H, Viana F (2009) Lipid raft segregation modulates TRPM8 channel activity. J Biol Chem 284: 9215-9224.

Morimoto RI (1998) Regulation of the heat shock transcriptional response: cross talk between a family of heat shock factors, molecular chaperones, and negative regulators. Genes Dev 12: 3788-3796.

Morita MT, Tanaka Y, Kodama TS, Kyogoku Y, Yanagi H, et al. (1999) Translational induction of heat shock transcription factor sigma32: evidence for a built-in RNA thermosensor. Genes Dev 13: 655-665.

Mosser DD, Kotzbauer PT, Sarge KD, Morimoto RI (1990) In vitro activation of heat shock transcription factor DNA-binding by calcium and biochemical conditions that affect protein conformation. Proc Natl Acad Sci U S A 87: 3748-3752.

Moulin M, Carpentier S, Levade T, Arrigo A (2007) Potential roles of membrane fluidity and ceramide in hyperthermia and alcohol stimulation of TRAIL apoptosis. Apoptosis 12: 1703-1720.

Mukherjee S, Maxfield FR (2004) Membrane domains. Annu Rev Cell Dev Biol 20: 839-866.

Multhoff G (2007) Heat shock protein 70 (Hsp70): membrane location, export and immunological relevance. Methods 43: 229-237.

Multhoff G (2009) Activation of natural killer cells by heat shock protein 70. 2002. Int J Hyperthermia 25: 169-175.

Murshid A, Chou S, Prince T, Zhang Y, Bharti A, et al. (2010) Protein kinase A binds and activates heat shock factor 1. PLoS One 5: e13830.

Nadeau SI, Landry J (2007) Mechanisms of activation and regulation of the heat shock-sensitive signaling pathways. Adv Exp Med Biol 594: 100-113.

Nagarsekar A, Hasday JD, Singh IS (2005) CXC chemokines: a new family of heat-shock proteins? Immunol Invest 34: 381-398.

Nagy E, Balogi Z, Gombos I, Akerfelt M, Björkbom A, et al. (2007) Hyperfluidization-coupled membrane microdomain reorganization is linked to activation of the heat shock response in a murine melanoma cell line. Proc Natl Acad Sci U S A 104: 7945-7950.

Nakamoto H, Vigh L (2007) The small heat shock proteins and their clients. Cell Mol Life Sci 64: 294-306.

Narasimhan SD, Yen K, Tissenbaum HA (2009) Converging pathways in lifespan regulation. Curr Biol 19: R657-66.

Nguyen VT, Bensaude O (1994) Increased thermal aggregation of proteins in ATP-depleted mammalian cells. Eur J Biochem 220: 239-246.

Nguyen VT, Morange M, Bensaude O (1989) Protein denaturation during heat shock and related stress. Escherichia coli beta-galactosidase and Photinus pyralis luciferase inactivation in mouse cells. J Biol Chem 264: 10487-10492.

Nivon M, Abou-Samra M, Richet E, Guyot B, Arrigo A, et al. (2012) NF-κB regulates protein quality control after heat stress through modulation of the BAG3-HspB8 complex. J Cell Sci 125: 1141-1151.

Nomura DK, Long JZ, Niessen S, Hoover HS, Ng S, et al. (2010) Monoacylglycerol lipase regulates a fatty acid network that promotes cancer pathogenesis. Cell 140: 49-61.

O'Flaherty JT, Chadwell BA, Kearns MW, Sergeant S, Daniel LW (2001) Protein kinases C translocation responses to low concentrations of arachidonic acid. J Biol Chem 276: 24743-24750.

Ohno K, Fukushima M, Fujiwara M, Narumiya S (1988) Induction of 68,000-dalton heat shock proteins by cyclopentenone prostaglandins. Its association with prostaglandin-induced G1 block in cell cycle progression. J Biol Chem 263: 19764-19770.

Parasassi T, De Stasio G, Ravagnan G, Rusch RM, Gratton E (1991) Quantitation of lipid phases in phospholipid vesicles by the generalized polarization of Laurdan fluorescence. Biophys J 60: 179-189.

Parasassi T, De Stasio G, d'Ubaldo A, Gratton E (1990) Phase fluctuation in phospholipid membranes revealed by Laurdan fluorescence. Biophys J 57: 1179-1186.

Parasassi T, Gratton E, Yu WM, Wilson P, Levi M (1997) Two-photon fluorescence microscopy of laurdan generalized polarization domains in model and natural membranes. Biophys J 72: 2413-2429.

Parasassi T, Ravagnan G, Sapora O, Gratton E (1992) Membrane oxidative damage induced by ionizing radiation detected by diphenylhexatriene fluorescence lifetime distributions. Int J Radiat Biol 61: 791-796.

Park HG, Han SI, Oh SY, Kang HS (2005) Cellular responses to mild heat stress. Cell Mol Life Sci 62: 10-23.

Parsell DA, Taulien J, Lindquist S (1993) The role of heat-shock proteins in thermotolerance. Philos Trans R Soc Lond B Biol Sci 339: 279-86.

Patra SK (2008) Dissecting lipid raft facilitated cell signaling pathways in cancer. Biochim Biophys Acta 1785: 182-206.

Patriarca EJ, Kobayashi GS, Maresca B (1992) Mitochondrial activity and heat-shock response during morphogenesis in the pathogenic fungus Histoplasma capsulatum. Biochem Cell Biol 70: 207-214.

Pearl LH, Prodromou C, Workman P (2008) The Hsp90 molecular chaperone: an open and shut case for treatment. Biochem J 410: 439-453.

Peer AJ, Grimm MJ, Zynda ER, Repasky EA (2010) Diverse immune mechanisms may contribute to the survival benefit seen in cancer patients receiving hyperthermia. Immunol Res 46: 137-154.

Perl A, Gergely PJ, Nagy G, Koncz A, Banki K (2004) Mitochondrial hyperpolarization: a checkpoint of T-cell life, death and autoimmunity. Trends Immunol 25: 360-367.

Perrin M (1926) Polarisation de la Lumiere de Fluorescence. Vie Moyenne des Molecule dans L'etat excite. J Phys Radium 7: 390-393.

Pessin JE, Salter DW, Glaser M (1978) Use of a fluorescent probe to compare the plasma membrane properties in normal and transformed cells. Evaluation of the interference by triacylglycerols and alkyldiacylglycerols. Biochemistry 17: 1997-2004.

Peter M, Balogh G, Gombos I, Liebisch G, Horvath I, et al. (2012) Nutritional lipid supply can control the heat shock response of B16 melanoma cells in culture. Mol Memb Biol Early Online: 1-16.

Piazza JR, Almeida DM, Dmitrieva NO, Klein LC (2010) Frontiers in the use of biomarkers of health in research on stress and aging. J Gerontol B Psychol Sci Soc Sci 65: 513-525.

Pike LJ (2006) Rafts defined: a report on the Keystone Symposium on Lipid Rafts and Cell Function. J Lipid Res 47: 1597-1598.

Pike LJ (2009) The challenge of lipid rafts. J Lipid Res 50 Suppl: S323-8.

Pike LJ, Han X, Chung K, Gross RW (2002) Lipid rafts are enriched in arachidonic acid and plasmenylethanolamine and their composition is independent of caveolin-1 expression: a quantitative electrospray ionization/mass spectrometric analysis. Biochemistry 41: 2075-2088.

Pike LJ, Han X, Gross RW (2005) Epidermal growth factor receptors are localized to lipid rafts that contain a balance of inner and outer leaflet lipids: a shotgun lipidomics study. J Biol Chem 280: 26796-26804.

Piper PW (1995) The heat shock and ethanol stress responses of yeast exhibit extensive similarity and functional overlap. FEMS Microbiol Lett 134: 121-127.

Pockley AG (2001) Heat shock proteins in health and disease: therapeutic targets or therapeutic agents? Expert Rev Mol Med 3: 1-21.

Pockley AG, Muthana M, Calderwood SK (2008) The dual immunoregulatory roles of stress proteins. Trends Biochem Sci 33: 71-79.

Pollak M (2008) Insulin and insulin-like growth factor signalling in neoplasia. Nat Rev Cancer 8: 915-928.

Pomorski T, Menon AK (2006) Lipid flippases and their biological functions. Cell Mol Life Sci 63: 2908-2921.

Pratt WB, Morishima Y, Osawa Y (2008) The Hsp90 chaperone machinery regulates signaling by modulating ligand binding clefts. J Biol Chem 283: 22885-22889.

Pratt WB, Toft DO (2003) Regulation of signaling protein function and trafficking by the hsp90/hsp70-based chaperone machinery. Exp Biol Med (Maywood) 228: 111-133.

Price BD, Calderwood SK (1991) Ca2+ is essential for multistep activation of the heat shock factor in permeabilized cells. Mol Cell Biol 11: 3365-3368.

Pruett ST, Bushnev A, Hagedorn K, Adiga M, Haynes CA, et al. (2008) Biodiversity of sphingoid bases ("sphingosines") and related amino alcohols. J Lipid Res 49: 1621-1639.

Páli T, Finbow ME, Marsh D (1999) Membrane assembly of the 16-kDa proteolipid channel from Nephrops norvegicus studied by relaxation enhancements in spin-label ESR. Biochemistry 38: 14311-14319.

Páli T, Garab G, Horváth LI, Kóta Z (2003) Functional significance of the lipid-protein interface in photosynthetic membranes. Cell Mol Life Sci 60: 1591-1606.

Qian L, Song X, Ren H, Gong J, Cheng S (2004) Mitochondrial mechanism of heat stress-induced injury in rat cardiomyocyte. Cell Stress Chaperones 9: 281-293.

Quinn PJ (1981) The fluidity of cell membranes and its regulation. Prog Biophys Mol Biol 38: 1-104.

Quinn PJ (2010) A lipid matrix model of membrane raft structure. Prog Lipid Res 49: 390-406.

Quinn PJ, Joo F, Vigh L (1989) The role of unsaturated lipids in membrane structure and stability. Prog Biophys Mol Biol 53: 71-103.

Raviol H, Sadlish H, Rodriguez F, Mayer MP, Bukau B (2006) Chaperone network in the yeast cytosol: Hsp110 is revealed as an Hsp70 nucleotide exchange factor. EMBO J 25: 2510-2518.

Reers M, Smith TW, Chen LB (1991) J-aggregate formation of a carbocyanine as a quantitative fluorescent indicator of membrane potential. Biochemistry 30: 4480-4486.

Revathi CJ, Chattopadhyay A, Srinivas UK (1994) Change in membrane organization induced by heat shock. Biochem Mol Biol Int 32: 941-950.

Richter K, Haslbeck M, Buchner J (2010) The heat shock response: life on the verge of death. Mol Cell 40: 253-266.

Ritossa F (1962) A new puffing pattern induced by temperature shock and DNP in Drosophila. Experimentia 18: 351-366.

Rodes JF, Berreur-Bonnenfant J, Trémolières A, Brown SC (1995) Modulation of membrane fluidity and lipidic metabolism in transformed rat fibroblasts induced by the sesquiterpenic hormone farnesylacetone. Cytometry 19: 217-225.

Roshchupkin DI, Murina MA (1998) Free-radical and cyclooxygenase-catalyzed lipid peroxidation in membranes of blood cells under UV irradiation. Membr Cell Biol 12: 279-286.

Roussou I, Nguyen VT, Pagoulatos GN, Bensaude O (2000) Enhanced protein denaturation in indomethacin-treated cells. Cell Stress Chaperones 5: 8-13.

Rydberg B (2001) Radiation-induced DNA damage and chromatin structure. Acta Oncol 40: 682-685.

Sachidhanandam SB, Lu J, Low KSY, Moochhala SM (2003) Herbimycin A attenuates apoptosis during heat stress in rats. Eur J Pharmacol 474: 121-128.

Saidi Y, Domini M, Choy F, Zryd J, Schwitzguebel J, et al. (2007) Activation of the heat shock response in plants by chlorophenols: transgenic Physcomitrella patens as a sensitive biosensor for organic pollutants. Plant Cell Environ 30: 753-763.

Saidi Y, Finka A, Muriset M, Bromberg Z, Weiss YG, et al. (2009b) The heat shock response in moss plants is regulated by specific calcium-permeable channels in the plasma membrane. Plant Cell 21: 2829-2843.

Saidi Y, Muriset M, Bromberg Z, Weiss YG, Maathuis FJM, et al. (2009a) The heat shock response in moss plants is regulated by specific calcium-permeable channels in the plasma membrane. The Plant Cell 21: 1-15.

Saidi Y, Peter M, Finka A, Cicekli C, Vigh L, et al. (2010) Membrane lipid composition affects plant heat sensing and modulates Ca(2+)-dependent heat shock response. Plant Signal Behav 5: 1530-1533.

Samples BL, Pool GL, Lumb RH (1999) Polyunsaturated fatty acids enhance the heat induced stress response in rainbow trout (Oncorhynchus mykiss) leukocytes. Comp Biochem Physiol B Biochem Mol Biol 123: 389-397.

Sangwan V, Orvar BL, Beyerly J, Hirt H, Dhindsa RS (2002) Opposite changes in membrane fluidity mimic cold and heat stress activation of distinct plant MAP kinase pathways. Plant J 31: 629-638.

Santoro MG (2000) Heat shock factors and the control of the stress response. Biochem Pharmacol 59: 55-63.

Sarge KD (1995) Male germ cell-specific alteration in temperature set point of the cellular stress response. J Biol Chem 270: 18745-18748.

Sarge KD, Bray AE, Goodson ML (1995) Altered stress response in testis. Nature 374: 126.

Sarge KD, Murphy SP, Morimoto RI (1993) Activation of heat shock gene transcription by heat shock factor 1 involves oligomerization, acquisition of DNA-binding activity, and nuclear localization and can occur in the absence of stress. Mol Cell Biol 13: 1392-1407.

Sato SB, Ishii K, Makino A, Iwabuchi K, Yamaji-Hasegawa A, et al. (2004) Distribution and transport of cholesterol-rich membrane domains monitored by a membrane-impermeant fluorescent polyethylene glycol-derivatized cholesterol. J Biol Chem 279: 23790-23796.

Schroeder F, Nemecz G, Wood WG, Joiner C, Morrot G, et al. (1991) Transmembrane distribution of sterol in the human erythrocyte. Biochim Biophys Acta 1066: 183-192.

Selye H (1936) A syndrome produced by diverse nocuous agents. Nature 138: 32.

Selye H (1950) Stress and the general adaptation syndrome. British Medical Journal 1: 1383-1392.

Shack S, Gorospe M, Fawcett TW, Hudgins WR, Holbrook NJ (1999) Activation of the cholesterol pathway and Ras maturation in response to stress. Oncogene 18: 6021-6028.

Shamovsky I, Ivannikov M, Kandel ES, Gershon D, Nudler E (2006) RNA-mediated response to heat shock in mammalian cells. Nature 440: 556-560.

Shamovsky I, Nudler E (2008) New insights into the mechanism of heat shock response activation. Cell Mol Life Sci 65: 855-861.

Shigapova N, Török Z, Balogh G, Goloubinoff P, Vígh L, et al. (2005) Membrane fluidization triggers membrane remodeling which affects the thermotolerance in Escherichia coli. Biochem Biophys Res Commun 328: 1216-1223.

Shimizu T, Yamaguchi N, Okada S, Lu L, Sasaki T, et al. (2007) Roles of brain phosphatidylinositol-specific phospholipase C and diacylglycerol lipase in centrally administered histamine-induced adrenomedullary outflow in rats. Eur J Pharmacol 571: 138-144.

Shimizu T, Yokotani K (2008) Bidirectional roles of the brain 2-arachidonoyl-sn-glycerol in the centrally administered vasopressin-induced adrenomedullary outflow in rats. Eur J Pharmacol 582: 62-69.

Shinitzky M (1984) Membrane fluidity in malignancy. Adversative and recuperative. Biochim Biophys Acta 738: 251-261.

Shinitzky M, Barenholz Y (1978) Fluidity parameters of lipid regions determined by fluorescence polarization. Biochim Biophys Acta 515: 367-394.

Siddle K (2011) Signalling by insulin and IGF receptors: supporting acts and new players. J Mol Endocrinol 47: R1-10.

Simons K, Sampaio JL (2011) Membrane Organization and Lipid Rafts. Cold Spring Harb Perspect Biol 3: a004697.

Singer SJ, Nicolson GL (1972) The fluid mosaic model of the structure of cell membranes. Science 175: 720-731.

Singh IS, Viscardi RM, Kalvakolanu I, Calderwood S, Hasday JD (2000) Inhibition of tumor necrosis factor-alpha transcription in macrophages exposed to febrile range temperature. A possible role for heat shock factor-1 as a negative transcriptional regulator. J Biol Chem 275: 9841-9848.

Skinner MK, Griswold MD (1983) Fluorographic detection of radioactivity in polyacrylamide gels with 2,5-diphenyloxazole in acetic acid and its comparison with existing procedures. Biochem J 209: 281-284.

Sklar LA (1984) Fluorescence polarization studies of membrane fluidity: where do we go from here? In: Kates MM and Lionel A (Eds.), Membrane Fluidity. Plenum Publishing Corp, New York. pp 99-131.

Smith WL, Marnett LJ (1991) Prostaglandin endoperoxide synthase: structure and catalysis. Biochim Biophys Acta 1083: 1-17.

Snyder F, Lee T, Wykle R (2004) Ether-linked lipids and their bioactive species. In: Vance D and Vance J (Eds.), Biochemistry of Lipids, Lipoproteins and Membranes. Elsevier, Amsterdam. pp 233-262.

Somero GN (1992) Adaptations to high hydrostatic pressure. Annu Rev Physiol 54: 557-577.

Spandl J, White DJ, Peychl J, Thiele C (2009) Live cell multicolor imaging of lipid droplets with a new dye, LD540. Traffic 10: 1579-1584.

Sreedhar AS, Srinivas UK (2002) Activation of stress response by ionomycin in rat hepatoma cells. J Cell Biochem 86: 154-161.

Stangl S, Gehrmann M, Riegger J, Kuhs K, Riederer I, et al. (2011) Targeting membrane heat-shock protein 70 (Hsp70) on tumors by cmHsp70.1 antibody. Proc Natl Acad Sci U S A 108: 733-738.

Stevenson MA, Calderwood SK, Hahn GM (1987) Effect of hyperthermia (45 degrees C) on calcium flux in Chinese hamster ovary HA-1 fibroblasts and its potential role in cytotoxicity and heat resistance. Cancer Res 47: 3712-3717.

Storch J, Shulman SL, Kleinfeld AM (1989) Plasma membrane lipid order and composition during adipocyte differentiation of 3T3F442A cells. Studies in intact cells with 1-[4-(trimethylamino)phenyl]-6-phenylhexatriene. J Biol Chem 264: 10527-10533.

Storey JD, Tibshirani R (2003) Statistical significance for genomewide studies. Proc Natl Acad Sci U S A 100: 9440-9445.

Söti C, Csermely P (2000) Molecular chaperones and the aging process. Biogerontology 1: 225-233.

Söti C, Csermely P (2007) Protein stress and stress proteins: implications in aging and disease. J Biosci 32: 511-515.

Söti C, Nagy E, Giricz Z, Vígh L, Csermely P, et al. (2005) Heat shock proteins as emerging therapeutic targets. Br J Pharmacol 146: 769-780.

Taipale M, Jarosz DF, Lindquist S (2010) HSP90 at the hub of protein homeostasis: emerging mechanistic insights. Nat Rev Mol Cell Biol 11: 515-528.

Takai S, Tokuda H, Matsushima-Nishiwaki R, Hanai Y, Kato K, et al. (2006) Phosphatidylinositol 3-kinase/Akt plays a role in sphingosine 1-phosphate-stimulated HSP27 induction in osteoblasts. J Cell Biochem 98: 1249-1256.

Tang X, Edwards EM, Holmes BB, Falck JR, Campbell WB (2006) Role of phospholipase C and diacylglyceride lipase pathway in arachidonic acid release and acetylcholine-induced vascular relaxation in rabbit aorta. Am J Physiol Heart Circ Physiol 290: H37-45.

Tissières A, Mitchell HK, Tracy UM (1974) Protein synthesis in salivary glands of Drosophila melanogaster: relation to chromosome puffs. J Mol Biol 84: 389-398.

Tsvetkova NM, Horváth I, Török Z, Wolkers WF, Balogi Z, et al. (2002) Small heat-shock proteins regulate membrane lipid polymorphism. Proc Natl Acad Sci U S A 99: 13504-13509.

Török Z, Goloubinoff P, Horváth I, Tsvetkova NM, Glatz A, et al. (2001) Synechocystis HSP17 is an amphitropic protein that stabilizes heat-stressed membranes and binds denatured proteins for subsequent chaperone-mediated refolding. Proc Natl Acad Sci U S A 98: 3098-3103.

Török Z, Horváth I, Goloubinoff P, Kovács E, Glatz A, et al. (1997) Evidence for a lipochaperonin: association of active protein-folding GroESL oligomers with lipids can stabilize membranes under heat shock conditions. Proc Natl Acad Sci U S A 94: 2192-2197.

Török Z, Tsvetkova NM, Balogh G, Horváth I, Nagy E, et al. (2003) Heat shock protein coinducers with no effect on protein denaturation specifically modulate the membrane lipid phase. Proc Natl Acad Sci U S A 100: 3131-3136.

Van Blitterswijk WJ, Van Hoeven RP, Van der Meer BW (1981) Lipid structural order parameters (reciprocal of fluidity) in biomembranes derived from steady-state fluorescence polarization measurements. Biochim Biophys Acta 644: 323-332.

Vance D (2004) Phospholipid biosynthesis in eukaryotes. In: Vance D and Vance J (Eds.), Biochemistry of Lipids, Lipoproteins and Membranes. Elsevier, Amsterdam. pp 205-231.

Vane JR (1971) Inhibition of prostaglandin synthesis as a mechanism of action for aspirin-like drugs. Nat New Biol 231: 232-235.

van Meer G (2011) Dynamic transbilayer lipid asymmetry. Cold Spring Harb Perspect Biol 3: a004671.

van Meer G, Voelker DR, Feigenson GW (2008) Membrane lipids: where they are and how they behave. Nat Rev Mol Cell Biol 9: 112-124.

van Meer G, de Kroon AIPM (2011) Lipid map of the mammalian cell. J Cell Sci 124: 5-8.

van Rossum DB, Patterson RL (2009) PKC and PLA2: probing the complexities of the calcium network. Cell Calcium 45: 535-545.

Vereb G, Szöllosi J, Matkó J, Nagy P, Farkas T, et al. (2003) Dynamic, yet structured: The cell membrane three decades after the Singer-Nicolson model. Proc Natl Acad Sci U S A 100: 8053-8058.

Vest R, Wallis R, Jensen LB, Haws AC, Callister J, et al. (2006) Use of steady-state laurdan fluorescence to detect changes in liquid ordered phases in human erythrocyte membranes. J Membr Biol 211: 15-25.

Vigh L, Escribá PV, Sonnleitner A, Sonnleitner M, Piotto S, et al. (2005) The significance of lipid composition for membrane activity: new concepts and ways of assessing function. Prog Lipid Res 44: 303-344.

Vigh L, Horváth I, Maresca B, Harwood JL (2007a) Can the stress protein response be controlled by 'membrane-lipid therapy'? Trends Biochem Sci 32: 357-363.

Vigh L, Literáti PN, Horváth I, Török Z, Balogh G, et al. (1997) Bimoclomol: a nontoxic, hydroxylamine derivative with stress protein-inducing activity and cytoprotective effects. Nat Med 3: 1150-1154.

Vigh L, Los DA, Horváth I, Murata N (1993) The primary signal in the biological perception of temperature: Pd-catalyzed hydrogenation of membrane lipids stimulated the expression of the desA gene in Synechocystis PCC6803. Proc Natl Acad Sci U S A 90: 9090-9094.

Vigh L, Maresca B (2002) Dual role of membranes in heat stress: as thermosensors they modulate the expression of stress genes and, by interacting with stress proteins, re-organize their own lipid order and functionality. In: Storey K and Storey J (Eds.), Sensing, Signaling and Cell Adaptation. Elsevier, Amsterdam. pp 173-187.

Vigh L, Maresca B, Harwood JL (1998) Does the membrane's physical state control the expression of heat shock and other genes? Trends Biochem Sci 23: 369-374.

Vigh L, Nakamoto H, Landry J, Gomez-Munoz A, Harwood JL, et al. (2007b) Membrane regulation of the stress response from prokaryotic models to mammalian cells. Ann N Y Acad Sci 1113: 40-51.

Vigh L, Török Z, Balogh G, Glatz A, Piotto S, et al. (2007c) Membrane-regulated stress response: a theoretical and practical approach. Adv Exp Med Biol 594: 114-131.

Voellmy R, Boellmann F (2007) Chaperone regulation of the heat shock protein response. Adv Exp Med Biol 594: 89-99.

Vos MJ, Hageman J, Carra S, Kampinga HH (2008) Structural and functional diversities between members of the human HSPB, HSPH, HSPA, and DNAJ chaperone families. Biochemistry 47: 7001-7011.

Wakelam MJ (1998) Diacylglycerol--when is it an intracellular messenger? Biochim Biophys Acta 1436: 117-126.

Welch WJ, Suhan JP (1985) Morphological study of the mammalian stress response: characterization of changes in cytoplasmic organelles, cytoskeleton, and nucleoli, and appearance of intranuclear actin filaments in rat fibroblasts after heat-shock treatment. J Cell Biol 101: 1198-1211.

Welch WJ, Suhan JP (1986) Cellular and biochemical events in mammalian cells during and after recovery from physiological stress. J Cell Biol 103: 2035-2052.

Wenk MR (2010) Lipidomics: new tools and applications. Cell 143: 888-895.

Westerheide SD, Morimoto RI (2005) Heat shock response modulators as therapeutic tools for diseases of protein conformation. J Biol Chem 280: 33097-33100.

Whiteman EL, Cho H, Birnbaum MJ (2002) Role of Akt/protein kinase B in metabolism. Trends Endocrinol Metab 13: 444-451.

Wilton D, Waite M (2004) Phospholipases. In: Vance D and Vance JE (Eds.), Biochemistry of Lipids, Lipoproteins and Membranes . Elsevier, Amsterdam. pp 291-314.

Wu KK (1998) Biochemical pharmacology of nonsteroidal anti-inflammatory drugs. Biochem Pharmacol 55: 543-547.

Wymann MP, Schneiter R (2008) Lipid signalling in disease. Nat Rev Mol Cell Biol 9: 162-176.

Xu Q, Schett G, Li C, Hu Y, Wick G (2000) Mechanical stress-induced heat shock protein 70 expression in vascular smooth muscle cells is regulated by Rac and Ras small G proteins but not mitogen-activated protein kinases. Circ Res 86: 1122-1128.

Yamamoto N, Smith MW, Maki A, Berezesky IK, Trump BF (1994) Role of cytosolic Ca2+ and protein kinases in the induction of the hsp70 gene. Kidney Int 45: 1093-1104.

Yamashita A, Sugiura T, Waku K (1997) Acyltransferases and transacylases involved in fatty acid remodeling of phospholipids and metabolism of bioactive lipids in mammalian cells. J Biochem 122: 1-16.

Yan D, Saito K, Ohmi Y, Fujie N, Ohtsuka K (2004) Paeoniflorin, a novel heat shock protein-inducing compound. Cell Stress Chaperones 9: 378-389.

Yan L, Rajasekaran NS, Sathyanarayanan S, Benjamin IJ (2005) Mouse HSF1 disruption perturbs redox state and increases mitochondrial oxidative stress in kidney. Antioxid Redox Signal 7: 465-471.

Yatvin MB, Clifton KH, Dennis WH (1979) Hyperthermia and local anesthetics: potentiation of survival of tumor-bearing mice. Science 205: 195-196.

Yatvin MB, Cramp WA (1993) Role of cellular membranes in hyperthermia: some observations and theories reviewed. Int J Hyperthermia 9: 165-185.

Young JC (2010) Mechanisms of the Hsp70 chaperone system. Biochem Cell Biol 88: 291-300.

Young JC, Agashe VR, Siegers K, Hartl FU (2004) Pathways of chaperone-mediated protein folding in the cytosol. Nat Rev Mol Cell Biol 5: 781-791.

Yu W, So PT, French T, Gratton E (1996) Fluorescence generalized polarization of cell membranes: a two-photon scanning microscopy approach. Biophys J 70: 626-636.

Yukawa O, Nakajima T, Miura Y, Ueda J, Ozawa T (2005) Induction of radical scavenging ability and suppression of lipid peroxidation in rat liver microsomes following whole-body, low-dose X-irradiation. Int J Radiat Biol 81: 681-688.

Zaragoza A, Díez-Fernández C, Alvarez AM, Andrés D, Cascales M (2001) Mitochondrial involvement in cocaine-treated rat hepatocytes: effect of N-acetylcysteine and deferoxamine. Br J Pharmacol 132: 1063-1070.

Zemski Berry KA, Murphy RC (2004) Electrospray ionization tandem mass spectrometry of glycerophosphoethanolamine plasmalogen phospholipids. J Am Soc Mass Spectrom 15: 1499-1508.

Zeyda M, Stulnig TM (2006) Lipid Rafts & Co.: an integrated model of membrane organization in T cell activation. Prog Lipid Res 45: 187-202.

Zhang Y, Li X, Becker KA, Gulbins E (2009) Ceramide-enriched membrane domains--structure and function. Biochim Biophys Acta 1788: 178-183.

Zhou YN, Kusukawa N, Erickson JW, Gross CA, Yura T (1988) Isolation and characterization of Escherichia coli mutants that lack the heat shock sigma factor sigma 32. J Bacteriol 170: 3640-3649.

APPENDIX 1 – PUBLICATION LIST

Publications related to the thesis

1. **Balogh G**, Maulucci G, Gombos I, Horvath I, Torok Z, Peter M, Fodor E, Pali T, Benko S, Parasassi T, De Spirito M, Harwood JL, Vigh L (2011) Heat stress causes spatially-distinct membrane re-modelling in K562 leukemia cells. Plos One 6: e2182.
2. **Balogh G**, Peter M, Liebisch G, Horvath I, Torok Z, Nagy E, Maslyanko A, Benko S, Schmitz G, Harwood JL, Vigh L (2010) Lipidomics reveals membrane lipid remodelling and release of potential lipid mediators during early stress responses in a murine melanoma cell line. Biochim Biophys Acta 1801: 1036-1047.
3. Nagy E, Balogi Z, Gombos I, Akerfelt M, Bjorkbom A, **Balogh G**, Torok Z, Maslyanko A, Fiszer-Kierzkowska A, Lisowska K, Slotte PJ, Sistonen L, Horvath I, Vigh L (2007) Hyperfluidization-coupled membrane microdomain reorganization is linked to activation of the heat shock response in a murine melanoma cell line. Proc Natl Acad Sci U S A 104: 7945-7950.
4. **Balogh G**, Horvath I, Nagy E, Hoyk Z, Benko S, Bensaude O, Vigh L (2005) The hyperfluidization of mammalian cell membranes acts as a signal to initiate the heat shock protein response. FEBS J 272: 6077-6086.

Other publications

5. Gombos I, Crul T, Piotto S, Burcin G, Torok Z, **Balogh G**, Peter M, Slotte JP, Campana F, Pilbat A, Toth N, Literati-Nagy Z, Vigh L Jr., Glatz A, Brameshuber M, Schutz G, Hevener A, Febbraio MA, Horvath I, Vigh L (2011) Membrane-lipid therapy in operation: The HSP co-inducer BGP-15 activates stress signal transduction pathways by remodeling plasma membrane rafts. Plos One (accepted).
6. Sipos E, Kurunczi A, Feher A, Penke Z, Fulop L, Kasza A, Horvath J, Horvat S, Veszelka S, **Balogh G**, Kurti L, Eros I, Szabo-Revesz P, Parducz A, Penke B, Deli MA (2010) Intranasal delivery of human beta-amyloid peptide in rats: effective brain targeting. Cell Mol Neurobiol 30: 405-413.
7. Brunelli R, **Balogh G**, Costa G, De Spirito M, Greco G, Mei G, Nicolai E, Vigh L, Ursini F, Parasassi T (2010) Estradiol binding prevents apob-100 misfolding in electronegative ldl(-). Biochemistry 49: 7297-7302.
8. **Balogh G**, Peter M, Torok Z, Horvath I, Vigh L (2010) Lipidomika. Magyar Tudomány 171: 1078-1082.
9. Horvát S, Fehér A, Wolburg H, Sipos P, Veszelka S, Tóth A, Kis L, Kurunczi A, **Balogh G**, Kürti L, Eros I, Szabó-Révész P, Deli MA (2009) Sodium hyaluronate as a mucoadhesive component in nasal formulation enhances delivery of molecules to brain tissue. Eur J Pharm Biopharm 72: 252-259.
10. Greco G, **Balogh G**, Brunelli R, Costa G, De Spirito M, Lenzi L, Mei G, Ursini F Parasassi T (2009) Generation in Human Plasma of Misfolded, Aggregation-Prone Electronegative Low Density Lipoprotein. Biophys J 97: 628-635.
11. Eder K, Vizler C, Kusz E, Karcagi I, Glavinas H, **Balogh GE**, Vigh L, Duda E, Gyorfy Z (2009) The role of lipopolysaccharide moieties in macrophage response to Escherichia coli. Biochem Biophys Res Commun 389: 46-51.

12. De Palma M., Grillo S, Massarelli I, Costa A, **Balogh G**, Vigh L, Leone A (2008) Regulation of desaturase gene expression, changes in membrane lipid composition and freezing tolerance in potato plants. Mol Breeding 21: 15–26.

13. Vigh L, Torok Z, **Balogh G**, Glatz A, Piotto S, Horvath I (2007) Membrane-regulated stress response: a theoretical and practical approach. Adv Exp Med Biol 594: 114-131.

14. Balogi Z, Torok Z, **Balogh G**, Josvay K, Shigapova N, Vierling E, Vigh L, Horvath I (2005) "Heat shock lipid" in cyanobacteria during heat/light-acclimation. Arch Biochem Biophys 436: 346-354.

15. Shigapova N, Torok Z, **Balogh G**, Goloubinoff P, Vigh L, Horvath I (2005) Membrane fluidization triggers membrane remodeling which affects the thermotolerance in Escherichia coli. Biochem Biophys Res Commun 328: 1216-1223.

16. Cinege G, Kereszt A, Kertész S, **Balogh G**, Dusha I (2004) The roles of different regions of the CycH protein in c-type cytochrome biogenesis in Sinorhizobium meliloti. Mol Genet Genomics 271: 171-179.

17. Török Z, Tsvetkova NM, **Balogh G**, Horváth I, Nagy E, Pénzes Z, Hargitai J, Bensaude O, Csermely P, Crowe JH, Maresca B, Vígh L (2003) Heat shock protein co-inducers with no effect on protein denaturation specifically modulate the membrane lipid phase. Proc Natl Acad Sci U S A 100: 3131-3136.

18. Csont T, **Balogh G**, Csonka Cs, Horváth I, Vígh L, Ferdinándy P (2002) Hyperlipidemia induced by high cholesterol diet inhibits heat-shock response after ischemic and heat stress in rat hearts. Biochem Biophys Res Comm 290: 1535-1538.

19. Török Z, Goloubinoff P, Horváth I, Tsvetkova NM, Glatz A, **Balogh G**, Varvasovszki V, Los DA, Vierling E, Crowe JH, Vígh L (2001) Synechocystis HSP17 is an amphitropic protein that stabilizes heat-stressed membranes and binds denatured proteins for subsequent chaperone-mediated refolding. Proc Natl Acad Sci U S A 98: 3098-3103.

20. Lahdes E**, Balogh G**, Fodor E, Farkas T (2001) Adaptation of composition and biophysical properties of phospholipids to temperature by the Crustacean, Gammarus spp. Lipids 35: 1093-1098.

21. Horváth I, Glatz A, Varvasovszki V, Török Z, Pali T, **Balogh G**, Kovacs E, Nadasdi L, Benko S, Joo F, Vígh L (1998) Membrane physical state controls the signaling mechanism of the heat shock response in Synechocystis PCC 6803: identification of hsp17 as a "fluidity gene". Proc Natl Acad Sci U S A 95: 3513-3518.

22. Pataricza J, Penke B, **Balogh GE**, Papp JG (1998) Polarographic detection of nitric oxide released from cardiovascular compounds in aqueous solutions. J Pharmacol Toxicol Methods 39: 91-95.

23. Torday LL, Pataricza J, **Balogh GE**, Zarándi M, Penke B, Papp JG (1998) Endothelium-dependent vasorelaxant and anti-aggregatory effect and mechanism of action of some antifibrinogen RGD (Arg-Gly-Asp-containing) peptides. J Pharm Pharmacol 50: 667-671.

24. Győrfy Z, Horváth I, **Balogh G**, Domonkos A, Duda E, Maresca B, Vígh L (1997) Modulation of lipid unsaturation and membrane fluid state in mammalian cells by

stable transformation with the delta9-desaturase gene of Saccharomyces cerevisiae. Biochem Biophys Res Commun 237: 362-366.

25. Török Z, Horváth I, Goloubinoff P, Kovács E, Glatz A, **Balogh G**, Vígh L (1997) Evidence for a lipochaperonin: association of active protein-folding GroESL oligomers with lipids can stabilize membranes under heat shock conditions. Proc Natl Acad Sci U S A 94: 2192-2197.
26. Vígh L, Literáti PN, Horváth I, Török Z, **Balogh G**, Glatz A, Kovács E, Boros I, Ferdinandy P, Farkas B, Jaszlits L, Jednákovits A, Korányi L, Maresca B (1997) Bimoclomol: a nontoxic, hydroxylamine derivative with stress protein- inducing activity and cytoprotective effects. Nat Med 3: 1150-1154.
27. Szabó AC, **Balogh EG**, Pataricza J, Papp JG (1994) Nitroglycerin induced acute "desenzitisation" is inhibited by ATP-sensitive potassium channel openers in isolated rabbit aorta. Polish J Pharmacol 46: 247-248.

Abstracts in journals

28. Vigh L, **Balogh G**, Torok Z, Gombos I, Peter M, Gungor B, Crul T, Toth N, Hunya A, Pilbat A, Vigh Jr. L, Glatz A, Horvath I (2011) Membranes in stress management: How membranes control the expression and cellular distribution of stress proteins. Chem Phys Lipids 164: S10.
29. Horvath I, **Balogh G**, Peter M, Gombos I, Glatz A, Crul T, Burcin G, Torok Z, Vigh, L (2010) Interrelationship between lipid droplet (LD) biogenesis and heat shock protein (Hsp) response. Chem Phys Lipids 163:S60.
30. **Balogh G**, Peter M, Liebisch G, Maslyanko A, Nagy E, Horvath I, Schmitz G, Harwood JL, Vigh L (2009) Membrane origin of stress response in B16 cells: a lipidomic approach. Chem Phys Lipids 160: S18-S19.
31. **Balogh G**, Liebisch G, Szilvassy Z, Peidl B, Nagy ZL, Tory K, Peter M, Torok Z, Benko S, Horvath I, Schmitz G, Vigh, L (2008) Membrane lipids as drug targets: lipidomic fingerprint of antidiabetic treatment. Chem Phys Lipids 154: S43.
32. Vigh L, Torok Z, **Balogh G**, et al. (2008) Membranes as stress sensors fine-tune the stress protein expression. Chem Phys Lipids 154: S18.
33. Benko S, **Balogh G**, Horvath I, Liebisch G, Maslyanko A, Schmitz G, Harwood JL, Vigh L (2007) Variations in culture conditions profoundly alter the lipid composition of mammalian cells: implications for the stress response modulation. Blodd Reviews 21: S94.
34. **Balogh G**, Horvath I, Liebisch G, Maslyanko A, Nagy E, Schmitz G, Harwood JL, Vigh L (2006) Variations in culture conditions profoundly alter the lipid composition of mammalian cells: Implications for the stress response modulation. Chem Phys Lipids 143: S67.
35. Horvath I, Torok Z, **Balogh G**, Maslyanko A, Nagy E, Balogi Z, Gombos I, Vigh L (2006) Stress protein responses in mammalian cells under the control of lipid composition and microdomain organization of membranes. Chem Phys Lipids 143: S46.
36. **Balogh G**, Horvath I, Nagy E, Torok Z, Parasassi T, Vigh L (2004) Rapid plasma membrane reorganisation in response to heat and membrane perturbation. Chem Phys Lipids 130: S46.

37. Horvath I, Glatz A, Balogi Z, **Balogh G**, Puskas L, Josvay K, Liberek K, Debreczeny M, Hunyadi-Gulyas M, Medzihradszky E, Goloubinoff P, Vigh L (2004) The emerging role for small heat shock proteins in the regulation of composition and dynamics of cell membranes. Chem Phys Lipids 130: S29.

38. **Balogh G**, Horváth I, Nagy E, Török Z, Parasassi T, Vígh L (2004) Rapid plasma membrane reorganisation in response to heat and membrane perturbation. Chem Phys Lipids 130: S46.

39. Horváth I, Glatz A, Balogi Z, **Balogh G**, Puskás L, Jósvai K, Liberek K, Debreczeny M, Hunyadi-Gulyás É, Medzihradszky K, Goloubinoff P, Vígh L (2004) The emerging role for small heat shock proteins in the regulation of composition and dynamics of cell membranes. Chem Phys Lipids 130: S29.

40. **Balogh G**, Horváth I, Nagy E, Török Z, Győrfy Z, Hoyk Z, Benkő S, Bensaude O, Vígh L (2002) Membrane as thermosensor modulate the expression of stress genes. Chem Phys Lipids 118: S84.

41. Horváth I, Török Z, Tsvetkova NM, Balogi Z, **Balogh G**, Vierling E, Crowe JH, Vígh L (2002) Small heat-shock proteins regulate membrane lipid polymorphism. Chem Phys Lipids 118: S15.

42. Győrfy Z, Horváth I, **Balogh EG**, Vígh L, Maresca B, Duda E (1996) Alteration of TNF sensitivity and membrane viscosity of target cells. Eur Cytokine Netw 7: 173.

43. Győrfy Z, Galiba E, **Balogh EG**, Horváth I, Vígh L, Duda E, Maresca B (1996) Increased sensitivity of target cells to cytotoxic cells and cytokines after expression of fungal desaturase gene. Cell Biol Intl 20: 222.

44. Pataricza J, **Balogh EG**, Papp JG (1996) Effect of selective inhibitors of cyclic nucleotide phosphodiesterase isoenzymes on platelet aggregation. J Mol Cell Cardiol 28: A98.

45. Pataricza J, Penke B, **Balogh EG**, Papp JG (1995) Polarographic measurement of nitric oxide released by "NO-donor" compounds in aqueous solutions. J Mol Cell Cardiol 27: A102.

46. Torday L, Pataricza J, **Balogh EG**, Penke B, Zarándi M, Papp JG (1994) Vasorelaxant properties and mechanism of action of some RGD- (Arg-Gly-Asp-containing) peptides. J Mol Cell Cardiol 26: 339.

47. **Balogh EG**, Pataricza J, Papp JG (1993): Kinetic analysis of the effects of vinpocetine, zaprinast and 8-bromo-cGMP on agonist induced endothelium dependent relaxation. J Mol Cell Cardiol 25: S93.

48. Pataricza J, **Balogh G**, Jakab I, Papp JG (1993) Interaction of vinpocetine and acetylcholine on endothelium dependent relaxation and cyclic GMP content in isolated rabbit aorta. J Mol Cell Cardiol 25: S93.

49. Pataricza J, **Balogh G**, Papp JG (1993) Vinpocetine prolongs endothelium dependent vascular relaxation induced by thrombin stimulated platelets in vitro. J Mol Cell Cardiol 25: S94.

50. Torday L, **Balogh EG**, Pataricza J, Zarándi M, Papp JG, Penke B (1993): The vasodilator property and mechanism of action of GRGDS an Arg-Gly-Asp(RGD)-containing peptide. J Mol Cell Cardiol 25: S93.

APPENDIX 2 – COPYRIGHT PERMISSIONS

Re-used material	Adapted from	Copyright holder	Permission received or not required*
Figure 1.1	Richter et al., 2010	Elsevier	✓
Figure 1.2	Finka et al., 2011	Springer Science+Business Media	✓
Tables 1.1–1.5	Kampinga et al., 2009	Springer Science+Business Media	✓
Figure 1.3	Kampinga and Craig, 2010	Nature Publishing Group	✓
Table 1.6	Vos et al., 2008	ACS	✓
Figure 1.4	Björk and Sistonen, 2010	John Wiley & Sons, Inc.	✓
Figure 1.6	Vigh et al., 2007a	Elsevier	✓
Figure 1.7	Morimoto, 1998	CSH Laboratory Press	✓
Figure 1.8	Shamovsky et al., 2006	Nature Publishing Group	✓
Figure 1.17	Pomorski and Menon, 2006	Springer Science+Business Media	✓
Figure 1.18	Simons and Sampaio, 2011	CSH Perspectives	✓
Figure 1.19	Horváth et al., 1998	National Academy of Sciences	✓
Figure 1.20	Escribá et al., 2008	John Wiley & Sons, Inc.	✓
Figures 3.1–3.8	Balogh et al., 2005	John Wiley & Sons, Inc.	✓
Figure 4.1	Nagy et al., 2007	National Academy of Sciences	✓
Figure 4.5–4.15	Balogh et al., 2010	Elsevier	✓
Tables 4.1–4.2	Balogh et al., 2010	Elsevier	✓
Figures 5.1–5.9	Balogh et al., 2011	Creative Commons Attribution License	✓
Table 5.2	Balogh et al., 2011	Creative Commons Attribution License	✓

*: The list was made according to "THE STM PERMISSIONS GUIDELINES (2012)" (www.stm-assoc.org) through the Copyright Clearance Center and/or according to the copyright holder instructions.